VISIBLE LIGHT COMMUNICATION BASED ON HIGH-POWER LED

by

MOSTAFA HUSSEN A. AHFAYD

A thesis submitted to the University of Huddersfield in partial fulfilment of the requirements for the degree of Doctor of Philosophy

School of Computing and Engineering

University of Huddersfield

UK

December 2019

ABSTRACT

In this research, a Visible light communication (VLC) system using a high power (30W) white single LED is evaluated. Initial experiments were performed on a 30 W warm LED, measuring the bandwidth (BW) and data rate. Previous research has shown that these can be implemented in VLC but at limited data rates of less than 10 Mbps due to the LED bandwidth of around 3MHz. An RC compensator circuit was used to increase the bandwidth above 10MHz and a cool LED was used to increase the bandwidth by up to three times. Three differently rated LEDs (20, 30, and 50W) were examined to study the rating power effect on the performance. Experimental systems have shown that this change affects bandwidth, with increasing power resulting in a reduction in bandwidth.

A further focus of the work was to study the effect of six different colour temperature LEDs on bandwidth and data rate. The results show that increasing the colour temperature from within the range of 3,000K to 35,000K leads to an increase in bandwidth from 10MHz to 84MHz and improves data transmission by reducing the bit error rate (BER) to 10^{-11}. The drawback of increasing the colour temperature results in changing the lighting colour from white to blue, which can adversely affect the human eye.

The second objective of this research was to improve the functionality of the VLC system by choosing the appropriate modulation technique. Three types of pulse position modulation (PPM) technique (DiPPM, Duo PPM, and Offset PPM) were implemented based on VLC using high power LEDs. The study found all techniques have similar performance with a minimal difference in the data rate. However, the offset PPM was distinguished from other techniques by recording the minimum BER at a data speed of 20 Mbps. This is due to the working technique of the offset PPM which converts signal pulses from 3- to 4-bits, whereas, other techniques were based on the end of each pulse. Thus, the intersymbol interference (ISI) is reduced in offset PPM compared to other techniques. To verify the results, the 30W LED was compared to a 1W LED which had been used by previous researchers. The results confirm that the high-power LED has the same performance as the low-power LED in VLC applications. Theoretical simulations are also presented.

ACKNOWLEDGEMENTS

First, I would like to express my sincere gratitude to Dr Martin Sibley for his continued support and assistance to move the obstacles to reach the required level of research. I appreciate his patience, motivation and skills that have greatly enriched my graduate experience. I would like also to thank him for the guidance and opportunity to write, publish and participate in international conferences.

I would also like to thank the second supervisor Dr Peter Mather, whose experience, encouragement and direction were vital in completing my research projects and writing this thesis. He enabled me to continue, understand and be kind to the development of a strong theoretical framework in a logical and consistent way and lead me to perform the experimental work at the highest standard. These words fail to express my appreciation and deepest gratitude.

I would also like to express my thanks to all colleagues, especially at engineering department and generally at the University of Huddersfield, research colleagues, faculty members, laboratory staff and supervisors, who have worked over the years to make my experience wonderful on a professional and personal level.

Last but not least, I would particularly like to thank and dedicate this thesis to my wonderful family, my wife and my children: Narjes, Ahmed, Razan, Rahf for their continued support, encouragement and love. Special thanks and gratitude to my mother, soul of my father and all my brothers and sisters for their high expectations, faith and trust in me.

COPYRIGHT

LIST OF PUBLICATIONS

1. Farhat, Z. A., Ahfayd, M. H., Mather, P. J., & Sibley, M. J. "Improved BER for offset pulse position modulation using priority decoding over VLC system," Wireless Days (WD), Manchester, United Kingdom, 24-26 April 2019, pp. 1-4.

In this paper, the main contribution is error correction for Offset-PPM with priority-decoding method.

2. Ahfayd, M. H., Farhat, Z. A., Sibley, M. J., Mather, P. J., & Lazaridis, P. I. "Selection of high power LEDs for Li-Fi applications," 25th International Conference on Telecommunications (ICT), Saint Malo, France, 26-28 June 2018, pp. 170-174.

   In this paper for the first time different types of commercial LEDs are compared to find their efficiency and characteristics in terms of use in VLC.

3. Farhat, Z. A., Ahfayd, M. H., Mather, P. J., & Sibley, M. J. "Practical implementation of duobinary pulse position modulation using FPGA and visible light communication,"*IEEE 15th Student Conference on Research and Development (SCOReD),* Putrajaya, Malaysia, 13-14 December 2017, pp. 253-256.

   The contribution of this paper is practical implementation of Duo-PPM based on VLC using 30 W LED.

4. Ahfayd, M. H., Farhat, Z. A., Sibley, M. J., Mather, P. J., & Lazaridis, P. I. "Visible light communication based system using high power LED and dicode pulse position modulation technique," *25th Telecommunication Forum (TELFOR),* Belgrade, Serbia, 21-22 November 2017, pp. 1-4.

   The novelty of this paper is successful practical implementation of DiPPM on VLC using 30 W LED.

5. Ahfayd, M. H., Sibley, M. J., Mather, P. J., & Lazaridis, P. I. "Visible light communication based on offset pulse position modulation (Offset-PPM) using high power LED," *XXXIInd General Assembly and Scientific Symposium of the International Union of Radio Science (URSI GASS),* Montreal, Canada, 19-26 August 2017, pp. 1-4.

The main contribution of this paper is the use of high power LED (30 W) in visible light communication (VLC), and practical implementation of offset-PPM based on VLC.

TABLE OF CONTENTS

Contents

LIST OF FIGURES

LIST OF TABLES

LIST OF ABBREVIATIONS

AGC	Automatic Gain Control
APD	Avalanche Photodiode
ASK	Amplitude-Shift-Keying
BW	Bandwidth
BER	Bit Error Rate
CAP	Carrierless Amplitude and Phase
CDMA	Code Division Multiple Access
DD	Direct Detection
DD-LMS	Decision-Directed Least Mean Square
DiPPM	Dicode Pulse Position Modulation
DPPM	Differential Pulse Position Modulation
DMT	Discrete Multitone Modulation
Duo-PPM	Duobinary Pulse Position Modulation
GPS	Global Positioning System
HDL	Hardware Description Language
IFFT	Inverse Fast Fourier Transform
ISI	ISI Inter-Symbol Interference
ITS	Intelligent Transportation Systems
LAN	Local Area Network
LASER	Light Amplification by Stimulated Emission of Radiation
LED	Light Emitting Diode
Li-Fi	Light-Fidelity
LOS	Line-Of-Sight
MEPPM	Multilevel Expurgated Pulse Position Modulation
MLSD	Maximum Likelihood Sequence Detection
MPPM	Multiple Pulse Position Modulation
NRZ	Non-Return to Zero
OOK	On-Off Keying
OWC	Optical Wireless Communication
PAM	Pulse Amplitude Modulation
PC	Personal Computer
PCB	Printed Circuit Board
PCM	Pulse Code Modulation
PD	Photodiode
PHY	Physical Layer
PIM	Pulse Interval Modulation
PLL	Phase-Locked Loop

PPM	Pulse Position Modulation
PRBS	Pseudo Random Binary Sequence
PSD	Power Spectral Density
QAM	Quadrature Amplitude Modulation
RF	Radio Frequency
RS	Reed Solomon
SNR	Signal-to-Noise Ratio
TIA	Trans-impedance Preamplifier
VHDL	VHSIC Hardware Description Language
VHSIC	Very High-Speed Integrated Circuit
VLC	Visible Light Communications
WDM	Wavelength Division Multiplexing
Wi-Fi	Wireless Fidelity

Chapter 1
Introduction

1.1 Introduction

Optical telecommunications has become a topic of academic interest in the field of data communication systems. In this emerging technology, light is used as a data transferring medium. In ancient days, people used to manipulate light sources as well as smoke in order to convey messages to their allies. However, with the advent of the technological revolution, wireless optical communication systems (OWC) became part of radio-frequency (RF) communications. OWC systems use two types of light spectra for communication: infrared (IR) and visible light. Therefore, accessibility to the wide spectral range of OWC (approximately 670 THz) has the potential to provide wireless communication with high data transferability [1]. Additionally, OWC systems with 390–700 nm wavelength are commonly used for visible light communications (VLCs); thus, the light emitting diode (LED) can be used for the dual purpose of communication and illumination. VLC is an economical and green hybrid technology, with the potential to revolutionise the near future of communication [2]. However, apart from communication, the primary purpose of light is to illuminate the surroundings. The technological advancements made in the field of visible LEDs have influenced the researchers to develop VLC-related systems. The motive of using LEDs is to provide communications as well as illumination. This sharing of resources can save electric power and raw materials. The most important benefit of using LEDs instead of ordinary bulbs for communications is LEDs' fast switching capability [3].

Considering the recent development in high-power, visible-light-emitting LEDs, VLC is a more energy efficient and clean substitute than RF technology. Furthermore, the current progress in OWC allows a consumer to use existing lighting infrastructure for VLC systems. VLC refers to optical wireless communication systems that use light as an information carrier in the visible spectrum range (400–700 nm) [4].

In the past couple of years, with the widespread use of LEDs in lighting, the study related to VLC using LED has been increased. The major reasons for the growing interest on LEDs over ordinary lamps and fluorescent tubes are low power consumption, long life, lower cost than competing technologies and, importantly for use in data transmission, fast switching. Optical wireless communication (OWC) and

Visible Light Communication (VLC) which use LEDs have become techniques for high data transmission, which are potentially faster than other systems such as infrared (IR) or radio-frequency (RF). Due to progress in the field of optical electronics, more precisely concerning illumination sources, the data transferring technology is evolving with a new perspective through OWC [5]. However, researchers are trying to develop an OWC system depending on the visible electromagnetic spectrum to the human eye, which will serve the purpose of communication as well as illumination [4, 6-9]. Communication systems, such as the VLC systems, are different from the conventional communication standards [6, 10]. As mentioned earlier, VLC systems can fulfil basic illumination needs and standard communication medium [11]. However, during the practical application of VLC systems, several issues have been faced by the developers of the systems, such as the practical implementation of the channel model, transmitter and receiver front-end [12]. On the other hand, to achieve a higher data rate and more secure data, especially when using white phosphoric LEDs, different modulation techniques are used, such as on-off keying (OOK), pulse-position modulation (PPM), etc. [4, 5].

The purpose of this study was to focus on the current development and analysis of energy-efficient LEDs. Furthermore, the development of VLCs using high power LEDs system was also investigated throughout the thesis.

Experimental tests have been performed on some LEDs. Moreover, comparisons have been drawn in order to find the most appropriate technique. The main aim of the study was to develop a reliable and new cost-effective VLC technology based on high-power LEDs.

This motivation led us to contribute to the knowledge of the use of high-power LEDs in communication systems as well as lighting. From this perspective, a database was built to find the most appropriate LEDs in these applications. Finally, some types of pulse position modulation techniques were employed to find the optimum performance of optical communication systems.

1.2 Historical Development of VLC

Although researchers have been trying to develop VLC systems from the late nineties, the biggest breakthrough related to this technology was introduced in Japan in 2004, where the efficiency of LEDs in high-speed data transmission for vehicle-borne

and hand-held computing gadgets was demonstrated. Moreover, in 2005, Japan introduced a VLC system that was comprised of fluorescent light and LEDs, which could transfer information to mobile phones at a speed of several Mbps. Furthermore, in 2007, Japan's Fuji Television company introduced LED-backlit liquid crystal display, in which data could be transferred through light [5].

However, with the introduction of new technologies, Japan Electronics and Information Technology Industries Association (JEITA) also proposed two standards of VLC systems, such as the visible light ID system standard (JEITA CP-1222) and the VLC system (JEITA CP-1221) standard. Additionally, in 2008, a European-Union-funded project named OMEGA proposed a global standard for the domestic use of OWC after considering the VLC and IR technology. The OMEGA project demonstrated a VLC system that could transfer information at a rate higher than 100 Mbps. According to the OMEGA guidelines, the data transmission may reduce if the distance is longer than a few metres. Furthermore, in 2008, the Infrared Data Association (IrDA) and Visible Light Communications Consortium (VLCC) in Japan started collaborating in order to develop a VLC standard for the United States. In 2009, VLCC and IrDA defined the allowable wavelength of the visible spectrum for VLC technology. After the declaration of VLC standards, this technology became an efficient medium to connect electronic gadgets such as computers, laptops, smartphones, high-definition television, digital cameras, etc. Aside from these applications of VLCs, in 2010, Japan demonstrated the application of VLCs in indoor global positioning systems (GPS). In the same year, a German institute developed an FM-VLED system that could transmit information at a rate of 500 Mbps over 5 m. It was also the year when a team of researchers from the University of Edinburgh, UK, demonstrated the OFDM-based VLC system. They demonstrated that a VLC system consisting of phosphorescent white LEDs was able to transfer data at rate of 124 Mbps in real time. Further progress in VLC technology found a way to transfer data through a local area network (LAN) by 2012 [13]. In 2013, the visible light beacon system was a new standard that was proposed in JEITA as JEITA CP-1223. Moreover, Bellè et al. developed a VLC system based on the IEEE802.15.7 standard for intelligent transportation systems (ITS) [14]. In 2014, a VLC system was tested as a complementary technology of the RF indoor communication system and the dual-mode (white LED and IR) VLC conference system [15, 16]. Furthermore, an indoor localisation device, which provided localised

information and underwater VLC systems, was developed in 2015 [17, 18]. In the subsequent years (i.e., 2016 and 2017), VLCs were developed using optical image sensors and employed in the intelligent transport system [19-22]. In 2018, a subsystem of Li-Fi technology was developed based on VLC communication [23]. In 2019, Meister et al. designed a VLC system that could transfer data between VLC and Wi-Fi [24].

1.3 Applications of VLC

Applications of VLC can be found in daily-life instances such as [4]:

- Wi-Fi and cellular wireless connectivity within a confined space
- Wireless communication for connecting interrelated computing devices
- Communication support to the intelligent transport system (ITS)
- Wireless communication devices in medical facilities
- Smart toys and theme-based entertainment parks
- Dynamic information produced with the help of a smartphone camera

1.4 Advantages of VLC

VLCs have certain advantages when compared with existing RF-based communication systems, which are as follows:

1.4.1 VLC spectrum

The wide spectrum of visible light can be experienced from 400 THz to 780 THz, whereas the RF spectrum is between the 3 kHz–300 GHz range. The wide spectrum of visible light can increase the rate of data transfer by replacing the congested RF spectrum.

1.4.2 Electromagnetic interference

As in VLC systems, light works as a data transferring medium and causes zero electromagnetic interferences. This VLC can be used in aeroplanes, hospitals, and nuclear power plants.

1.4.3 Implementation

VLC systems can be organised as compact and small devices which can be readily implemented into the existing artificial illuminating sources. Furthermore, the control unit and digital-to-analogue signal converter, among others, can be installed within the LEDs or as an external receiver.

1.4.4 Cost

The execution of a VLC system is comparatively easier than that of other communication systems. VLCs can be installed within the existing lighting infrastructure by simple attachments or extensions, which is the main reason why VLCs have lower cost and better compatibility.

1.4.5 Energy efficiency

As the LEDs have the advantage of lesser energy consumption, these systems are considered to be green illuminating devices. According to research, LEDs consume less than 80% of the energy consumed by conventional artificial illuminating devices [25]. Moreover, if all the conventional lighting sources are replaced by LEDs, the worldwide energy consumption is expected to reduce by 50% [26]. According to a current forecast from the Department of Energy, US, up to 217 TWh of energy can be saved till 2025 by replacing conventional lights with LEDs [27].

1.4.6 Health safety

As LEDs do not produce any harmful RF or microwave, they are safe for human health and can be used as large optical sources.

1.4.7 Information security

Data security is the biggest concern for any communication system. An RF-based system employs radio waves that can pass through walls. However, visual light-based communication systems do not possess properties similar to radio waves. As light cannot pass through walls, the data in VLCs stays confined within walls. However, this characteristic leads to better indoor and outdoor communication. The huge demand for high-speed internet access for indoor smart computing devices can be resolved through the application of VLCs. As people spend most of their time in the workplace, school, and home, it would be convenient for them to be able to access the internet by using modified LED-lighting sources. The wide bandwidth range of visible light can provide better and faster data transferring experiences than conventional Wi-Fi and existing internet facilities. VLC devices equipped with proper modules can transfer data at up to a gigabit per second. Moreover, zero electronegative interference of visible light ensures safe data transfer in the electromagnetic sensitive environment, which enables the VLC system to function without hampering electrical gadgets.

The aforementioned various indoor and outdoor applications of VLCs enable them to reach the consumers of smart devices, who influence the developers to think

about the various possibilities of VLCs in different aspects. Moreover, the low energy consumption of VLC systems can influence a better market demand than the existing communication system [28].

1.5 The VLC Principle

Simple operating procedures enable VLC systems to achieve better connectivity by controlling the communications with the on-and-off switching of LED intensity, which is significantly faster than the perception of the human eye. A photodiode (PD) present into the VLC is used to sense the rapid on-and-off regulation of light. A photodiode is a device that can produce currents in the presence of photons. The amount of currents induced in a PD is proportional to the quantity of photons incident on the surface of a photodetector. This simple working principle of photodiode enables scientists to develop a hybrid system which can fulfil the multiple purposes of both data transfer and illumination. Figure 1–1 shows the schematic diagram of a VLC system which uses LED and photodiodes in order to fulfil the previously stated purpose. Moreover, the presence of an illuminating source with the communication outlet enables consumers to identify the communication service area. Unlike the RF-communication system, where dedicated accessories are required to identify the service area, VLC systems can be easily recognised by this illumination source. Visible light consists of a wide range of frequencies of 385–789 THz, enabling VLCs to convey information at a faster rate [3].

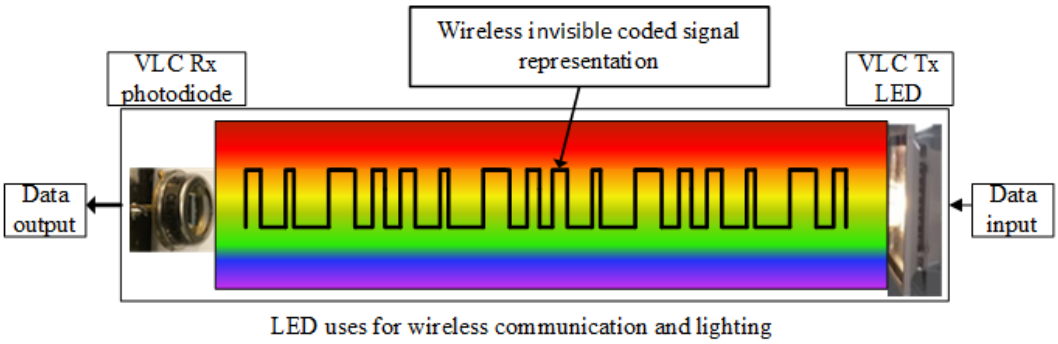

Figure 1–1: Principle of visible light communications [3]

1.6 System Description

Figure 1-2 presents the block diagram of a typical VLC system, through which it can be observed that the precise control of the dimming appearance of incandescent lamps is difficult, while the light intensity of LEDs can be controlled easily. Moreover, it can be

observed that the response time of an LED during off-and-on operation is around a few nanoseconds. Therefore, by controlling the high frequency current, VLCs are capable of maintaining a moderate on-and-off state of an LED-based system in a faster way. Thus, it is easy to generate a low average power pulse and high frequency information stream from an LED-based system. However, the average photon flux produced from LED is controlled by the width of a dimming signal. A similar kind of system can be designed using a semiconductor laser, serving a similar purpose for data communication according to the safety requirements. An advantage of using LED in the OWC is that it fulfils the purposes of both illumination and communication [29].

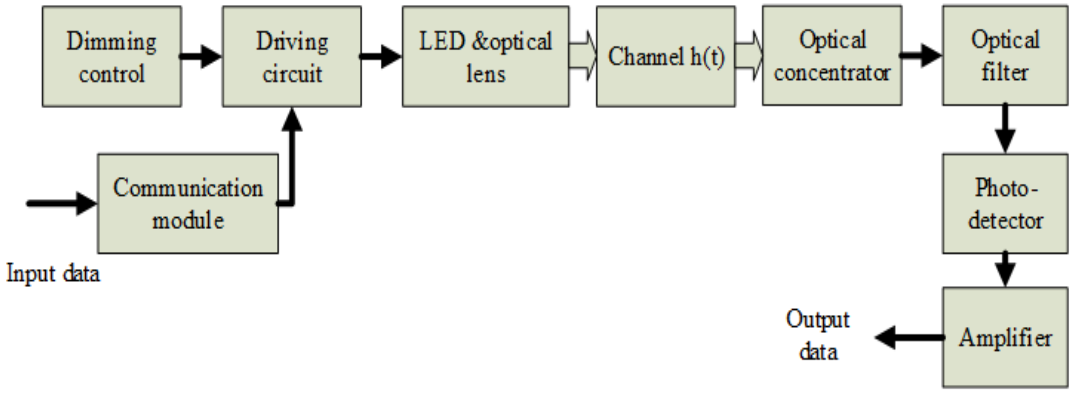

Figure 1-2: Block diagram of a VLC [29]

1.7 VLC's Key Components

As shown in Figure 1-3, the functionality of a successful VLC system depends on the key components of the system, such as LED, PD and physical layer (PHY). The purpose of LED is to convert an electrical signal into an optical signal. This optical signal is used to provide illumination and a data-carrying medium for communication. Further, the data encoding and modification is done by the PHY module. Afterward, the data is transferred from PHY as an optical signal to the receiver. Then, PD, present in the receiver end and translates the optical signal into an electrical signal, depending on the intensity of the optical signal. Once again, the PHY layer receives an electrical signal and decodes it for the user. However, the main drawback of VLC systems is the interference from the noise produced by secondary illumination sources such as sunlight or any other light-emitting object. Due to these secondary sources, it is difficult to produce a signal with a high signal-to-noise ratio (SNR). The SNR of the VLC system can be optimised by implementing a careful design that includes optical filtering, concentrators and electrical signal processing [3].

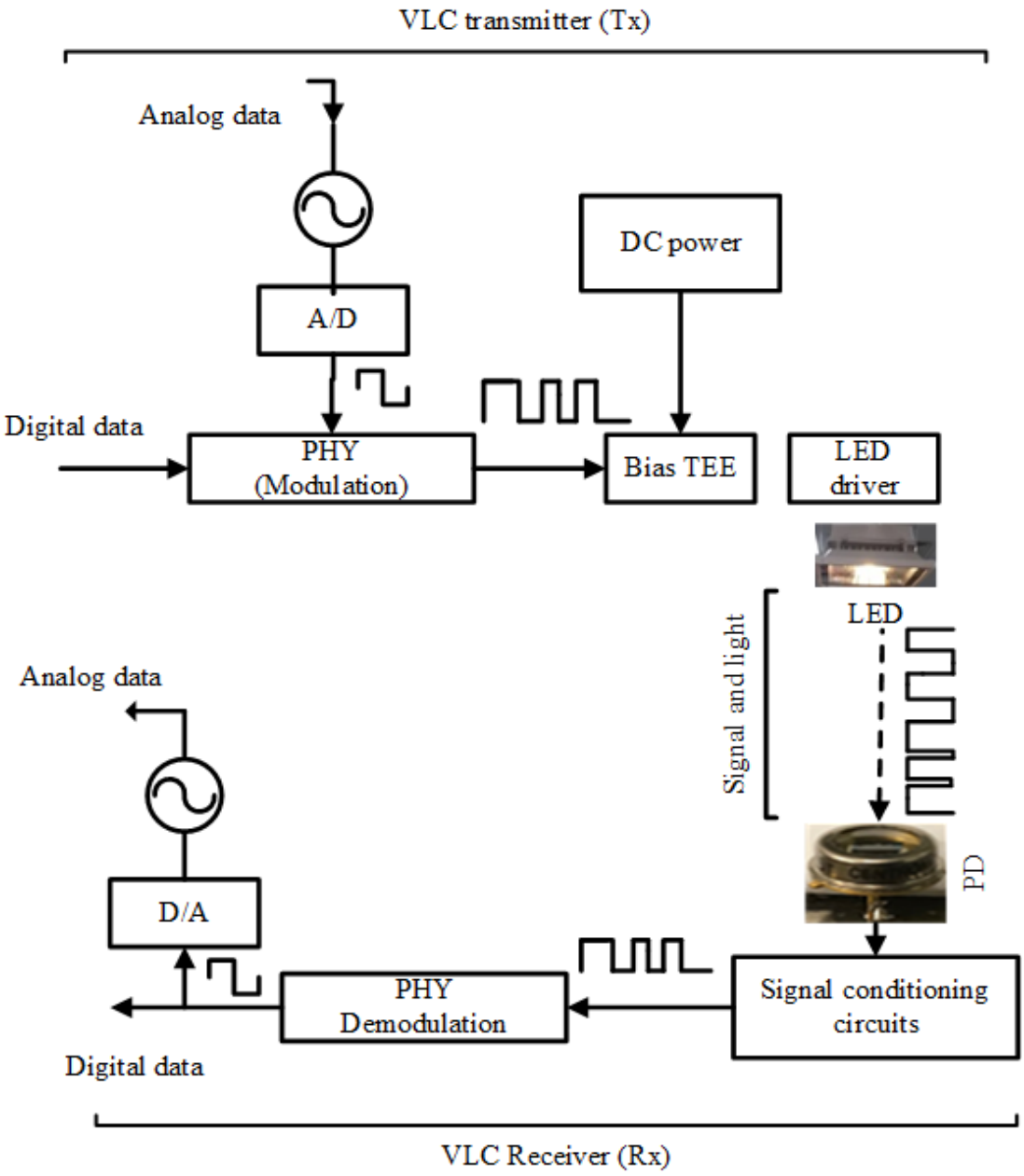

Figure 1-3: VLC key components [3]

1.8 VLC Approaches

Presently, environmental safety and green technology play a significant role in the marketing of a new product. VLC is an emerging green technology that can satisfy consumer needs with better efficiency than the existing communication system. LED-based illuminating sources are well established in mark-to-manufacture devices such as indication sign, traffic signal, transportation light, TV, etc. This increased popularity of LED as a lighting source will provide LED-based VLC technology with a marketing benefit.

LED- and VLC-based fusion technology can be used to connect multiple computing devises with higher data transferring ability. Furthermore, communication can be done by using an LED display. Moreover, wireless communication system in a restricted area can be implemented by using VLCs. VLCs can also provide communication network with less electronic interference. This feature enables VLCs to use it in electronically sensitive areas. Additionally, the intelligent transport system can be manufactured using a VLC system [3].

1.9 Motivation

Several factors have influenced researchers to develop a communication system based on the visible light spectrum. The most convincing cause is to develop a VLC system that is more energy efficient than conventional communication systems. The idea is to develop a system which will convey information by means of modified illumination sources. However, the acceptance of a newly-developed VLC system depends on factors such as secure data transfer and environment compatibility rather than the existing RF-based systems [4]. The application of LEDs can be observed in different areas in order to make the systems more economical, energy saving and reliable. Considering the previously mentioned advantages, researchers are trying to use an LED-based system in transport systems as well as VLC-based systems. The major focus of the researchers is to develop a system that can be used as an alternative and complementary system of an RF-based system. This alternative system should be able to connect millions of electronic system efficiently. Furthermore, the efficiency of VLC systems was affected by different factors such as modulation techniques and LED power, which can be considered for improving the system performance. Although OWC has been utilised in the communication sector for several years, in recent times, VLC systems have emerged as a promising technology for data transferring and wireless communication [2]. From these principles, the motivation for this research was the study and practical implementation of high-power LEDs for VLC applications, in addition to lighting.

1.10 Research Aims

Due to the rapid development of communication technology, especially in the wireless communications area, which makes researchers seek the best alternatives to

improve communication in terms of speed, security and cost, the main aims of this research are as follows:

- To build the test rig for studying commercial high-power LEDs in terms of data transmission and lighting.
- To implement and optimise a VLC transceiver system based on different schemes of the PPM technique by using high-power LEDs in order to transmit high data rate along with illumination.
- To optimise and select the appropriate LED for lighting and data transmission based on an appropriate modulation scheme.

1.11 Research Objectives

A key goal of this study was to investigate the possibility of using high power LEDs in visible light communication systems. To achieving this, several key objectives were identified and prioritised, which are as follows:

- To review previous studies in order to determine the most important research on visible light communications and knowledge of methods, techniques and results that have been obtained in order to reach the highest data rate.
- To implement a cost-efficient transmitter in terms of less complexity and noise reduction using additional circuits.
- To design, implement and improve a receiver in order to obtain the highest data rate.
- To implement different modulation techniques in VLC based on high-power LEDs.
- To optimise the appropriate modulation technique among the proposed techniques by using different approaches.
- To select the appropriate white, high-power LED so as to determine the optical bandwidth and its improvement.
- To conduct a mathematical investigation of the receiver sensitivity.
- To investigate the effect of the transmission distance and elevation angle based on VLC by using high-power LEDs.

1.12 Thesis Structure

The structure of the present thesis has been divided into eight chapters, which

are as follows: ***Chapter 1*** provides a concise overview of VLC systems and presents the history of their evolution. Moreover, it describes the applications and advantages of VLC. ***Chapter 2*** provides a review of the literature on the existing VLCs based on different modulation schemes. Previous studies were reviewed in relation to the types of LEDs as well as modulation methods based on VLC required to access higher data rate. This ensures that the replication of previous studies is avoided. ***Chapter 3*** describes the LEDs' basic principles in order to understand their optical and electrical characteristics as well as properties. ***Chapter 4*** studies several types of pulse position modulation that are used in optical systems of communication. ***Chapter 5*** explores the properties of high-power LEDs by conducting experiments to measure their bandwidth and expandability. ***Chapter 6*** investigates the practical implementation of VLCs based on high-power LEDs by using different modulation techniques. ***Chapter 7*** presents the mathematical models of the offset PPM, DiPPM, and duo PPM by using the Mathcad software. Finally, ***Chapter 8*** provides conclusions based on the key findings and contributions of this study, such as using high-power LEDs, selecting the most appropriate commercial LED in terms of lighting and data communication, specifying three modulation techniques for the VLC applications as well as identifying the most appropriate technique, and identifying recommendations for future research.

Chapter 2
Literature Review

2.1 Introduction

Recently, significant studies have focused on the development of white LEDs used in various areas of life as an alternative to ordinary lamps and fluorescence in achieving lower power consumption [10, 30]. In addition, data transmission has become possible as it offers many advantages such as faster switching, longer lifespan and lower cost compared with most technologies [31, 32]. Moreover, the use of LEDs in VLC and OWC has become key for high transmission of data, which, when compared to other systems such as IR and RF, is potentially faster [11, 33, 34].

In studies related to VLC systems, two main variable parameters need to be investigated in order to determine the reliability of the system in terms of transmission: data speed (data rate), which is the rate of bit transmission speed per second, and bit error rate (BER), which is the number of bits that have error ratio to the total number of received bits.

2.2 Light-emitting Diode Based on VLC

In this section, studies where LEDs have been applied in data communication, lighting and VLC were reviewed. Some of the reasons why such techniques are being utilised include greater brightness and extensive durability compared to other bulbs, higher bandwidth and data rate, low energy consumption and low risks. Recent studies that used VLC have succeeded in the transfer of data that is higher than 500 Mbit/s [5]. Most of the previous studies on VLC relied on low-power LEDs. 1 W RGB (i.e., red, green, and blue) LEDs have been implemented for a data rate of up to several Gbps [18, 35-38]. A transmission distance of less than 1 m was achieved with a BER of 3.8×10^{-3} by using RGB LED and filter. Some of the disadvantages of using the RGB LEDs are high manufacturing cost, colour dispersion, colour offset, and other phenomena. In general, they cannot be used for the purpose of lighting [39].

A white LED was implemented in several studies in order to acquire higher transmission of data in an optical wireless system with several Mbps [11, 40-43]. Wang et al. (2012) stated that their test was carried out over the illumination in the photodiode surface with various distances between the photodiode receiver and 3 W white LED.

Moreover, the impact of background light was also taken into consideration. The results of their experiment concluded that by setting the average indoor illumination at 40 lux for a distance of 1.5 m, there was a possibility of data transmission at 111 kbit/s. Moreover, the illumination on the surface of the photodiode was absent after a distance of 1.2 m [44]. Furthermore, the proposition and demonstration of a VLC system, including a real-time phosphor LED and 37 Mbit/s throughputs in a length of 1.5 m free-space transmission, were also conducted. The highest achieved bit rate by the VLC system was 37 Mbit/s. The proposed system of VLC demonstrated a video transmission using 28.419 Mbit/s [45]. According to Chow (2015), the investigation was conducted over the visible light communication by using white LEDs (7.5 W). 190 Mbps was the highest bit rate, achieved at high illuminance [46].

A white LED with 1 W rating with an upper limit of transmission rate achieved up to 2 Mbit/s, with BERs being lower than 10^{-6} when used between two computers [47]. Moreover, a prototype of 20.0 mW white LED transmitted data at 100 kHz towards a 160^{o} view field with a 1.7 m radius [6]. The transmitting bandwidth, specified as the modulation bandwidth for 4 mW white LEDs, was 2 MHz [48]. One disadvantage of low-power LEDs is that it provides insufficient energy for lighting. In addition, transmission signal has a limited propagation distance. Therefore, for high illumination, the array of 16 white LEDs (1.5 W) was implemented. Moreover, a 40 Mb/s data rate was transmitted, covering a link radius of 0.5m and a distance of 2 m [49]. One main disadvantage of using LEDs array was that the synchronous driving of all the LED chips can be a difficult task as it requires a careful design of the length of the cable and the spacing between the LED chips. A huge amount of difference in electrical signal paths from a common point of distribution to each of the LED chips can lead to ISI [50].

2.3 Requirements of Transceiver System for High Data Speed

It is known that the white LED bandwidth is relatively small because the time constant of the phosphor is relatively slow [2], where it is not reliable to send high data rate. Therefore, it seeks to use additional circuits for the purpose of increasing the speed of transmission and the spread distance. Such circuits include equalisation circuits, pre-emphasis circuits, and the blue filter. However, these kinds of additional circuits have disadvantages such as noise, high cost, and a complicated transmitter. Furthermore, pre-emphasis circuits and post-equalisation technology have been added to the transmitter

and receiver, respectively, in order to achieve a data rate of up to hundreds of Mbps. In addition, blue filters have been implemented based on 1W LEDs [35, 51-54]. However, in these cases, the transceiver circuit becomes more complicated and expensive. The transmitter distance can be increased to 2 m for a 1 W RGB LEDs (with a speed of 4.5 Gb/s at the BER of $3.8x10^{-3}$) by adding the Volterra nonlinear equaliser circuit at the transmitter (Tx) [39]. Moreover, by optimally designing the analogue pre-equalisation in the LED transmitter (Tx) and the receivers' (Rx) automatic gain control (AGC), the modulation VLC bandwidth can be increased from 1MHz to 30 MHz without the use of any optical blue filter [46]. For instance, the bandwidth for the phosphor LED, which was approximately 1 MHz, was extended to approximately 12 MHz by using a pre-equalisation circuit without a blue filter [45]. Additionally, a technique with multiple-resonant-driving equalisation was implemented in order to increase the white LED-based VLC systems modulation bandwidth to 25 MHz [49].

Presupposed optimal analogue equalisers were used for extending the 3-dB bandwidth of the VLC link from 3 MHz to 143 MHz. The maximum achievable rate of the transmission data and the resultant bit-error-ratio (BER) at a distance of 1 m were 682 Mbit/s and 2.5×10^{-3}, respectively [55]. A white LED, blue-filter-based VLC system was demonstrated and used to increase the bandwidth of the modulation and reducing the BER. Furthermore, according to [39], a drastic reduction in BER at 50 MHz bandwidth for VLC was based on the wide stop-band blue filter and the blue filter.

Using the post-equalisation and pre-emphasis circuits, the 3-dB VLC system bandwidth increased from 3MHz to 233 MHz. The distance between the receiver and the LED, with BER and the data rate of 2.3×10^{-7} and 480 Mbit/s, respectively, could be extended to 1.6 m. Moreover, for alleviating the VLC link data rate and the 3-dB bandwidth, pre-emphasis circuits were applied along with the post-equalisation. Additionally, the highest data rate (550Mbit/s) was acquired at a free-space distance of 0.6 m and BER of 2.6×10^{-9} [41].

For alleviating the phosphor white LED bandwidth through a thorough inspection by VLC, one active equaliser was conducted between two passive equalisers circuits. The distance of the link operation was 0.43 m, which was infused with a 1W white LED. BER yielded less than 2×10^{-3} from the operation of on-off keying non-return to zero (OOK-NRZ) The VLC link of data transmitted at the rate of 340 Mbit/s [40].

On the side of the LED transmitter, an optimal analogue pre-equalisation RLC circuit was designed to compensate for the phosphor LED impedance matching, while on the side of the receiver, the automatic gain control (AGC) circuit was used to increase the sensitivity of the signal to maintain and enhance the orthogonal frequency division multiplexing (OFDM) signal linearity [56]. The results from the data transmission demonstrated that the measured carrier bandwidth could be enhanced from 0.8 MHz to about 1.7 MHz through the use of a high-pass RC filter such as a post-equaliser, especially utilised for compensating a 3 W white LED response [51]. The RLC equalisation circuit component and blue filtering was used in improving the frequency response of white LEDs. The VLC system modulation bandwidth was increased from 3 MHz to about 180 MHz at 0.5m radius, with a NRZ-OOK data transmission of up to 400 Mb/s [54].

The pre-emphasis circuits, with cascaded T-bridge and maximal ratio combining (MRC) differential receivers, were utilised with an RGB LED in a VLC system with high speed. Moreover, a data rate of 9.51 Gbps was experimentally achieved at over 1 m indoor free space transmission [35].

A VLC system with a carrier wave of 1 KHz–1 MHz was built at a transmission distance of 1.8 m by using a 1 W white LED (Edixeon A series EDEW-1LA5-F1), having a 105 lm⁄W flux with pre- and post-equalisation [57]. However, it is known that an increase in the design of the electronic circuit means an increase in the number of electronic components in the transceiver system. Therefore, the signal noise caused by circuit components increased, leading to the design of additional filtering circuits to reduce the noise. In this case, the transceiver circuit became more complicated and expensive.

2.4 Modulation Techniques Based on Visible Light Communications

The most common types of modulation techniques used in visible light communications are: pulse-amplitude modulation (PAM), carrierless amplitude and phase (CAP), discrete multitone modulation (DMT), on-off keying (OOK), amplitude-shift keying (ASK), pulse-position modulation (PPM), and orthogonal frequency division multiplexing (OFDM).

CAP modulation was used in VLC in order to achieve a high data rate up to several Gbps [38, 39, 58]. High speed wavelength division multiplexing, carrierless

amplitude, and a phase WDM CAP64 VLC system, which makes use of the Volterra series-based nonlinear equaliser, was used in mitigating the nonlinearity of the LED [39]. Moreover, a volterra series-based nonlinear equaliser, a linear equaliser and a decision-directed least mean square (DD-LMS) equaliser were employed to obtain a high data rate of up to 8 Gbps [58]. Additionally, an overall data rate of 1.35Gbps over a transmission distance of 0.3m was achieved successfully, with BER under 7% and 3.8×10^{-3} FEC limit [59]. CAP modulation, two and single cascaded constant-resistance symmetrical T-bridged amplitude hardware pre-equalisers and a three-stage hybrid post-equaliser consisting of a linear equaliser based on M-CMMA, a DD-LMS-based equaliser, and a Volterra series-based nonlinear equaliser were proposed and combined to implement a high-speed VLC system [60]. However, CAP modulation requires very complex equalisers and carrier waves.

In the demonstration of a high-speed wavelength division multiplexing, the CAP WDM-CAP64 VLC system, with a nonlinear equaliser based on the Volterra series, was used for the attenuation of the 1 W RGB LED nonlinearity. Over an indoor free-space transmission of 2 m at 3.8×10^{-3} BER, an aggregate data rate of 4.5 Gbps was attained [18]. PAM and DMT were demonstrated and compared with (OOK for VLC based on white LEDs with blue filtering, where the data rates for PAM and DMT were higher than that of OOK, being 101 Mbps and 40 Mbps, respectively. [61]. The total BER of 1.5×10^{-3}, along with the highest data rate at 420 lx (10 cm) and 10 lx (50 cm) of 1 Gb/s and 640 Mb/s, respectively, were acquired by DMT modulation based on a commercial phosphorescent white LED [62]. While DMT modulation is more complex when compared to CAP modulation (where fast Fourier transform [FTT] and inverse FFT are needed). The spectral efficiency is seen to reduce due to the inclusion of a training sequence and cyclic prefix [63]. A data rate of 10 Mbps with a BER of 10^{-10} through the VLC was achieved by using a white LED, with 1 W power rating and 1 MHz bandwidth through OOK modulation and first-order RC-equalisation at the side of the receiver [64]. Moreover, the demonstration of OOK-NRZ modulation regarding linking the real-time VLC on a phosphorescent 1 W white LED was conducted. The resultant BER was 2.6×10^{-9} at 60 cm with a data rate of 550 Mbit/s [41]. Furthermore, VLC, using a phosphorescent 1 W white LED with pre-emphasis and blue-filtering circuit at 1.1 m, was investigated based on NRZ–OOK. The VLC system bandwidth and data rate transmission increased from 3 to 77.6 MHz and 86 to

200 Mb/s, respectively, with the BER being below 10−6 [53]. In case of the power LEDs being used as an information source, Latal et al. concluded that the OOK NRZ modulation scheme cannot be applied for a high data rate (i.e., a data rate of more than 100 Mbps) [65]. The OOK modulation is a coherent modulation technique that is normally used when there is a presence of an undesired signal. One key disadvantage of using this type of modulation is that it has a very poor bandwidth efficiency. However, the main advantage of using this technique is that it is very simple to implement, although it can be highly prone to noise.

Further investigation was conducted on the quaternary-amplitude-shift-keying (4-ASK) modulation, including digital filtering to improve the direct speed of modulation of a single white LED (Cree, XLamp XR-E LED) in a VLC system. In a free space transmission of 1 m, where an optical blue filter was not used, a data rate of 20 Mbit/s was attained with a BER of less than 10^{-10} [66]. However, this modulation was more prone to noise and BW inefficient scheme. Further, it operated in linear regions. On the other hand, an integrated OFDM-based DSP chip VLC system for real-time operation achieved a data rate of up to 37 Mbit/s and 28.419 Mbit/s video signals [45]. Besides, the data rate was modulated from 200 Mb/s to 350 by using 32-QAM modulation at a fixed distance of 40 cm between the receiver and the white LED.

A consideration of VLC with increased brightness LEDs has been examined through the OFDM in contextual intensity modulation. Nevertheless, the experiment proved that covering a maximum distance of 1 m with BER of 10^{-3}, excluding a channel or source coding with a single LED, is possible [67]. Higher rate of data transmission can be provided by VLC in an indoor ambience in a credible and affordable way with regards to commercialisation. For VLC, several suitable techniques of modulation have been thoroughly researched. Such technique includes the OFDM and multilevel expurgated pulse-position modulation (MEPPM) as they have the ability of supplying the needed spectral efficiency of up to several Gbit/s [68]. Moreover, a demonstration of visible-light communication with full-duplex wireless between two computers for direct detection (DD) and intensity modulation (IM) schemes (based on the OOK-NRZ data) was achieved at a data rate of up to 2 Mbit/s and BERs of less than 10^{-6} [47]. In order to increase the rate of transmission in the VLC systems, arrays of white LEDs, propositioned over numerous techniques, was applied, where expurgated pulse-position modulation (EPPM) was used. Between PPM and EPPM, the presupposed interleaving

technique made the former, which is a more eligible modulation option for the systems of VLC [69]. A reduction in the effectiveness was observed in the system bandwidth with the incorporation of a repeater and the time it dispersed extensively in the channel, bringing the channel bandwidth to 3–5 MHz. The rate of data transmission was 1 Mbps, with a BER of 10^{-3} by using a 2-PPM modulation scheme. One disadvantage of using the repeaters was the introduction of interference into the network caused by the delay added to the signal at the repeater circuit [48]. Moreover, an investigation on the reported link of phosphor-based 682 Mbps white LED VLC by using 16QAM-OFDM modulation excluding the modulation of blue filter was conducted [55].

Besides, the presentation of a bidirectional real-time VLC prototype based on the OFDM modulation technique was demonstrated, with a speed of up to 500 Mb/s at 2 m [34]. The drawback of using the OFDM is its problems of frequency synchronisation, Doppler shift sensitivity, need for the linear transmitter circuitry suffering from poor power efficiency and high peak-to-average-power ratio (PAPR) [70]. The demonstration of the proposed system of phosphor LED, with 1 W white VLC, comprising of an OFDM and an adaptive 16QAM of 84.44–190 Mbit/s, was carried out. At a practical transmission distance of 0.75–2 m and BERs of $< 3.8 \times 10^{-3}$ at 30 MHz, the ~1 MHz phosphor LED modulation bandwidth was stretched. At 513 Mbit/s, on the basis of using a white LED and DMT modulation within BER of $2x10^{-3}$, a higher data rate was attained [71].

On the basis of using only one commercially available RGB-type LED, a comparison was made between CAP signals and the OFDM performances in the VLC system at a free-space distance of 25 cm. For the OFDM signals, the highest data rates of green, blue, and red chips were 0.87 Gbps, 1.05 Gbps and 1.01 Gbps, respectively. The blue chip helped in achieving the data rate of a single-channel of 1.32 Gb/s and, as regards the CAP signals, the highest pre-emphasised data rates for green, blue, and red chips were 0.92 Gb/s, 1.15 Gb/s, and 1.15 Gbps, respectively, which, altogether, led to a BER of less than 10^{-3} [36, 37]. The PPM technique has improved power efficiency and requires less optical power compared to OOK [72]. A major disadvantage of differential PPM and digital pulse interval modulation (PIM) is that they cannot operate with continuous data due to their coding characteristics and must also code blocks of data [73]. For the improvement of the quality of transmission and mitigate any effect of intersymbol interference (ISI), an investigation on dicode pulse-position modulation

technique (DiPPM) was conducted. This technique increased the performance of the system (receiver sensitivity) from 3.47 dB to 3.5 dB compared with digital PPM as well as reduced the BER from 10^{-6} to 10^{-9} [74].

In conclusion, to improve the data transmission rate, it is essential to consider the type of modulation technique, type of LED, the distance between the transmitter and the receiver, and the use of a blue filter. Table 2-1 provides the summary of some of the results obtained from previous studies with the most important variables. The motivation in this study has made it possible to use high-power, single-LED (30 W), visible-light communication based on different modulation techniques in order to achieve high data transmission rate with low BER.

2.5 Summary

After reviewing the previous studies, the following points have been summarised:

- Previous studies focused on the use of low-power LEDs in VLC applications, the limitations of which included insufficient illumination as well as transmitter distance. Hence, in this study, high-power LEDs were implemented in VLC.
- To increase the bandwidth of LEDs, additional circuits were used for both the transmitter and receiver, making the final circuit more complicated and expensive. Hence, in this study, the simplest transceiver circuits in VLC were designed at low cost.
- Several types of modulation techniques were used to improve the design performance in terms of an increased speed of data transmission. In this study, different types of PPM techniques (DiPPM, Duo-PPM and offset-PPM) were used and compared in order to overcome the defects found in previously used modulations. The PPM technique improves power efficiency, requires less optical power and increases the receiver sensitivity. In the next two chapters, the characteristics of LEDs and different types of PPM techniques will be studied and described in detail.

Table 2-1: The summary of previous studies results

Types of LED	Modulation	Data rate	Tx-Rx Distance	BER	Blue filter	Reference	Year
RGB LED Module (LED ENGIN LZ4-20MC00)	CAP	R/B/ 1.15 Gbps G/0.92 Gbps	About 25cm	$R/3.29.10^{-4}$ $G/3.17.10^{-4}$ $B/2.54.10^{-4}$	R/G/B filter	[36]	2013
RGB LED Module (LED ENGIN LZ4-20MC00)	OFDM	R/ 1.01 Gbps G/0.87 Gbps B/1.05 Gbps	About 25cm	$R/9.33.10^{-4}$ $G/9.13.10^{-4}$ $B/9.98.10^{-4}$	R/G/B filter	[36]	2013
RGB LED (Cree PLCC, output power: 1 W; red: 620 nm; green: 520 nm; blue: 470 nm)	WDM CAP64	Aggregate data rate of 4.5 Gbps	Over 200cm	$3.8.10^{-3}$	R/G/B filter	[75]	2015
Phosphor LED	OFDM	37Mbps	Under 150cm	-	Without	[45]	2013
White LED (1w, beam angle 120o)	NRZ-OOK	2Mbps (full duplex wireless)	-	$< 10^{-6}$	Without	[47]	2013
White LED (cree XLamp XR-ELED)	4-ASK	20Mbps	100cm	$<10^{-10}$	Without	[66]	2012
Phosphorescent white LED (OSTAR® LE CW E2B)	QAM-DMT	513Mbps	30c m	$<2.10^{-3}$	Blue filter	[71]	2010
White phosphor LED (Edison, EDEW 3LS5)	16-QAM-OFDM	84.44 Mbps 190 Mbps	200cm 75cm	$2.6.10^{-3}$ $2.54.10^{-3}$	Without	[56]	2014
Phosphor-based White LED (cree XLamp XR-ELED)	OFDM	325 Mbps	50cm	$3.8.10^{-3}$	Designed blue filter	[39]	2015
Phosphorescent white LED (OSRAM LUW W5AM)	NRZ-OOK	550 Mbps 480 Mbps	60cm 160cm	$2.6.10^{-9}$ $2.3.10^{-7}$	Blue filter	[41]	2014
Phosphorescent white LED (OSRAM LUW W5AM)	16-QAM-OFDM	682 Mbps 520 Mbps 390 Mbps	100cm 180cm 220cm	$2.5.10^{-3}$ $3.76.10^{-3}$ $3.4.10^{-3}$	Without	[55]	2015
Phosphorescent white LED (OSRAM LUW W5AM)	OOK-NRZ	340 Mbps	43cm	$<2.10^{-3}$	Blue filter	[40]	2014
Phosphor-based White LED (13lm at 80mA)	DMT	1Gbps 640	10cm 50cm	$1.5.10^{-3}$	Blue filter	[62]	2012
Red LED	DFT-S OFDM	1.2 Gbps	40 cm	$3.8.10^{-3}$	Without	[76]	2016
Red LED	64QAM	2.1 Gbps	100 cm	$<10^{-4}$	Without	[77]	2017
µLED array	PWM	2 Mbps	12.5 cm	$<10^{-6}$	Without	[78]	2018
µLED array	OOK	1 Gbps	30 cm	$<10^{-5}$	Without	[79]	2019

Chapter 3
Characteristics of LEDs

3.1 Introduction

LEDs are a p-n junction semiconductor that under appropriate, forward-biased conditions can emit radiation in the visible, ultraviolet and infrared regions of the spectrum [5, 80, 81]. The application of a forward-biased voltage across the p-n junction enables electrons to be energised inside the material, thereby becoming excited and unstable. During the process, the energy is released by the energised electrons while returning to a stable condition in the form of photons. LEDs can be applied widely and classified into three groups: display, illumination and application. The examples of displays include panel displays in calculators, computer screens, automobiles, etc., while that of illumination are replacements for old incandescent light bulbs. Moreover, an example of application includes sourcing light for systems of optical-fibre communication with moderate and low data rates (< 1 Gb/s) through short and moderate distances (< 10 km).

3.2 LED Current-Voltage Characteristics

The following is a summary of the electrical aspects of p-n junctions [82]. An acceptor concentration (N_A) and a donor concentration (N_D) is created in consideration of an abrupt p-n junction. Complete ionisation is expected in all the dopants so that $n = N_D$ and $p = N_A$, providing free electron concentration and free hole concentration, respectively. Moreover, the occurrence of dopants is assumed without compensation from unintentional disputes and contamination. Around the unbiased p-n junction, the donors originates electrons on the side of the n-type, which spreads across the side of the p-type, encountering numerous holes and using them for recombination. The holes make a corresponding process occur which is diffused on the side of the n-type. It results in an area around the p-n junction where free carriers deplete. The name of this area is the depletion region. Only the ionised acceptors and donors provide charge while free carriers are absent in the depletion region. A region of space charge is formed by those dopants, i.e., donors and acceptors on the n-type side and the p-type side, respectively. A potential diffusion voltage V_D is generated by this space-charge region. The voltage of the diffusion is attained through:

$$V_D = \frac{kT}{e} ln \frac{N_A N_D}{n_i^2} \qquad 3–1$$

Here, the donor and acceptor concentrations are N_D and N_A, respectively. As for the semiconductor, k, Te and ni are the Boltzmann constant (1.38×10^{-23} J/Ko), temperature (ko), electric charge equal to 1.6×10^{-19} C and the crucial carrier concentration, respectively [83].

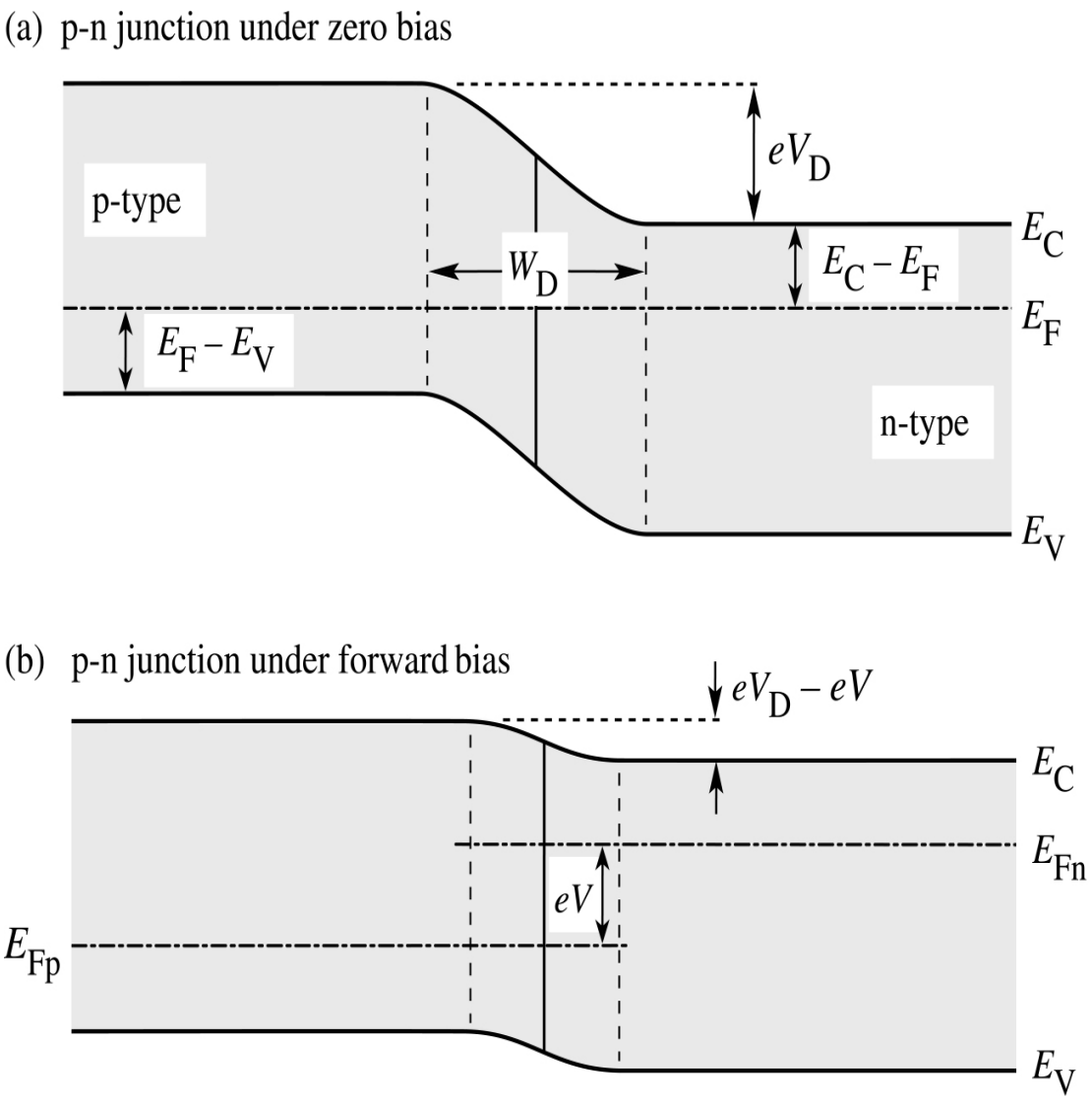

Figure 3-1: p-n junction and energy diagram[82]

The restriction that requires the free carriers to overcome is represented by the diffusion voltage for reaching the neutral zone of the type of opposite connectivity, as illustrated in Figure 3-1. The width of the depletion layer is attained through [82, 83]:

$$W_D = \sqrt{\frac{2\varepsilon}{e}(V_D - V)\left(\frac{1}{N_A} + \frac{1}{N_D}\right)}\ 3 \qquad 3\text{–}2$$

Where, $\varepsilon = \varepsilon_r \times \varepsilon_0$ and V are the semiconductor dielectric permittivity and the voltage of diode bias, respectively. Over the depletion zone, the voltage dips after applying the bias voltage on the p-n junction. Owing to the depletion of the free carriers, high resistance can be found in this zone. The barrier of p-n junction regarding reverse or forward bias increases or decreases, respectively, through an external bias. Conditioned with forward bias, zones, including the type of opposite conductivity, are injected with holes and electrons. The zones of the opposite conductivity type are diffused with carriers, leading to the eventual recombination and, finally, emission of a photon. Shockley was the first to build the current-voltage (I–V) aspect of a p-n junction, which is why the equation is called the Shockley equation, as it depicts the I-V curve of a p-n junction diode. For a diode, the Shockley equation (including the cross-sectional area A) is attained through [82]:

$$I = eA\left(\sqrt{\frac{D_P}{\tau_P}}\ \frac{n_i^2}{N_D} + \sqrt{\frac{D_n}{\tau_n}}\ \frac{n_i^2}{N_A}\right)\left(e^{eV/KT} - 1\right) \qquad 3\text{–}3$$

Here,τ_n,τ_P and D_n,D_P represent the electron and carrier of the hole minority for lifetime as well as the electron and constants of the hole diffusion, respectively. Conditioned with reverse bias, the saturation is conducted by the diode current and the preceding factor of the exponential function of the Shockley equation, providing the saturation current. The diode I-V aspect are:

$$I = I_S\left(e^{eV/KT} - 1\right) \qquad 3\text{–}4$$

Where,

$$I_S = eA\left(\sqrt{\frac{D_P}{\tau_P}}\ \frac{n_i^2}{N_D} + \sqrt{\frac{D_n}{\tau_n}}\ \frac{n_i^2}{N_A}\right) \qquad 3\text{–}5$$

The diode voltage is $V >> KT/e$, and $\left(e^{\frac{eV}{KT}} - 1\right) \approx \left(e^{\frac{eV}{KT}}\right)$ for the common states of forward bias. Using Eq. 3-1, The Shockley equation with respect to the forward-bias conditions will be:

$$I = eA\left(\sqrt{\frac{D_P}{\tau_P}}\ \frac{n_i^2}{N_D} + \sqrt{\frac{D_n}{\tau_n}}\ \frac{n_i^2}{N_A}\right) e^{e(V-V_D)/KT} \qquad 3\text{–}6$$

The strong increase can be delineated by the exponent from the exponential function of Eq. 3-4, while the voltage heads off to the diffusion voltage, meaning V ≈ V_D. The name of the voltage is threshold voltage, which powerfully increases the current, while Vth ≈ VD generates this voltage. As depicted in Fig. 3-1, the dissociation from the valence band edge and the conduction of the Fermi level is illustrated in the p-n junction band diagram. Boltzmann statistics can infer the differences in the energy between the band edges and the Fermi level, which will be the following for the n-type side:

$$E_C - E_F = -KT\ ln\frac{n}{N_C}3 \qquad 3\text{–}7$$

As for the n-type side, it will be the following:

$$E_F - E_V = -KT\ ln\frac{P}{N_V} \qquad 3\text{–}8$$

The band diagram of Fig. 2.1 describes the sum of the following energies as zero:

$$eV_D - E_g + (E_F - E_V) + (E_C - E_F) = 0 \qquad 3\text{–}9$$

With greatly doped semiconductor, the band gap energy $E_F - E_C \ll E_g$ on the p-type side and $E_C - E_F \ll E_g$ on the n-type side – is greater than the dissociation between the Fermi level and the band edges. Therefore, Eq. 3-8 can be rewritten as:

$$V_D \approx E_g/e \qquad 3\text{–}10$$

The following band gap energy provides emission energy from the emitted photon of a semiconductor, having an energy gap (E_g) of:

$$hv \approx E_g \qquad 3\text{–}11$$

Each electron produces a photon, which is fed to the active zone. Therefore, energy conservation needs the energy injecting electron as much as photon energy. Therefore, energy conservation is in the need of:

$$eV = hv\,3 \qquad 3\text{–}12$$

It means that the photon energy and the elementary charge, multiplying when applying voltage to LEDs, are equal to each other. Therefore, the diode voltage will come out from:

$$V = hv/e \approx E_g/e3 \qquad 3\text{–}13$$

3.3 LED Efficiencies

Each injected electron is counted for the emission of one photon around the active zone in the ideal LED. One light quantum particle (photon) is generated by every charge quantum particle (electron). Therefore, quantum unity efficiency is present in the perfect active zone [5, 82, 84].

3.3.1 Internal quantum efficiency

This term has a relation while the carriers are converted into photons in the device. Hence, it can be concluded as the proportion of internally emitted number of photons, corresponding to the number of carriers sweeping across the p-n junction. It means:

$$\eta_{int} = \frac{No.\,of\ photons\ emitted\ from\ active\ region\ per\ second}{No.\,of\ electrons\ injected\ into\ LED\ per\ second}$$

$$= \frac{P_{int}/(hv)}{I/e} = \frac{(P_{int})e}{I(hv)} \qquad 3\text{–}14$$

Here, I and P_{int} are the injection current and emitted optical power out of an active zone respectively. A relation between the internal quantum efficiency and injected carrier fractions that make radiative recombination with the total recombination can be observed; the following equation links it directly to the carrier lifetimes:

$$\eta_{int} = \frac{R_r}{R_t} = \frac{R_r}{R_r+R_{nr}} = \frac{\tau_r}{\tau_r+\tau_{nr}} \qquad 3\text{-}15$$

Here, R_{nr} and R_r represent nonradiative and radiative rates of recombination respectively with R_t being the total number of recombination and τ_{nr} and τ_r being the nonradiative and radiative lifetimes respectively. Moreover, the following represents the total recombination lifetime τ:

$$\frac{1}{\tau} = \frac{1}{\tau_r} + \frac{1}{\tau_{nr}} \quad \text{3-16}$$

3.3.2 Extraction efficiency

The outline of light extraction efficiency will be:

$$\eta_{extraction} = \frac{No.of\ photons\ emitted\ free\ space\ per\ second}{No.of\ photons\ emitted\ from\ active\ region\ per\ second}$$

$$= \frac{P/(h\nu)}{P_{int}/(h\nu)} = \frac{P}{P_{int}} \quad \text{3-17}$$

Here, emitted optical power in free space is symbolized by P. The high-performance LEDs can be severely limited by the extraction efficiency. Increasing the extraction efficiency above 50% is a very difficult task involving expensive and advanced device techniques.

3.3.3 External quantum efficiency

The ratio between internally generated photons and emitted photons in the device is defined as the external quantum efficiency.

$$\eta_{ext} = \frac{No.of\ photons\ emitted\ free\ space\ per\ second}{No.of\ electrons\ injected\ into\ LED\ per\ second}$$

$$= \frac{P/(h\nu)}{I/e} = \frac{Pe}{I(h\nu)} = \eta_{extraction}\eta_{int} \quad \text{3-18}$$

3.3.4 The power efficiency

The ratio of the electrical power input and the optical power output in LED is known as the power efficiency, i.e.:

$$\eta_{power} = \frac{optical\ power\ output}{electrical\ power\ input} = \frac{P}{IV} \quad \text{3-19}$$

Here, the electrical power supplied to LED is represented by *IV*.

3.4 LED Modulation

LEDs are applied most widely as the source of light in the local-area communication systems with very short (< 1 m) to moderate (5 km) operating distances [82]. There are many common bit rates ranging to 1 Gbit/s from 10 Mbit/s. The capacitance, shunt resistance and series resistance of LEDs rely on the voltage of application. These should be accounted for through an extensive investigation. Nevertheless, they can be learned by considering the LED as a linear device, although some important aspects of the LED modulation behaviour cannot be deduced from the linear model. First, the LEDs will be analysed as linear devices; then, its modulation aspects with certain non-linear modulation aspects will be discussed.

3.5 Rise and Fall Times

Figure 3-2(a) illustrates a simple RC circuit. The following brings forth increase in output voltage when heading for the input pulse of a step-function:

$$V_{out}(t) = V_0\left[1 - e^{(-t/\tau_1)}\right] \qquad 3\text{-}20$$

Here, the time constant in RC circuit is depicted though τ_1= RC. The following brings forth decrease in the output voltage at the time of return of input voltage:

$$V_{out}(t) = V_0 e^{(-t/\tau_2)} \qquad 3\text{-}21$$

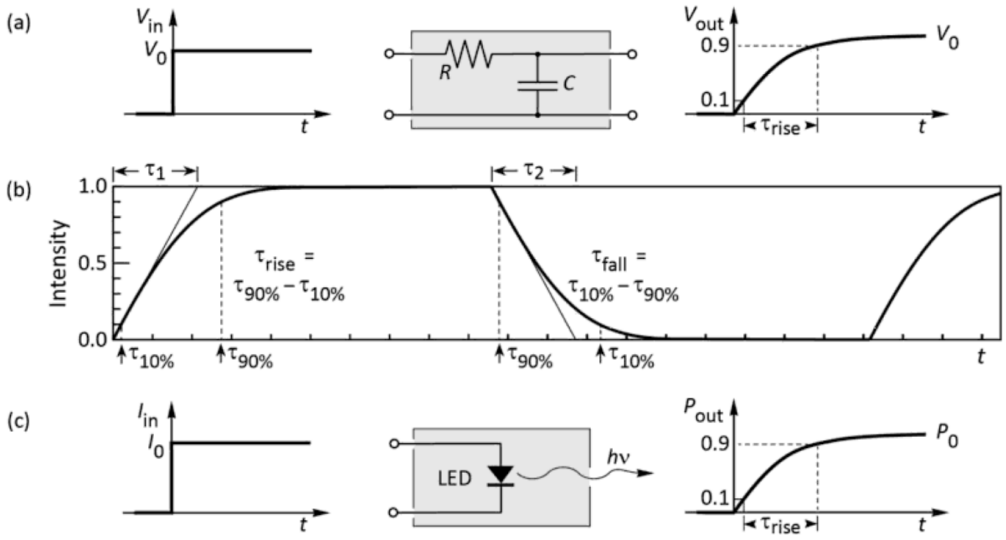

Figure 3-2: a)- Linear RC circuit with rise time; b)- Rise and fall time with time constants τ_1 and τ_2; c)- output power of an LED [82]

An RC circuit requires $\tau_1 = \tau_2$. As Figure 3-2(b) depicts, the gap between 90% and 10% voltage points defines the fall and rise times respectively. Figure 3-2(c) shows the output power of LED as a function of time with rise time. The relation between τ_1 and τ_2 and signal rise and fall times respectively is:

$$\tau_r = (ln9)\tau_1 \approx 2.2\tau_1 \qquad 3\text{-}22$$

$$\tau_f = (ln9)\tau_2 \approx 2.2\tau_2 \qquad 3\text{-}23$$

The following generates the function of voltage transfer $H(\omega)$:

$$H(\omega) = \frac{1}{(1+i\omega\tau)} \qquad 3\text{-}24$$

3.5.1 LED modulation bandwidth

The determining factors in the modulation response and the bandwidth of frequency of an LED are the parasitic capacitance, the junction capacitance and the injected current

[5, 84]. The values of capacitance are almost static whereas increasing current increases the response [12]. Superimposing the AC signal upon a persistent DC bias can decrease the impact of the factor mentioned above. Supposing P_o as the given DC power and its frequency as ω, by$P(\omega)$, the frequency can be anything in this yielded output of relative optical power:

$$\frac{P(\omega)}{P_o} = \frac{1}{\sqrt{1+(\omega\tau)^2}} \qquad 3\text{-}25$$

The frequency of power transmission via the system and the system bandwidth Δf corresponds with each other. Thus, the condition should be: $|H(\omega)|^2 = 1/2$. And the bandwidth in the RC circuit then will be:

$$\Delta f = f_{3dB} = \frac{1}{2\pi\tau} = \frac{ln9}{2\pi\tau_r} = \frac{ln9}{\pi(\tau_r+\tau_f)} \approx \frac{0.35}{\tau_r} \approx \frac{0.7}{(\tau_r+\tau_f)} \qquad 3\text{-}26$$

Another name of the bandwidth is 3 dB frequency as at this frequency, the transmitted power is decreased by 3 dB than its value of low frequency. After that, an LED is considered in Figure 3-2(c) where the rise time is τ_r. The application of current is done in terms of input of step-function increasing the optical output power as:

$$P_{out}(t) = P_0\left[1 - e^{(-t/\tau_r)}\right] \qquad 3\text{-}27$$

At the LED 3 dB frequency, the absolute power transfer function value is decreased to a half:

$$\Delta f = f_{3dB} = \frac{\sqrt{3}}{2\pi\tau} = \frac{\sqrt{3}ln9}{2\pi\tau_r} = \frac{\sqrt{3}ln9}{\pi(\tau_r+\tau_f)} \approx \frac{1.2}{(\tau_r+\tau_f)} \qquad 3\text{-}28$$

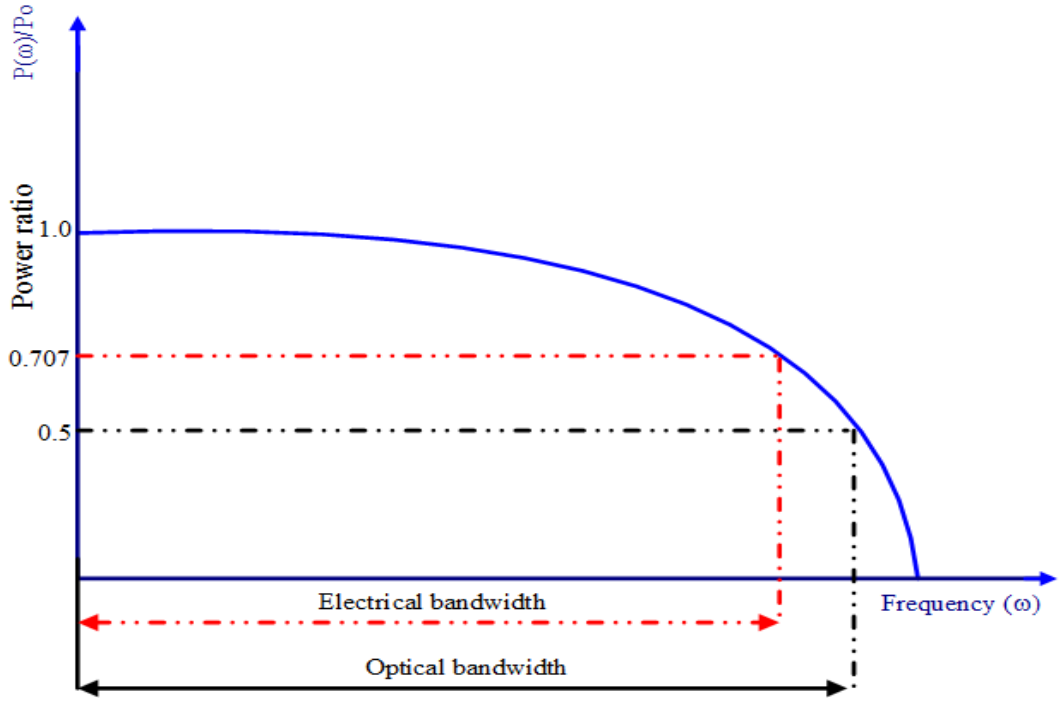

Figure 3-3: An electrical and optical bandwidth [5, 84]

Eq. 3-28 is set at 0.5 for acquiring the bandwidth of optical 3 dB whereas the same expression is set at 0.707 for acquiring the equivalent electrical bandwidth (referred to Figure 3-3).

3.6 Colour Temperature

The ranges of colour temperatures of man-made light sources (incandescent lamp and wax candle) as well as natural light sources (sun and moon under different conditions) are illustrated in FFigure 3-4. Achromatic white light (also called 'pure' white light) is located close to the equal energy point in the chromaticity diagram. Achromatic white has no hue and is used as the white point of colour displays. It may be noted that LEDs can generate light of any colour temperature by mixing the light from multiple LED chips or by using phosphors [83].

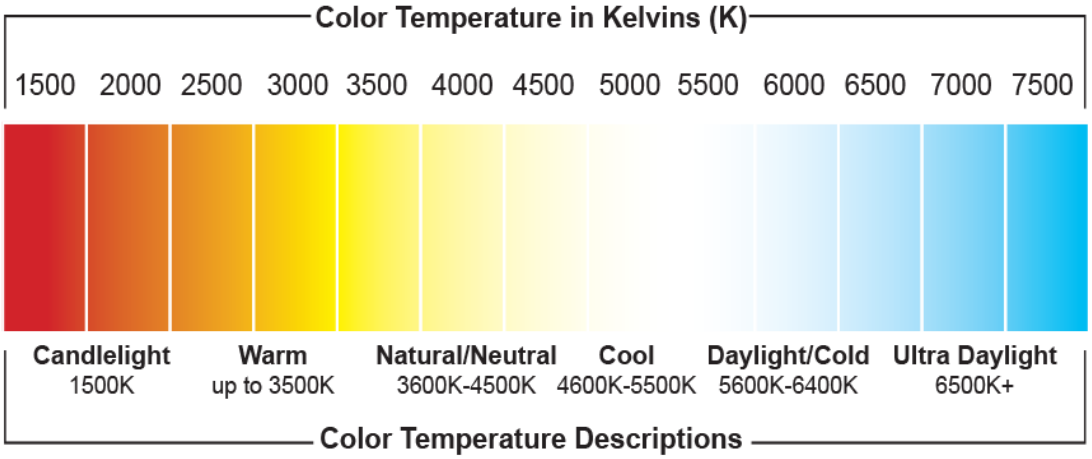

Figure 3-4: Colour temperature of light sources [83]

3.7 White Light Emitting Diode

The definition of 'white light' is guided by natural white light such as sunlight (under various conditions). As pointed out earlier, sunlight resembles black-body radiation and therefore has a chromaticity on or close to the Planckian locus [83].

White LEDS are regarded as very efficient sources of light. Demonstration of conversion efficiencies of electrical-to-optical power and external quantum efficiencies exceeds 50%. With the continuing fashion of greater efficiencies of LEDs, increase in application number is also noticed. General illumination is a very intriguing application where sources of conventional illumination like fluorescent lamps and incandescent lamps and LEDs compete with each other [82, 85]. Blue, green, red and sometimes amber combine in creating white LED light. The result of this combination is indicated

as white lights that are RGB-generated [82, 86]. An alternative method of white light generation is from the use of an LED that is blue or near ultraviolet in colour or a LED coated with phosphor. The colour temperatures in this type of LED can be very high, leading to a cool blue or white appearance. The white colour that is warmer can be possibly obtained by adding phosphorus emissions in the visible spectrum red zone, even with 50% reduction in the efficacy of its luminosity.

3.8 Summary

In this chapter, the properties of the photodiode were studied. Emphasis was placed on the efficiency of diode and methods of calculation, the rise and fall time was measured and calculated, and the LED modulation bandwidth in addition to the classification of LEDs in terms of colour temperature are also calculated. In Chapter 5, the bandwidth will be measured practically for different types of high-power commercial LEDs to be compared in terms of VLC applications.

Chapter 4
Modulation Techniques Based on VLC

4.1 Introduction

Of the presently deployed systems, the majority of practical optical wireless communication (OWC) systems apply the intensity modulation with direct detection (IM/DD) strategy for outdoor as well as indoor applications. The prevailing issue in heavy fog is the atmospheric conditions because the propagation of light intensity into a dense fog is considerably reduced. Thus, hypothetically, high attenuation could be solved best by pumping more and providing optical power and power respectively in the small regions. Nevertheless, the quantity of transmitting optical power is limited by eye safety. The eye safety limit is more rigid in transmit optical power of indoor applications. There is a significant difference between the optical channel and the RF channels. Phase, frequency and amplitude related to carrier signals in the RF systems undergo modulation whereas optical carrier intensity in optical systems undergoes modulation where most systems operate below data rates of 25 Gbps. Normally, external modulation is taken for data rates more than 25 Gbps. Moreover, the average of thousand wavelengths of the incident wave facilitates the surface area of photodetectors much greater than the optical wavelength. This chapter discusses some popular modulation methods concerning bandwidth efficiency and power efficiency in case of both outdoor and indoor OWC applications [82, 85, 86]. Types of modulation methods are outlined in Figure 4-1.

Optical modulation techniques can be divided into two main types—internal modulation and external modulation. Internal modulation is a direct modulation of the light source. Practically, internal modulation may cause changes in the density of the carrier, thus causing a shift in carrier frequency, which results in the dispersion. Eliminating this problem using the external modification isolates the processes of modulation and generation of light. In the external modulation technique, the light source is focused through an external system, where the propagation properties are changed by the modulation signal. These systems can use the full capacity of the power. The external modulation techniques are coherent binary polarization shift keying (BPOLSK), Multilevel Polarization Shift Keying (MPolSK) and intensity modulation (IM).

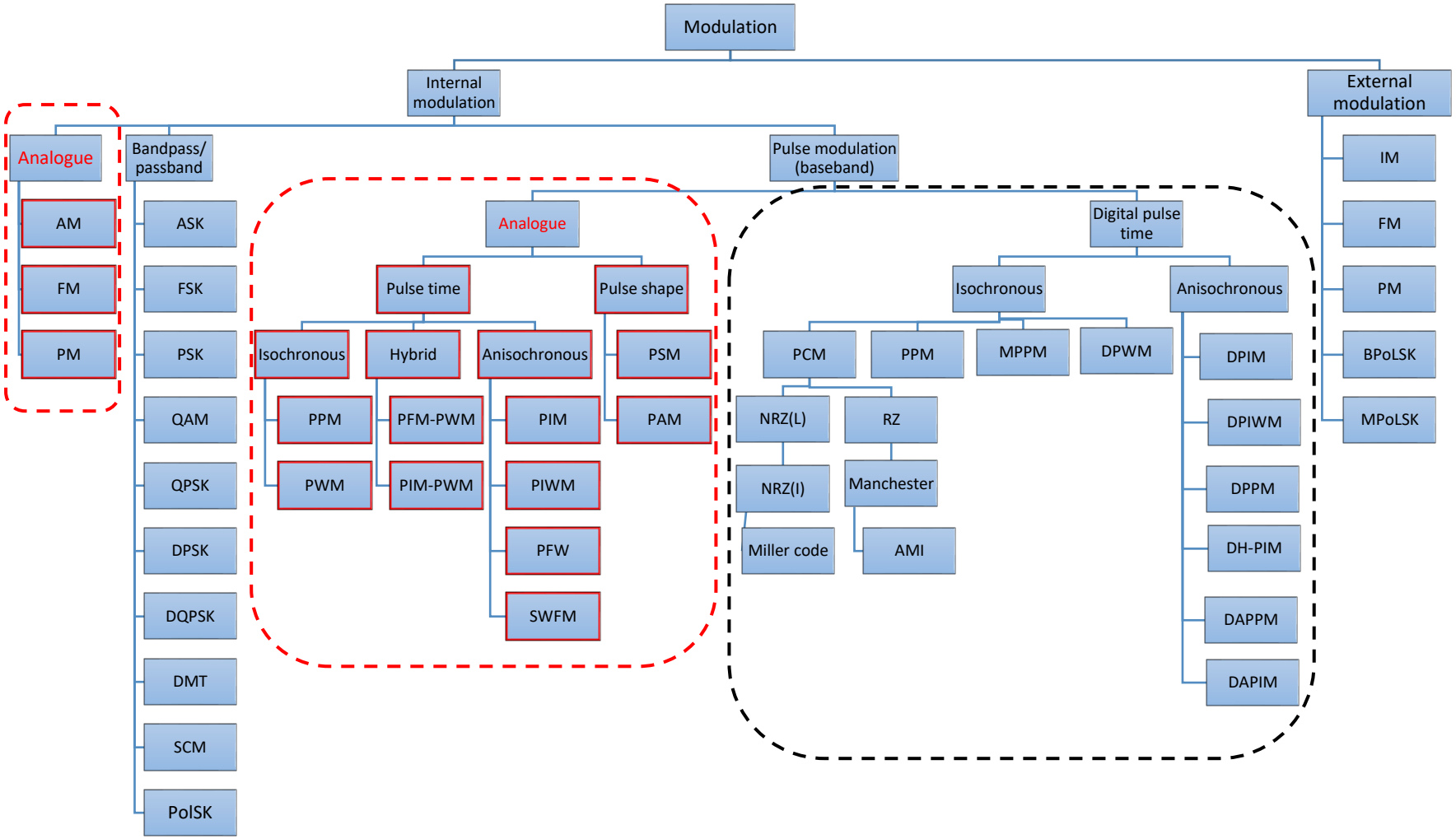

Figure 4-1: Modulation tree [29]

Internal modulation scheme as digital pulse time has the following two types:

An isochronous: It needs a synchronization clock at the transmitter and receiver part, such as digital pulse interval modulation (DPIM), digital pulse interval and width modulation (DPIWM) and digital pulse-position modulation.

Isochronous: The synchronization clock does not require such multiple pulse position modulation (MPPM), Pulse Code Modulation (PCM) and pulse position modulation (PPM).

Generally, internal modulation has the advantages of compactness and being simple and cost-effective, while external modulation is used for high data transmission [5, 87]. The widely used modulation methods are used for optical wireless communication. In this chapter, the modulation techniques used in this research will be addressed.

4.2 Pulse Position Modulation (PPM)

The block diagram in Figure 4-2 depicts how PPM is generated from PAM. The signal modulation is formed by pulse-position modulation (PPM) where a single pulse in one of the required 2^M probable time-shifts is transmitted to encode M message bits [88]. Its repletion happens every T seconds, making the transmitted bit rate as M/T bits per second as shown in Figure 4-3. Primarily, it is very useful to optical communication systems with a slight tendency of multi-path interference.

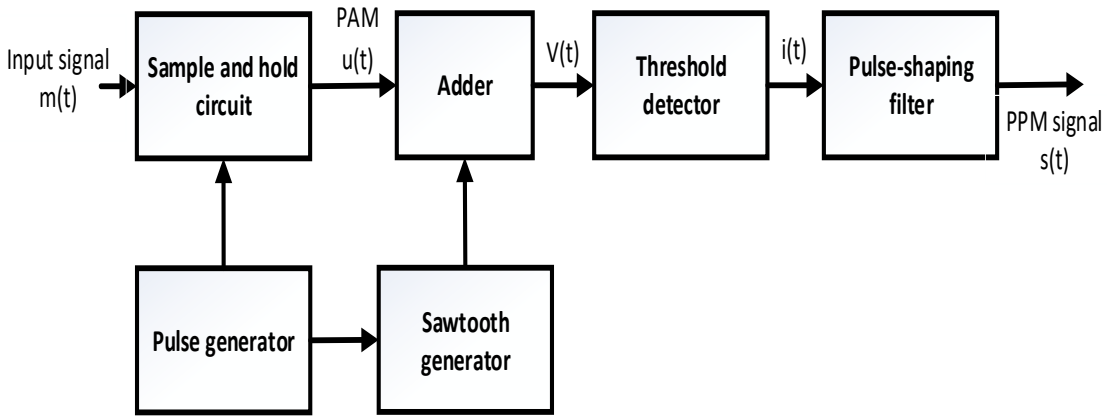

Figure 4-2: Block diagram of PPM generator [89]

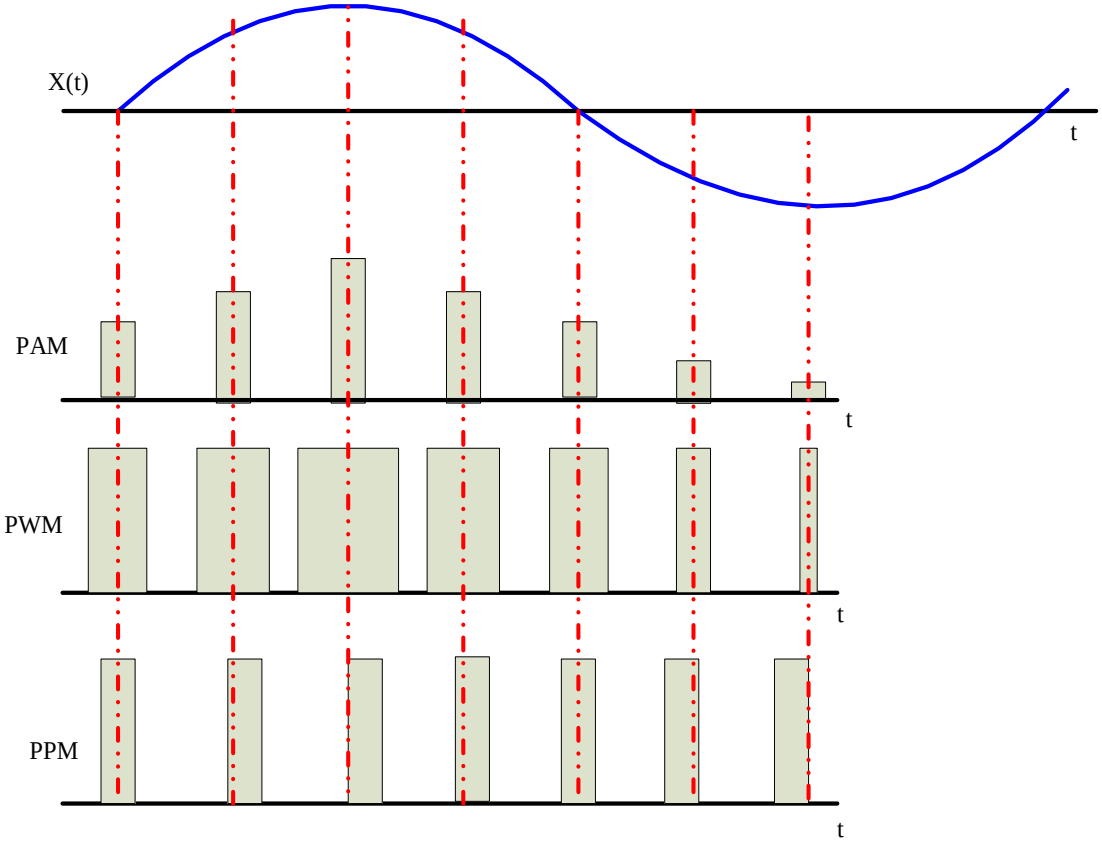

Figure 4-3: Output signal of PPM [90]

The required bandwidth is not a major concern in line-of-sight (LOS) OWC; thus, PPM was the most appropriate modulation scheme among the options owing to its efficient battery power regarding application range [90]. PPM can be defined as a method of orthogonal modulation belonging to the pulse modulation family. The power efficiency of On-Off-Key (OOK) is improved due to the PPM method, but higher bandwidth is required and more complications [5]. A constant power pulse is contained within a symbol of Single-pulse position modulation (L-PPM) which occupies one duration of a slot within $L=2^M$ [91-93]. The probable time slots including the remaining slots are empty. Information is encoded inside the pulse position that is commensurate of the decimal value of input data of M-bit [28]. For L-PPM, the shape of transmit pulse will be:

$$x(t)_{PPM} = \begin{cases} 1 & for \quad t \in [(m-1)T_s, mT_s] \\ 0 & elsewhere \end{cases} \qquad 4\text{-}1$$

where, sample duration, $m \in \{1,2, \ldots . L\}$ is represented by T_s.

The signal of PPM will be:

$$s(t)_{PPM} = \sum_{n=-\infty}^{\infty} g(t - n\,T_s - k_p m(nT_s)) \qquad 4\text{-}2$$

where a standard pulse of interest and the PPM sensitivity are denoted by $g(t)$ and k_p respectively.

Many pulse position modulation techniques are used in VLC such as DPPM, L-PPM, MPPM, DiPPM, Duo PPM and Offset PPM. In the next section, DiPPM, Duo PPM and Offset PPM will be described.

4.2.1 Dicode Pulse Position Modulation (DiPPM)

Satellite systems [94], optical fibre [95-97] and optical communication systems utilize intensity modulation and digital PPM extensively. The format of newly emerged dicode pulse position modulation (DiPPM) facilitates sensitivity across digital PPM but the line-rate is reduced as shown in Table 4-1. Digital PPM and dicode signalling are combined to develop DiPPM. Analysis of the workability of the new code has been conducted, and it is also relatively evaluated with PCM and digital PPM to assess its usability in optical fibre links [74, 96, 97].

Table 4-1: DiPPM Symbol Alphabet

PCM	DiPPM
00	No pulse (N)
01	Set (S)
10	Rest (R)
11	No pulse (N)

The DiPPM sensitivity has been improved up to 5.12 dB by using Reed Solomon (RS) codes [98], and across digital PPM and PCM systems, 7.5 and 2.4 dB respectively has been improved by sensitivity. On the basis of performance of erasure error and false alarm, a comparison is made among a dicode, multiple and digital PPM [94, 95]. DiPPM yields the lowest rate of error and the bandwidth was equal to twice the expansion of PCM rate. Figure 4-4 exemplifies the generation of a DiPPM from PCM. The reset pulses (R) and set pulses (S) will be generated when the PCM data transitions from zero-to-one or one-to-zero respectively and no pulses if the data is constant, as shown in Table 4-1.

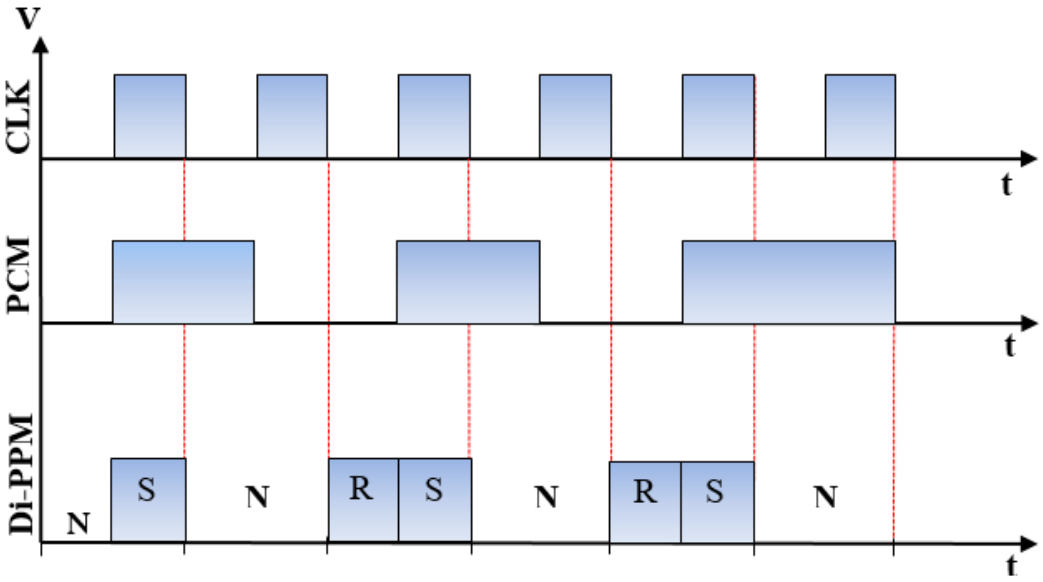

Figure 4-4: Conversion into DiPPM from PCM data with zero guard [94, 95]

An empty slot (guard) is usually used in DiPPM technique to protect the signal from intersymbol interference (ISI). The DiPPM time slot duration T_s can be expressed as:

$$T_s = \frac{T_b}{2+gu} \qquad 4\text{-}3$$

where $T_b = \frac{1}{B}$ is the bit time of PCM, B denotes the data rate and gu is the slot guard intervals.

One downside of using guards is to increase the line rate, which requires a higher bandwidth of the channel [99, 100]. In Figure 4-4, zero guard was used, which was carried out in this research.

Third order Butterworth filter has been used to reduce the impact of ISI in DiPPM by painstakingly selecting the cut off frequency of the single pole preamplifier and the equalising third order Butterworth filter [101, 102]. The maximum likelihood sequence detection (MLSD) has been implemented with DiPPM to eliminate wrong-slot errors and reduce false-alarm and erasure errors [102-105]. OOK, PPM and DPPM have been compared with DiPPM, In general, DiPPM is an alternative modulation technique for optical wireless communications [106]. The power spectral density (PSD) of DiPPM has been implemented and compared; the agreement was obtained between experimental, theoretical and simulation [107, 108].

4.2.2 Duobinary Pulse Position Modulation (Duo-PPM)

The problem of signalling at a speed higher than the Nyquist rate is the focus. The new approach to this problem, which results in a technique that permits signalling at twice

the Nyquist frequency, has been termed duobinary, where the word ‘duo’ indicates the doubling of the straight-binary bit capacity of the system. Suppose two sequences of digits are considered [109]. Duo PPM pulse is positioned at 0 or 1, when the data is constant in slot 0 or 1 respectively. When the data is changed from high to low or low to high, no pulse is transmitted as shown in Table 4-2 and Figure 4-5 [110]. The Duo PPM time slot duration T_s can be expressed as:

$$T_s = \frac{T_b}{2} \qquad 4\text{-}4$$

Table 4-2: Symbol Alphabet of Duo PPM

Data	Probability	Duo PPM	Symbol
00	1/4	Pulse in slot 0	0
01	1/4	No pulse	No change
10	1/4	No pulse	No change
11	1/4	Pulse in slot 1	1

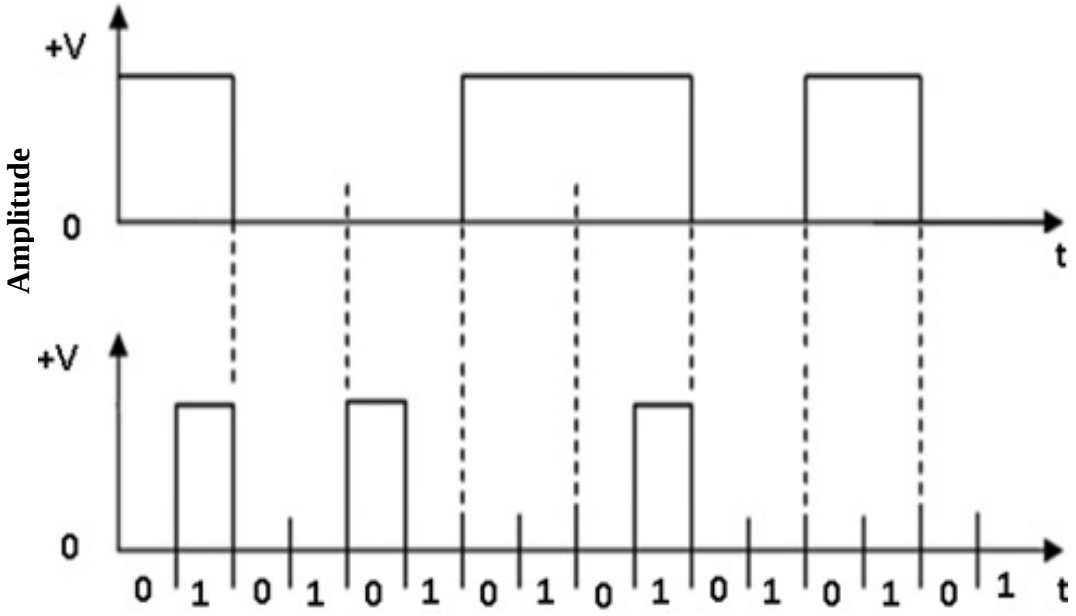

Figure 4-5: Conversion of PCM data into Duo-PPM [110]

4.2.3 Offset Pulse Position Modulation (Offset PPM)

Offset PPM is a novel digital PPM version that operates at half the digital PPM line rate and offers an increasing sensitivity as illustrated in Table 4-3 [111]. The Offset PPM gives more than 3.1 dB sensitivity improvement at low bandwidths over the digital PPM; it also has a better sensitivity than multiple PPM [111, 112]. As the next number in codewords is unknown, the Maximum Likelihood Sequence Detector (MLSD)

cannot be applied for Offset PPM application. However, Offset PPM, at the frame repetition frequency, gives a discrete line, when compared with DPPM, which has a stronger frame component [113]. To generate the Offset PPM from DPPM, all code-word positions are initially reset to zero to the first sequence. The least significant bit (LSB), for the second sequence, is replaced with one. The subsequent code-words in sequence will be produced by removing the one from the LSB to the most significant bit. The most significant bit is kept simultaneously with the following code-word formation by replacing the LSB with one as shown in Table 4-3 [111]. The average slot width T_s for Offset PPM can be expressed as:

$$T_s = \frac{T_n}{n} \qquad 4\text{-}5$$

where

$$T_n = \frac{N}{B} \qquad 4\text{-}6$$

where T_n denotes the frame time for N bits of PCM, B is the original data rate and n is a number of bits of Offset PPM keywords.

Table 4-3: Generation of Offset PPM and DPPM, from three bits of PCM [111, 112]

PCM	DPPM	Offset PPM
000	0000 0001	0 000
001	0000 0010	0 001
010	0000 0100	0 010
011	0000 1000	0 100
100	0001 0000	1 000
101	0010 0000	1 001
110	0100 0000	1 010
111	1000 0000	1 100

4.3 Error Sources of PPM

The PPM has three types of errors – wrong slot, false alarm and erasure [99, 100, 114-118]. Figure 4-6 demonstrates the PCM signal as an example of how these errors occur. In this section, the probability of these errors will be addressed. In addition to these errors, there is ISI, which occurs when the interval between pulses is greater than the rise and fall times.

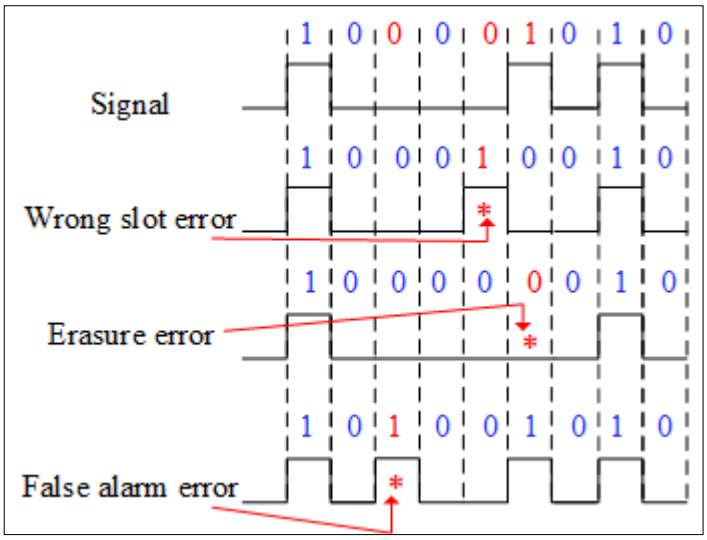

Figure 4-6: Representation of error types [5]

4.3.1 Wrong slot errors

This type of error occurs when the noise on the pulse front edge appears in an adjacent time slot. The pulse appears in a slot before or after the original slot as seen in Figure 4-6. To reduce this type of error, the pulse must be detected in the centre of the time slot. The probability of wrong slot errors (p_s) is given by [99]:

$$p_s = 0.5erfc\left(\frac{Q_s}{\sqrt{2}}\right) \quad 4\text{-}7$$

where

$$Q_s = \frac{T_s\, slope(t_d)}{2\sqrt{\langle n_o^2 \rangle}} \quad 4\text{-}8$$

The receiver mean square noise is denoted by $\langle n_o^2 \rangle$; the slope of the received pulse at the instant t_d is denoted by $slope(t_d)$.

4.3.2 False alarm errors

This type of error occurs due to a signal threshold crossing in a slot in which there is no presence of any signal as shown in Figure 4-6. The probability of these errors is given by [100]:

$$p_f = \left(\frac{t_s}{\tau_r}\right) 0.5erfc\left(\frac{Q_t}{\sqrt{2}}\right) \quad 4\text{-}9$$

where

$$Q_t = \frac{v_d - v_{oISI}}{\sqrt{\langle n_o^2 \rangle}} \quad 4\text{-}10$$

t_s is the uncorrelated samples, and τ_r is the time at which the autocorrelation function has become small. v_{oISI} is the ISI induced voltage at the time slot.

4.3.3 Erasure errors

Erasure errors arise when the signal voltage is reduced to below the threshold level, due to great noise, i.e. erase an existing pulse as illustrated in Figure 4-6. The probability p_{er} is given by [99, 100]:

$$p_{er} = 0.5erfc\left(\frac{Q_{er}}{\sqrt{2}}\right) \quad 4\text{-}11$$

$$\mathrm{Q_{er}} = \frac{\mathrm{v_{pk}} - \mathrm{v_d}}{\sqrt{\langle \mathrm{n_o^2} \rangle}} \quad 4\text{-}12$$

v_d is the receiver output signal at a time t_d, and v_{pk} is the receiver peak output signal at a time t_{pk}.

4.4 Summary

In this chapter, the methods of modulation used in optical communication systems were discussed. Several types of modulation techniques have been used to improve design performance in terms of increasing the speed of data transmission. Emphasis was placed on the study of species carried out in this research. Three PPM types (DiPPM, Duo PPM and Offset PPM) were used and compared in order to overcome the defects in previously used modulations. The PPM technique has improved power efficiency, requires less optical power and increases the receiver sensitivity. The principle of the work of each technique has been explained.

There is a similarity in the process of coding signals for DiPPM and Duo PPM, where the method of signal encryption depends on the end of each pulse. Regarding the Offset PPM, the signal is encrypted by converting the codeword from 3 bits to 4 bits, which means the method of encoding signal depends on the middle of pulse. Finally, different error sources of PPM were addressed.

Chapter 5

VLC System Implementation

5.1 Introduction

In this chapter, the practical aspect will be discussed in three stages. Firstly, two types of commercial LEDs (warm and cool) were compared in terms of the bandwidth and bit error rate. In the second stage of the experiments, different types of cool LEDs were compared in terms of colour temperature. Four different colour temperatures which were commercially available in the markets were selected (6000–6500 K, 10000–15000 K, 20000–25000 K and 30000–35000 K). 10000–15000 K was selected, which has better performance in terms of communication and illumination. In each of the previous stages, in parallel, three different rating power of LEDs (20, 30 and 50 W) were employed and compared to find the most appropriate. In the final stage of the comparison, which is addressed in the next chapter, the three types of modulation techniques are compared (DiPPM, Duo-PPM and Offset-PPM) using 30 W LED (10000–15000 K) in terms of the BER and data transmission.

5.2 System Architecture

Figure 5-1 illustrates the block diagram of the proposed scheme of the visible light communication system (VLC), which contains the basic circuit blocks.

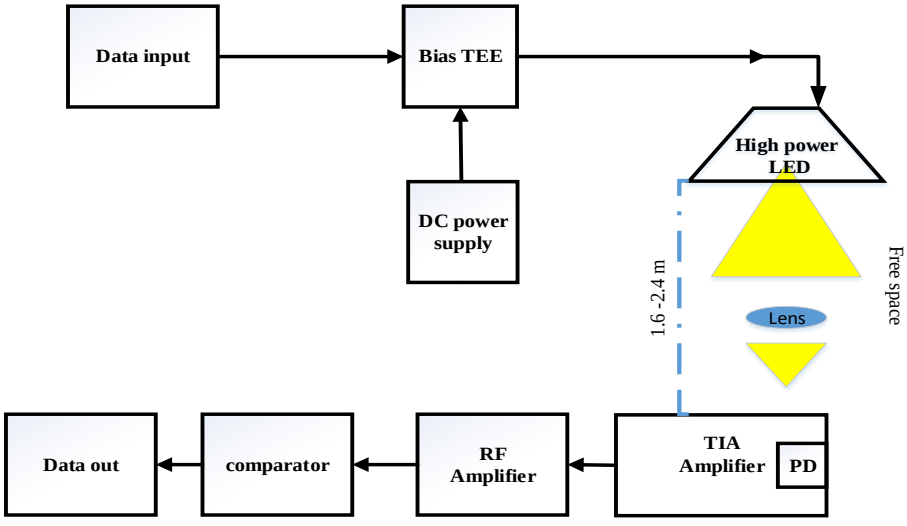

Figure 5-1: VLC system block diagram

The transmitter has a bias tee and a high-power LED. The receiver is composed of three main parts, namely photodiode with transimpedance (TIA), RF amplifier and

comparator. No additional circuitry has been used in the transmitter, just bias tee with the high-power LED. However, the signal has been fed onto the LED bias current, through a bias tee (Picosecond Pulse Labs 5575A) [119]. The output from the bias tee has been directly delivered to high power-white LED. The practical aspect will be addressed as described in Figure 5-2

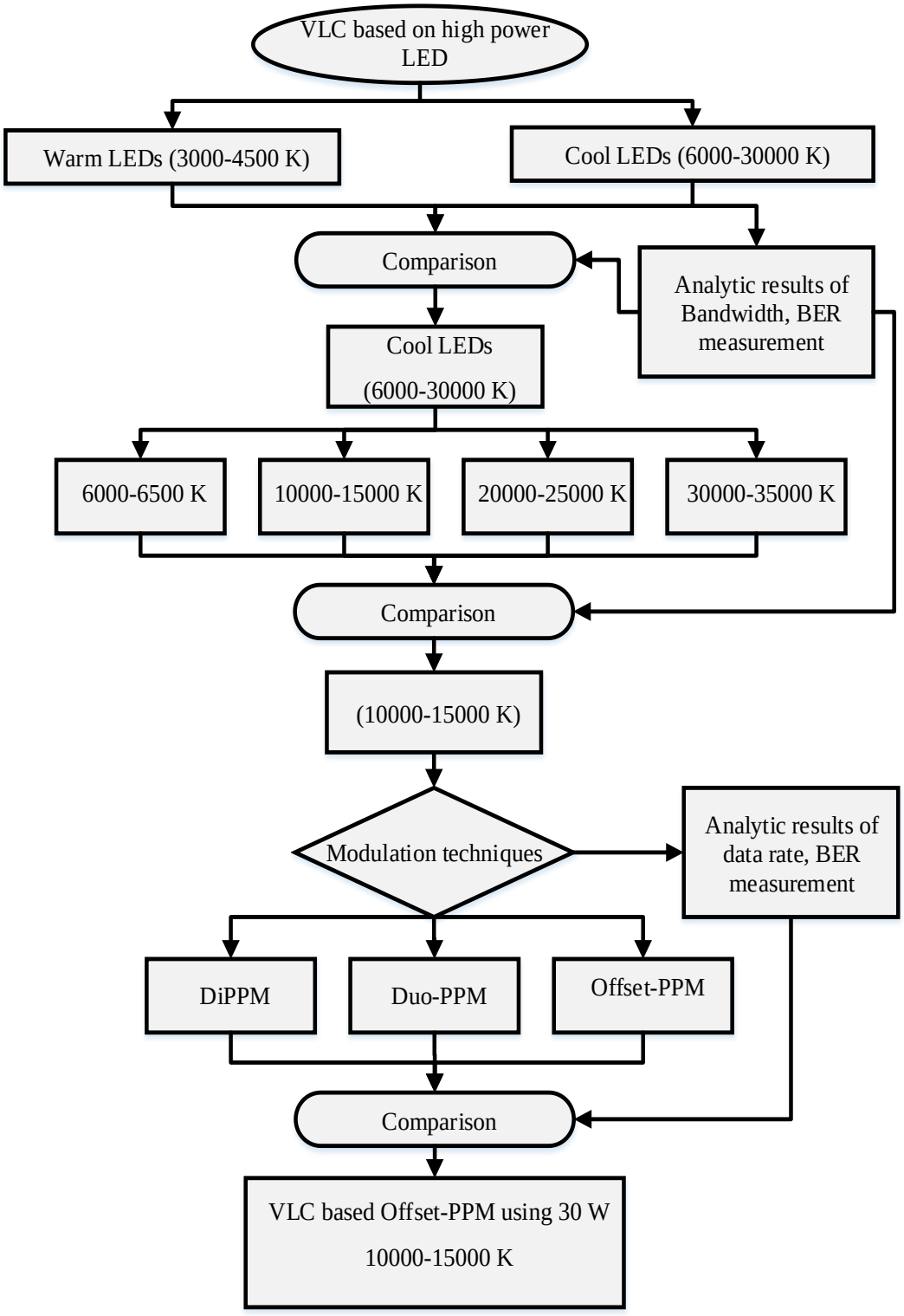

Figure 5-2: Experiments work and the developed scheme flowchart

5.3 Receiver Circuit Design and Development

An optical receiver basic structure, as seen in Figure 5-3, consists of a low noise pre-amplifier (TIA), the post-amplifier and a comparator. One key point to note here is the unsaturation of the pre and post amplifiers, where the maximum detected data rate would be limited by the charge storage on the transistor if the amplifiers are non-saturated [120].

The receiver has been designed with three different types of Si PIN photodiode (PD) that are commercially available, to select the most appropriate photodiode in terms of performance. The first photodiode is BPW34 with 7.02 mm^2 active area, the second is OSD5-5T 5 mm^2 sensitive area and the third is FDS010 with an active area of 0.8 mm^2. The photodiode current is transformed to a voltage equivalent of the transmitted data through a transimpedance amplifier (TIA). The output of the TIA is sent to the comparator (MAX942) to recover the original data. It should be noted that in this research, three TIAs with the same elements and dimensions (60 x 50 mm) were designed, only with differing photodiodes.

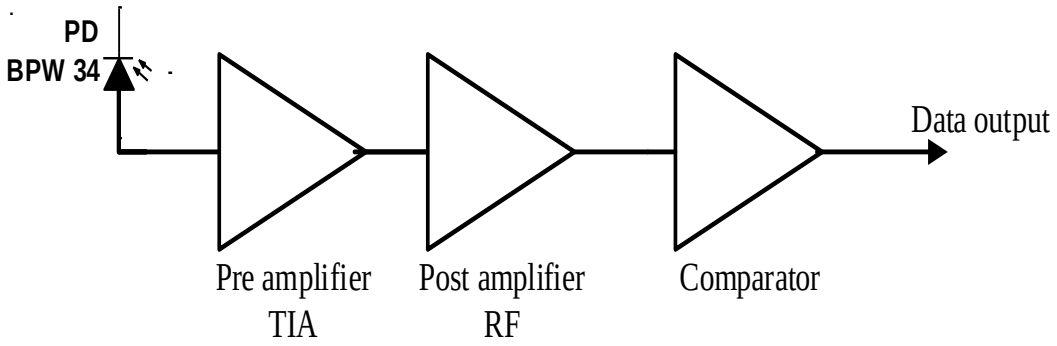

Figure 5-3: Structure of a VLC receiver

5.3.1 Transimpedance circuit design

Figure 5-4 depicts a simple emitter follower transimpedance preamplifier (TIA) circuit (PCB layout and printed circuit illustrated in appendix A). In this design, the transistor BFR92A was employed, which has higher bandwidth and low noise. Between two buffers (Q3 and Q1) is Q2, for which an amplifying circuit of 20 dBm has been designed with Si PIN preamplifier. To obtain a high sensitivity wideband response, a receiver with a CC (common collector) front end has been used. One key benefit of using the CC front end is to eliminate the Miller capacitance at the first stage. For this current design, the CC stage output impedance and the second-stage noise current gain are high enough to be insignificant when compared with the first-stage noise.

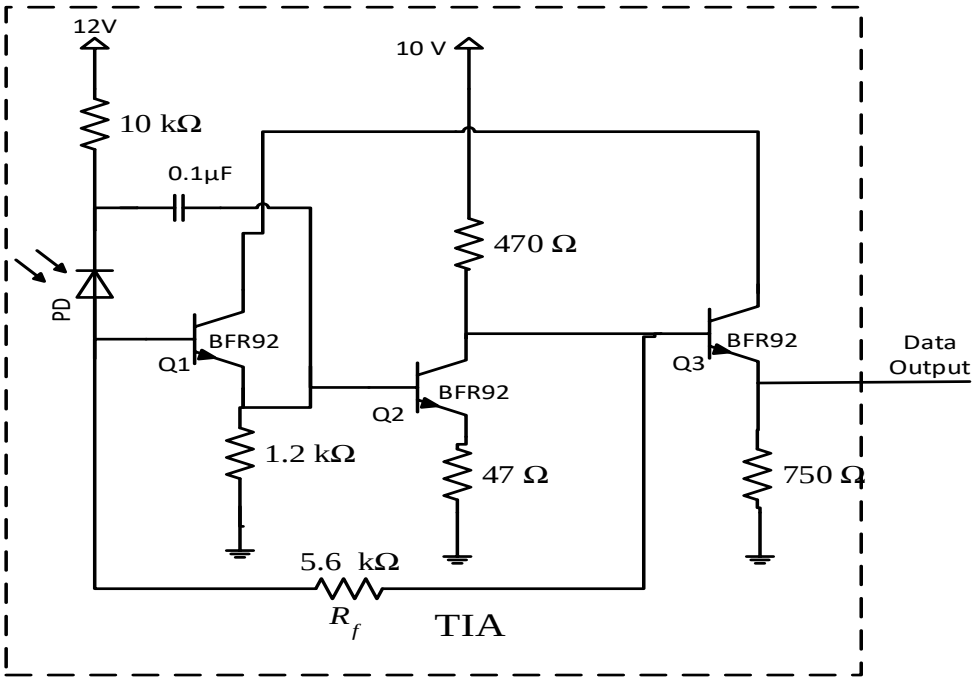

Figure 5-4: Transimpedance (TIA) circuit design

The frequency response of the trans-impedance (TIA) circuit is given by [120]:

$$f_{-3dB} = \frac{1+A}{2\,\pi R_f[(1-A_{Q1})C_d + C_c + (1+A)C_f]}\,5 \qquad 5\text{–}1$$

Where f_{-3dB} is the bandwidth of the TIA, A is the gain of the amplifying circuit (second stage), R_f is the feedback resistor, C_d is the photodiode capacitance (C_j), C_c is the transistor capacitance, C_f is the capacitance of the feedback resistor and A_{Q1} is the AC gain for transistorQ_1.

In this circuit, $A = \frac{470}{47} = 10$, $R_f = 5.6$ kΩ, (C_c = 0.35 pF, C_f = 0.1 pF) from transistor datasheet and $A_{Q1} = \frac{v_o}{v_{in}}$.

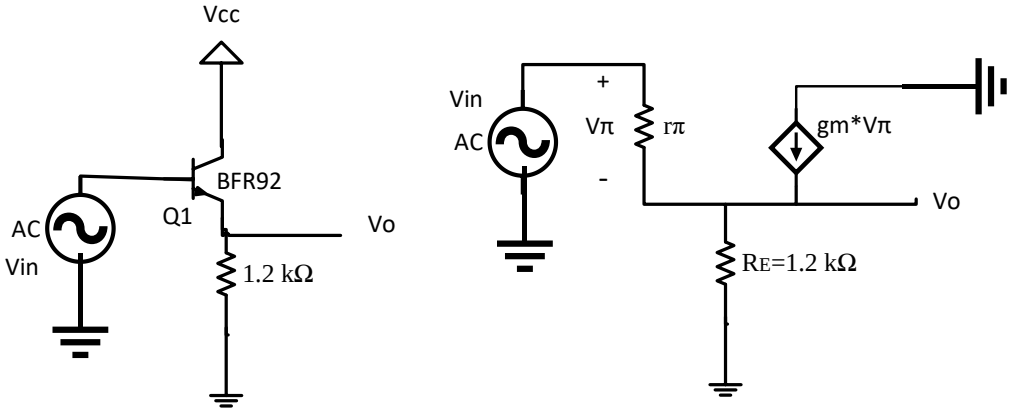

Figure 5-5: Illustration of how to calculate the gain (A_{Q1}) for the first stage of the TIA

From Figure 5-5:

$$v_\pi = v_{in} - v_o \quad (5\text{-}2)$$

$$v_o = g_m v_\pi R_E \quad (5\text{-}3)$$

$$v_o = g_m (v_{in} - v_o) R_E \quad (5\text{-}4)$$

$$v_o = g_m v_{in} R_E - g_m v_o R_E \quad (5\text{-}5)$$

$$v_o (1 + g_m R_E) = v_{in} g_m R_E \quad (5\text{-}6)$$

$$\frac{v_o}{v_{in}} = \frac{g_m R_E}{(1 + g_m R_E)} \quad (5\text{–}7)$$

$$g_m = \frac{I_c}{25\ mV} \quad (5\text{-}8)$$

$$I_c \approx \frac{0.7}{R_E} \approx 0.583\ mA \quad (5\text{-}9)$$

$$g_m = \frac{0.583\ mA}{25\ mV} = 23.3 \frac{mA}{V} \quad (5\text{-}10)$$

$$A_{Q1} = \frac{v_o}{v_{in}} = \frac{0.0233 \times 1200}{(1 + 0.0233 \times 1200)} = 0.966 \quad (5\text{-}11)$$

5.3.2 RC compensator design

Compensation circuits are used in many applications, particularly in cases where sudden changes in the input signal frequency is noticed and, as a result, an enhancement in the frequency response of the system and of the bandwidth occur. Three types of compensation networks are common – phase lead, phase lag or lead-lag circuits [121]. Figure 5-6 illustrates the RC lead compensator which has been used in this project, where enhancement of the bandwidth is achieved by increasing the transmission speed of the system [122].

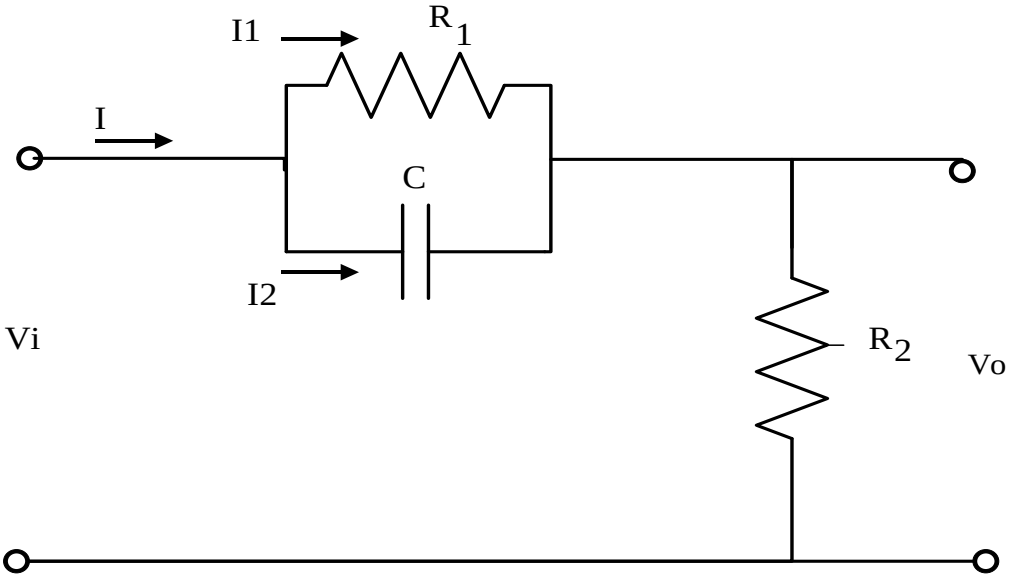

Figure 5-6. Lead Compensation circuit

From the above circuit, the transfer function can be written as:

$$G_{(s)} = \frac{V_o}{V_i} = \alpha \frac{1+S\tau}{1+\alpha S\tau} = \alpha \left[\frac{S+\frac{1}{\tau}}{S+\frac{1}{\alpha\tau}}\right] \qquad 5\text{-}12$$

where

$$\alpha = \frac{R_2}{R_1+R_2}, \text{ and } T = R_1C \qquad 5\text{-}13$$

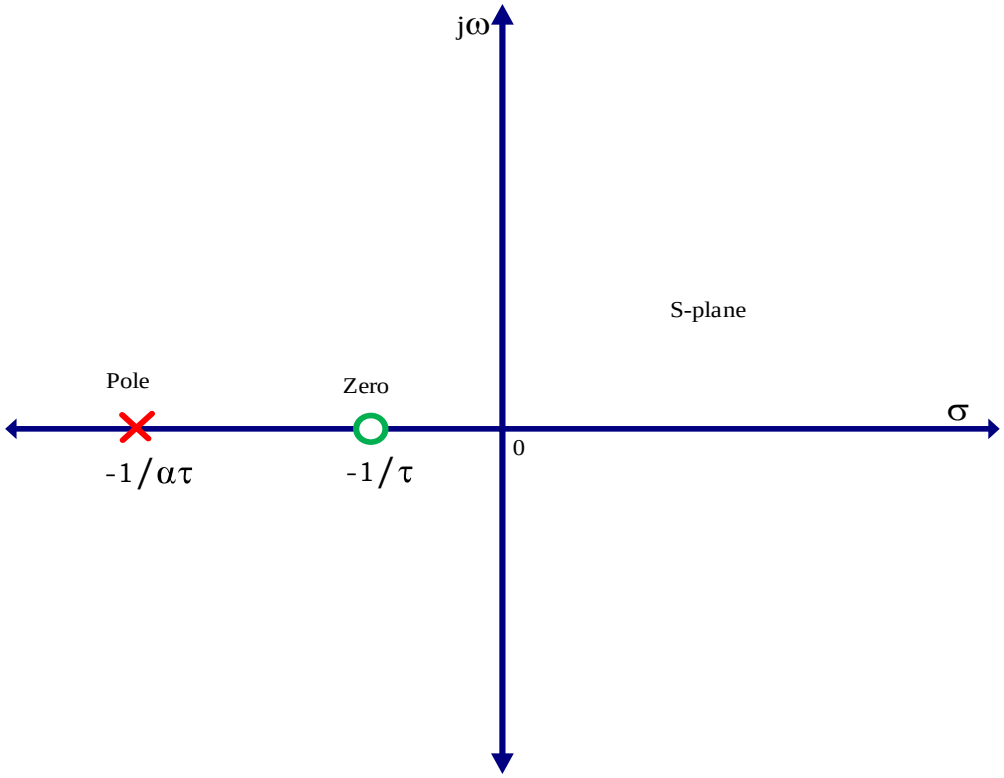

Figure 5-7: Pole and Zero Plot of Lead Compensation Network

Figure 5-7 above shows the S-plane for the transfer function of the lead compensator, where the zero ($-\frac{1}{T}$) is closer to the origin, which is more dominating than the pole ($-\frac{1}{\alpha T}$). First and foremost, the TIA has been developed by the addition of an RC lead compensator having dimensions of 60 x 50 mm to improve the system's response by reducing the rise time. The lead compensator output, using an SMA plug of 50 Ω (SMA RP Jack to SMA RP Jack Adaptor), has been connected to an RF amplifier in order to amplify the signal as shown in Figure 5-8. The variable resistor (10 KΩ) and the RC lead compensator capacitor has been calculated to increase the bandwidth above 3 MHz according to the equation below.

The capacitor of 47pF has been used, for wide bandwidth, to match 50 Ω load resistor. Then, the resistor R will be calculated according to 3.3 MHz 30 W LED bandwidth and 47 pF.

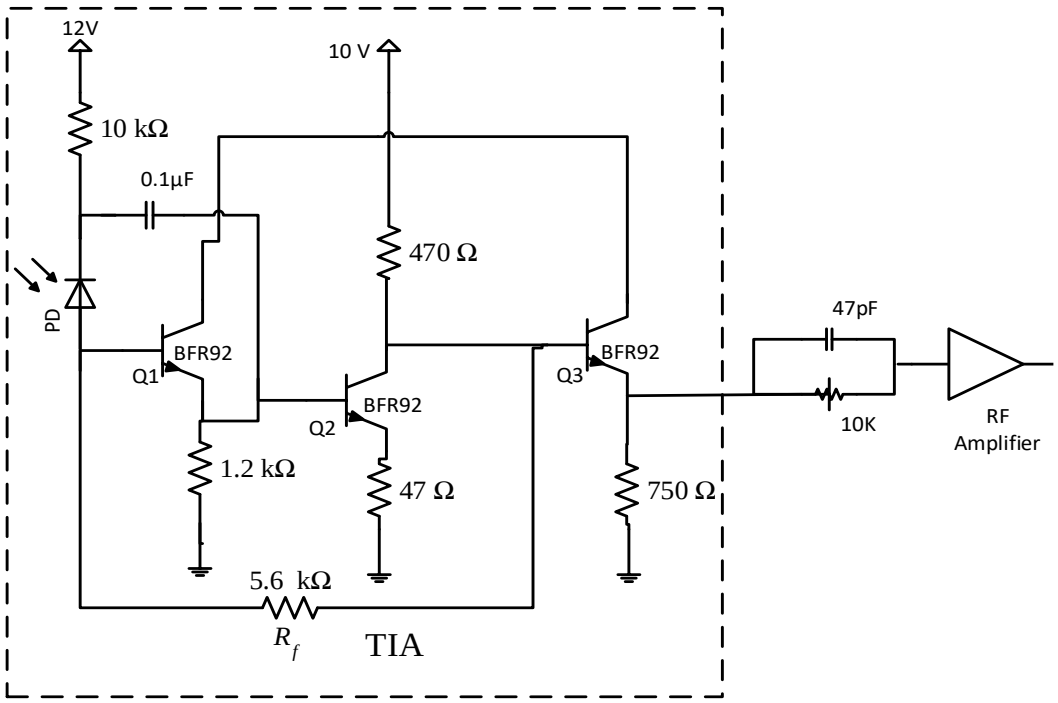

Figure 5-8: Receiver circuit a) circuit diagram. b) PCB Printed circuit

Figure 5-9 shows the frequency response of the compensator and the cool 30 W LED, where the resistance value is calculated according to the LED bandwidth. The figure shows how LED bandwidth is compensated and increased.

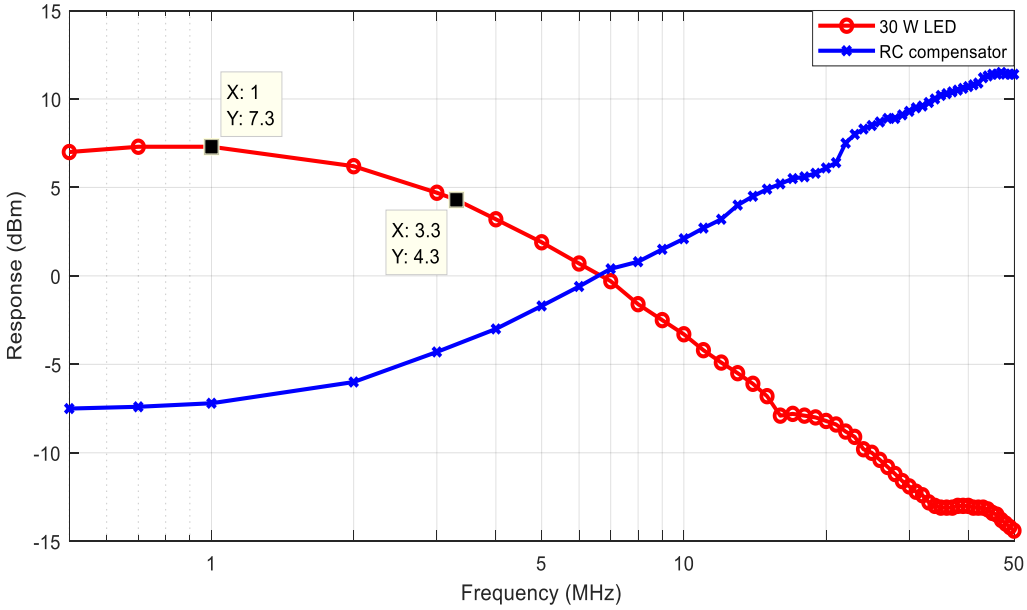

Figure 5-9: Frequency response for 30 W LED and RC compensator

5.3.3 Comparator circuit design

The comparator has been used in order to standardize the digital output of the receiver, where the receiver output can be either 0 V volts or 5 V. The comparator compares the output signal of the receiver with a reference signal; if the signal is below the reference signal, the output of the comparator is zero. Furthermore, if the input signal is greater than the reference voltage, the comparator output is 5 V as shown in Figure 5-10.

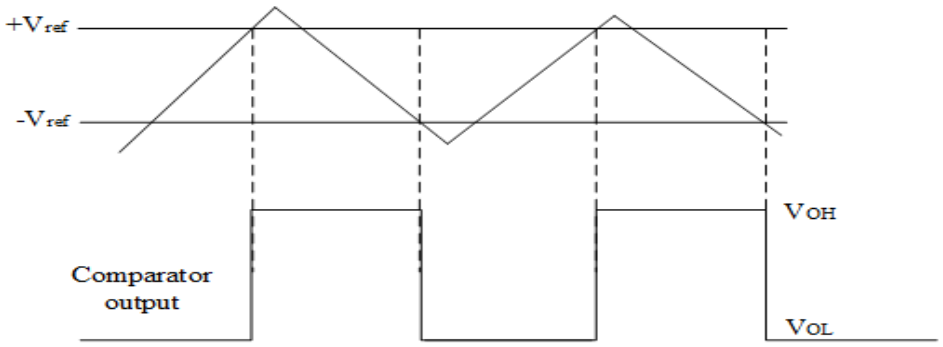

Figure 5-10: Comparator input versus output signal

A high-speed and low-power comparator (MAX942) has been used for this research in comparing the levels of the voltage as depicted in Figure 5-11 (PCB layout and printed circuit illustrated in appendix B). The operation voltage of the comparator ranged from 2.7 V to 5.5 V with only 350µA supply current with 80 ns of propagation delay (datasheet).

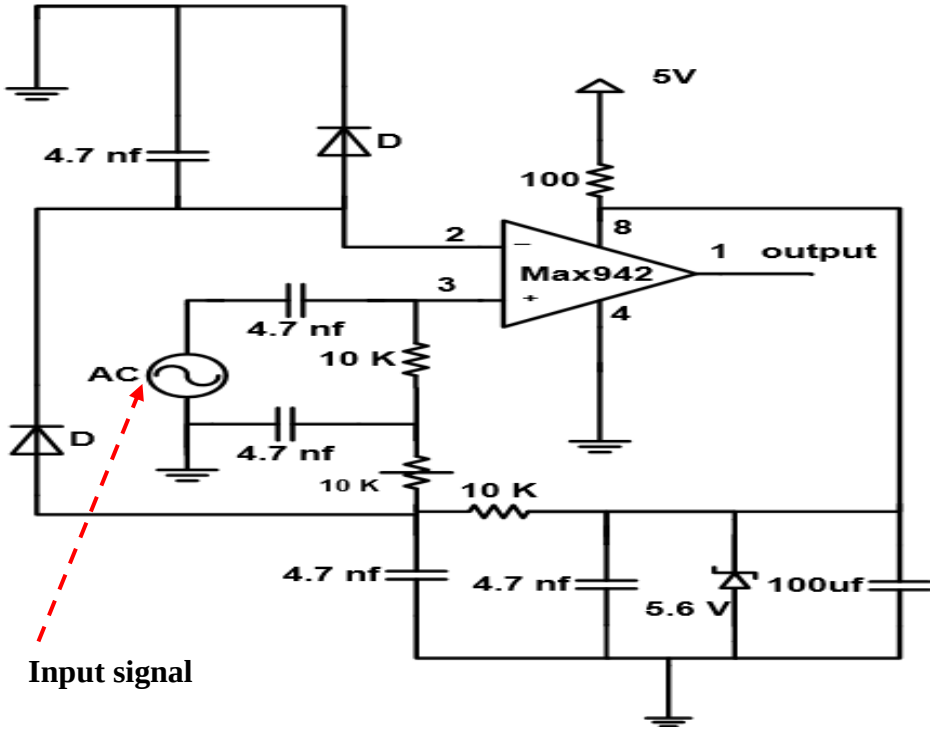

Figure 5-11: Comparator circuit design

5.3.4 Photodiode selection

A photodiode has been used as an optical receiver in converting the optical signal in the visible light spectrum to an electrical signal. When a photodiode absorbs a photon with sufficient energy, the electron moves to the conduction band from the valence band, resulting in a pair of electron-hole generation [123]. Typically, a reverse voltage drives the photodiode, where the cathode connects to the positive terminal and the anode is connected to the negative terminal. If absorption occurs in the depletion zone, the built-in electric field would separate the electron-hole pairs. The electrons would drift toward the cathode while the holes drift toward the anode, thereby generating the photocurrent [28, 123]. The built-in field can be strengthened by the reverse voltage in the depletion zone in order to accelerate the photon-induced carriers drift and also enlarge the depletion zone length in addition to decreasing the capacitance in shortening the response time. For the photodiode, both the indirect-bandgap (Si, Ge) and the direct-bandgap (InGaAs, GaAs, etc.) semiconductors can be used. When compared with semiconductors with the indirect-bandgap, the direct-bandgap counterparts often have higher absorption coefficients [123, 124]. The absorption region of the direct-bandgap semiconductors, when absorbing the same amount of the light, is thinner than that of the indirect-bandgap semiconductors. Ideally, materials such as InGaAs and Ge are mostly chosen in fabricating photodiodes in order to be able to receive long-wavelength light (range of infrared spectral). As for light with shorter wavelength (200–1600 nm), Si is preferred as the ideal material for the receiver, thus, making photodiodes with Si-based material usually used for VLC systems. Photodiodes are of numerous types. They include the avalanche photodiode (APD), PIN photodiode and PN photodiode [5, 80, 81]. The PN photodiode comprises a highly doped layer, a thin n-type and a p-type substrate. Its frequency response shows double cutoff –the lifetime cutoff (in MHz) – due to the time period the carrier spends at n-type and p-type sides of the diffusion regions – and the RC cutoff (in GHz) – due to the capacitance effects and the transit time. The PN photodiode performance is usually limited by the carrier lifetime having a 100–200 MHz maximum cutoff frequency [123].

Initially, three types of photodiodes were selected to be used as the transimpedance amplifier, with the most appropriate chosen by comparing bandwidth and bit error rate. Table 5-1 shows the specifications of the three types.

Table 5-1: Photodiodes characteristic

Parameters	BPW34	OSD5-5T	FDS010	Unit
Wavelength range (λ)	400–1100	430–900	200–1100	nm
Peak Wavelength (λ_p)	850	850	730	nm
Active area	7.02	5	0.8	mm^2
DC reverse voltage (V_r)	32	15	25	V
Peak DC current (I)	5	10	5	mA
Rise/Fall time (t_r/t_f)	20	9	1	ns
Capacitance (C_j)	72 at Vr = 0 15 atVr=12 V	130 at Vr = 0 35 at V_r= 12 V	6 atVr = 10 V	PF
Responsivity ($\Re$) at (λ_p)	0.62	0.44	0.44	A/W
Dark current (I_d)	2	0.5	0.3	nA

In this experiment, three types of TIA are designed, with each type containing different photodiode. A blue laser diode (TO 38, 80 mW, 450 nm) was used instead of LED to verify the maximum bandwidth of photodiodes. On the other hand, the bit error rate of each type was measured at the same operating conditions. From the table, an active area, rise/fall time, and capacitance are the most important parameters in photodiode types, which had a clear impact on the results of experiments. Figure 5-12 shows the TIA frequency response for the three types of photodiodes. It can be seen that the highest bandwidth was about 79 MHz for FDS010, with a bandwidth reduction to about 22 MHz for BPW34, and the lowest recorded bandwidth was about 13.2 MHz for OSD5-5T. This difference is due to the different capacitance for each photodiode. Furthermore, there is a significant difference between the calculated and measured bandwidth due to the transit time of the photodiodes [125]. Furthermore, the free BER was recorded at 20 Mbps and 1.6 m free space distance for the OSD5-5T, where the output signal was identical with the input signal, and 10-10 BER was reached for BPW34, and the highest BER was recorded for FDS010 ($>10^{-2}$). An increase in the error rate can be explained by the increase in the rise/fall time for BPW34 compared to OSD5-5T. As for the FDS010 type, it is due to the small size of the active area, where it would not be able to receive all the light sent from the LED. The BER is manifested due to ISI, which occurred due to the comparator circuit. It can be concluded that the OSD5-5T has better performance, with higher speed and low BER when compared to other photodiodes.

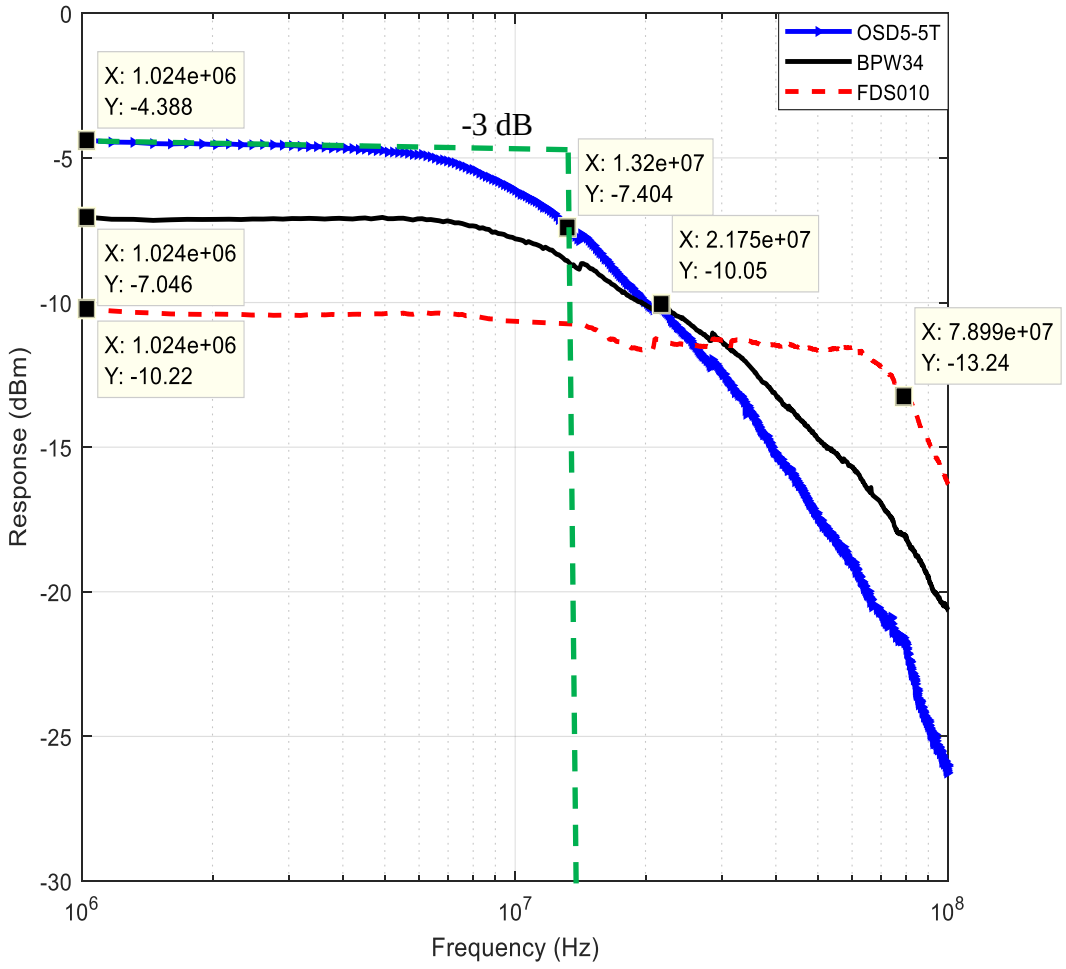

Figure 5-12: Frequency response of the TIA for the three types of photodiodes

5.4 Calculation of the TIA Bandwidth by Measuring the Rise Time

In this experiment, the Pseudorandom Binary Sequence (PRBS) signal has been sent directly to the laser diode, while the signal via three types of TIA will be received and plotted using an oscilloscope to measure the rise time for each case. Finally, Eq. 5-14 is used to calculate the TIA bandwidth.

$$f_{3dB} = \frac{0.35}{\tau_r} \qquad 5\text{-}14$$

The rise (τ_r) time has been determined using:

$$\tau_r = \sqrt{\tau_{TIA}^2 - \tau_{PRBS}^2} \qquad 5\text{-}15$$

where, τ_{TIA} denotes the rise time of the TIA and τ_{PRBS} is the rise time of the input signal (PRBS). Figure 5-13 illustrates the rise time for the PRBS signal and three cases of TIA.

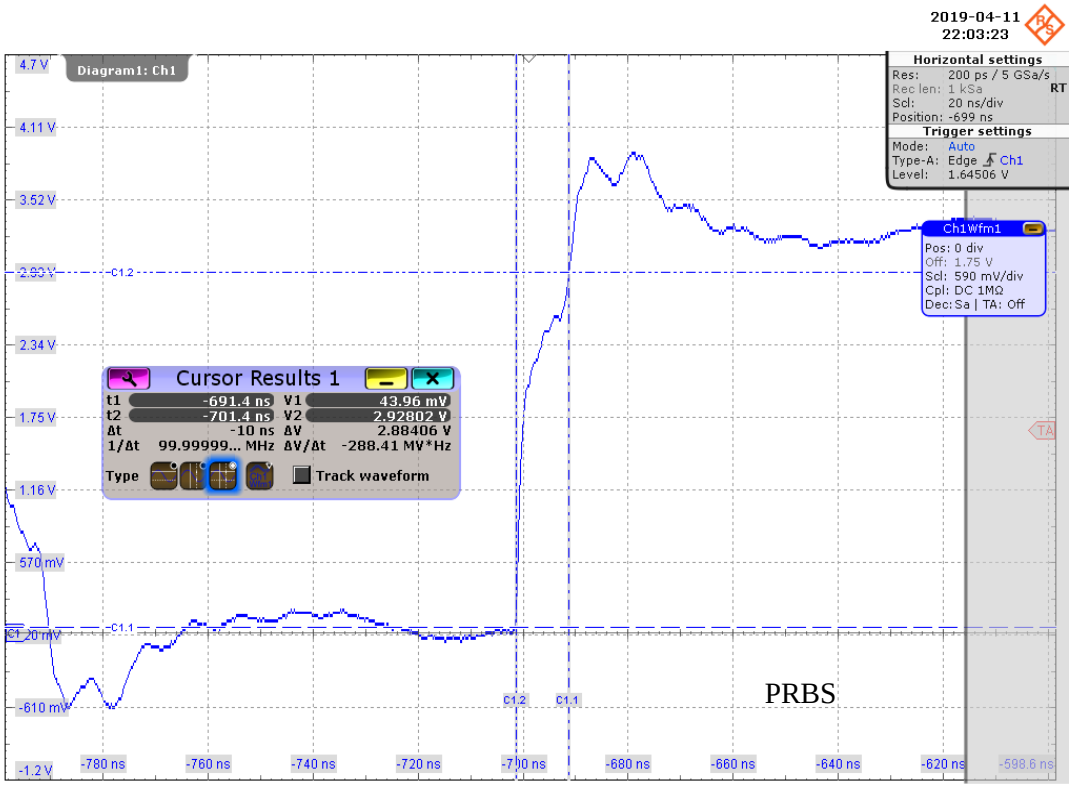

Figure 5-13: Measured rise time for PRBS

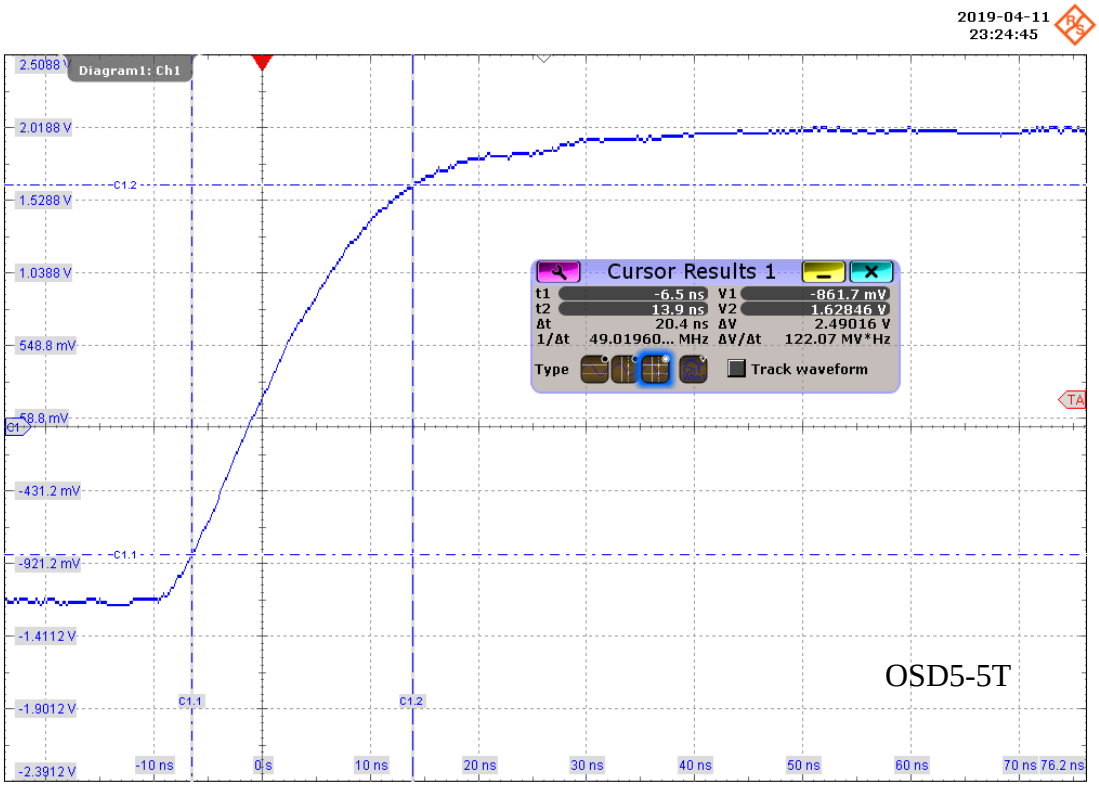

Figure 5-14: Measured rise time for TIA using (OSD5-5T) photodiode

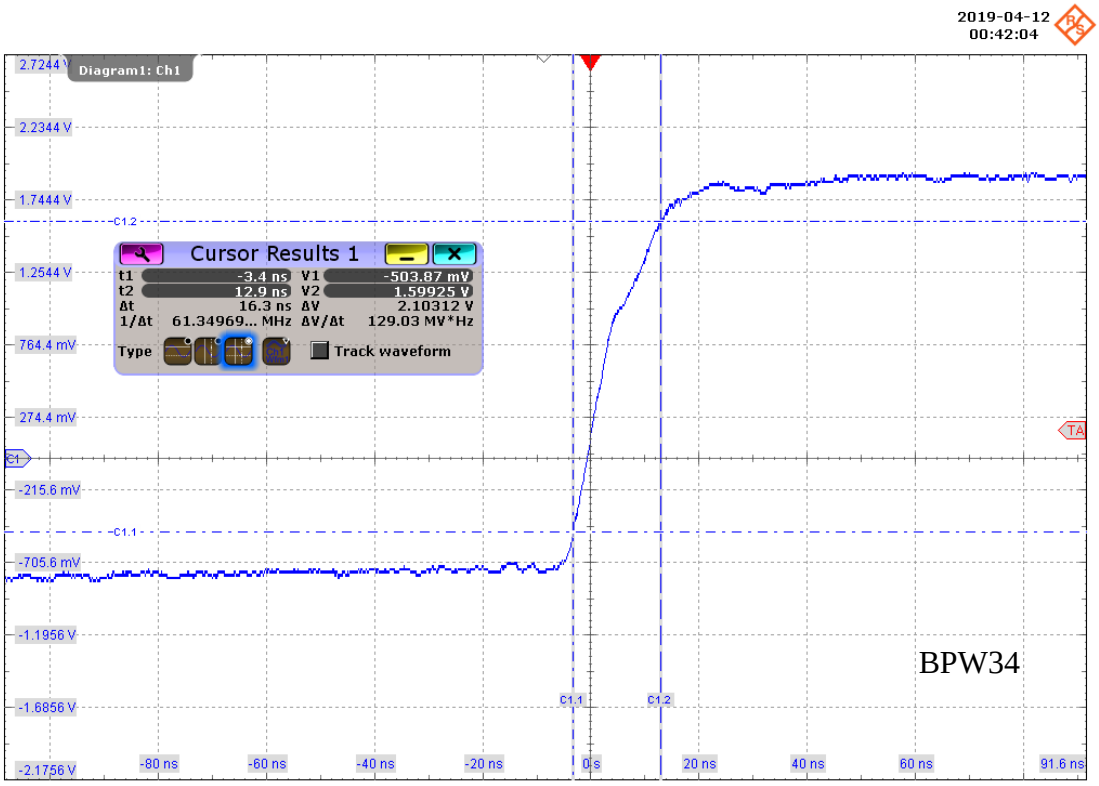

Figure 5-15: Measured rise time for TIA using (BPW34) photodiode

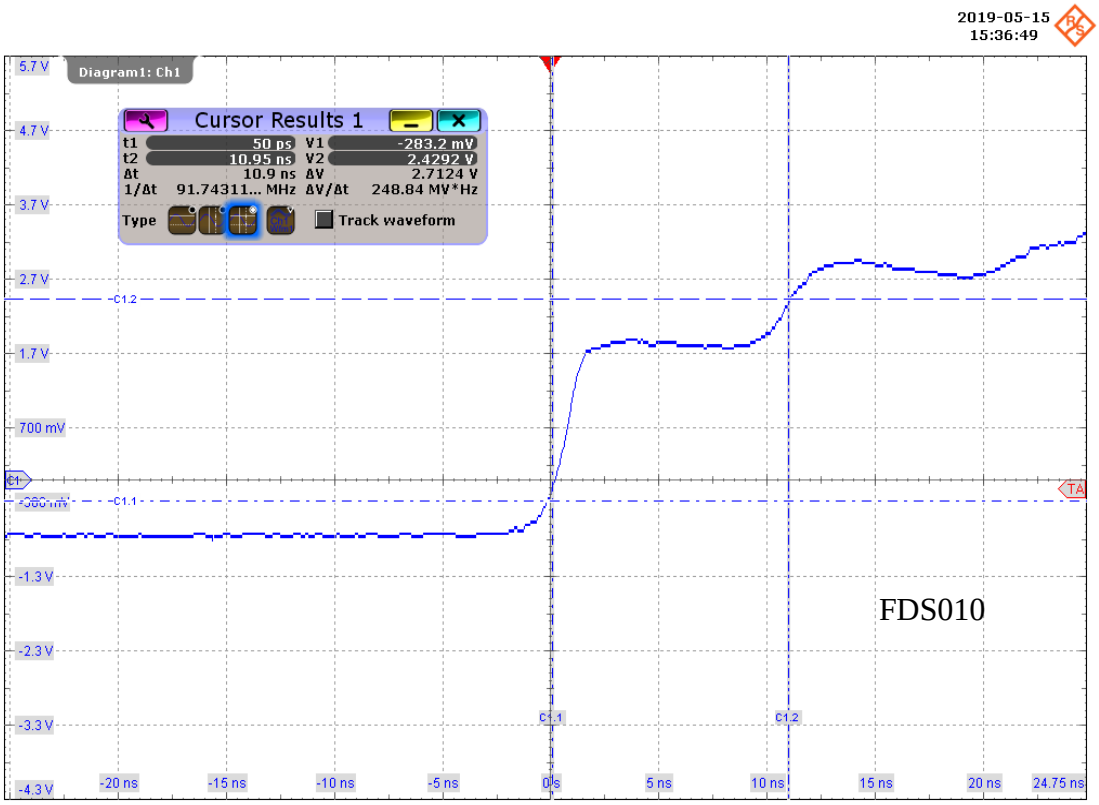

Figure 5-16: Measured rise time for TIA using (FDS010) photodiode

Figure 5-13 represents the rise time of a PRBS signal which is equal to 10 ns. Figure 5-14 depicts the rise time for TIA with OSD5-5T photodiode, which is about 20.4 ns. Figure 5-15 shows the rise time for TIA with BPW34 photodiode, which is equal to 16.3 ns. Figure 5-16 illustrates the rise time for TIA with FDS010 photodiode of about 10.9 ns. Using the figures above, the bandwidth can be calculated for each TIA using the equations 5-14 and 5-15. Table 5-2 shows the calculation results of the bandwidth for different types of TIA.

Table 5-2: Calculated bandwidth for each type of TIA

TIA	Rise time (ns)	Bandwidth (MHz)
OSD5-5T	20.4	19.7
BPW34	16.3	27.1
FDS010	10.9	81.4

It can be seen that the calculated bandwidth for the rise time is nearly the same as the measured bandwidth from the experiments.

5.5 Selection of High-Power LEDs

Once high-power LEDs have been chosen to be used for the VLC, the next step is to select a particular LED(s) that can reliably transmit, as far as possible, a modulated signal in free space. In this section, the characteristics of the commercial high-power LEDs have been studied and analysed in order to be used for these type of VLC applications as well as illumination, by measuring the LED bandwidth and the BER of the data transmission.

Generally, there are two common types of high-power LEDs in commercial markets – warm (3000–3500 K) and cool (6000–6500 K). However, in some markets, there are other classifications in terms of the colour temperature (from 3000 K to 30000 K). Therefore, the comparison of these two types has been made in the first stage (warm and cool); for the second stage, comparison in terms of different colour temperature will be made.

Figure 5-17 illustrates the experimental setup of the LEDs' bandwidth measurements and their comparison. For this experiment, the PIN photodiode transimpedance preamplifier (TIA) type, in combination with an RC lead compensator on the same board, has been developed, as the TIA aims to improve the system response by rise time reduction. The lead compensator output has been connected to an RF

amplifier for the signal amplification that the signal analyser was set to evaluate. A 13 dBm sine-wave generated by the signal generator has been superimposed via a bias tee onto the LED bias current. The output from the bias tee was supplied directly to the individual white LEDs. After a direct LOS has been established, the module of the receiver was placed, from the LED, between 1.35 to 2.5 m free space distances. Furthermore, a convex lens was used to focus the light onto the photodiode of the receiver. To ensure the accuracy of the results, a wide-band (150 MHz) amplified photodetector (PDA10A-EC) was used to measure the LED's bandwidth.

Figure 5-18 shows the experimental link of the BER measurement using an Offset PPM technique. The coding system was programmed onto the FPGA board of type (Cyclone IV GX-EP4CGX150DF31C7) via the Quartus II software using Very High Speed Integrated Circuits (VHSIC) Hardware Description Language (VHDL), which describes how the device functions. First, the FPGA generates a PRBS (pseudorandom binary sequence) signal through Quartus II, which is delivered directly to a LED with high power (about 20, 30 or 50 W) through a bias-T (Picosecond Pulse Labs 5575A). Between the LED and the PD, 1.9 m free space distance has been used, where a 60 mm focal length optical convex lens has been fixed in front of the BPW34 (PIN photodiode) built into the TIA board to amplify the current output of PD and covert to voltage. An RF amplifier (0.01–1000 MHz) bandwidth with 32 dB gain has been used to amplify the TIA output voltage.

Lastly, a high-speed low-power comparator (MAX942) has been applied to compare the voltage levels. The comparator output was sent to the FPGA board to be compared with the input signal, with the result displayed on the PC by means of the USB cable via the logic analyser signal tap II. In addition, the plotting of the signals was done using a four-channel digital oscilloscope (Rohde & Schwarz RTO1044 Oscilloscope; 4 GHz).

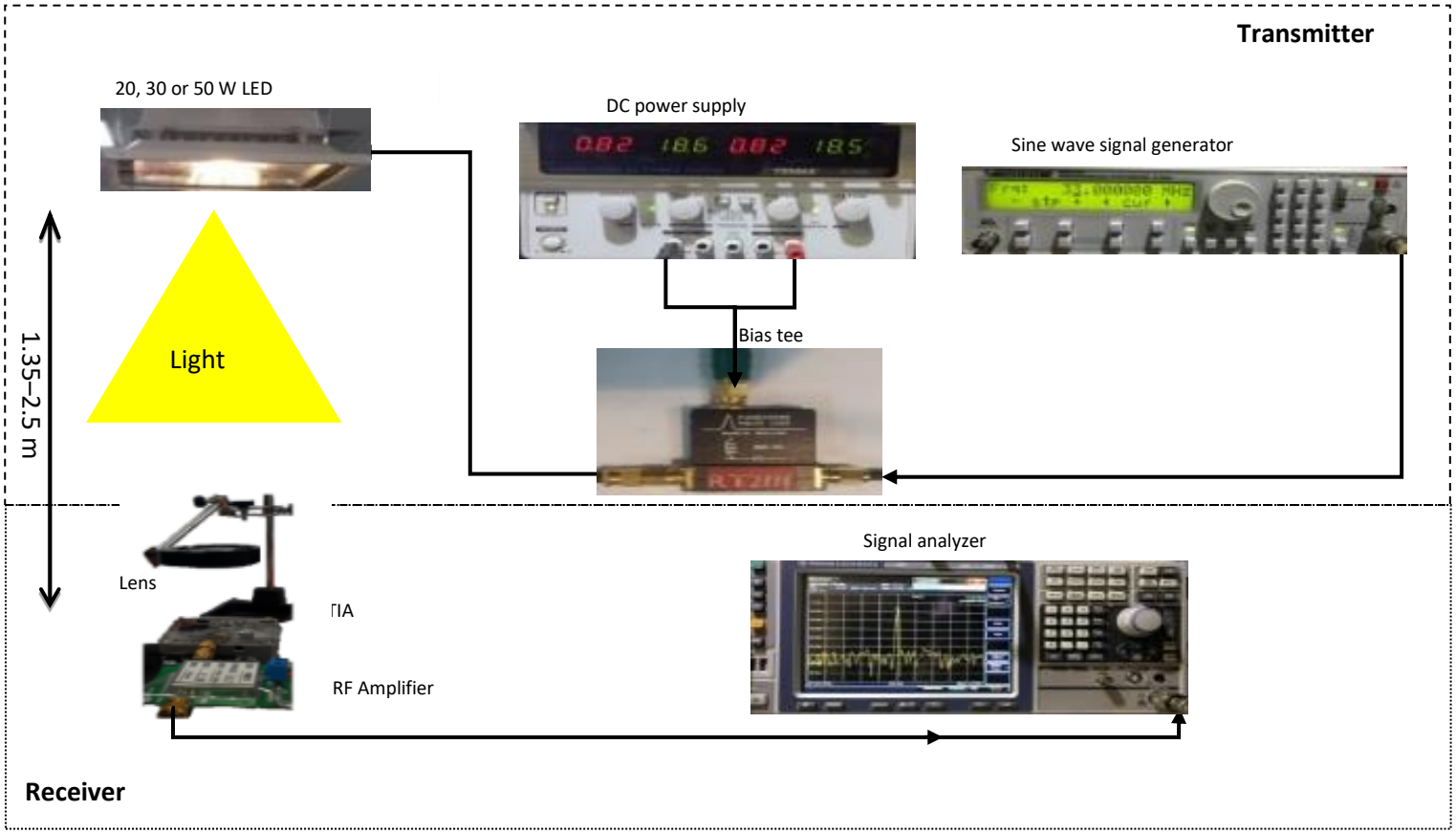

Figure 5-17: Experimental setup for the LEDs bandwidth measurements

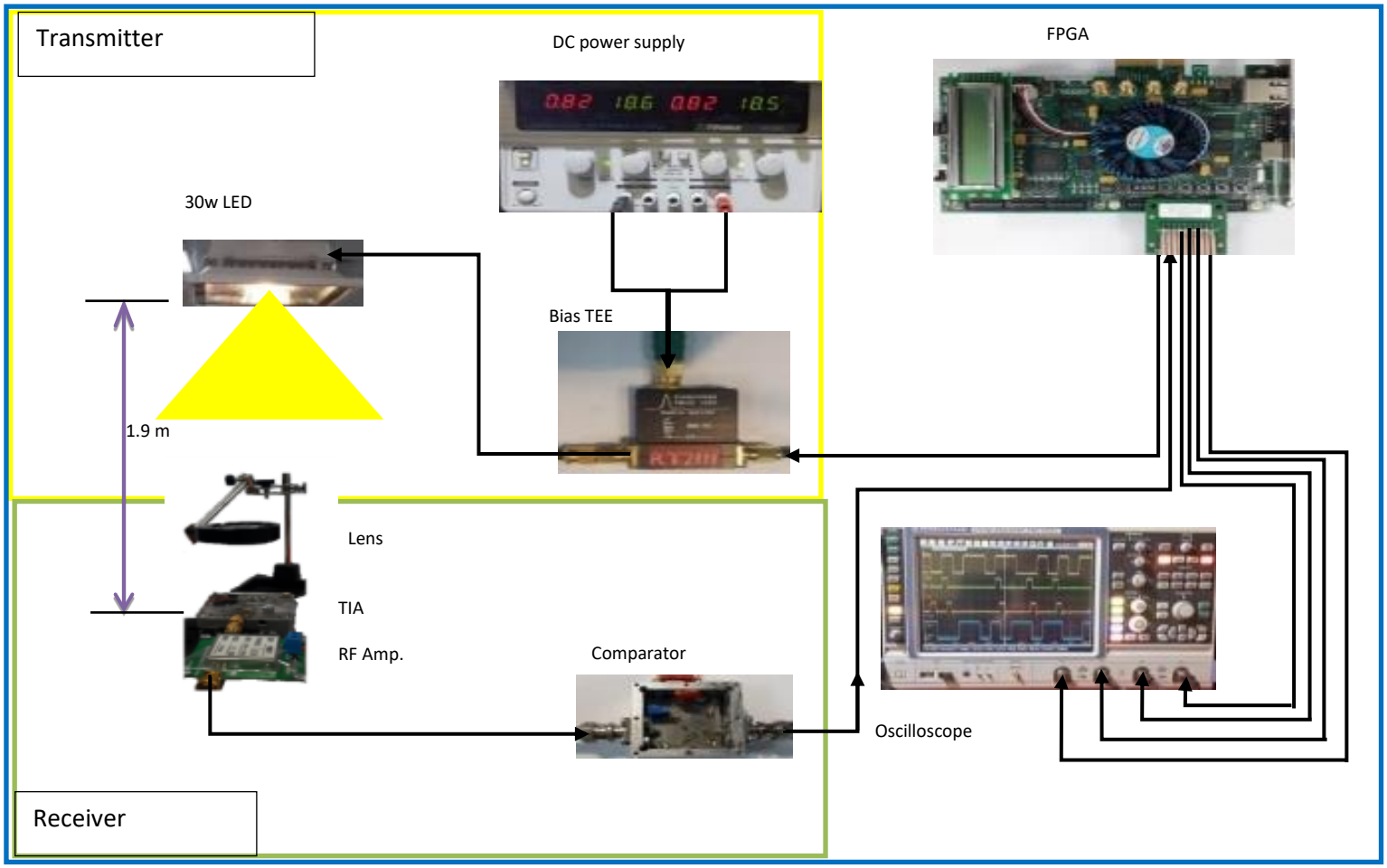

Figure 5-18: Experimental setup of the BER measurement

5.5.1 Comparison of warm and cool LEDs

When purchasing a commercial LED, the source of the manufacturing process must be taken into consideration. Experiments have shown that LEDs with the same specifications but from different sources give different results when used in optical communication systems. High-power LEDs that are commercially available are of two types – cool white with a 5800–6000 K colour temperature and warm white with a 2800–3200 K colour temperature. Different values of power have been selected for each type of high-power LEDs (50, 30 and 20 W) having the same size of the chip as depicted in Figure 5-19.

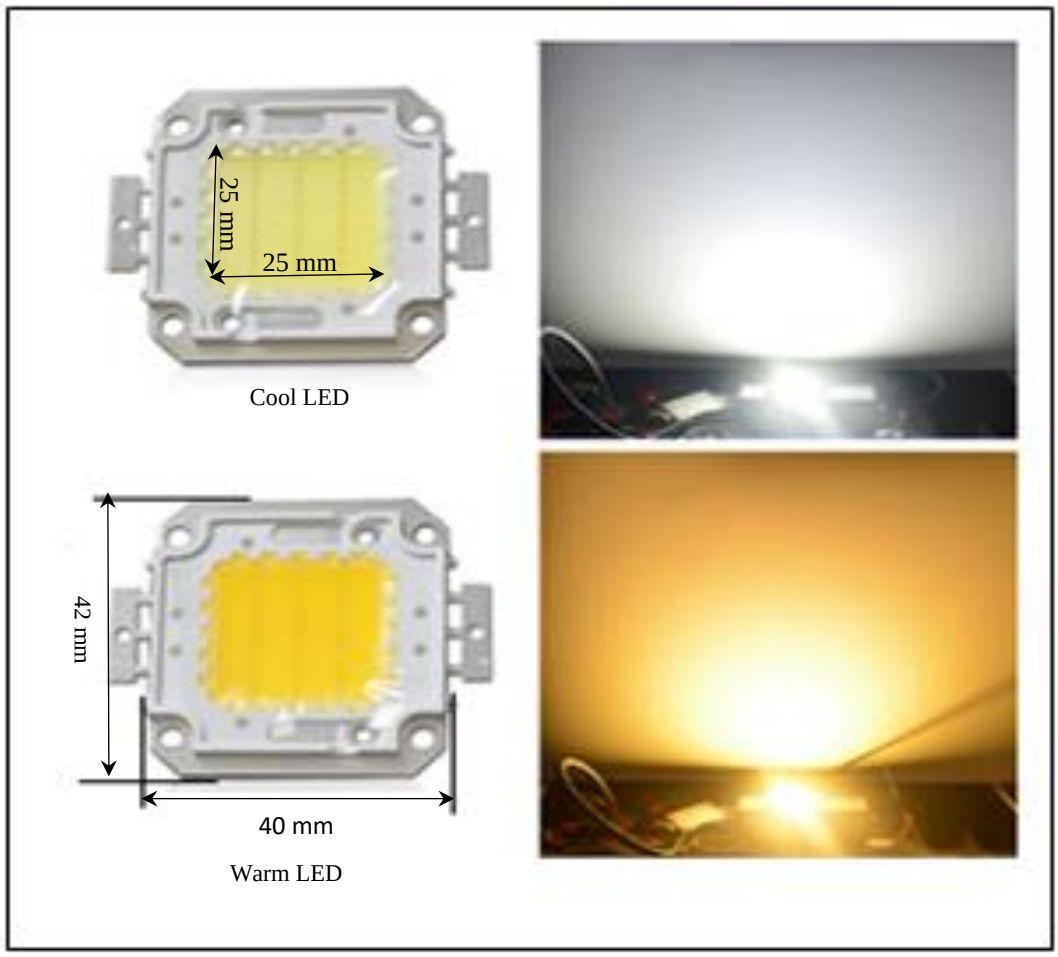

Figure 5-19: High power LEDs chip

All the LEDs' bandwidths have been compared both before and after the extension of the bandwidth in selecting the suitable LED as the experiments for all the LEDS were carried out under similar conditions. In order to extend the LED bandwidth, a circuit with RC lead compensator has been provided. This circuit has been embedded on the TIA circuit. With regards to high-power LED data transmission, the Li-Fi

application, using FPGA (field-programmable gate array), has been implemented based on the Offset PPM scheme [126]. In this research, the resulting BER from data transmission, through each LED, has been measured and compared to find the highest data rate and the distance of transmission having the least BER. The results showed that cool LEDs have a higher frequency bandwidth and lower BER than warm LEDs. On the other hand, high-power LEDs have lower bandwidth and a higher BER than low power [127]. The experiment was also carried out on other LEDs with the same specifications but from a different supplier source. First, the warm LEDs, at different power values, were compared at 1.9 m free space.

Figure 5-20a shows the LED's frequency response before the use of the compensator. It has been noted here that, for all LEDs, the -3 dB bandwidth is approximately around 3 MHz (which is, for white LEDs, the normalized bandwidth [128]), with a response difference ranging from 3 to 5 dBm for 50 W and 20 W respectively. Figure 5-20b depicts the frequency response after the compensator has been used. Additionally, the LED's bandwidth increased approximately to 10 MHz and 13 MHz for 50, 20 and 30 W respectively, with varying response LEDs' rates ranging from -18 dBm to -19 dBm.

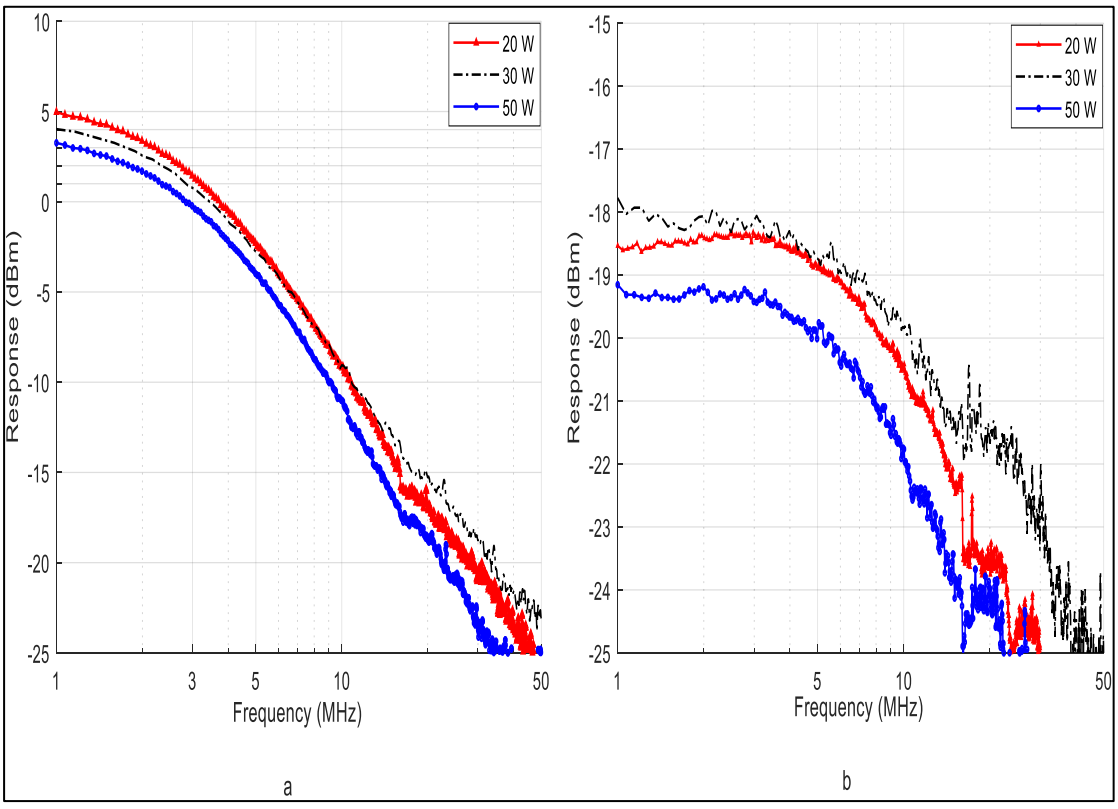

Figure 5-20: Warm LED frequency response a) without a compensator, b) with compensator

The second stage of the LEDs comparison is between cool and warm type for different power values. Figure 5-21a shows a 20 W frequency response for the warm and cool LEDs. The bandwidth was found to be between 3 and 2.7 MHz, with the optical power approximately between 7 and 5 dBm for cool and warm LED types respectively. The extended bandwidth increased to 38 MHz for the cool LED, which is about thrice the warm bandwidth. Figure 5-21b and c illustrate the frequency response difference between the cool and warm type LEDs for 50 and 30 W respectively. The figures show that the LEDs have the same characteristics of bandwidth with a decrease in response at the rate of 1 dB with increasing the LED power. Large variations have been observed as the bandwidth increases for cool LED, which is equivalent to three times that of the warm LED. It can be again seen that the warm LED has a lower response and bandwidth than that of the cool LED. This lower bandwidth is due to added phosphors emitting coating that reduces the switching speed and luminous efficacy.

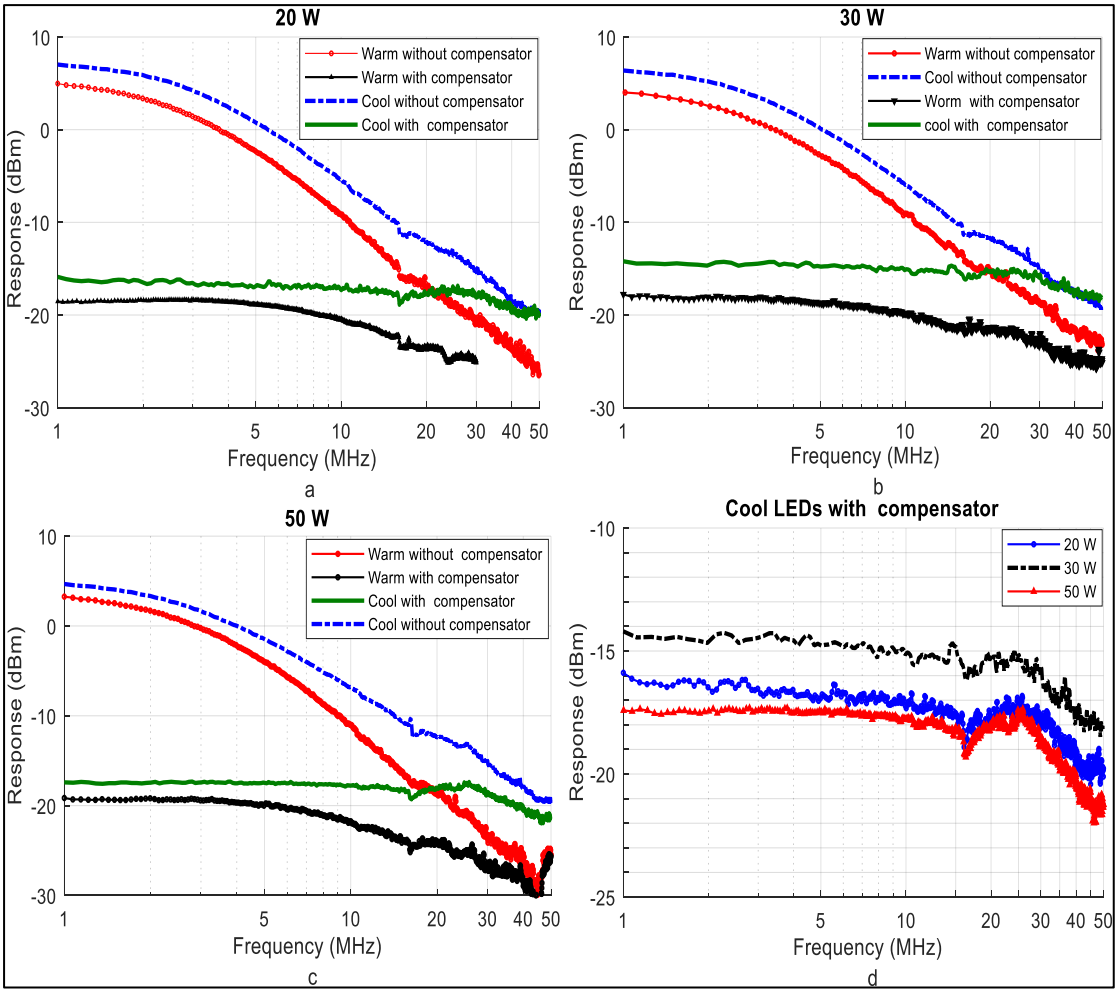

Figure 5-21: Frequency response for warm and cool LEDs

The final stage of this analysis involves comparing the cool LEDs of different power values to find the most optimum and appropriate LED in terms of their bandwidth and response to their optical power. Figure 5-21d shows the different LED power frequency response values. It is seen from the figure that all the LEDs have approximately the same 38 MHz bandwidth with a response difference ranging from -14.5 dBm to-16 dBm to -17.4 dBm for 30, 20 and 50 W respectively. In addition, the Li-Fi application that has been based on Offset PPM, using white LEDs with high power at 20 Mbps data rate and 1.9 m free space distance, was implemented and compared for different types of LEDs. A higher BER was recorded using warm LEDs with 10^{-2} of BER, and a low BER was recorded using cool LEDs with 1.3×10^{-7}, 2×10^{-6}, and 3.5×10^{-5} of BER for 20, 30, and 50 W LED respectively.

Furthermore, analysis has been performed in investigating additional room lighting effect using two experimental setups – only lighting from the LED and with extra lighting inside the room. The results showed that room lightening has zero effect on the LEDs with high power.

Table 5-3 shows a comparison summary between the different LED types. The table depicts that warm LEDs have an inferior performance than cool LEDs. Also shown in the table is the similar performance characteristics between the 30 and 20 W cool LEDs, making them more suitable, compared to the 50 W warm LED for same Li-Fi applications.

Table 5-3: Comparison between different types of LEDs

Type of LED	**Basic bandwidth**	**Extended bandwidth**	**BER at 20Mbps &1.9 m**
	$f_{-3\ dB}$ (MHz)	$f_{-3\ dB}$ (MHz)	
20 W warm	2.7	13	1.6×10^{-2}
20 W cool	3	38	1.3×10^{-7}
30 W warm	2.8	13	2×10^{-2}
30 W cool	3	38	2×10^{-6}
50 W warm	2.8	10	3.9×10^{-2}
50 W cool	3	38	3.5×10^{-5}

Comparing these results with the results previously published [127], it can be seen that the cool LEDs have better optical communications performance than warm LEDs, taking into account the source of manufacture of the commercial LEDs, which had a difference in optical characteristics (bandwidth and data speed) depending on the source supplier.

The results establish that high-power LEDs can be used for Li-Fi applications in achieving similar bandwidths to that of LEDs with low power. Furthermore, the LEDs with high-power, when compared to LEDs with low power, have higher optical power and enable increased data transmission distance being used for lighting. In addition, LEDs with high-power have been compared with two basic types of white LEDs – the warm and cool – in terms of data transmission and lighting. It has been also concluded that the white cool LEDs, compared to the warm, have a larger bandwidth, leading to faster transmission of data. In general, the 30 and 20 W cool LEDs achieved optimum performance regarding data transmission rate and better distance, in addition to the illumination of the environment.

5.5.2 Comparison of colour temperature LEDs

In the second part of the comparison, the colour temperature of each LED is compared. In this experiment, LEDs with different power were selected and compared at different colour temperatures. The experiments were conducted for commercially available colour temperatures which are of six types (3000–3500 K, 4000–4500 K, 6000–6500 K, 10000–15000 K, 20000–25000 K and 30000–35000 K) as shown in Figure 5-22.

The figure illustrates that by increasing the colour temperature, the colour of the light changes from yellow to blue. The categories have been classified according to the colour temperature. They are the warm at 3000–3500 K, natural at 4000–4500 K, and cool at 6000–30000 K. Moreover, three different LEDs' power ratings were selected for each colour temperature, again for 20, 30 and 50 W. To avoid any errors in the results, a high-speed TIA with photo-diode type FDS010 was selected and positioned at a free space distance of 1.9 m from an LED.

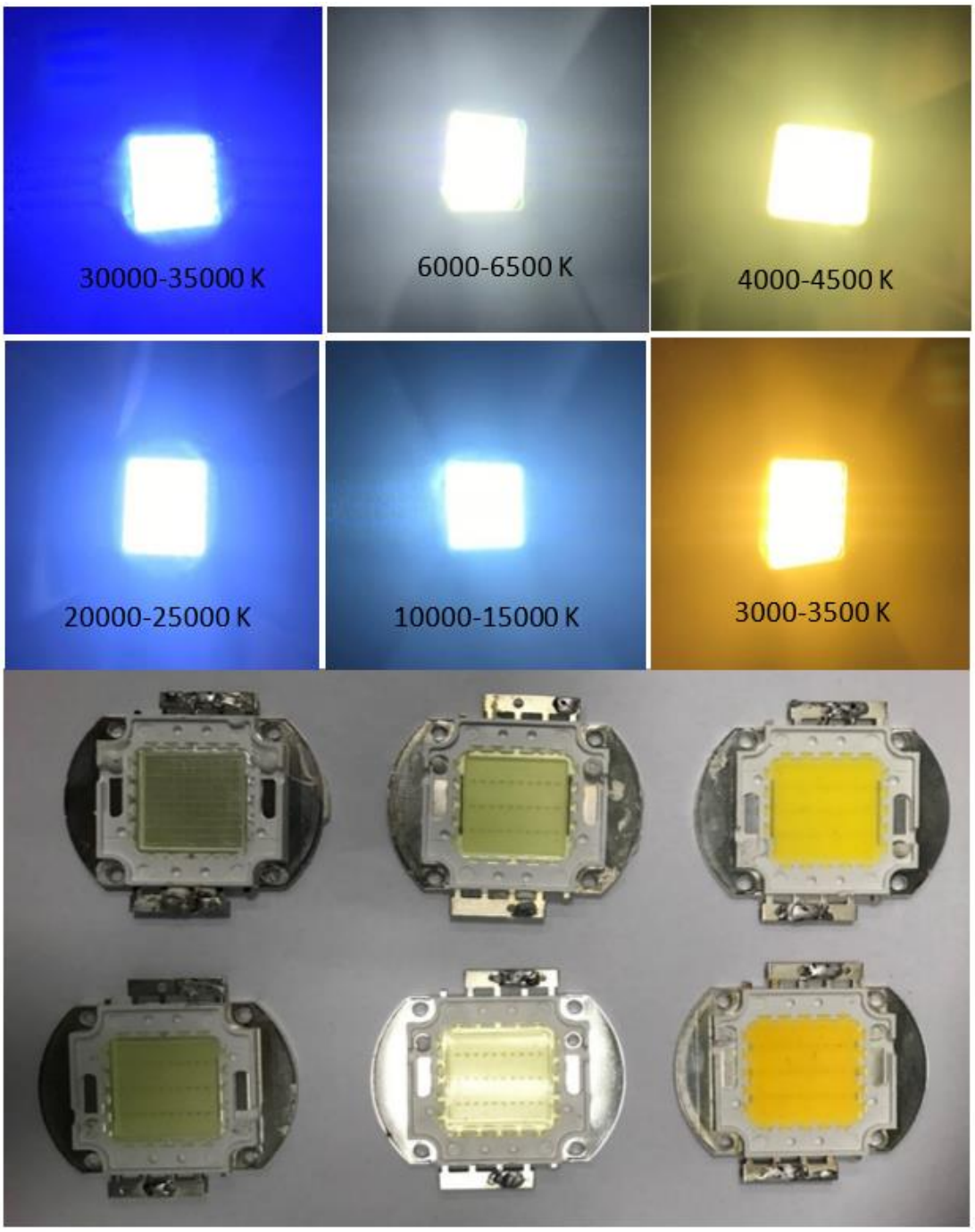

Figure 5-22: Commercially available colour temperature LEDs

Figure 5-23 illustrates the standard frequency response of LEDs at different colour temperatures. A trend was observed for the LED's bandwidth at the same colour temperature. In addition, a slight increase in bandwidth can be observed by increasing the colour temperature. A slight increase in bandwidth can be noticed as the colour temperature increases. About 2.8 MHz bandwidth was recorded at 3000–3500 K colour temperature, and about 5 MHz at 30000–35000 K for 50 W LED. Furthermore, a slight change was observed in response with increased colour temperature.

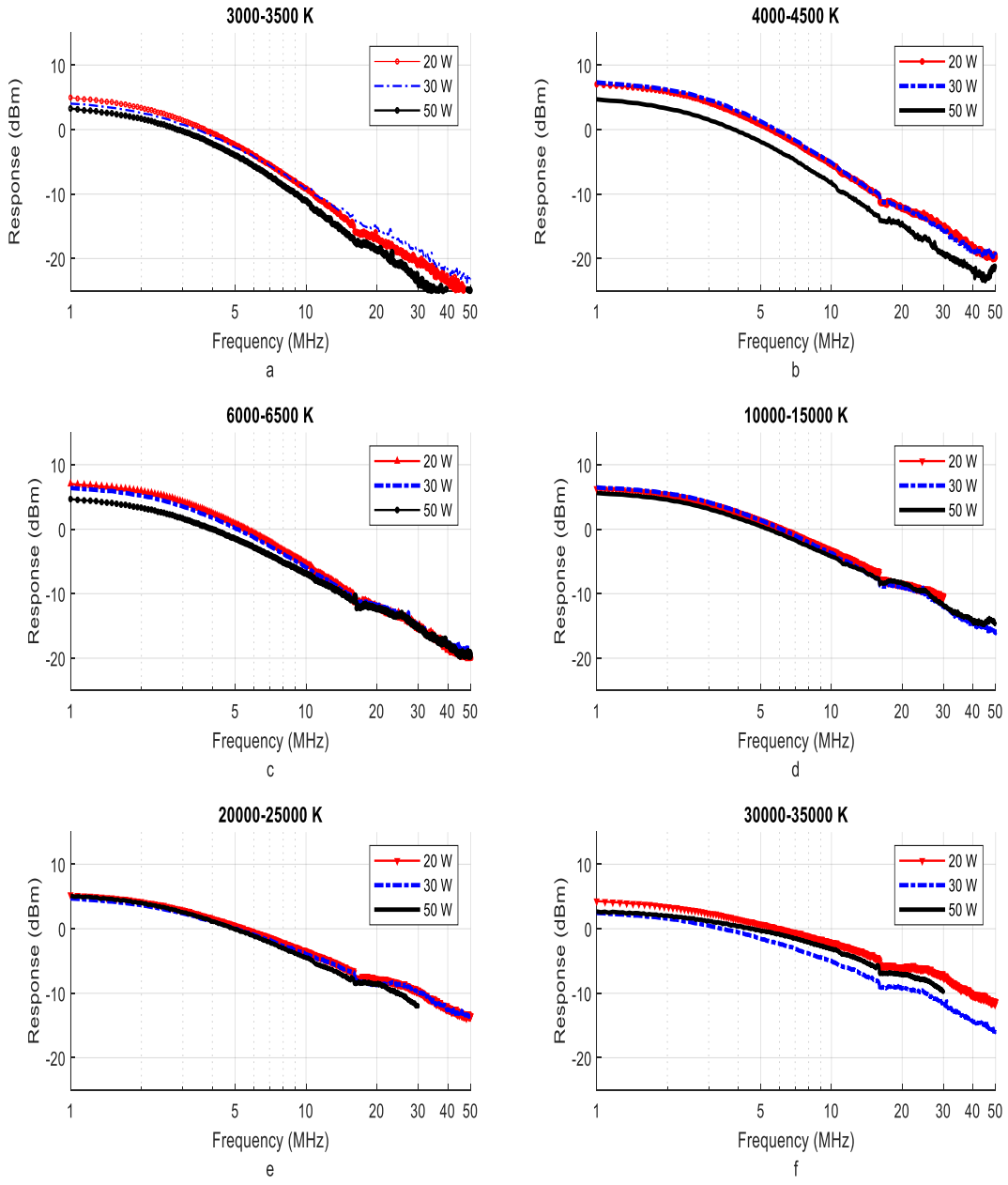

Figure 5-23: Frequency response of LEDs at different colour temperature: a) 300–3500 K, b) 400–4500 K, c) 6000–65000 K, d)10000–15000 K, e) 20000–25000 K and d) 30000–35000 K

Figure 5-24 represents the frequency response of LEDs after the bandwidth has been extended. Note that there is a significant increase in bandwidth due to the colour temperature increase. In addition, there was a slight variation in bandwidth, depending on the power of each LED. A bandwidth of 13 MHz for 20 and 30 W LEDs and 10 MHz for 50 W LED has been recorded for the colour temperature of 3000–3500 K. The bandwidth gradually increases as the colour temperature increases while maintaining the same difference in bandwidth depending on the power of LEDs. A bandwidth of

56, 45 and 42 MHz for 20, 30, and 50 W LEDs respectively was recorded at 10000–15000 K, while the bandwidth reached above 80 MHz at 30000–35000 K colour temperature for all the power of LEDs.

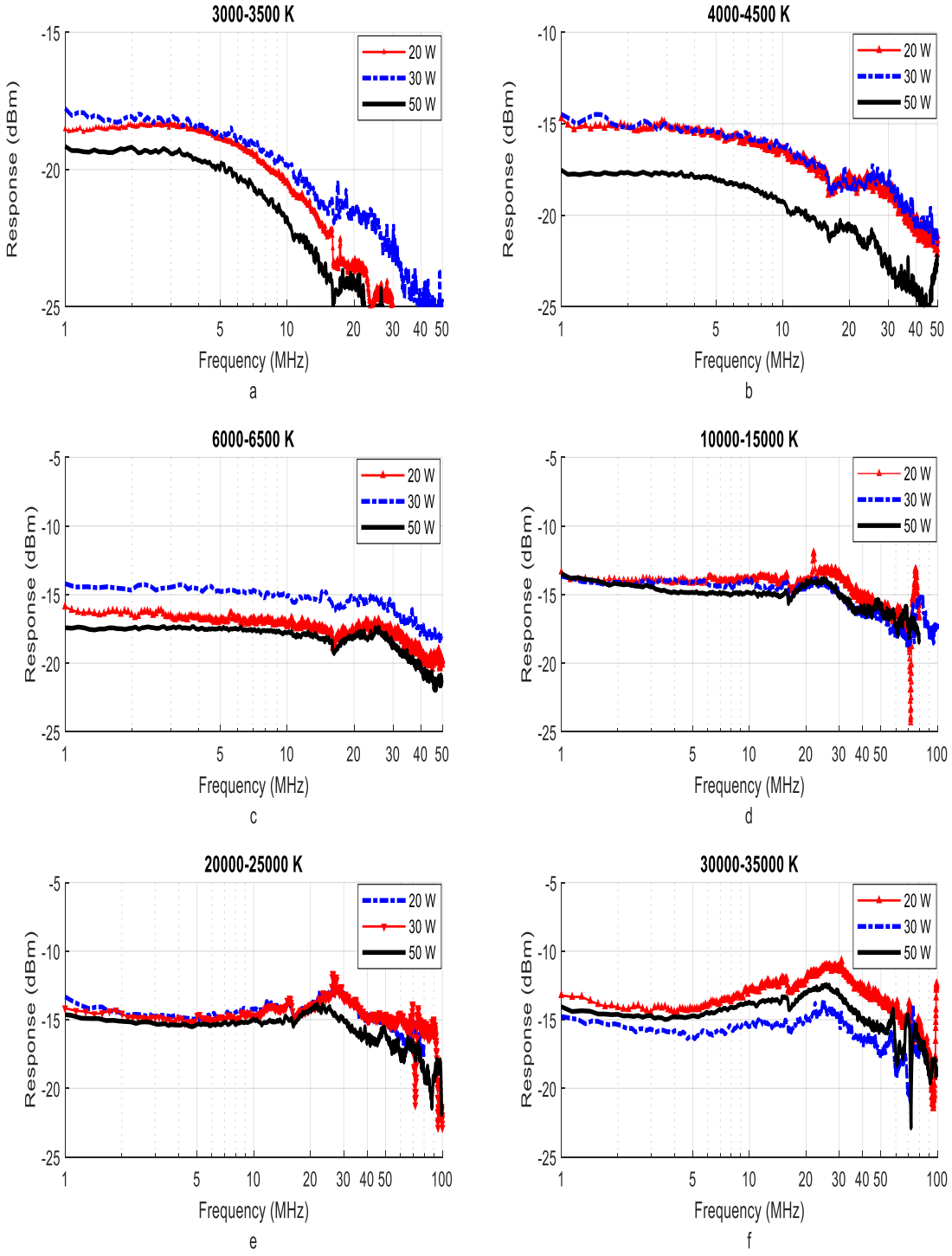

Figure 5-24: Frequency response of LEDs after extended bandwidth: a) 3000–3500 K, b) 4000–4500 K, c) 6000–65000 K, d)10000–15000 K, e) 20000–25000 K and d) 30000–35000 K

From Figure 5-24 above, the differential increase in bandwidth can be observed by increasing the colour temperature. It can be seen that the bandwidth of the LEDs depends on the colour temperature. In general, there are slight differences in responses for all LEDs due to colour temperature and LED power rating. However, vertical scale error affects the obtained responses for all the LEDs because of the manual nature of the experimental set up in collecting data. It should be noted here that this error will have no affect at -3 dB. Furthermore, the BER was measured at a fixed transmission distance of 1.9 m at 20 Mbps data speed for each LED at different colour temperatures as well as for different values of power. The results showed that higher BER was recorded at a lower colour temperature. In contrast, increasing the colour temperature leads to a decrease in the BER as shown in Table 5-4.

Table 5-4: Bandwidth (BW) and BER results for a different type of LEDs, N= Not extended, E =Extended

Colour temperature (K)	BER			BW (MHz)					
	LED Power (W)			LED Power (W)					
	20	30	50	20		30		50	
				N	E	N	E	N	E
3000–3500	1.6×10^{-2}	2×10^{-2}	3.9×10^{-2}	2.7	13	2.8	13	2.8	10
4000–4500	7.5×10^{-5}	2×10^{-4}	1.3×10^{-3}	3	15	3	15	2.9	15
6000–6500	1.3×10^{-7}	2×10^{-6}	3.5×10^{-5}	3	38	3	38	3	38
10000–15000	2.5×10^{-10}	1.6×10^{-9}	3.2×10^{-9}	3.5	56	3.5	45	3.5	42
20000–25000	6.6×10^{-11}	9.5×10^{-11}	2.7×10^{-10}	3.5	75	3.5	70	3.5	60
30000–35000	5.2×10^{-11}	8.3×10^{-11}	2×10^{-10}	4.2	84	3.9	82	5	80

5.6 The Effect of Distance and Angle on the Rate of Data Transmission

The effect of transmission distance was studied by measuring the bit error rate (BER) of the signal transmitted at different free space distances. In this experiment, an offset PPM based on cool LEDs (20, 30 and 50 W), with a colour temperature range of 10000–15000K was implemented at 20 Mbps data speed. Figure 5-25 shows the relationship between BER and the free space distances. The results showed that free BER was achieved up to 1.6 m for all LEDs. A BER of $< 10^{-10}$ was recorded at 1.8 m for 20 W, whereas the same BER was achieved for 30 and 50 W LEDs at 1.7 m.

The error rate due to the light deviation angle (Θ) from the receiver was measured at different angles. A 20 Mbps data rate and 1.9 m free space distance was selected with 10000–15000K LEDs colour temperature with 20, 30, and 50 W rating powers, as shown in Figure 5-26.

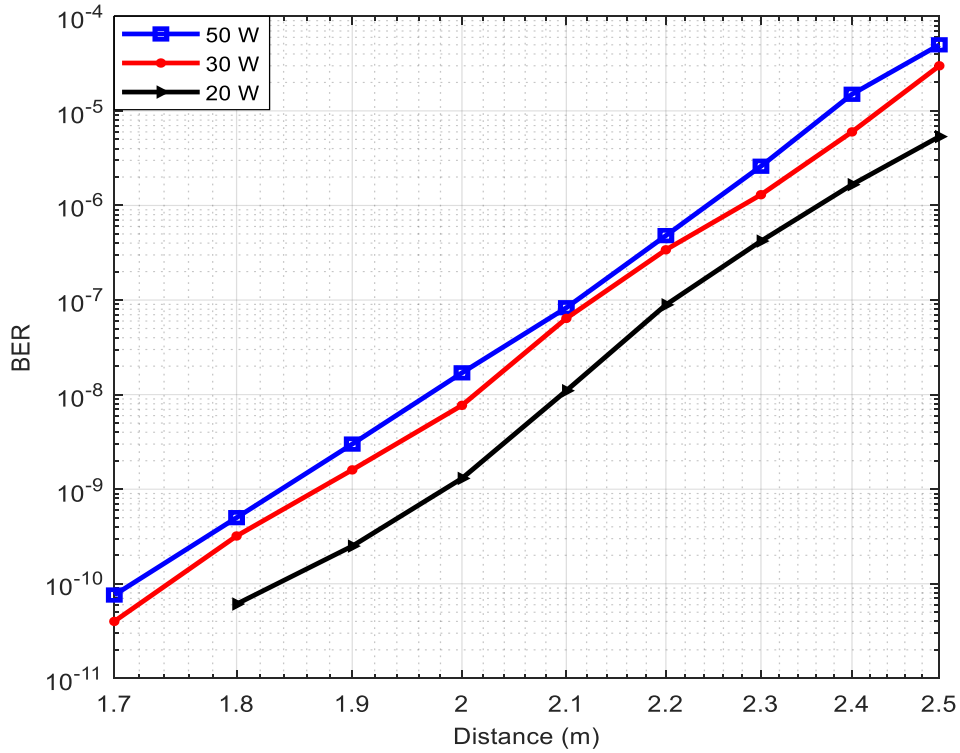

Figure 5-25: Relationship between BER and distance

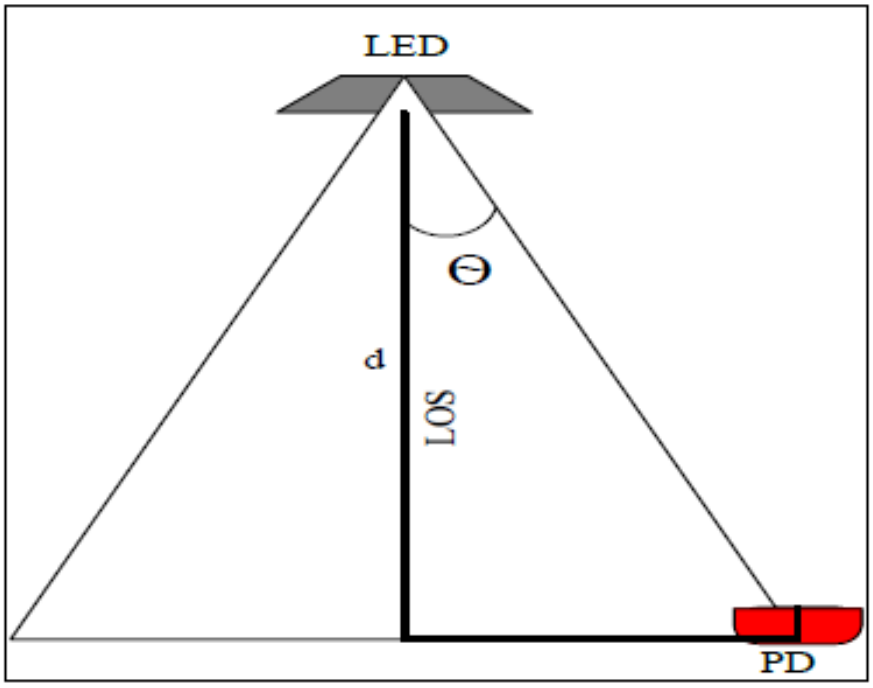

Figure 5-26: Geometry of deviation angle (Θ) between Tx and Rx

Figure 5-27 illustrates the results obtained from the experiment. The figure shows that the error rate increased by increasing the angle, with a clear difference in the increase, depending on the power of the LEDs. This variance was reduced by increasing the angle, where the BER for all LEDs was approximated to 10^{-4} at a 40^{o} angle; this was due to systematic errors. The angle was measured manually and, consequently, the varying degrees of values and directions were recorded, which makes it difficult to determine the exact values for all LEDs and angles.

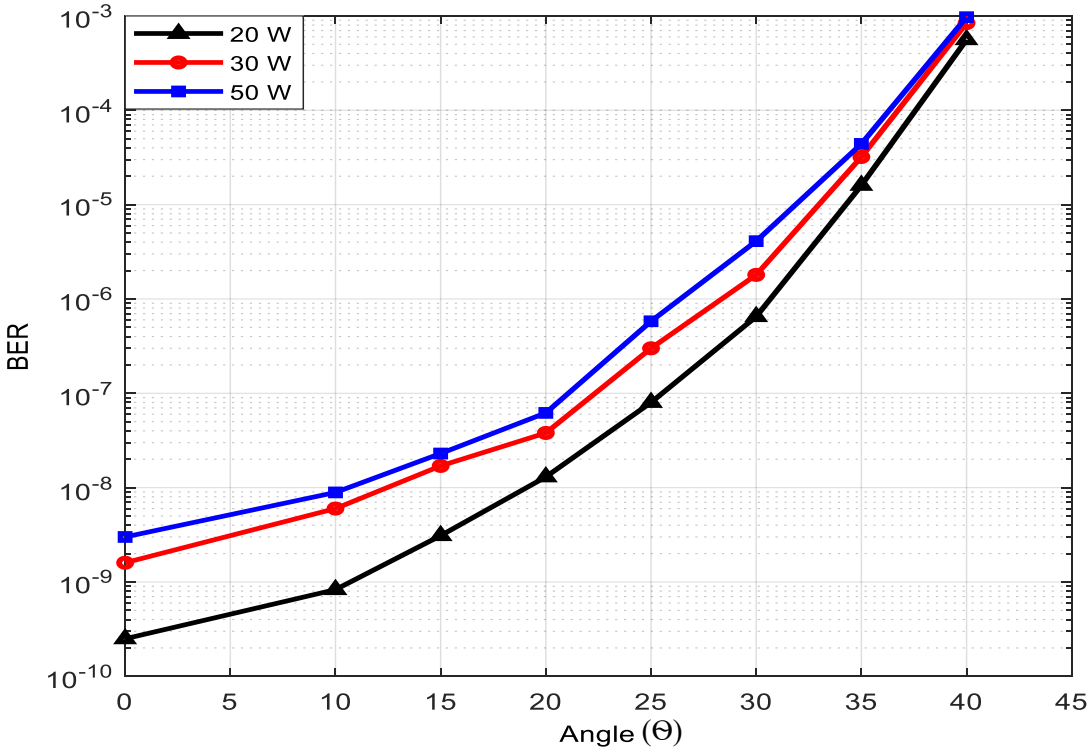

Figure 5-27: Relationship between BER and angle

To conclude, the figures show the apparent variations in the error rate, where the lowest BER was recorded with the 20 W LED. The error rate increased with the increase in the power rate as well as the distance (d) and angle (Θ).

5.7 Uncertainty Measurement

To avoid errors resulting from lab devices and the effects of the surrounding environment, measurement uncertainty was calculated by repeating experiments and measurements at different time periods. The LED bandwidth measurement was repeated 20 times and observed to run all devices simultaneously. Measurements were taken for different periods for more than 24 hours. As a result, the standard deviation (STD) of these periods for different frequencies were calculated and plotted,, as

depicted in Figure 5-28. It can be observed that the values of the standard deviation range from (0.18–0.22), indicating that the error rate is minimal enough to be neglected.

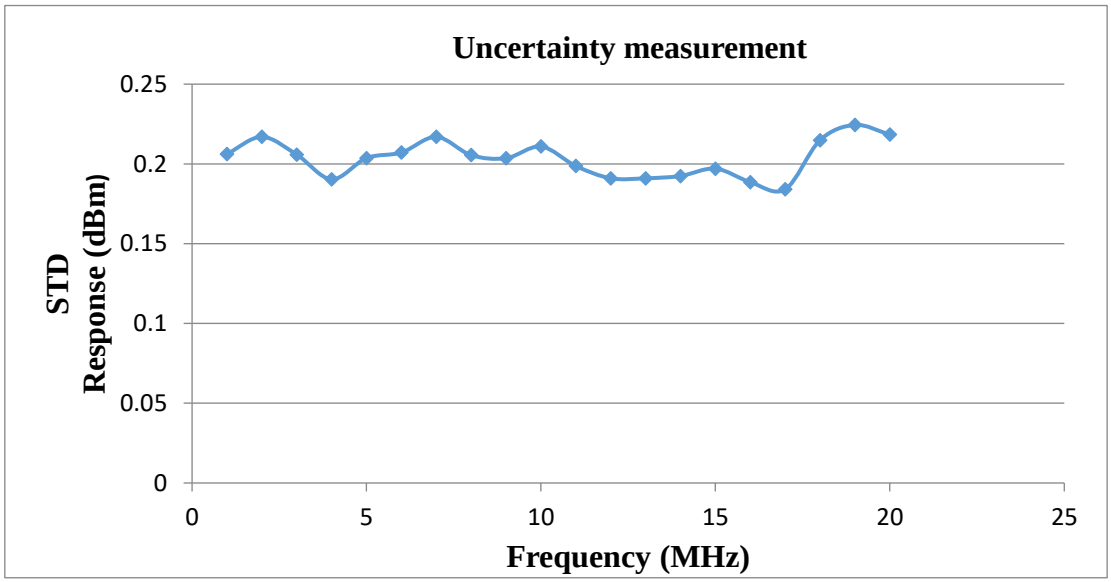

Figure 5-28: Uncertainty measurement for the LED bandwidth measurements at different times

5.7.1 Impact of additional lighting

The experiments were performed for complete lighting and repeated in the absence of any lighting, except for a 30 W LED. The measurements and results were found to be an exact match, meaning that the lab lighting had no significant effect.

5.7.2 Effect of equipment and devices

The devices and equipment used in these experiments were calibrated and evaluated through the direct connection between them, without the use of test rigs. The devices used for the bandwidth measurement were all calibrated, with the signal generator connected directly to the spectrum analyser via a coaxial cable. The measurements obtained were recorded and plotted, as depicted in Figure 5-29. It shows that the response increased sharply at 14 MHz, with a 0.7 dBm difference in amplitude and the response fluctuating after 14 MHz due to the noise input and, as a result, the effect of this oscillation was observed in the obtained results.

The test rig was calibrated, including the FPGA board and the coaxial cables by measuring the bit error rate, which achieved a transmission data rate of up to 40 MHz with free BER. However, there was some additional BER caused by the effects of electronic devices in the lab.

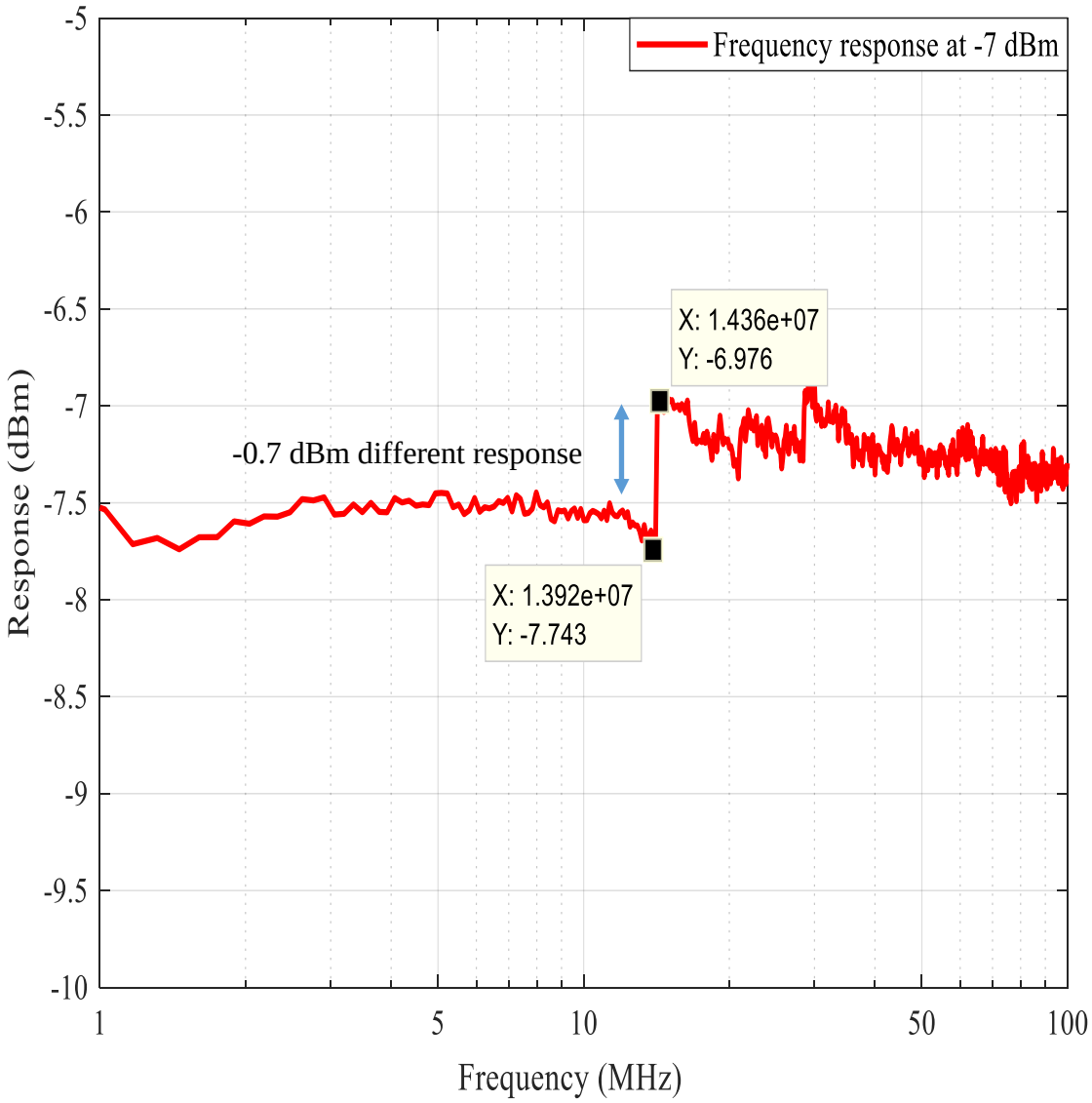

Figure 5-29: Systematic error through bandwidth measurement devices

5.8 Practical Validation of Using High Power LEDs

For high power LEDs to be used in VLC applications, particular LEDs were chosen since the goal is to enable signal transmissions for as far as possible. The ability of high power LEDs has been checked to send data at high rates, where it has been compared with phosphorescent white LEDs (OSRAM LUW, W5AM), used in many previous researches (see Table 2-1).

In this experiment, a 30 W LED at 6000–6500K was chosen to be compared with the OSRAM LUW W5AM, as they have the same colour temperature. The comparison was based on the bandwidth and bit error rate measurements. Figure 5-30 shows the frequency response of both LEDs.

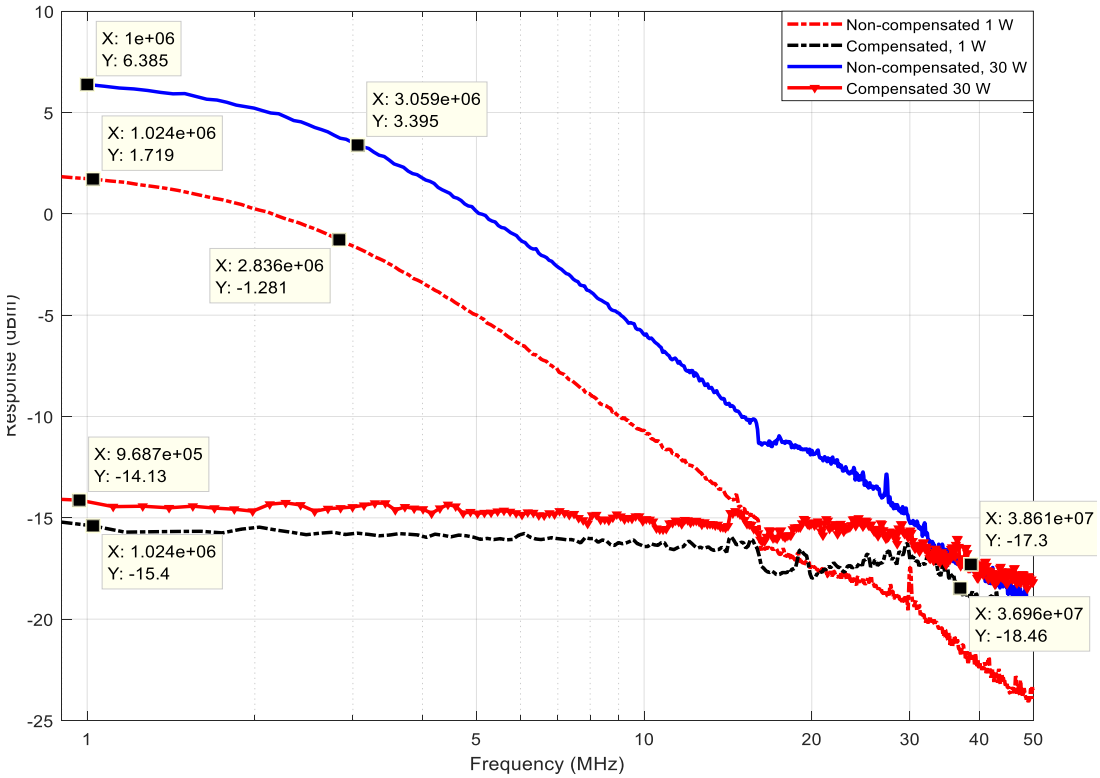

Figure 5-30: Frequency response of 1 W and 30 W LEDs

A convergence of bandwidth for both LEDs was observed. The bandwidth was around 3 MHz and 30 MHz before and after compensation, respectively. Furthermore, the BER was measured for both LEDs at a 20 Mbps data rate. The different distances were taken for both LEDs in order to eliminate the signal for 1 W at a higher distance, whilst saturating the signal for 30 W at a short distance. A 10^{-6} of BER was recorded for both the 1 W and 30 W at free space distances of 0.75 m and 1.6 m, respectively.

It can be seen clearly that both LEDs have the same bandwidth with a slight difference in the response, helping the conclusion that the high power LED (30 W) can be used to send data at higher rates of up to several hundred Mbps, as compared to the low power one (1 W) [129-131].

5.9 Summary

The simplest transceiver circuit was implemented, and successfully, the data was achieved according to the ethernet speed. In the transmitter, an LED with bias-T was employed. At the receiver part, the TEA was improved to increase the bandwidth through the RC compensator circuit. On the other hand, three types of photodiodes were selected and tested to investigate the best performance. Thus, it was concluded that the

OSD5-5T performed better, with a higher speed and lower BER, as compared to other photodiodes.

Previous research has focussed on the use of low power LEDs (1 W) or RGB in VLC applications. For the first time in this research, high-power LEDs (20, 30, 50 W) were employed for VLC. The results showed the success of high-power LEDs in transmitting data, such as low-power LEDs. From this principle, a set of commercial high-power LEDs were compared in order of type, power and colour temperature.

In terms of type, there are two common commercial types – warm LEDs and cool LEDs. Experiments have proved that the cool LEDs performed better than warm LEDs, where it was found that the bandwidth of the cool LED was three times higher than the warm one, recorded at 38 MHz. Moreover, these LEDs were compared in terms of data transmission. The results showed that the cool LED had a higher data rate. The source supplier of the LEDs was also considered. The results proved that the optical characteristics of LEDs are dependent on the source supplier (manufacturing). Where there was a disparity in bandwidth and data speed, stability was preferred in terms of the cool LED over warm.

In terms of power, three types of rated powers (20, 30, and 50 W) were implemented on the VLC. It was found that the three types had similar characteristics with little variation. The results confirmed that the increase in rating power led to reducing the bandwidth and data speed. It was found that the 20 W LED performed better than the 30 W, and the 30 W was better than the 50 W.

In terms of colour temperature, the experiments comprised commercially available colour temperatures, which contained six types (3000–3500K, 4000–4500K, 6000k–6500K, 10000–15000 K, 20000–25000 K and 30000–35000 K).

It can be concluded that the bandwidth of the LEDs depend on the colour temperature. The bandwidth was gradually increased by increasing the colour temperature while maintaining the same difference in bandwidth, depending on the power of the LEDs. A 13 MHz bandwidth was recorded for the 3000–3500 K colour temperature, and a 84 MHz (the maximum bandwidth) was recorded at a colour temperature of 30000–35000 K. In terms of data transmission, a 20 Mbps data rate at a fixed transmission distance of 1.9 m was implemented, at different colour temperatures. The results showed that the higher BER was recorded at a lower colour temperature,

where a BER $< 10^{-2}$ was recorded at 3000–3500 K, and a BER $< 10^{-10}$ was recorded for a range between 10000K to 30000 K.

The error rate for 20 Mbps data rate was measured at the different transmission distances. The results proved that the data could be transmitted over a distance of up to 1.6 m with free BER. The error rate is directly proportional to the distance; it was less than 10^{-5} at a distance of up to 2.4 m. This result is acceptable for transmission in optical communication systems. Moreover, the BER, due to the light deviation angle from the receiver, was measured at 20 Mbps data rate and 1.9 m free space distance. It can be summarised that the BER increases due to the increasing angle, where the BER was approximated < 10^{-5} at an angle of 30^{o}.

However, the practical validation of using high power LEDs was implemented by comparing it with a low power LED (1 W). The results showed that both LEDs had the same performance in terms of VLC applications.

Chapter 6

Modulation Schemes Implementation

6.1 Introduction

In this chapter three types of pulse position modulation techniques are addressed and implemented to verify the optimum type used in VLC based high-power LEDs. The test rig was calibrated, including the FPGA board and coaxial cables, by measuring the bit error rate, which achieved a transmission data rate up to 40 MHz with free BER.

6.2 Field Programmable Gate Array Board (FPGA)

The Altera Cyclone IV GX-FPGA development kit is a complete design environment that includes both the software and hardware needed to develop Cyclone IV GX FPGA designs. Cyclone IV GX devices are targeted towards high-volume and cost sensitive applications, enabling system designers to meet increasing bandwidth requirements while lowering costs. Figure 6-1 shows the field programmable gate array board (FPGA), which is employed for programming the modulation techniques. A very high-speed integrated circuits (VHSIC) for hardware description language (VHDL) was used to programme the FPGA, which requires knowledge of how the device functions. The reason behind utilising the FPGA is that the resultant system will have lower levels of external noise and any internal delays than in the previous implementations [132].

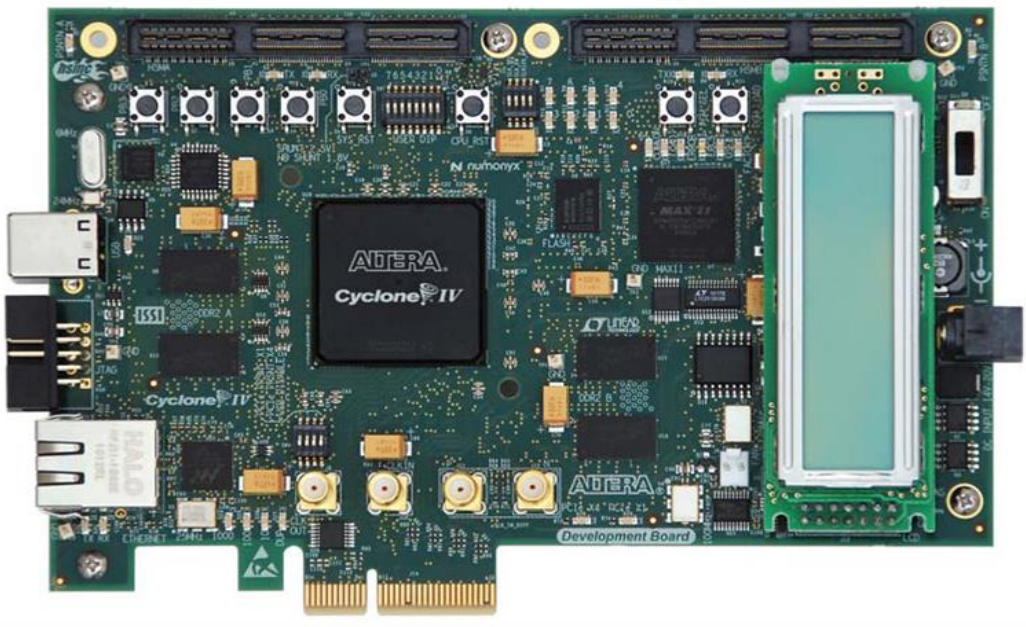

Figure 6-1: Field-Programmable-Gate-Array board Cyclone IV GX (FPGA) [132]

6.3 Implementation of the Dicode Pulse Position Modulation (DiPPM)

Figure 6-2 and Figure 6-3 describe the block diagram and the logic circuit schematics of the experimental VLC system, based on DiPPM using a 30 W LED. The test rig explained in Chapter Five, Figure 5-18 comprises two parts, software system design and hardware system design. In software design, FPGA via the Quartus II software, the VHDL is used for data generation in PRBS form, BER measurement and the DiPPM coder and decoder. First, the 125 MHz clock was generated by the FPGA which was sent to the phase-locked loop (PLL) to generate the required frequency. The desired frequency was applied to generate the PRBS signal (PCM). Afterwards, the PRBS signal was encrypted by the DiPPM encoder which was sent to the LED via the bias-T and the digital oscilloscope, for observation through the pins (DiPPM/DiPPM1).

The hardware design encompasses the VLC transmitter circuit and receiver circuit. In the transmitter circuit, the commercially available high-power LED (cool white 30 W) was connected to the data and power supply via a bias-T. Furthermore, the receiver circuit was composed of the photodiode (PD) and transimpedance amplifier (TIA), with a gain of 20 dB to recover the signal.

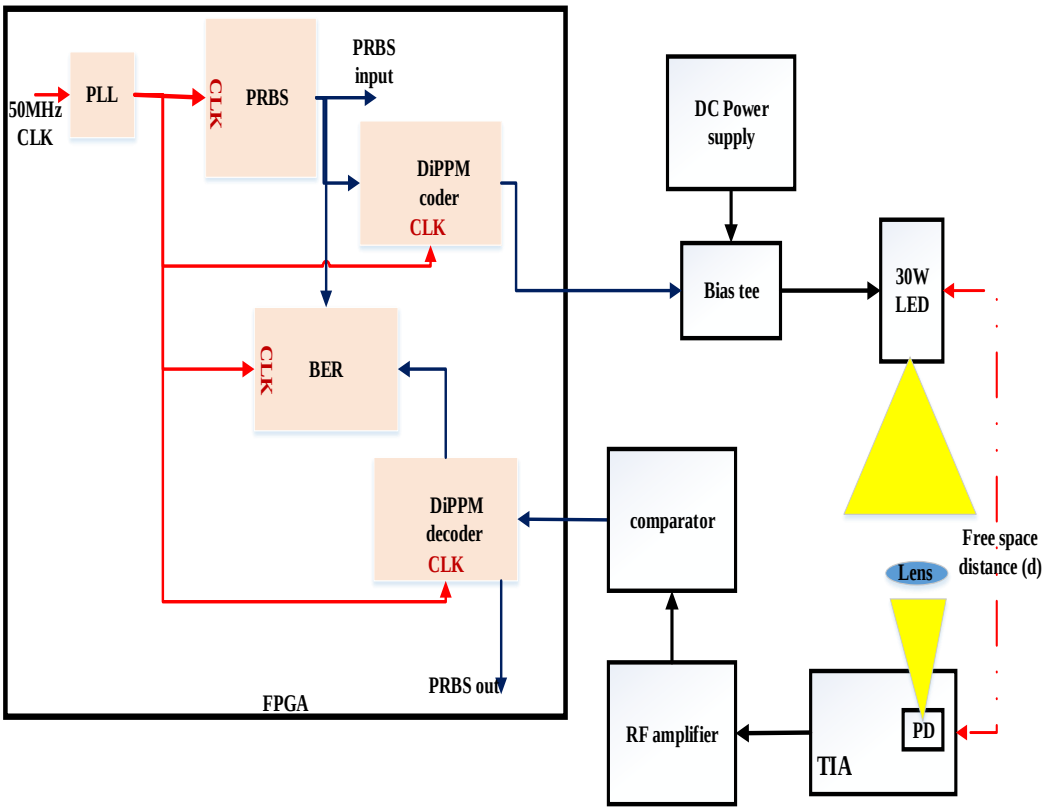

Figure 6-2: Block diagram of the DiPPM based on VLC

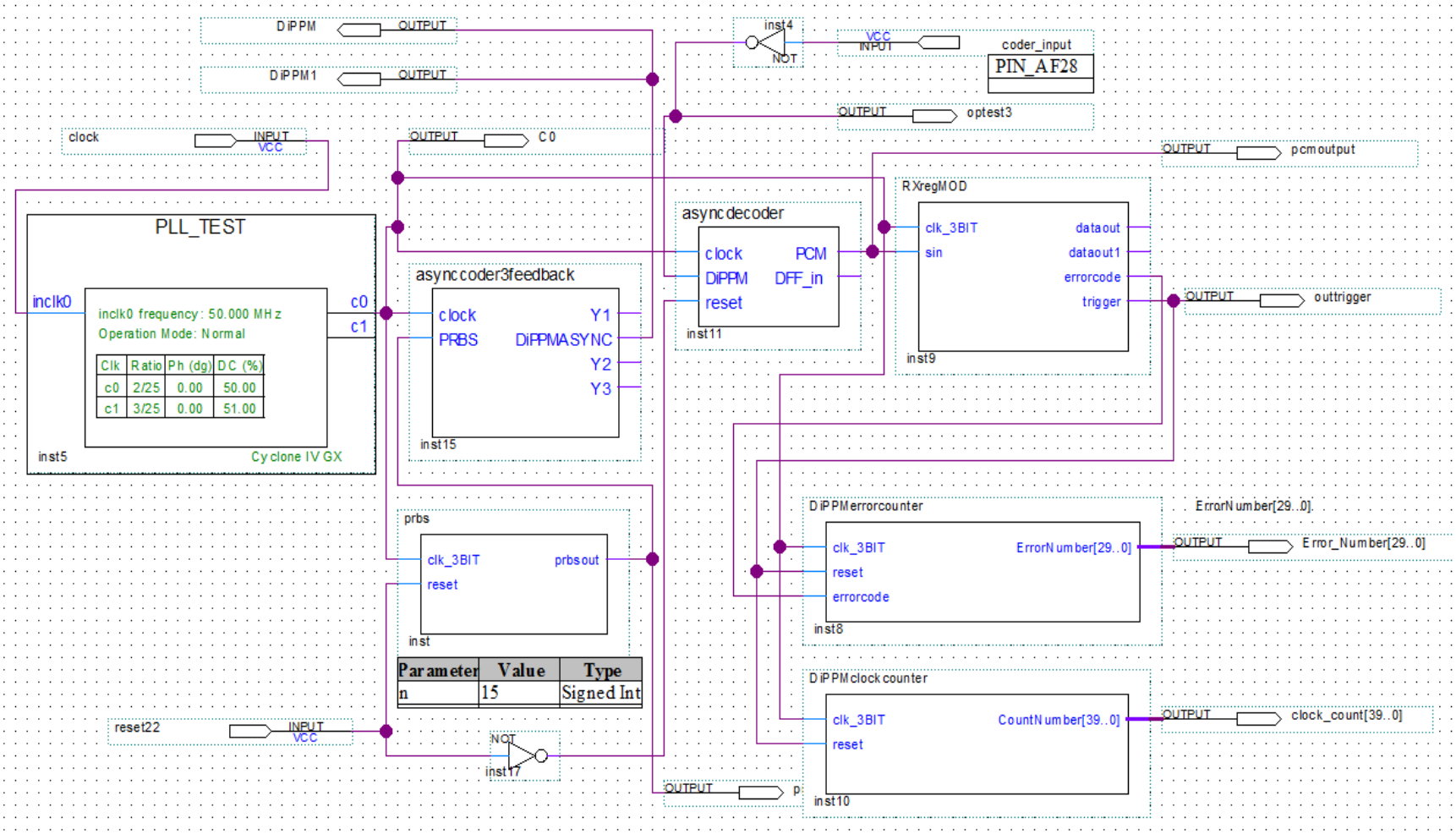

Figure 6-3: Logic circuit schematic of DiPPM

The photodiode received the signal from the LED lighting to be converted from current to voltage, and then amplified by the TIA. The output signal from the TIA was sent directly to the RF amplifier for amplification. The amplified signal was sent to the comparator to equalise the receiver output to either zero or one. Finally, the output signal from the comparator was fed directly through the coaxial cable to the FPGA board via the pin (coder_input), which was observed via the digital oscilloscope through the pin (optest3) and the PC. On the other hand, the FPGA decoded the signal received from the comparator to retrieve the original signal. The original signal was sent to the oscilloscope via a pin (pcmoutput) for observation. Moreover, the BER was measured by counting the error numbers through the comparison between the decoder signal and the PRBS signal. Table 6-1 shows the characteristics of the experiment link parameters.

Table 6-1: Characteristics of the Experiment Setup Parameters.

Parameter	Characteristics
LED	Cool white 30 W, 10000–15000 K
Bias TEE	Picosecond Pulse Labs 5575A
Photodiode	OSD5-5T
RF amplifier	1 MHz-2GHz, 32 dB
Comparator	MAX942
FPGA	Cyclone IV GX-EP4CGX150DF31C7
Free space distance	1.9 m

6.3.1 Results and discussion

Figure 6-4 shows the measured real signals via the oscilloscope at transmission speeds of 14 Mbps. The top trace represents the PRBS signal, the middle traces represent the encoded signals, where the upper signal represents the transmitted signal to the LED (encoded), and the lower signal represents the output signal from the comparator (received). The bottom signal represents the decoded signal (decoded). From the shape of the signals, a good correlation can be observed between the input data (PRBS) and the output data (decoded), with time delay due to the logic circuit components, as well as between the coded signal in the transmitter (encoded) and receiver (decoded).

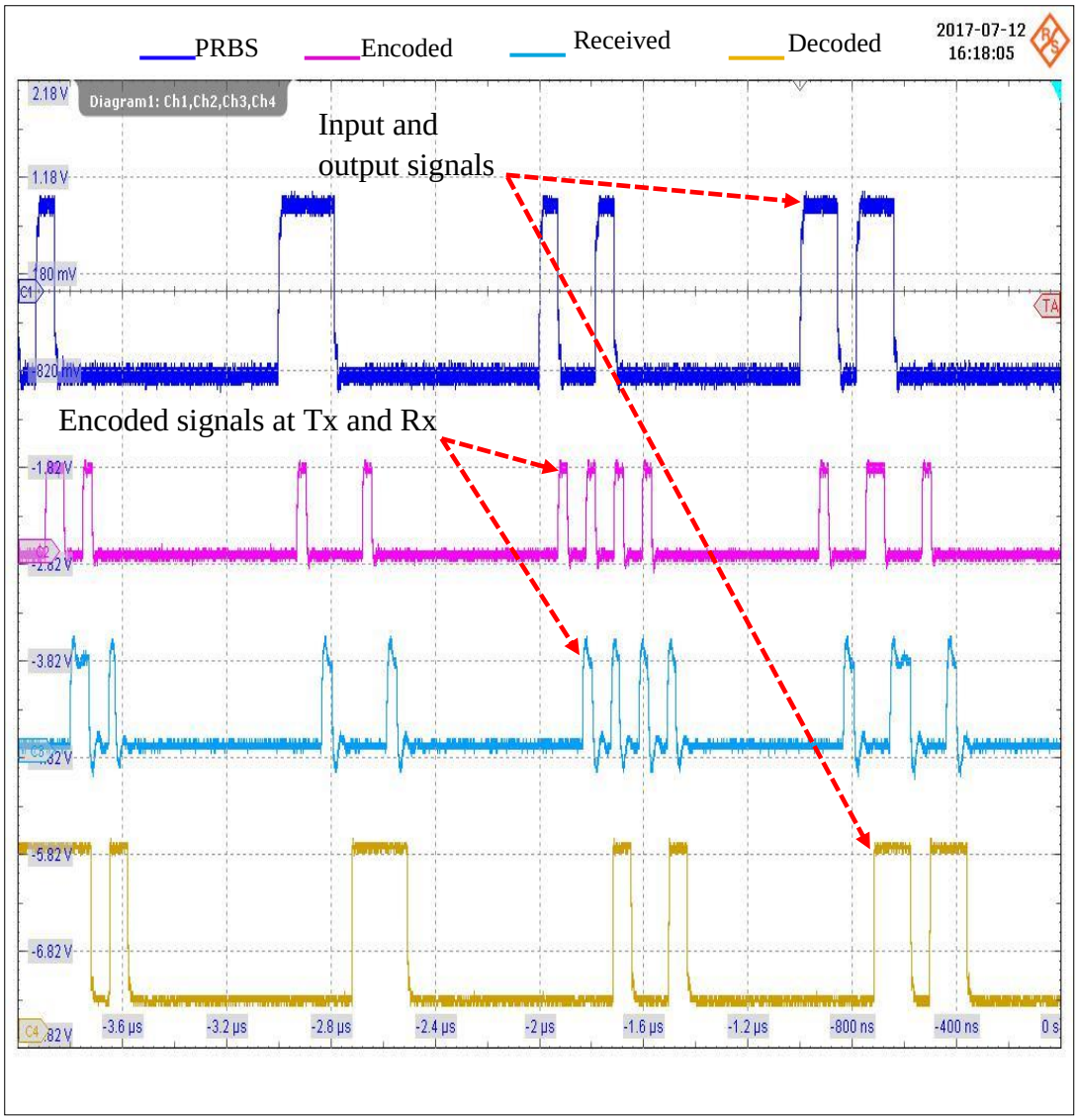

Figure 6-4: Transmitted and received signals of DiPPM via oscilloscope

Furthermore, the FPGA board has been connected to the PC to display the simulation signals through the signal tap II logic analyser, using the Quartus II software to measure the BER, as shown in Figure 6-5. Similarly, there is a match between the transmitted and received signals. The BER was measured by comparing the input signal (PRBS) and the output signal (decoded). The BER was less than 10^{-11} for up to 14 Mbps data rates. As the frequency increased up to 14.5 Mbps, the BER also increased to $>10^{-9}$. The reason for the increase in the BER was due to inter-symbol interference (ISI), since this modulation was generated with zero guard.

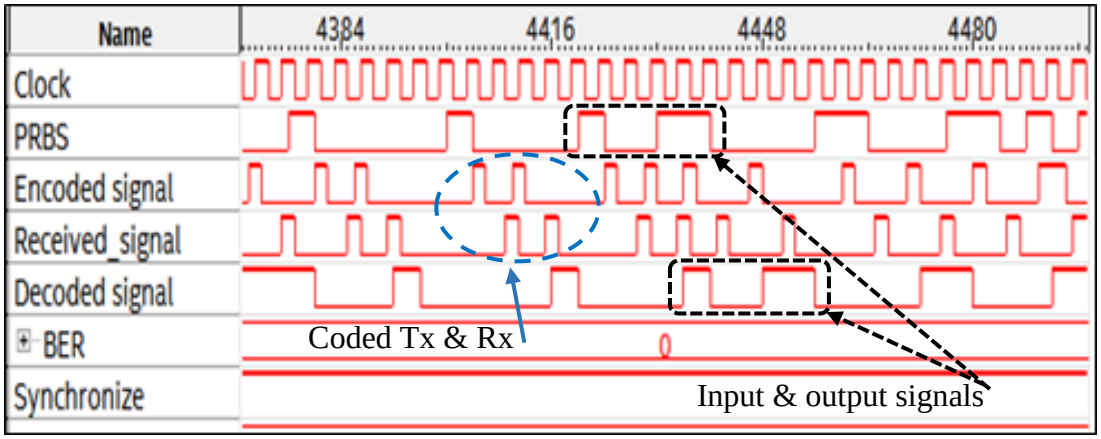

Figure 6-5: Waveforms of the DiPPM simulation

6.4 Implementation of Duobinary Pulse Position Modulation (Duo PPM)

Figure 6-6 depicts the block diagram of the VLC system-based Duo PPM. The experiment setup was implemented similarly to the steps of the previous modulation systems with switches, both the encoder and the decoder to the Duo PPM.

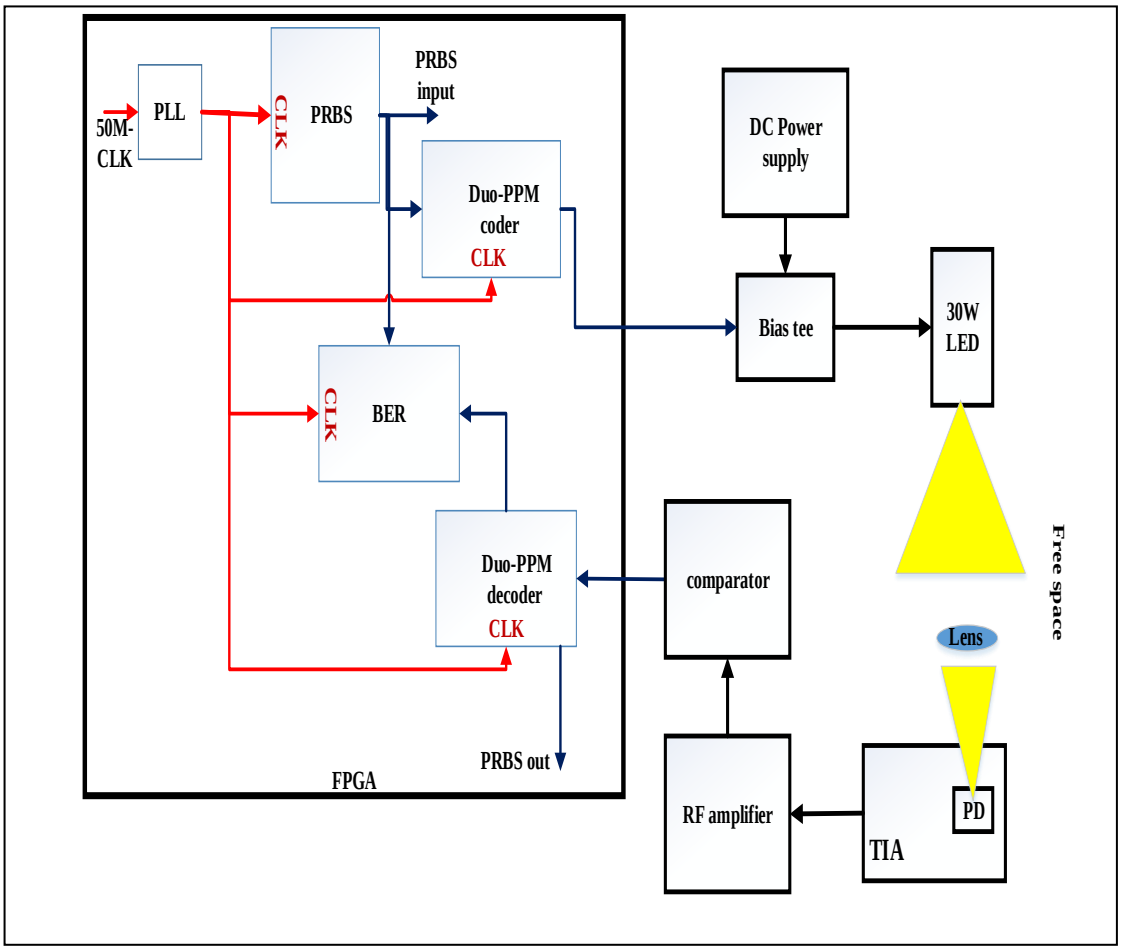

Figure 6-6:.Block diagram of the Duo-PPM based on VLC

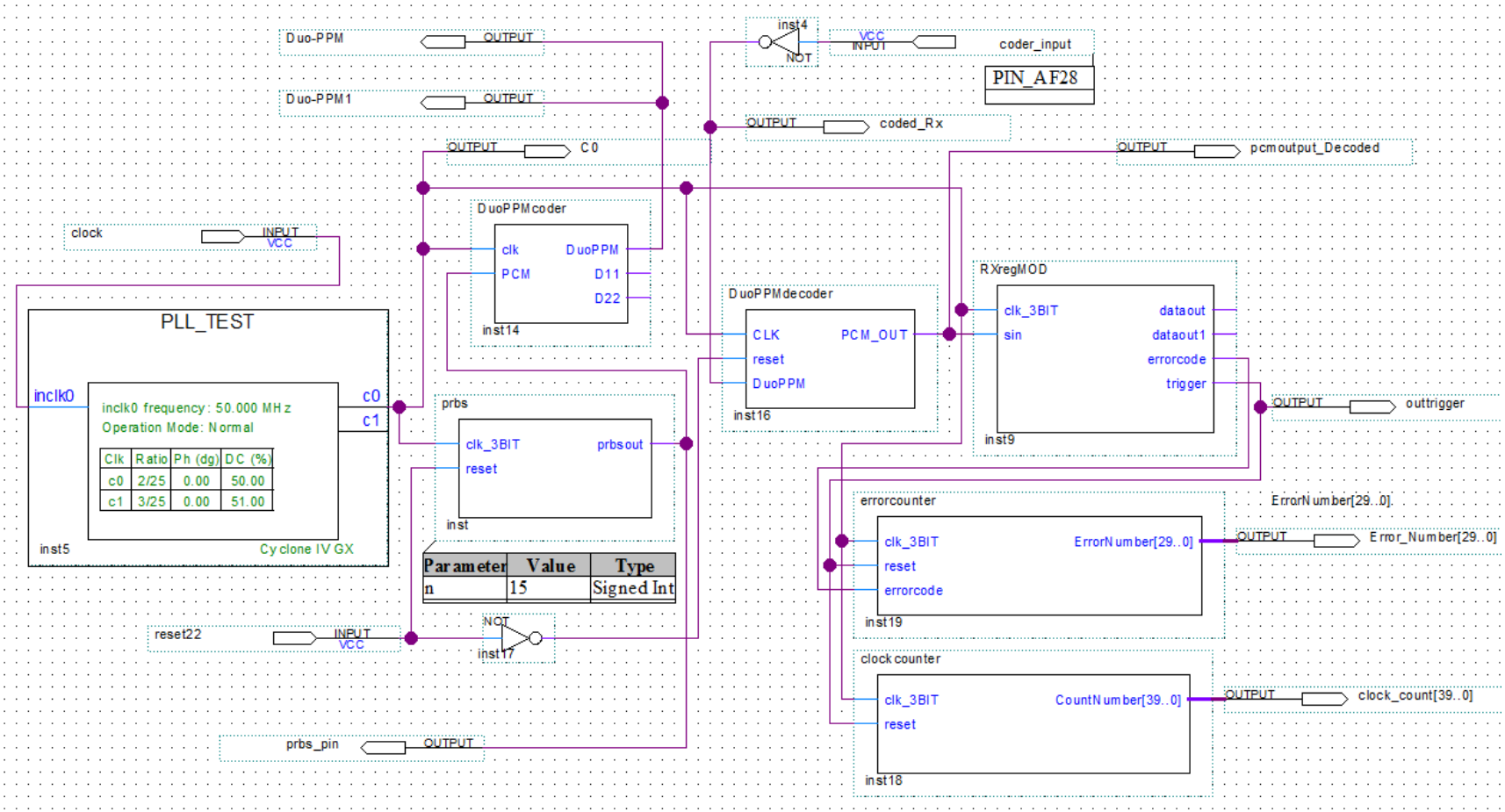

Figure 6-7: Logic circuit schematic of Duo-PPM

Figure 6-7 describes in full details the logic circuit schematic of Duo PPM using VHDL and the Quartus II software. The coder and decoder were improved by Farhat et al. to reach the maximum speed with the lowest error rates [133].

The clock pulses were generated using an FPGA, which was fed to the phase-locked loop (PLL) to control the selected frequency. The selection frequency was sent to the PRBS block to generate the PRBS signal using a VHDL code. The PRBS was delivered to the Duo PPM coder for signal coding, which was sent through the coaxial cable to an LED via the pin (Duo-PPM). The pin (Duo-PPM1) was connected to the oscilloscope to observe the transmitted signal. The received signal at the output of the comparator was sent to an FPGA to feed the Duo PPM decoder, to retrieve the original signal. Additionally, the output of the comparator was sent to the oscilloscope for comparison with the transmitted coded signal. The output signal from the Duo PPM decoder was delivered to the BER block for comparison with an original PRBS, as shown in Figure 6-7.

6.4.1 Results and discussion

Figure 6-8 presents the data pulses through oscilloscope at a transmission speed of 14 Mbps. The top trace and the bottom trace represent the input data signal (PRBS) and the received output data signal (decoded), respectively. The middle traces represent the encoded signals, where the upper signal represents the transmitted signal to the LED (encoded) and the lower signal represents the received signal from the comparator (received).

It can be seen that there is a match between the transmitted data and the received data. The decoded received signal is the same as the original PRBS signal. Moreover, there is a similarity between the encoded signal transmitted through the LED (encoded) and the received signal (received) at the receiver output. The FPGA board was connected to the computer to present the simulation signals via the signal tap II logic analyser using the Quartus II software to measure the BER, as shown in Figure 6-9. Similarly, there is a correspondence between the input signal (PRBS) and the output signal (decoded).

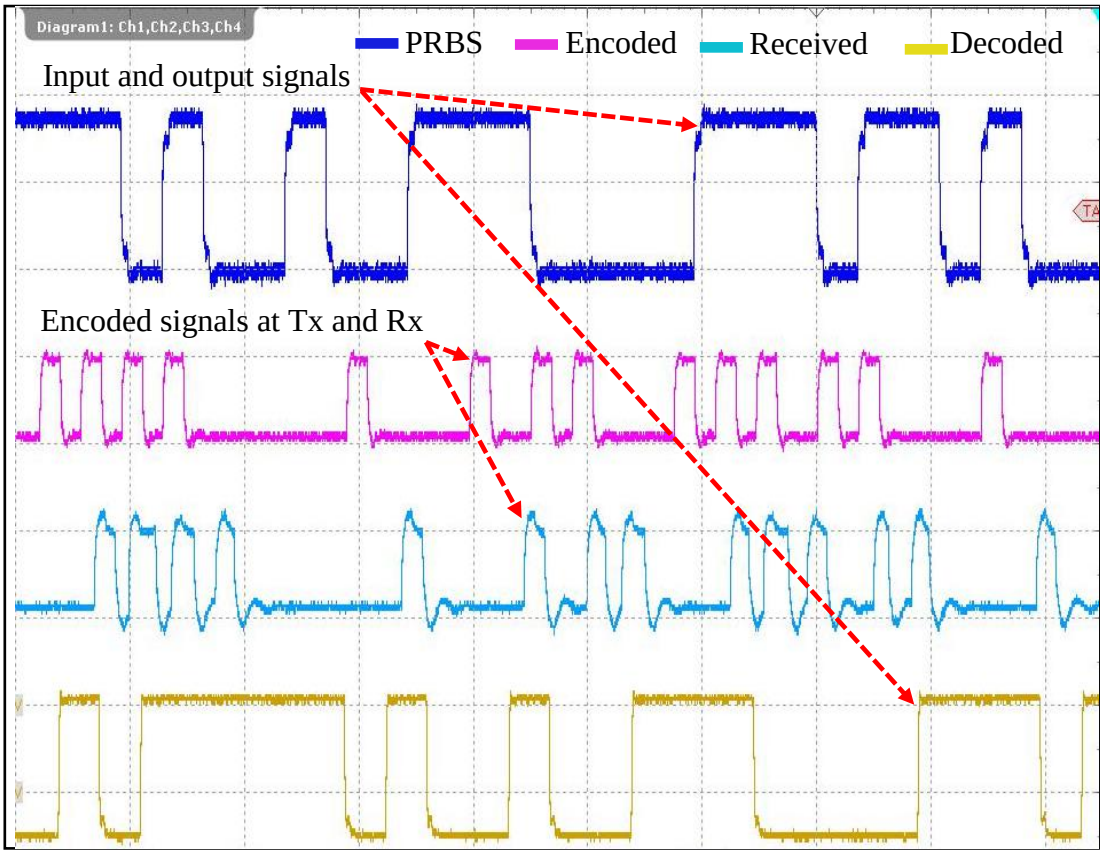

Figure 6-8: Real measurement signals of the Duo PPM via the oscilloscope

The same BER in the DiPPM was recorded which was < 10^{-11} up to 14 Mbps data rates, and above 10^{-9} at 14.5 Mbps. It was found that the BER increased for both modulations (DiPPM and Duo PPM) due to the ISI, which occurred due to the comparator bandwidth limitations, as shown in Figure 6-10.

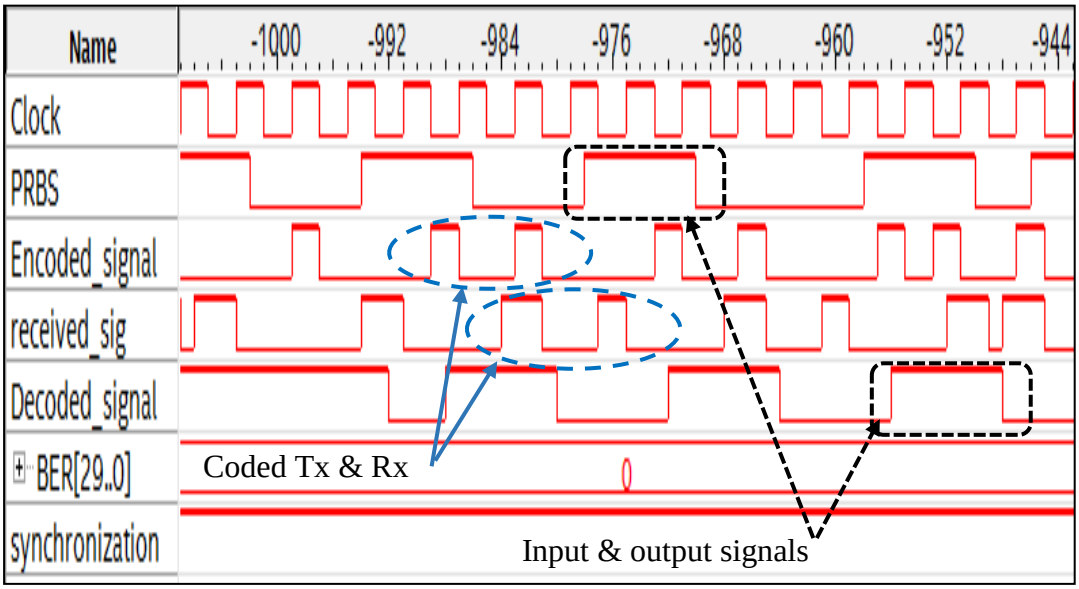

Figure 6-9: Waveforms of the Duo PPM simulation using signal tap II logic analyser

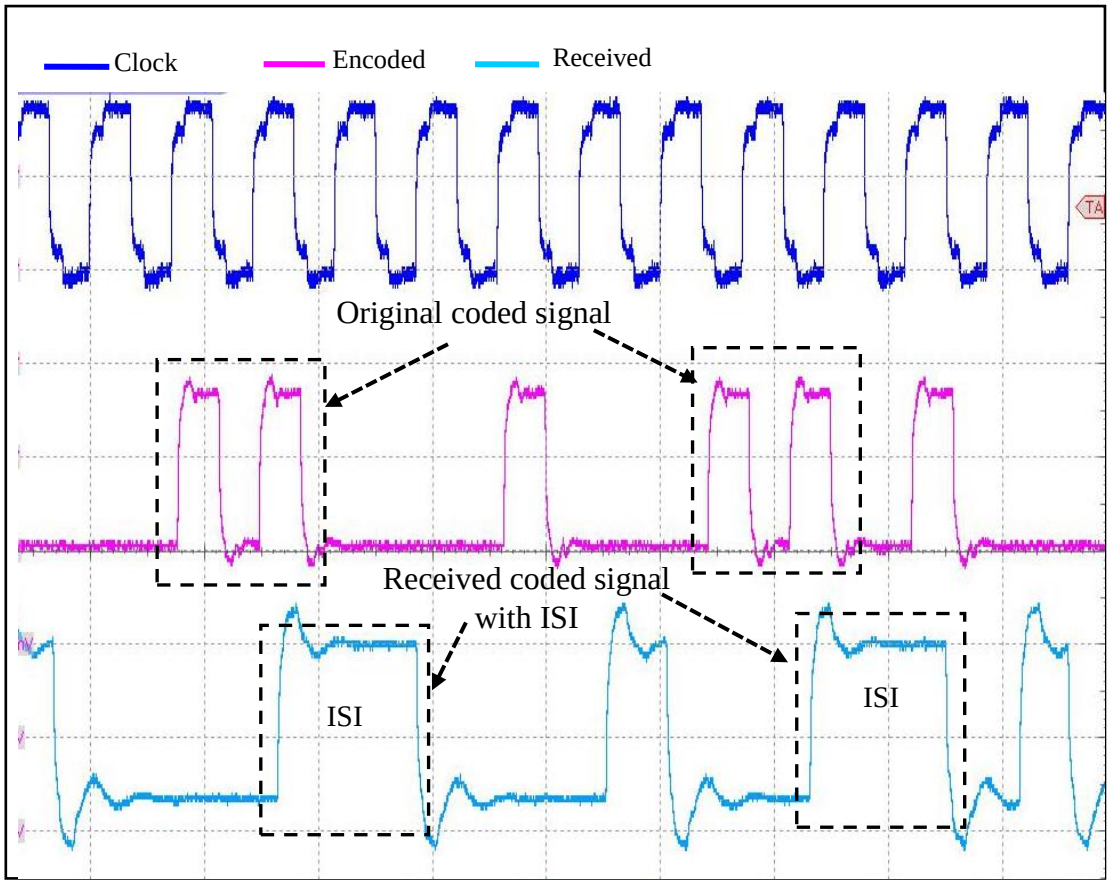

Figure 6-10: Typical effect of ISI

6.5 Offset Pulse Position Modulation (Offset PPM) Implementation

This was done applying the same measurements as mentioned earlier in the DiPPM but with the offset PPM coder and decoder, as illustrated in Figure 6-11. The simplicity of this technique is uncomplicated synchronization and in contrast to the DiPPM technique, where the signal is coded and converted from 3-bit to 4-bit. First, the 125 MHz clock was connected to the phase-locked-loop (PLL) to control the selection of the appropriate frequency. The selected frequency is fed to the 3-bit/4-bit clock signal via C0, which was fed the pseudorandom bit sequences (PRBS) and the offset PPM (coder/decoder). The PRBS signal was sent to the offset PPM coder to generate the offset PPM signal (convert from 3 bit to 4 bit), which was then sent to the high-power LED through the bias-T. The photodiode received the encoded transmitted signal that was sent through the light of an LED. The signal was processed through the TIA amplifier and the comparator, then sent to the FPGA through the coaxial cable via a pin (A27). The encoded signal was decoded through the offset PPM decoder to retrieve the original signal.

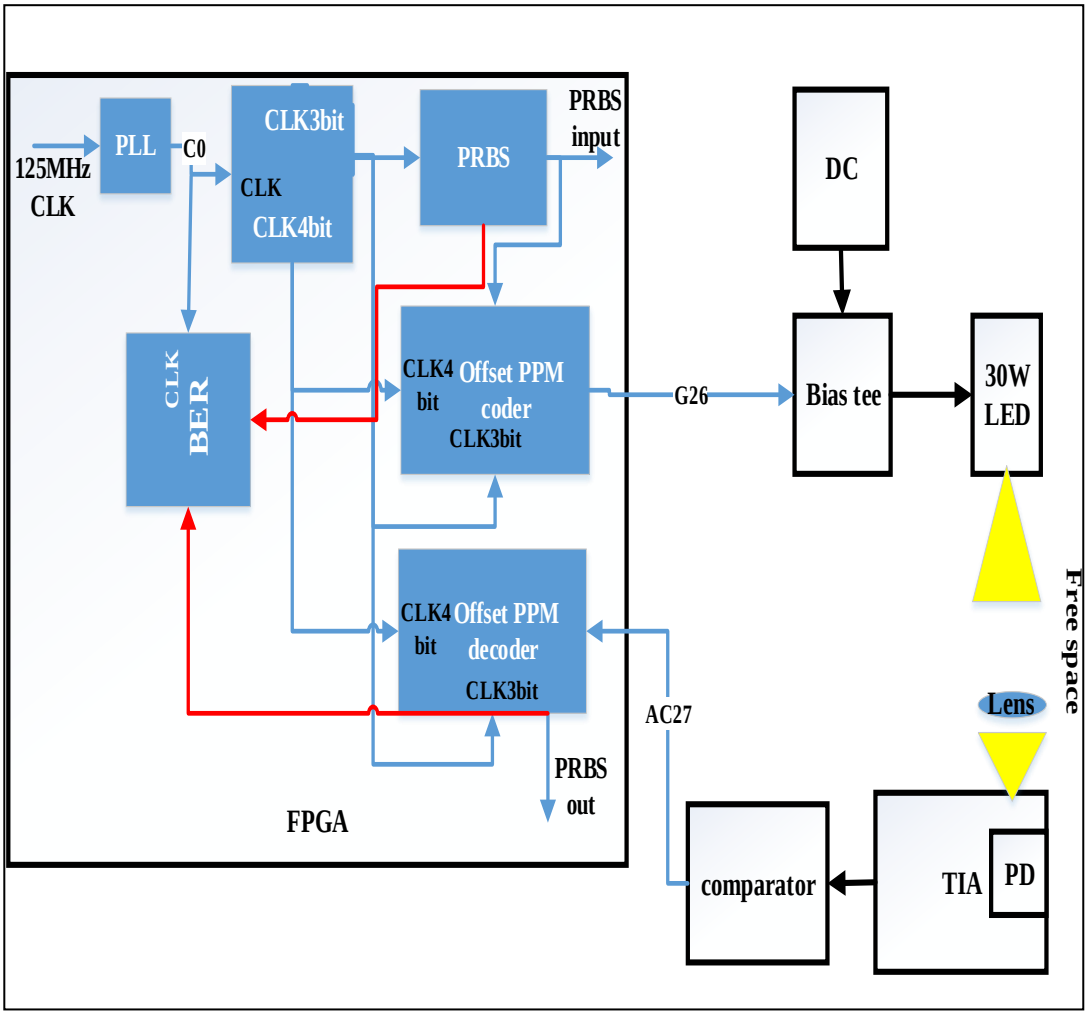

Figure 6-11: Block diagram of offset PPM based on VLC

Figure 6-12 depicts the block diagram of the offset PPM through the FPGA board using the VHDL programming language and Altera Quartus II software. A 125 MHz clock pulse was created using an FPGA, which was fed to the PLL to control the selected frequency. The selection frequency was sent to clock signal block to generate the 3-bit and 4-bit clock pulses. The 3-bit pulses were fed to the PRBS block to generate the PRBS signal, which was sent to the offset PPM coder. The encoded data was delivered to an LED through the bias-T via a pin (AE27), where the pin (AE26) was connected to the oscilloscope to observe the coded data. The LED was sent the encoded data with lighting to the photodiode.

The received data at the output of the comparator was sent to an FPGA to feed the offset PPM decoder, to retrieve the original data. Also, the output data from the offset PPM decoder was delivered to the oscilloscope for comparison with an original PRBS.

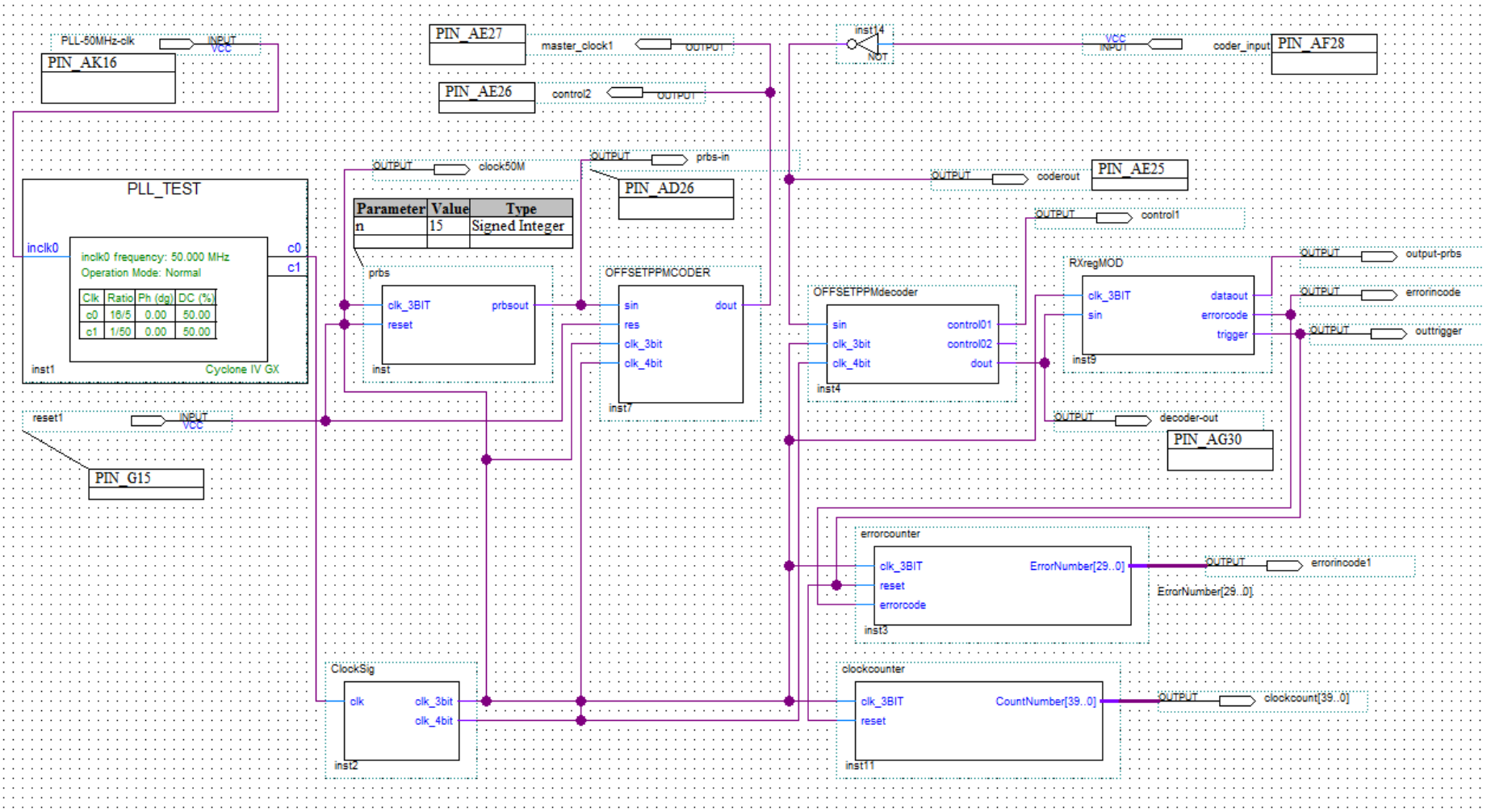

Figure 6-12: Logic circuit schematic of offset PPM

6.5.1 Results and discussion

The real signals via the oscilloscope are illustrated in Figure 6-13. The top trace represents the input data (PRBS), the second trace depicts the output decoded data (decoded). The third and bottom traces depict the encoded data which was transmitted to an LED (encoded), and the encoded data at the comparator output (received), respectively. It can be seen that there is a match in the signals between the input and the output signals, and there is a similarity between the transmitted signal, which was sent via LED with the received signal that was received from the receiver through the comparator output.

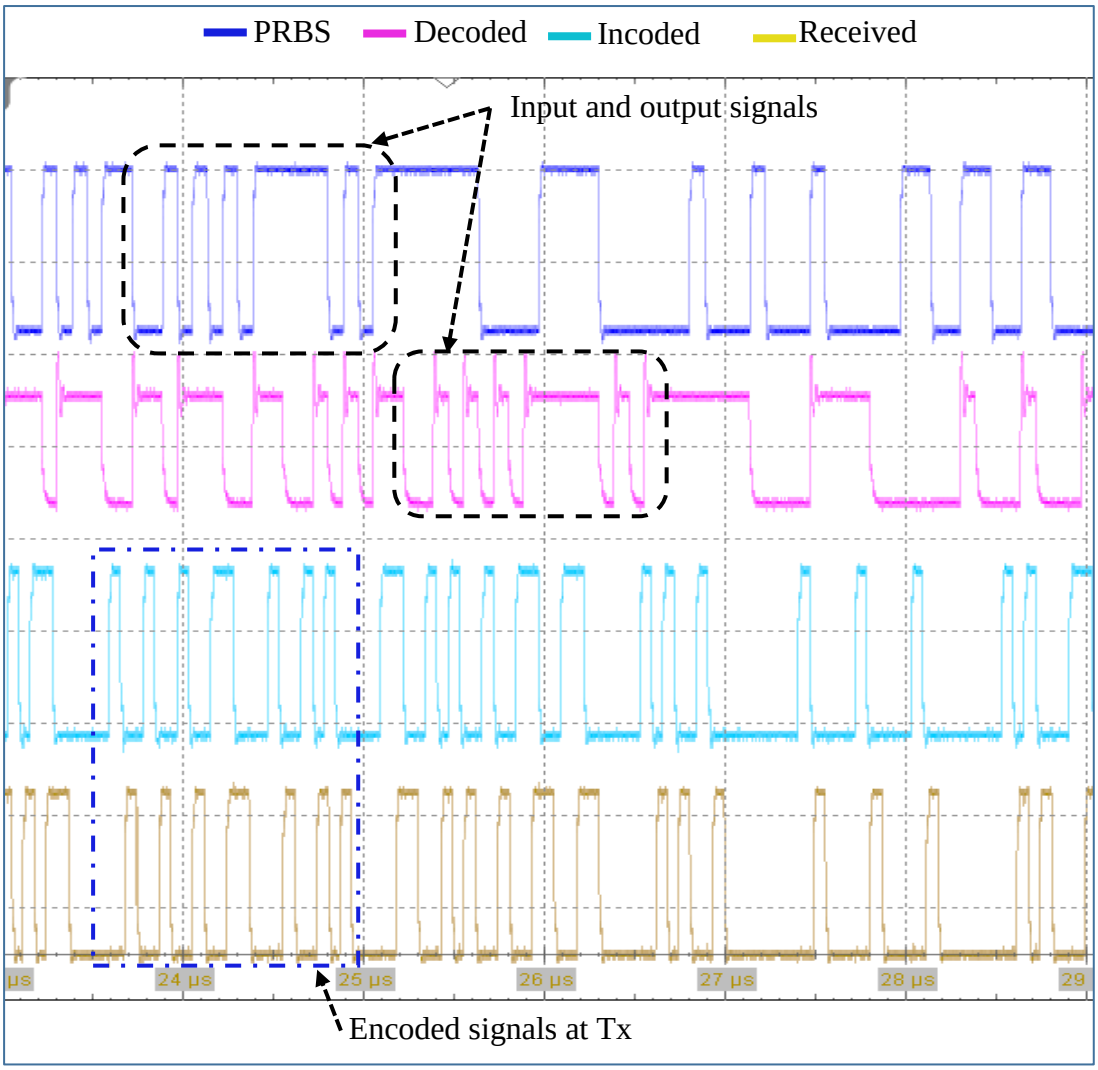

Figure 6-13: Real signals of offset PPM via the oscilloscope at 20 Mbps

Running the simulation of the offset PPM system with a clock and the PRBS input waveforms are illustrated on the timing diagram of the simulation in Figure 6-14. The waveforms of the input, output and coder signals are illustrated, and there is a

match between the input signal and the output signal including delays. There is also a similarity between the transmitted coded signals (coder Tx) with the received coded signal (coder Rx). However, the free error was recorded at 1.6 m free space distance at a 20 Mbps data rate, whilst 1.6×10^{-9} of BER was measured at 1.9 m distance with the same data rate.

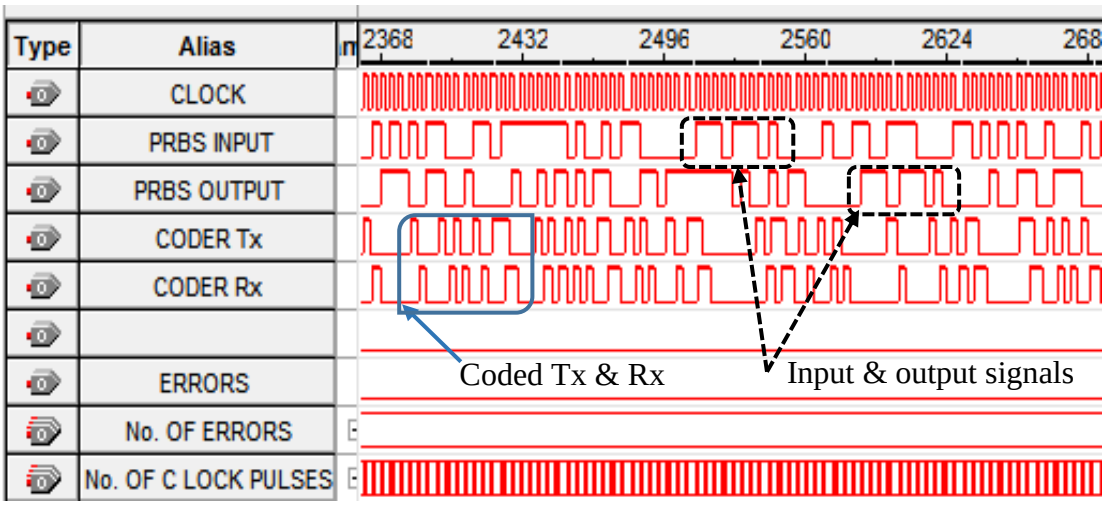

Figure 6-14: Waveforms of the offset PPM simulation

6.6 Summary

In conclusion, comparing the three types of modulation schemes have been summarised as follows.

The results were completely identical for both the DiPPM and Duo PPM, where the BER was less than 10^{-11} for up to 14 Mbps data rates. As the frequency increased to 14.5 Mbps, the BER also increased to $>10^{-9}$. The reason for the increase in the BER was due to the ISI, since both modulations were generated with zero guard. Whilst the offset PPM free error was recorded at 1.6 m free space distance and at a 20 Mbps data rate, whilst 1.6×10^{-9} of BER was measured at 1.9 m distance, at the same data rate.

It is clear that the offset PPM has higher speed and lower error rates than the DiPPM and Duo PPM, due to the offset PPM has the least impact on the ISI, where the coded signal occurs in the middle of pulses. Whereas, the encoding of the PPM and Duo PPM occur at the end edge of each pulse, which makes it more susceptible to ISI.

Chapter 7

VLC Simulation Model using MATHCAD

7.1 Introduction

Important parameters were determined such as preamplifier input noise, DC channel gain, signal propagation delay, receiver noise, probability of pulse errors and receiver sensitivity. These elements are required knowledge for calculations depending on the design of the transceiver system (receiver sensitivity) including the MATHCAD program, which will be used in this chapter to calculate receiver sensitivity.

7.2 Channel Model for Single LED

A major step in VLC design is understanding the limitations of the optical wireless channel. It is necessary to have a precise channel model to accurately predict the performance of the VLC system. Figure 7-1 depicts the geometry of the optical transmitter, receiver and reflectors for indoor VLC with one LED. The figure shows the illumination pattern from an LED to the photodiode. It can be seen that the line of sight (LOS) light with incidence ($\varphi_{i,j}$) and irradiance ($\theta_{i,j}$) angles as well as diffused light are reflected from the walls to the photodiode with angles α and β.

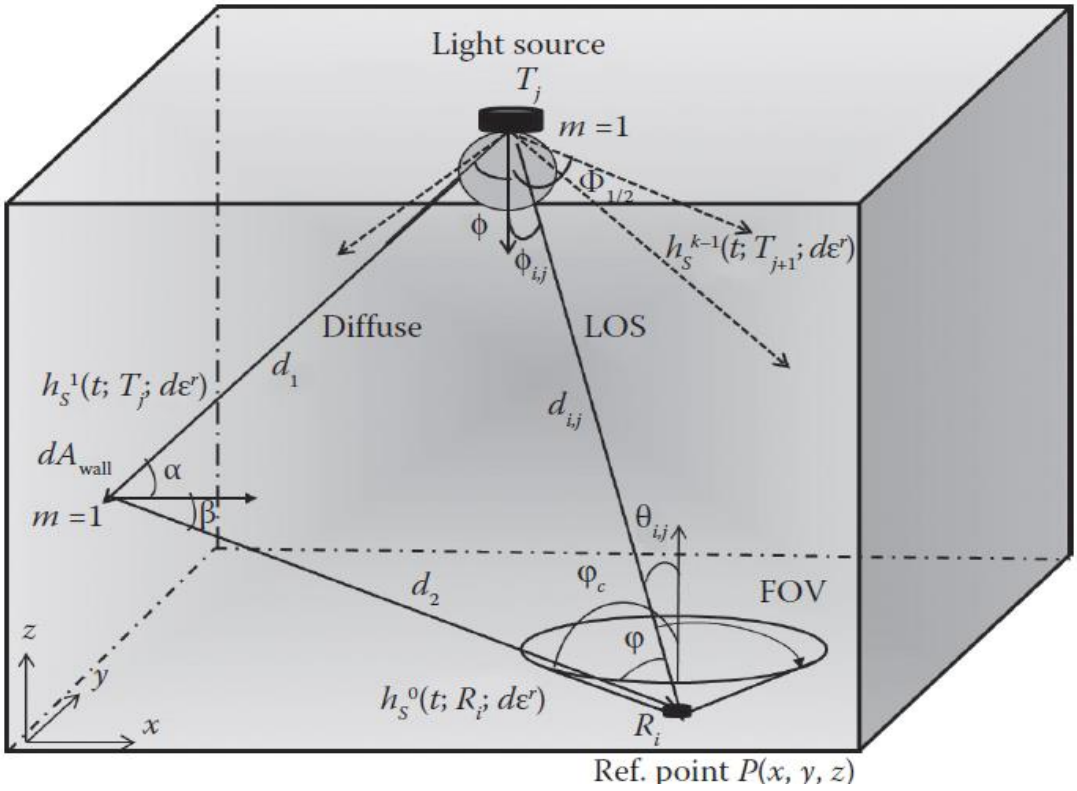

Figure 7-1: Geometry of optical Tx, Rx and reflectors [2]

In this chapter, channel modelling for the VLC system mainly focusses on a vertical LOS, which is addressed as shown in Figure 7-2. Experiments were carried out in a room with dimensions 8.5 m X 6 m X 3.5 m, and the 30 W LED was used with house dimensions of 0.22 m X 0.18 m, and beam angle (ϕ) of 120° at 1.9 m free space distance between the LED and the photodiode (PD), as shown in Figure 7-2. This makes the lighting more concentrated in the area with less room size. Therefore, the effect of reflection of lighting from the walls is too small and can be neglected as well as the incidence ($\varphi_{i,j}$) and irradiance ($\theta_{i,j}$) angles are set to zero degrees.

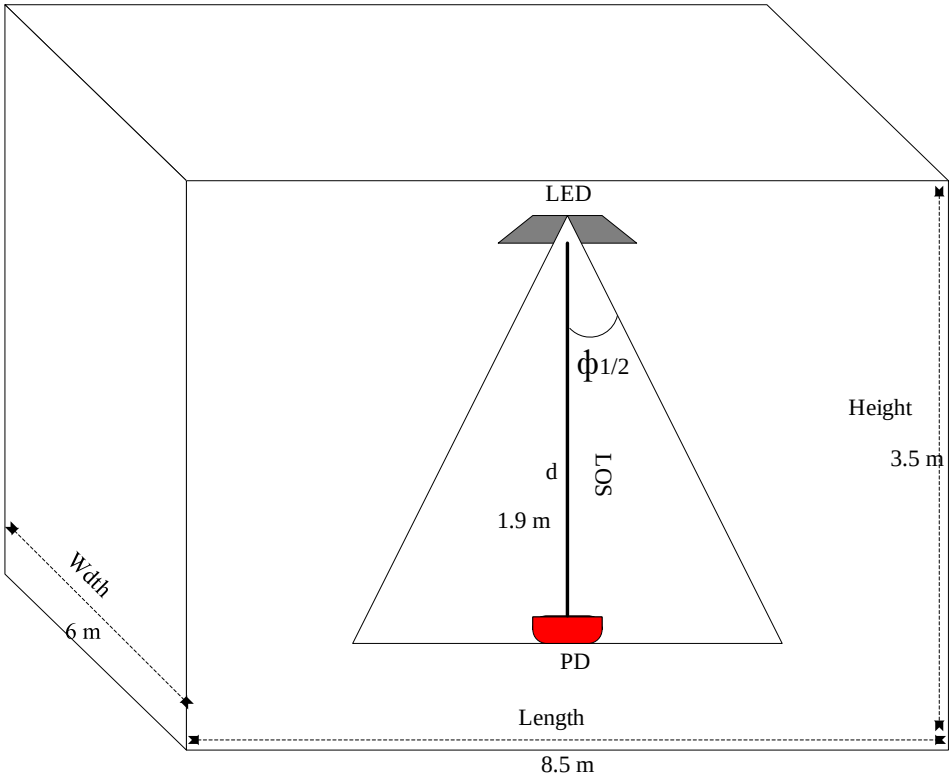

Figure 7-2: Geometry of the VLC system

In this simulation, a BER of 10^{-9} was employed, which was obtained in previous experiments, at a speed of 20 Mbps and 1.9 m distance transmission to determine the average received power required and receiver sensitivity. The system was evaluated according to the following main algorithms:

- Initially, a VLC impulse response signal $h_{(t)}$ was generated, which depended on the Gaussian input pulse shape (pulse (t)).
- In the second algorithm, the received pulse shape I_0 was determined and plotted. From the knowledge of the received pulse shape, the time at the

centre of the peak pulse t_{pk} and the peak voltage of the received pulse v_{pk} was found.

- The third algorithm calculated the noise bandwidth from the knowledge of the preamplifier cut-off frequency f_c.
- For the fourth algorithm, the probability error sources were determined, based on the knowledge of the previous algorithms.
- For the fifth algorithm, the standard of performance was that the probability of total error must be identical for the PCM (one error in 10^9).
- For the sixth algorithm, the received power was determined (P_r) regarding the minimum number of a photons (min(a)).
- Finally, the receiver sensitivity was defined in (dBm) using the knowledge of the received power which is, $P_{rdBm} = 10\log(\frac{P_r}{1mW})$.
- The improvement of the MATHCAD simulation was considered in order to achieve the reliability of the experimental and theoretical results.

7.3 Photodiode Responsivity

The definition of the photodiode responsivity $R(\lambda)$ is the ratio of the photodiode current in A to the radiant power in W (A/W), depended on the photodiode wavelength and is defined by [2, 28].

$$R(\lambda) = \frac{I_D}{P} = \frac{\eta q}{hv} \qquad 7\text{-}1$$

Where, I_D denotes the photodiode current, P is the radiant power, η is the quantum efficiency, q is an electron charge and hv denotes photon-energy, which is given by:

$$hv = \frac{h.c}{\lambda} \qquad 7\text{-}2$$

Where, h is a Planck's constant, c is the velocity of light and λ is the wavelength of the photodiode.

7.4 Analysis of Noise and Signal Response

7.4.1 DC channel gain of LOS

The Lambertian emission pattern (m) for emitted light from an LED is given by [83]:

$$m = \frac{-ln2}{\ln(\cos(\phi_{1/2}))} \quad 7\text{-}3$$

Where, $\phi_{1/2}$ represents the semi-angle at half illuminance of the transmitter. Therefore, the DC-channel gain of LOS is expressed by:

$$L_0 = \frac{(m+1)A_{PD}}{2\pi {d_0}^2}.cos^m(\phi_0).\cos(\theta_0)7 \quad 7\text{–}4$$

Where, A_{PD} represents the photodiode active, d_0 represents the LOS distance between the transmitter (LEDs in this research), the transmitter was positioned vertically on the receiver (photodiode), where ϕ_0 and θ_0 equal to zero, then the equation can be written:

$$L_0 = \frac{(m+1)A_{PD}}{2\pi {d_0}^2} \quad 7\text{-}5$$

7.4.2 VLC impulse response

Suppose the shape of input pulse property $h_p(t)$ is given by the following formula [97, 134, 135]:

$$\int_{-\infty}^{\infty} h_p(t)\,dt = 1 \quad 7\text{-}6$$

Then, the preamplifier output voltage is expressed as:

$$v_o(t) = bhvR_0\left(\ Z_{pre}(t) \times h_p(t)\right) \quad 7\text{-}7$$

$$v_0\,(t) = \frac{b\eta q}{2\pi}\int_{-\infty}^{\infty} H_p(\omega)\,Z_{pre}(\omega).e^{j\omega t}d\omega \quad 7 \quad 7\text{–}8$$

Where, b is the photons number per pulse, hv denotes the photon-energy, , $Z_{pre}(\omega)$ the frequency related to TIA, R_0 is the photodiode responsivity, η is the photodiode quantum efficiency, q denotes the charge of electron and $H_p(\omega)$ denotes the Fourier transform of $h_p(t)$.

The Gaussian input pulse shape is assumed as:

$$h_p(t) = \frac{1}{\sqrt{2\pi\alpha^2}}.\exp\left(-\frac{t^2}{2\alpha^2}\right) \quad 7\text{–}9$$

and

$$H_p(t) = \exp\left(-\frac{\alpha^2\omega^2}{2}\right) \quad 7\text{-}10$$

Where, α the pulse variance is given by:

$$\alpha = \frac{0.1874\,T_b}{f_n} \quad 7\text{-}11$$

Where, f_n is the normalised bandwidth of the system.

7.4.3 Input noise at TIA

The noise is another important aspect of a TIAs design, which is produced by the electronic components of the circuit. Combined effects of statistically independent noise sources have a significant impact on a TIA's performance [2, 136]. The total input mean square noise current for TIA is given by [120]:

$$\langle i^2 \rangle = \frac{4KT}{R_f} + 2qI_b + \frac{2qI_{c1}}{{g_{m1}}^2}\left[\frac{1}{R_f^2} + f^2(2\pi C_T)^2\right] \qquad 7\text{–}12$$

Where, K is Boltzmann's constant, $K = 1.38 \times 10^{-23}$, T is absolute temperature (kelvin) $T = 300K$, B is data rate, R_f is feedback resistor, $q = 1.6 \times 10^{-19}\ C$ is electron charge, $g_{m1} = \frac{1}{r_e} = \frac{I_{c1}}{25\ mV}$, and $C_T = C_d + C_{c1} + C_\pi$

$C_\pi = \frac{1}{2\pi f_T r_e} - c_c$ where, c_c is the collector capacitance and f_T is the transition frequency for the transistor BFR92A.

Table 7-1 illustrates the VLC system parameters for the simulation model. The collector current for the first stage of the TIA is:

$$I_{C1} \approx I_{E1} = \frac{V_{BE}}{R_E} = \frac{0.7}{1.2\ K\Omega} = 0.583\ mA$$

$$Then,\ r_e = \frac{25\ mV}{I_{C1}} = \frac{25\ mV}{0.583\ mA} = 42.88\ \Omega$$

$$g_m = \frac{1}{r_e} = 0.0233$$

$$C_\pi = \frac{1}{2\pi f_T r_e} - c_c = \frac{1}{2\pi \times 5\ GHz \times 42.88\ \Omega} - 0.6\ \text{PF}$$

$$C_\pi = 0.14\ \text{PF}$$

$$C_T = C_d + C_{c1} + C_\pi = 35\ PF + 0.6\ Pf + 0.14\ PF = 35.74\ PF$$

$$\langle i^2 \rangle = \frac{4KT}{R_f} + 2qI_bI_2 + \frac{2qI_{c1}}{{g_{m1}}^2}\left[\frac{1}{R_f^2} + B^2(2\pi C_T)^2\right]$$

$$\langle i^2 \rangle = 14.4 \times 10^{-24}\ \ {}^{A^2}/_{H}$$

Table 7-1: System Parameters for VLC

System Parameters	
PCM symbols	n = 10
PCM bits	N = 3
data rate	B = 20 Mbps
Quantum efficiency	$\eta = 100\%$
Electron charge	$q = 1.602 \times 10^{-19}$ C
Planck's constant	$H = 6.624 \times 10^{-34}$ Js
Velocity of light	3×10^{8} *m/s*
Photon-energy	$h.c/\lambda$
Boltzmann's constant	$K = 1.38 \times 10^{-23}$
TIA Parameters	
Bandwidth	13 MHz
Input noise	$\langle i^2 \rangle = 25 \times 10^{-24} A^2/Hz$
BER	10^{-9}
signal-to-noise parameter(Q) at BER of 10^{-9}	6
Transition frequency of the transistor	$f_T = 5\ GHz$
Si Photodiode Parameters (OSD5-5T)	
Wavelength Range (λ)	400 to 1100 nm
peak Wavelength (λ_p)	820 nm
Responsivity R(λ_p)	$R_o = 0.66$ A/W
Dark Current I_D	1 nA
Photodiode Load Resistor R_L	50 Ω
Active area (A_{PD})	*5 mm²*

7.4.4 Measurement of the input current white noise

To measure the input white noise, first the received power level in the absence of a signal needs to be measured. Knowing the power level, the input white noise (i^2) can be calculated as follows:

-138 dBm is the measured received power level when the signal is absent $P_{r.abs}$.

$$P_{r.abs} = 10\log(\frac{P_o}{1mW})$$

$$P_o = 1.6 \times 10^{-17}\ \frac{W}{Hz}$$

$$V^2 = P_o \times 50\ \Omega = 8 \times 10^{-17}\ \frac{V^2}{Hz}$$

$$i^2 = \frac{V^2}{{R_f}^2} = 25 \times 10^{-17}\ \frac{A^2}{Hz}$$

Where, $R_f = 5.6\ K\Omega$ is the feedback resistor for the TIA.

7.5 Error Sources Probability

Using the equations from 4–4 to 4–9 in Chapter Four, the total probability of errors can be calculated for each of the three types of modulation techniques, as mentioned below.

7.5.1 DiPPM and Duo PPM

- **Wrong slot errors**

Error probability of the equivalent PCM for [96, 137] is given by [100]:

$$P_{ewsSR} = P_{ewsRS} = \sum_{x=0}^{n-1} \left(\frac{1}{2}\right)^{x+3} P_s(x+1) + \left(\frac{1}{2}\right)^{x+2} P_s(\mathrm{n}+1) \qquad 7\text{-}13$$

Therefore, the total error probability can be expressed as follows [138]:

$$P_{ewsDiPPM} = P_{ewsSR} + P_{ewsRS}$$

$$P_{ewsDiPPM} = P_{ewsDuo\ PPM} = 2.\sum_{x=0}^{n-1} \left(\frac{1}{2}\right)^{x+3} P_s(x+1) + \left(\frac{1}{2}\right)^{x+2} P_s(\mathrm{n}+1) \qquad 7\text{-}14$$

- **Erasure Errors**

For a DiPPM and Duo PPM, the equivalent PCM error probability [137, 138] can be expressed as:

$$P_{erDiPPM} = P_{erDuo\ PPM} = 2.\left(\sum_{x=0}^{n-1} \left(\frac{1}{2}\right)^{x+3} P_{er}(x+1) + \left(\frac{1}{2}\right)^{x+2} P_{er}(\mathrm{n}+1)\right) \qquad 7\text{-}15$$

- **False-alarm Errors**

The total equivalent PCM error probability generated by a false alarm error for the DiPPM and Duo PPM is given by [96, 137-139]:

$$P_{efDiPPM} = P_{efDuo\ PPM} = 2.\left(\sum_{x=0}^{n-1}\sum_{k=0}^{x}\left(\frac{1}{2}\right)^{x+3} P_f(x+1-k) + \sum_{k=0}^{n}\left(\frac{1}{2}\right)^{x+2} P_f(\mathrm{n}+1-\mathrm{k})\right) \quad 7\text{-}16$$

7.5.2 Offset PPM

The probability of erasure errors in offset PPM occurs when any '1' positions of code-word are reset to '0'. The probability of false alarm errors in offset PPM occurs when any '0' positions of the code-word are reset to '1'. The probability of wrong slot errors in offset PPM occurs when any '1' positions of the code-word are moving to the left or right. Table 7-2 shows the error probability of each code-word and the average probability.

Table 7-2: Average Probability of Offset PPM Errors

PCM	Offset PPM	Probability of Erasure	Probability of False alarm	Probability of the Wrong slot	
				left	right
000	0000	0	1.25	0	0
001	0001	1	1	2	0
010	0010	1	1	1	2
011	0100	2	1.666	3	1
100	1000	1	1.3333	0	3
101	1001	1	2	2	2
110	1010	1	2	1	2
111	1100	1.5	2	0	1
average Probability (E_{av})		E_{av}= 0.35	E_{av}= 0.51	E_{Lav}= 0.375	E_{Rav}= 0.458

- **Wrong slot errors**

The error probability of the equivalent PCM for the offset PPM is given by [73]:

$$p_s = E_{Lav}(0.5erfc\left(\frac{Q_s}{\sqrt{2}}\right) + E_{Rav}(0.5erfc\left(\frac{Q_s}{\sqrt{2}}\right)7 \quad 7\text{–}17$$

Where, E_{av} the average probability of errors.

- **False Alarm Errors**

The probability of false alarm errors is given by [111-113]:

$$p_f = E_{av}\left(\frac{t_s}{\tau_r}\right) 0.5erfc\left(\frac{Q_t}{\sqrt{2}}\right) \quad 7\text{–}18$$

- **Erasure Errors**

The probability p_{er} for offset PPM is given by [112]:

$$p_{er} = E_{av}[0.5erfc\left(\frac{Q_{er}}{\sqrt{2}}\right)] \quad 7\text{-}19$$

7.6 Received Optical Power

The optical power is required for the DiPPM and Duo PPM systems and is given by [96]:

$$P_{DiPPM} = \left(\frac{bhv}{(gu+2}\right).\left(\frac{n+1}{2.n}\right).B \quad 7\text{-}20$$

Similar to the DiPPM, the optical power is required for the Duo PPM and is expressed as [113]:

$$P_{Duo\ PPM} = \left(\frac{bhv}{2}\right).\left(\frac{n+1}{2.n}\right).B \quad 7\text{-}21$$

Where, b represents the number of photons per pulse, n represents the maximum number of like symbols for the DiPPM, B is the bit rate and gu represents the guard intervals. In these experiments, the DiPPM is used with zero guard intervals.

Similarly, with the offset PPM, the required optical power is expressed as [113]:

$$P_{Offset\ PPM} = \left(\frac{bhv}{3}\right).B \quad 7\text{-}22$$

7.7 Simulation Results and Discussions

In this chapter, the simulation of the VLC system was performed by calculating the sensitivity of the receiver. The simulation has been subjected to operating conditions that have been used in practice experiments.

7.7.1 DiPPM simulation

The system simulation was carried out at the data transmission of 20 Mbps (appendix C). Figure 7-3 depicts the VLC received pulse for the DiPPM technique, which is used to find the peak time (t_{pk}) and peak voltage (v_{pk}). There are ripples in

the signal due to storage in the filter of the preamplifier filter combination and the short duration of the input pulse.

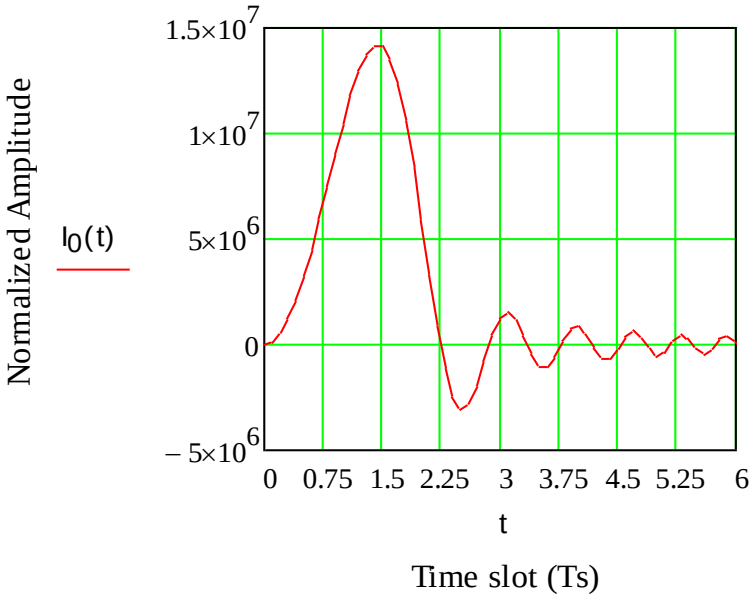

Figure 7-3: Received pulse for DiPPM at 20 Mbps

The simulation results have proved that the system has high sensitivity up to -36.6 dBm. From another perspective, to investigate the performance of the VLC system based on DiPPM, the VLC system was simulated at the data rate of 100 Mbps (appendix D). From Figure 7-4, it can be seen that the signal amplitude increased by up to five times with the increase in transmitter rates, which is an indication of the reduction of the sensitivity. The sensitivity diminished by -3.5 dBm at 100 Mbps data transmission.

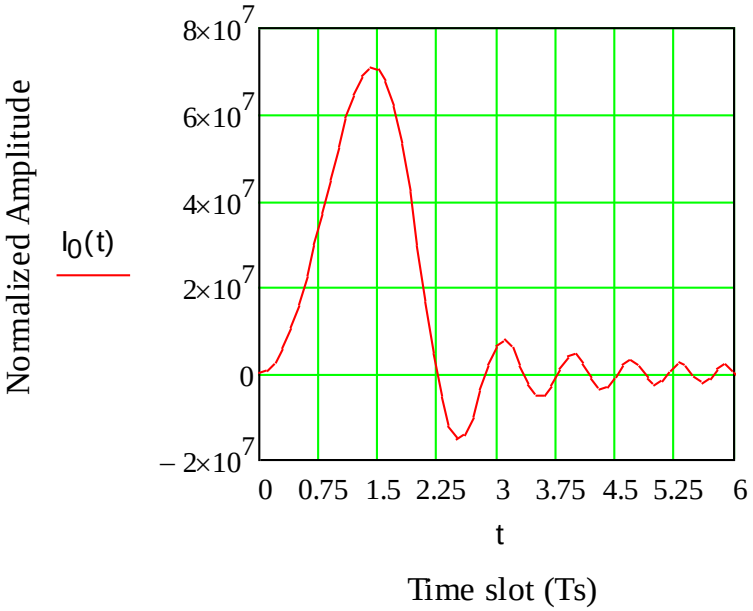

Figure 7-4: Received pulse for DiPPM at 100 Mbps

7.7.2 Duo PPM simulation

For a Duo PPM system, the process is similar to a DiPPM system. From Figure 7-5 and Figure 7-6, it can be observed that the received pulse for a Duo PPM is identical to a DiPPM received pulse. The difference was only in receiver sensitivity, which was caused by an error probability. The Duo PPM has -0.6 dBm better sensitivity than the DiPPM (appendix E).

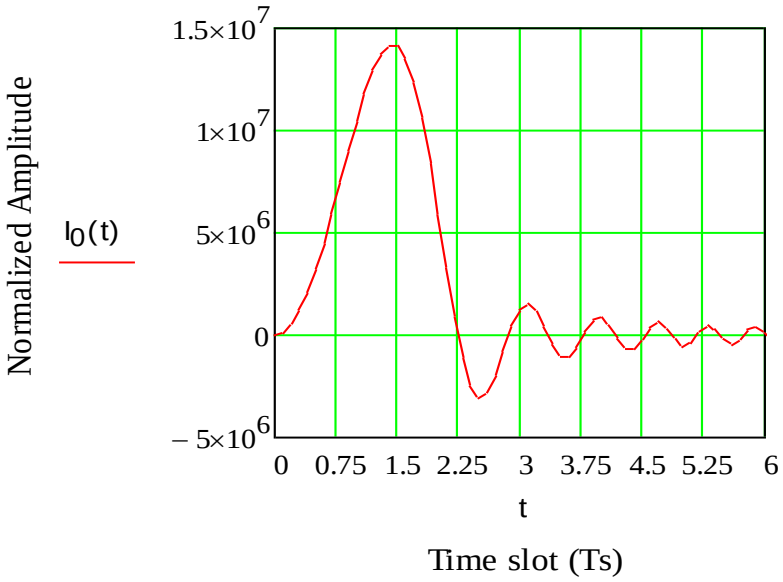

Figure 7-5: Received pulse for Duo PPM at 20 Mbps

The transmission speed was increased to 100 Mbps to ensure system scalability for high data rates. The results proved that the possibility of using Duo PPM for high speeds of up to100 Mbps, where the sensitivity was -33.73 (appendix F).

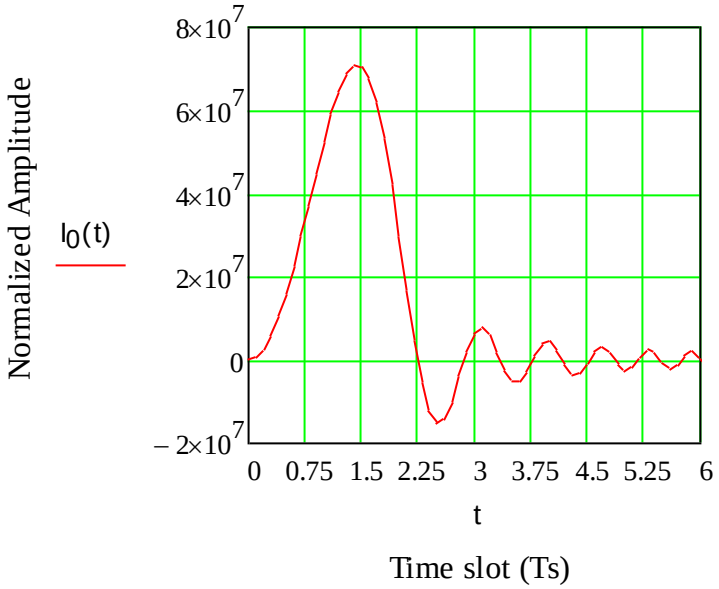

Figure 7-6: Received pulse for Duo PPM at 100 Mbps

7.7.3 Offset PPM simulation

Similar to the DiPPM, the system was simulated with the same conditions. Figure 7-7 shows the received pulse response at 20 Mbps data rate, the receiver sensitivity was achieved to -35.7 dBm, which was less than the DiPPM (appendix G).

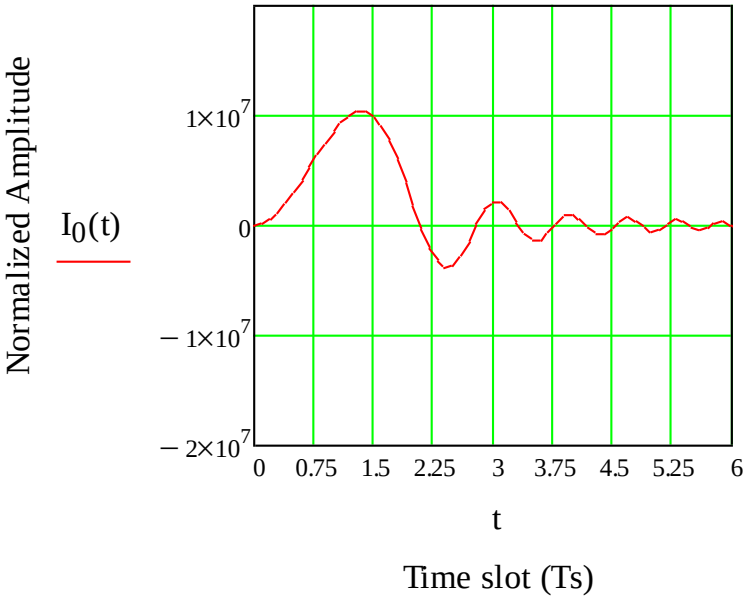

Figure 7-7: Received pulse for offset PPM at 20 Mbps

To investigate the performance of the VLC system based on Offset PPM, the VLC system was simulated at the data rate of 100 Mbps. From Figure 7-8, it can be seen that the amplitude is increased at by increasing transmitter rate, which the sensitivity was reduced to -32.21 dBm (appendix H).

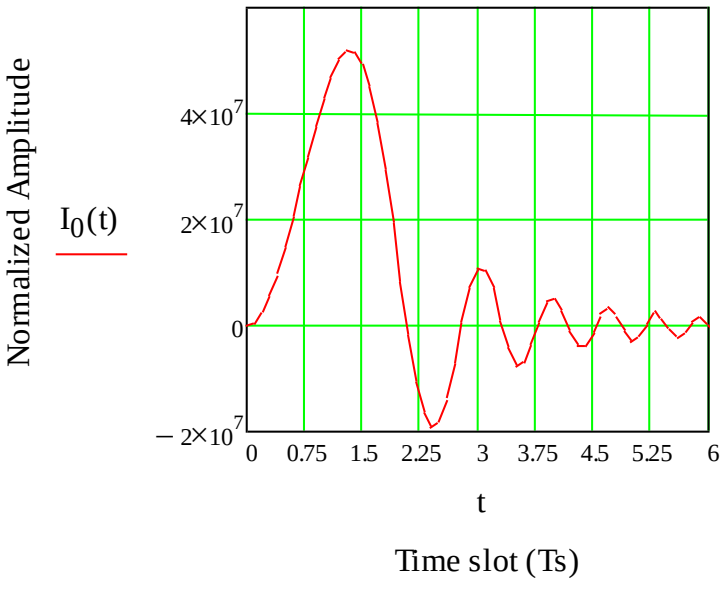

Figure 7-8: Received pulse for offset PPM at100 Mbps

Table 7-3 illustrates the results of the average received power and receiver sensitivity, obtained from the simulation using the MATHCAD software at 20 Mbps. From the table it can be seen that all techniques have a high sensitivity that goes beyond -35 dBm. The duo PPM has a higher sensitivity than the DiPPM and offset PPM by the rate of -0.6 dBm and -1.5 dBm respectively. Whilst received power required was recorded a maximum difference of 0.08 between an offset PPM and Duo PPM.

Table 7-3: Simulation Results at 20 Mbps

Modulation technique	**DiPPM**	**Duo PPM**	**Offset PPM**
Average received power (μW)	0.218	0.189	0.269
Sensitivity, dBm	-36.6	-37.22	-35.7

In Table 7-4 similarly, when the transmission rate is increased to 100 Mbps, The sensitivity rate is decreased by the constant average for all modulation techniques, which is -3.49 dBm, while the Duo PPM keeps the best sensitivity.

Table 7-4: Simulation Results at 100 Mbps

Modulation technique	DiPPM	Duo PPM	Offset PPM
Average received power (μW)	0.488	0.423	0.601
Sensitivity, dBm	-33.11	-33.73	-32.21

7.8 Model Evaluation of VLC Simulation

The receiver sensitivity is theoretically predicted, depending on the calculation of the input noise at the receiver. To take advantage of them, knowing the characteristic of noise at the output of the amplifier is required. Different methods will be used to evaluate the sensitivity of the receiver, which are listed as follows:

- **Method 1:**

The receiver sensitivity ($P_{rs(dBm)}$) is the minimum average optical power for a given BER, which can be calculated from the following equation:

$$P_{rs} = \frac{Q}{R_o}\sqrt{(noise_{BW}\langle i_n^2\rangle)} \qquad 7\text{-}23$$

$$P_{rs(dBm)} = 10\log(\frac{P_{rs}}{10^{-3}}) \qquad 7\text{-}24$$

Where, R_o is the responsivity of the photodiode, Q is the signal-to-noise parameter which depends on the BER, as shown in Figure 7-9, and $noise_{BW}$ is the bandwidth of the noise, which given by:

$$noise_{BW} = \frac{\pi}{2}.f_c \qquad 7\text{-}25$$

Where, f_c represents the cut-off frequency, which is expressed by:

$$f_c = 0.5/T_s \qquad 7\text{-}26$$

Where, T_s is the slot time, which depends on the modulation technique.

$$P_{rs} = \frac{6}{0.66}\sqrt{31.4 \times 10^6 \times 25 \times 10^{-24}} = 2.55 \times 10^{-7}\ W$$

$$P_{rs(dBm)} = -35.94\ dBm$$

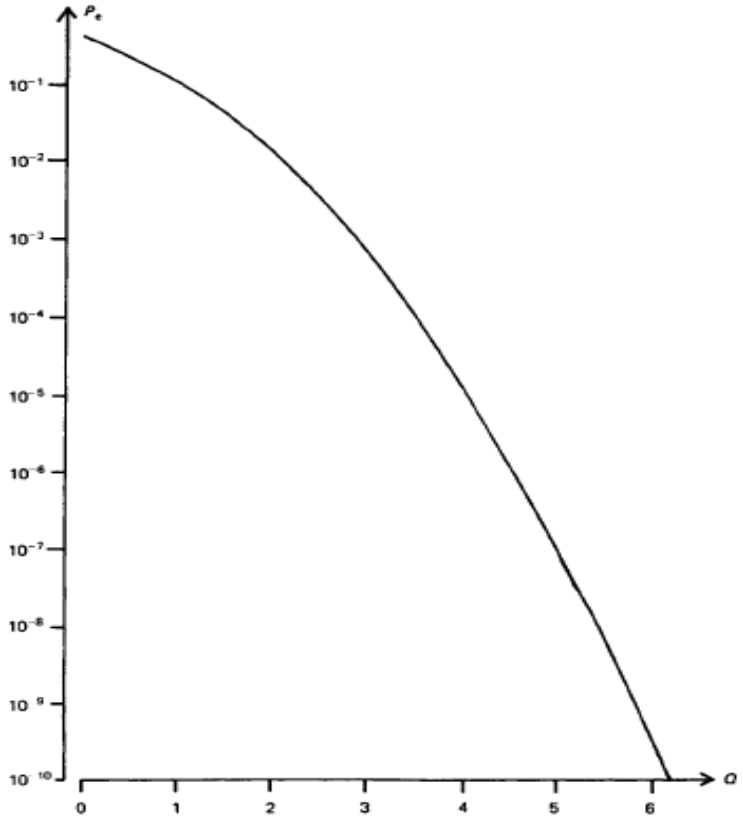

Figure 7-9: Error probability graph via Q parameter [120]

- **Method 2:**

In this way, the measurement method and the signal current (I_{PD}) received by the photodiode is measured using the picoammeter device. The challenge is the current measurement, which is very small compared to the total current delivered via an LED. The measurement steps were as follows:

The total current is measured in the absence of the signal (I_{abs}), then the total current is measured by the presence of the signal (I_{pr}), so the signal current is the difference between the two currents:

$$I_{PD} = I_{pr} - I_{abs} \qquad 7\text{-}27$$

The measured I_{abs} is equal to 138 µA. The measured I_{pr} is equal to 138.12 µA.

Then, $I_{PD} = 120\ nA$

Finally, the receiver sensitivity is determined by the following equations:

$$P_{rs} = \frac{I_{PD}}{R} = 0.182\ \mu W$$

$$P_{rs(dBm)} = -37.4\ dBm$$

- **Method 3:**

In this way, using the calculation method, the signal current (I_{PD}) will be determined using the following equation:

$$I_{PD} = Q\sqrt{(\langle i^2 \rangle . B . I_2)} = 1 \times 10^{-7}$$

Where, $\langle i^2 \rangle$ is the input noise, which is equal to 25×10^{-24}, B the data rate (20 Mbps) and $I_2 = 0.564$.

Then,

$$P_{rs} = \frac{I_{PD}}{R} = 0.153\ \mu W$$

$$P_{rs(dBm)} = -38.16\ dBm$$

Table 7-5 shows the summary results determined by the different methods. From the table it can be seen that there is a convergence of the calculated values by the three methods, where the insignificant difference sensitivity was recorded about -2.2 dBm whereas, the received power shows a difference approximately 0.1 µW.

Table 7-5: Model Evaluation Results

Method	**Method 1**	**Method 2**	**Method 3**
Received power	0.255	0.182	0.153
Receiver sensitivity	-35.94	-37.4	-38.16

7.9 Summary

In this chapter, the MATHCAD software was used to simulate the VLC based on high power LED, using three methods of modulation techniques. The simulation was carried out under the same conditions that were applied in experimental results, to verify the system profitability. The simulation results are summarised in the following points:

- At 20 Mbps data rate, the Duo PPM has the highest sensitivity, which was recorded to be at -37.22 dBm. Whilst, The DiPPM has a higher sensitivity than

the offset PPM, at -0.9 dBm, and less sensitivity than the Duo PPM at -0.6 dBm. The highest received power was recorded at Offset PPM with 0.269 µW. While the DiPPM and Duo PPM were recorded (decrease by) at 0.051 and 0.08, respectively, which were lower than the offset PPM.

- Increasing the speed of transmission rate up to 100 Mbps leads to a reduction in the sensitivity by -3.49 for the different modulation techniques. Conversely, the rate received power increased by 0.332 µW, 0.234 µW and 0.27 µW for the offset PPM, Duo PPM and DiPPM, respectively.
- The VLC simulation was evaluated by finding the receiver sensitivity using different methods. The methods used were based on practical measurements and mathematical calculations. Results have shown that the VLC system has high receiver sensitivity with an average of approximately -37 dBm. On the other hand, the methods were confirmed that there is a correlation between the theoretical results and mathematical calculations.
- In conclusion, the VLC simulation confirmed that the system has high reliability, capable of transmitting data at speeds of more than 100, where the sensitivity was slightly decreased.

Chapter 8
Conclusions and Future Work

8.1 Conclusions

This thesis investigated the use of high-power LEDs in VLC applications. The conclusions of the main findings of this study can be summarised in accordance with the objectives of this research as follows:

Conclusion #1: A critical revision was carried out on the LEDs in terms of their usage in VLC applications. The published works show that the LED has been mostly used in the low-power applications, and generally the concern revolves around how to improve the LED bandwidth. Additionally, the modulation techniques have been revised, as they were significant in the improvement of the performance of the VLC systems, where it was found that there is a possibility of using different techniques to achieve better performance.

Conclusion #2: A commercial high-power LED was used without any additional circuits (found in most of the transmitter component used in research), which offers a great possibility of decreasing the cost and eliminating the noise. It is worth mentioning that the overall implemented system performance was approximate to the performance obtained from the transmitter with the additional circuits in existence

Conclusion #3: A receiver was designed based on a simple emitter follower transimpedance preamplifier (TIA) circuit, using the transistor BFR92A which offers high bandwidth and low noise. Additionally, an RC compensator circuit was added to improve the LED bandwidth.

Conclusion #4: As the reviewed published studies revealed, there was a lack in information about the optimum modulation techniques to consider for high-power LED systems. Three different modulation schemes (DiPPM, Duo PPM and offset PPM) were used due to their high sensitivity, simplicity and the non-requirement of the carrier wave. Accordingly, the data transmission was successfully achieved at speeds above 10 Mbps. Moreover, The BER was less than 10^{-11}.

Conclusion #5: After the three types of pulse position modulation techniques were addressed and implemented, this step aimed to verify the optimum type used in

VLC based high-power LEDs. The optimisation criteria were defined (data transmission and BER). BER of 10^{-9} was recorded at a speed of 14.5 Mbps for both DiPPM and Duo-PPM, whereas 20 Mbps was recorded for the offset-PPM. Thus, it is clear that the offset-PPM has better data transmission reliability than the DiPPM and Duo-PPM.

Conclusion #6: This objective was achieved in two steps. First, the cool and warm LEDs were optimised and the results revealed that the cool LED showed better bandwidth, higher data rates and minimum BER. Second, using the same optimisation criteria, different colour temperatures were compared. Accordingly, a range of 10000–15000 K was selected. However, increases in the colour temperature resulted in changing the lighting colour from white to blue, which can adversely affect the human eye and was counted as a drawback of the high colour temperature.

Conclusion #7: The MATHCAD software was used to simulate the VLC based on high-power LEDs, using three methods of modulation techniques. The simulation was carried out under the same conditions which were used in the experimental study, to verify the system profitability. It was found that the three modulation techniques scored a high level of sensitivity (-35.94 to -38.16 dBm). Furthermore, the VLC simulation was evaluated by finding the receiver sensitivity using different methods, based on practical measurements and mathematical calculations. Results showed that the VLC system had high receiver sensitivity, with an average of approximately -37 dBm. It was also concluded that the VLC simulation confirmed that the system has high reliability, capable of transmitting data at speeds of more than 100.

Conclusion #8: Based on the optimisations carried out for the LEDs and modulation techniques, a reliable VLC system was achieved. Then, this reliable system was used to investigate the effects of the transmission distance and elevation angle on the VLC performance. The results proved that the data could be transmitted over a distance of up to 1.6 m with free BER. As the distance increased, the error rate increased. The error rate was less than 10^{-5} at a distance of up to 2.4 m. Moreover, the BER, due to the light deviation angle from the receiver, was measured at 20 Mbps data rate and 1.9 m free space distance. It can be summarised that the BER increases by increasing the angle, where the BER was approximated to $< 10^{-5}$ at a 30^{o} angle of inclination.

8.2 Contribution to Knowledge

A set of contributions is presented in this research which have not been addressed in previous researches. The summary of these contributions are as follows:

Contribution #1: The first contribution in the current work is successfully using high-power LEDs in optical communications as well as lighting. The current developed VLC system has been implemented using a simple transceiver. Moreover, it was validated through a comparison of the transmitting rate, bandwidth, BER and the illumination with the same low-power LED (1 W). The results show that both LEDs performed the same in terms of VLC applications.

Contribution #2: The second major contribution is represented in specifying the optimum commercial LED for better transmitting processes, which can enhance the overall performance of the VLC applications and has been done by comparing different types of LEDs and suppliers. This comparison helped establish a useful process for the selection of a proper commercial LED, particularly employable for VLC applications.

Contribution #3: The other major contribution of this research work is specifying three modulation techniques for the VLC applications, and then identifying the most appropriate technique by comparing the performance of the specified techniques (DiPPM, Duo PPM and offset PPM) in terms of data rate and BER. It is worth mentioning that the specified techniques have never been employed for high-power LEDs in VLC applications.

8.3 Future work

In this research, experiments and results proved that the high-power LEDs can be used in VLC applications. It is therefore recommended that future works focus on the following:

Outdoor applications: High-power LEDs can be used in street lighting systems to supply them with the necessary data. For example, vehicles can be located as follows: LED streetlight transmits the ID, then the camera can capture the LED image to find the image and the coordinates of the LED. After that it can look up the world coordinates of the LED. Finally, the camera geometric equations can be formulated to find the camera position.

It can be used for smart car technology to send data to a nearby vehicle, for example, by sending a stop signal, or sending turning indicators when turning left or right. Additionally, its usage in traffic lights serves several purposes, such as locating vehicles and sending signals by giving crossing and stop orders to smart vehicles.

Underwater applications: The use of high luminance can allow light propagation for long distances, this allows data to be transmitted to longer distances. The study of high-power LEDs needs to be deepen and expanded, in terms of their optical communications properties. Furthermore, studies should increase the data transmission rate by developing the receiver circuit and adding additional transmitter circuits, and design different types of modulation techniques and apply them to high power LEDs.

References

[1] S. Dimitrov and H. Haas, *Principles of LED light communications: towards networked Li-Fi*. Cambridge University Press, 2015.

[2] Z. Ghassemlooy, L. N. Alves, S. Zvanovec, and M.-A. Khalighi, *Visible light communications: theory and applications*. CRC press, 2017.

[3] S. Arnon, J. Barry, G. Karagiannidis, R. Schober, and M. Uysal, *Advanced optical wireless communication systems*. Cambridge university press, 2012.

[4] S. Arnon, *Visible light communication*. Cambridge University Press, 2015.

[5] Z. Ghassemlooy, W. Popoola, and S. Rajbhandari, *Optical Wireless Communications: System and Channel Modelling with MATLAB* (no. Book, Whole). GB: CRC Press Inc, 2013.

[6] S. C. Lo, "Visible Light Communications," *IEEE Transactions on Consumer Electronics*, vol. 50, no. 1, 2004.

[7] N. Chi, H. Haas, M. Kavehrad, and T. D. Little, "Visible light communications: demand factors, benefits and opportunities [Guest Editorial]," *Wireless Communications, IEEE*, vol. 22, no. 2, pp. 5-7, 2015.

[8] S. Rajagopal, R. D. Roberts, and S.-K. Lim, "IEEE 802.15. 7 visible light communication: modulation schemes and dimming support," *Communications Magazine, IEEE*, vol. 50, no. 3, pp. 72-82, 2012.

[9] F. Zafar, D. Karunatilaka, and R. Parthiban, "Dimming schemes for visible light communication: the state of research," *Wireless Communications, IEEE*, vol. 22, no. 2, pp. 29-35, 2015.

[10] D. C. O'Brien, L. Zeng, H. Le-Minh, G. Faulkner, J. W. Walewski, and S. Randel, "Visible light communications: Challenges and possibilities," in *Personal, Indoor and Mobile Radio Communications, 2008. PIMRC 2008. IEEE 19th International Symposium on*, 2008, pp. 1-5: IEEE.

[11] D. O'Brien *et al.*, "Indoor visible light communications: challenges and prospects," in *Optical Engineering+ Applications*, 2008, pp. 709106-709106-9: International Society for Optics and Photonics.

[12] K. Cui, G. Chen, Z. Xu, and R. D. Roberts, "Line-of-sight visible light communication system design and demonstration," in *Communication Systems Networks and Digital Signal Processing (CSNDSP), 2010 7th International Symposium on*, 2010, pp. 621-625: IEEE.

[13] P. Haigh, T. Son, E. Bentley, Z. Ghassemlooy, H. Le Minh, and L. Chao, "Development of a visible light communications system for optical wireless local area networks," in *2012 Computing, Communications and Applications Conference*, 2012, pp. 351-355: IEEE.

[14] A. Bellè, M. Falcitelli, M. Petracca, and P. Pagano, "Development of IEEE802. 15.7 based ITS services using low cost embedded systems," in *2013 13th International Conference on ITS Telecommunications (ITST)*, 2013, pp. 419-425: IEEE.

[15] H. Burchardt, N. Serafimovski, D. Tsonev, S. Videv, and H. J. I. C. M. Haas, "VLC: Beyond point-to-point communication," vol. 52, no. 7, pp. 98-105, 2014.

[16] L.-B. Chen *et al.*, "Development of a dual-mode visible light communications wireless digital conference system," in *The 18th IEEE International Symposium on Consumer Electronics (ISCE 2014)*, 2014, pp. 1-2: IEEE.

[17] H. Uema, T. Matsumura, S. Saito, Y. J. E. Murata, and C. i. Japan, "Research and development on underwater visible light communication systems," vol. 98, no. 3, pp. 9-13, 2015.

[18] K. Y. Yi, D. Y. Kim, K. M. J. J. o. E. E. Yi, and Technology, "Development of a localization system based on vlc technique for an indoor environment," vol. 10, no. 1, pp. 436-442, 2015.

[19] Y. Goto *et al.*, "A new automotive VLC system using optical communication image sensor," vol. 8, no. 3, pp. 1-17, 2016.

[20] N. Wang, C. Liu, Y. Lu, and J. Shen, "A Visible Light Communication (VLC) based Intelligent Transportation System for lorry fleet," in *2017 16th International Conference on Optical Communications and Networks (ICOCN)*, 2017, pp. 1-3: IEEE.

[21] M. T. Alresheedi, A. T. Hussein, and J. M. J. I. C. Elmirghani, "Uplink design in VLC systems with IR sources and beam steering," vol. 11, no. 3, pp. 311-317, 2017.

[22] V. Matus, N. Maturana, C. A. Azurdia-Meza, S. Montejo-Sánchez, and J. Rojas, "Hardware design of a prototyping platform for vehicular VLC using SDR and exploiting vehicles CAN bus," in *2017 First South American Colloquium on Visible Light Communications (SACVLC)*, 2017, pp. 1-4: IEEE.

[23] T. Adiono, S. Fuada, R. A. J. I. J. o. R. C. f. E. Saputro, Science, and IT, "Rapid development of system-on-chip (SoC) for network-enabled visible light communications," vol. 6, no. 1, pp. 107-119, 2018.

[24] R. Meister, J. Classen, M. S. Saud, M. Katz, and M. Hollick, "Practical VLC to WiFi Handover Mechanisms," in *Proceedings of the 2019 International Conference on Embedded Wireless Systems and Networks*, 2019, pp. 324-329: Junction Publishing.

[25] C. Chow, C. Yeh, Y. Liu, and Y. J. E. l. Liu, "Improved modulation speed of LED visible light communication system integrated to main electricity network," vol. 47, no. 15, pp. 867-868, 2011.

[26] M. J. I. C. M. Kavehrad, "Sustainable energy-efficient wireless applications using light," vol. 48, no. 12, pp. 66-73, 2010.

[27] N. Bardsley *et al.*, "Solid-State Lighting Research and Development," 2014.

[28] Z. Wang, Q. Wang, W. Huang, and Z. Xu, *Visible light communications: Modulation and signal processing*. John Wiley & Sons, 2017.

[29] Z. Ghassemlooy, W. Popoola, and S. Rajbhandari, *Optical wireless communications: system and channel modelling with Matlab®*. CRC press, 2012.

[30] T. Komine and M. Nakagawa, "Fundamental analysis for visible-light communication system using LED lights," *Consumer Electronics, IEEE Transactions on,* vol. 50, no. 1, pp. 100-107, 2004.

[31] M. Bhalerao, S. Sonavane, and V. Kumar, "A survey of wireless communication using visible light," *IJAET, Jan,* 2013.

[32] A. Jovicic, J. Li, and T. Richardson, "Visible light communication: opportunities, challenges and the path to market," *Communications Magazine, IEEE,* vol. 51, no. 12, pp. 26-32, 2013.

[33] M. Saadi, L. Wattisuttikulkij, Y. Zhao, and P. Sangwongngam, "Visible light communication: opportunities, challenges and channel models," *International Journal of Electronics & Informatics,* vol. 2, no. 1, pp. 1-11, 2013.

[34] L. Grobe *et al.*, "High-speed visible light communication systems," *Communications Magazine, IEEE,* vol. 51, no. 12, pp. 60-66, 2013.

[35] N. Chi, J. Shi, Y. Zhou, Y. Wang, J. Zhang, and X. Huang, "High speed LED based visible light communication for 5G wireless backhaul," in *Photonics*

Society Summer Topical Meeting Series (SUM), 2016 IEEE, 2016, pp. 4-5: IEEE.

[36] F. Wu *et al.*, "Performance comparison of OFDM signal and CAP signal over high capacity RGB-LED-based WDM visible light communication," *Photonics Journal, IEEE,* vol. 5, no. 4, pp. 7901507-7901507, 2013.

[37] F.-M. Wu, C.-T. Lin, C.-C. Wei, C.-W. Chen, Z.-Y. Chen, and K. Huang, "3.22-Gb/s WDM visible light communication of a single RGB LED employing carrier-less amplitude and phase modulation," in *Optical Fiber Communication Conference*, 2013, p. OTh1G. 4: Optical Society of America.

[38] X. Lu, M. Zhao, L. Qiao, and N. Chi, "Non-linear Compensation of Multi-CAP VLC System Employing Pre-Distortion Base on Clustering of Machine Learning," in *Optical Fiber Communication Conference*, 2018, p. M2K. 1: Optical Society of America.

[39] S.-W. Wang *et al.*, "A high-performance blue filter for a white-led-based visible light communication system," *Wireless Communications, IEEE,* vol. 22, no. 2, pp. 61-67, 2015.

[40] H. Li, X. Chen, B. Huang, D. Tang, and H. Chen, "High bandwidth visible light communications based on a post-equalization circuit," *Photonics Technology Letters, IEEE,* vol. 26, no. 2, pp. 119-122, 2014.

[41] H. Li, X. Chen, J. Guo, and H. Chen, "A 550 Mbit/s real-time visible light communication system based on phosphorescent white light LED for practical high-speed low-complexity application," *Optics express*, vol. 22, no. 22, pp. 27203-27213, 2014.

[42] T. Komine, J. H. Lee, S. Haruyama, and M. Nakagawa, "Adaptive equalization system for visible light wireless communication utilizing multiple white LED lighting equipment," *Wireless Communications, IEEE Transactions on,* vol. 8, no. 6, pp. 2892-2900, 2009.

[43] H. Sugiyama, S. Haruyama, and M. Nakagawa, "Brightness control methods for illumination and visible-light communication systems," in *Wireless and Mobile Communications, 2007. ICWMC'07. Third International Conference on,* 2007, pp. 78-78: IEEE.

[44] J.-y. WANG, N.-y. ZOU, W. Dong, I. Kentaro, I. Zensei, and Y. NAMIHIRA, "Experimental study on visible light communication based on LED," *The*

Journal of China Universities of Posts and Telecommunications, vol. 19, pp. 197-200, 2012.

[45] C.-H. Yeh, Y.-L. Liu, and C.-W. Chow, "Real-time white-light phosphor-LED visible light communication (VLC) with compact size," *Optics express,* vol. 21, no. 22, pp. 26192-26197, 2013.

[46] C. Chow, Y. Liu, C. Yeh, J. Sung, and Y. Liu, "A practical in-home illumination consideration to reduce data rate fluctuation in visible light communication," *Wireless Communications, IEEE,* vol. 22, no. 2, pp. 17-23, 2015.

[47] L. Ding, F. Liu, Y. He, H. Zhu, and Y. Wang, "Design of Wireless Optical Access System using LED," *Optics and Photonics Journal,* vol. 3, no. 02, p. 148, 2013.

[48] R. C. KIZILIRMAK, "Impact of repeaters on the performance of indoor visible light communications," *Turk J Elec Engin,* vol. 8, no. 1, 2013.

[49] H. Le Minh *et al.*, "High-speed visible light communications using multiple-resonant equalization," vol. 20, no. 14, pp. 1243-1245, 2008.

[50] J. Grubor, S. Randel, K.-D. Langer, and J. W. J. J. o. L. t. Walewski, "Broadband information broadcasting using LED-based interior lighting," vol. 26, no. 24, pp. 3883-3892, 2008.

[51] S.-z. Zhang, C.-t. Zheng, Y.-t. Li, W.-l. Ye, and Y. Liu, "Design and experiment of post-equalization for OOK-NRZ visible light communication system," *Optoelectronics Letters,* vol. 8, no. 2, pp. 142-145, 2012.

[52] C. Hongda *et al.*, "Advances and prospects in visible light communications," *Journal of Semiconductors,* vol. 37, no. 1, p. 011001, 2016.

[53] H. Li, X. Chen, J. Guo, D. Tang, B. Huang, and H. Chen, "200 Mb/s visible optical wireless transmission based on NRZ-OOK modulation of phosphorescent white LED and a pre-emphasis circuit," *Chinese Optics Letters,* vol. 12, no. 10, p. 100604, 2014.

[54] D. Kwon, S. Yang, and S. Han, "Modulation bandwidth enhancement of white-LED-based visible light communications using electrical equalizations," in *SPIE OPTO*, 2015, pp. 93870T-93870T-6: International Society for Optics and Photonics.

[55] H. Li *et al.*, "682Mbit/s phosphorescent white LED visible light communications utilizing analog equalized 16QAM-OFDM modulation without blue filter," *Optics Communications,* 2015.

[56] C. Yeh, C. Chow, H. Chen, J. Chen, and Y. Liu, "Adaptive 84.44-190 Mbit/s phosphor-LED wireless communication utilizing no blue filter at practical transmission distance," *Optics express,* vol. 22, no. 8, pp. 9783-9788, 2014.

[57] H.-C. Chen, C.-J. Liou, and S.-R. Siao, "Illumination distribution and signal transmission for indoor visible light communication with different light-emitting diode arrays and pre-equality circuits," *Optical Engineering,* vol. 54, no. 11, p. 115106, 2015.

[58] Y. Wang, L. Tao, X. Huang, J. Shi, and N. J. I. P. J. Chi, "8-Gb/s RGBY LED-based WDM VLC system employing high-order CAP modulation and hybrid post equalizer," vol. 7, no. 6, pp. 1-7, 2015.

[59] Y. Wang, L. Tao, Y. Wang, and N. J. I. C. L. Chi, "High speed WDM VLC system based on multi-band CAP64 with weighted pre-equalization and modified CMMA based post-equalization," vol. 18, no. 10, pp. 1719-1722, 2014.

[60] N. Chi, Y. Zhou, S. Liang, F. Wang, J. Li, and Y. J. J. o. L. T. Wang, "Enabling Technologies for High-Speed Visible Light Communication Employing CAP Modulation," vol. 36, no. 2, pp. 510-518, 2018.

[61] J. Grubor, S. Randel, K.-D. Langer, and J. Walewski, "Bandwidth-efficient indoor optical wireless communications with white light-emitting diodes," in *Communication Systems, Networks and Digital Signal Processing, 2008. CNSDSP 2008. 6th International Symposium on*, 2008, pp. 165-169: IEEE.

[62] A. Khalid, G. Cossu, R. Corsini, P. Choudhury, and E. Ciaramella, "1-Gb/s transmission over a phosphorescent white LED by using rate-adaptive discrete multitone modulation," *Photonics Journal, IEEE,* vol. 4, no. 5, pp. 1465-1473, 2012.

[63] N. M. Ridzuan, M. Othman, M. Jaafar, M. F. L. J. J. o. T. Abdullah, Electronic, and C. Engineering, "Comparison of Cap and QAM-DMT Modulation Format for In-Home Network Environment," vol. 9, no. 3-2, pp. 1-4, 2017.

[64] C. Chow, C. Yeh, Y. Liu, and Y. Liu, "Improved modulation speed of LED visible light communication system integrated to main electricity network," *Electronics letters,* vol. 47, no. 15, pp. 867-868, 2011.

[65] J. Latal, P. Koudelka, V. Vasinek, F. Dostál, and K. Sokansky, "Possible use of power LEDs for lighting and communication," *Przeglad Elektrotechniczny,* vol. 87, no. 4, pp. 25-28, 2011.

[66] C. Yeh, Y. Liu, C. Chow, Y. Liu, P. Huang, and H. Tsang, "Investigation of 4-ASK modulation with digital filtering to increase 20 times of direct modulation speed of white-light LED visible light communication system," *Optics Express*, vol. 20, no. 15, pp. 16218-16223, 2012.

[67] M. Z. Afgani, H. Haas, H. Elgala, and D. Knipp, "Visible light communication using OFDM," in *Testbeds and Research Infrastructures for the Development of Networks and Communities, 2006. TRIDENTCOM 2006. 2nd International Conference on*, 2006, pp. 6 pp.-134: IEEE.

[68] M. Noshad and M. Brandt-Pearce, "Can visible light communications provide Gb/s service?," *arXiv preprint arXiv:1308.3217*, 2013.

[69] M. Noshad and M. Brandt-Pearce, "Application of expurgated PPM to indoor visible light communications—Part I: Single-user systems," *Journal of Lightwave Technology*, vol. 32, no. 5, pp. 875-882, 2014.

[70] H. K. J. I. J. i. I. Channi and Engineering, "A Comparative Study of Various Digital Modulation Techniques," vol. 4, pp. 39-49.

[71] J. Vučič, C. Kottke, S. Nerreter, K. Langer, and J. W. Walewski, "513 Mbit/s Visible Light Communications Link Based on DMT-Modulation of a White LED," *Journal of Lightwave Technology*, vol. 28, no. 24, pp. 3512-3518, 2010.

[72] G. A. Mahdiraji and E. Zahedi, "Comparison of selected digital modulation schemes (OOK, PPM and DPIM) for wireless optical communications," in *2006 4th Student Conference on Research and Development*, 2006, pp. 5-10: IEEE.

[73] M. J. J. I. o. Sibley, "Analysis of offset pulse position modulation-a novel reduced bandwidth coding scheme," vol. 5, no. 4, pp. 144-150, 2011.

[74] A. M. Buhafa, B. M. Al-Nedawe, M. J. Sibley, and P. J. Mather, "VLC system performance using Dicode Pulse Position Modulation over an indoor diffuse link," in *Telecommunications Forum Telfor (TELFOR), 2014 22nd*, 2014, pp. 605-608: IEEE.

[75] Y. Wang, L. Tao, X. Huang, J. Shi, and N. Chi, "Enhanced performance of a high speed WDM CAP64 VLC system employing Volterra series based nonlinear equalizer."

[76] M. Shi, C. Wang, H. Guo, Y. Wang, X. Li, and N. Chi, "A high-speed visible light communication system based on DFT-S OFDM," in *2016 IEEE International Conference on Communication Systems (ICCS)*, 2016, pp. 1-5: IEEE.

[77] F. Wang, Y. Zhao, and N. Chi, "High speed visible light communication system using QAM-DMT modulation based on digital zero-padding and differential receiver," in *2017 16th International Conference on Optical Communications and Networks (ICOCN)*, 2017, pp. 1-3: IEEE.

[78] X. Li, W. K. Cho, B. Hussain, H. S. Kwok, and C. P. Yue, "66-3: Micro-LED Display with Simultaneous Visible Light Communication Function," in *SID Symposium Digest of Technical Papers*, 2018, vol. 49, no. 1, pp. 876-879: Wiley Online Library.

[79] E. Xie *et al.*, "High-speed visible light communication based on a III-nitride series-biased micro-LED array," vol. 37, no. 4, pp. 1180-1186, 2019.

[80] J. P. Colinge and C. A. Colinge, *Physics of Semiconductor Devices* (no. Book, Whole). Boston, MA: Springer, 2007.

[81] S. M. Sze and K. K. Ng, *Physics of semiconductor devices*. John Wiley & Sons, 2006.

[82] E. F. Schubert, *Light-emitting diodes* (no. Book, Whole). Cambridge; New York: Cambridge University Press, 2006.

[83] E. F. Schubert, *Light-emitting diodes*. E. Fred Schubert, 2018.

[84] J. M. Senior, *Optical fiber communications: principles and practice* (no. Book, Whole). Harlow: Prentice Hall, 2009.

[85] N. Hirosaki, N. Kimura, K. Sakuma, S. Hirafune, K. Asano, and D. Tanaka, "White light-emitting diode lamps for lighting applications," *Fujikura Technical Review*, vol. 35, p. 1, 2006.

[86] G. Held, *Introduction to light emitting diode technology and applications*. CRC Press, 2008.

[87] R. Ramirez-Iniguez, S. M. Idrus, and Z. Sun, *Optical wireless communications: IR for wireless connectivity*. Auerbach Publications, 2008.

[88] Z. Wang, Q. Wang, W. Huang, Z. Xu, I. Xplore, and Wiley, *Visible Light Communications: Modulation and Signal Processing*, 1 ed. (no. Book, Whole). Hoboken: Wiley, 2017.

[89] F. Xiong, *Digital modulation techniques*, 2nd ed. (no. Book, Whole). Boston, MA: Artech House, 2006.

[90] R. W. Middlestead, *Digital communications with emphasis on data modems: theory, analysis, design, simulation, testing, and applications*, 1 ed. (no. Book, Whole). Hoboken: Wiley, 2015.

[91] K. T. Wong, "Narrowband PPM semi-‘blind’spatial-rake receiver & co-channel interference suppression," *European transactions on telecommunications,* vol. 18, no. 2, pp. 193-197, 2007.

[92] Y. Fujiwara, "Self-synchronizing pulse position modulation with error tolerance," *Information Theory, IEEE Transactions on,* vol. 59, no. 9, pp. 5352-5362, 2013.

[93] N. Chi, "LED-Based Visible Light Communications," 2018.

[94] F. J. Ghosna, "Pulse Position Modulation Coding Schemes for Optical Inter-satellite Links in Free Space," University of Huddersfield, 2010.

[95] F. Ghosna and M. J. Sibley, "Pulse position modulation coding schemes for optical intersatellite links," *Electronics letters,* vol. 46, no. 4, pp. 290-291, 2010.

[96] M. J. Sibley, "Dicode pulse-position modulation: a novel coding scheme for optical-fibre communications," *IEE Proceedings-Optoelectronics,* vol. 150, no. 2, pp. 125-131, 2003.

[97] M. J. Sibley, "Analysis of dicode pulse position modulation using a PINFET receiver and a slightly/highly dispersive optical channel," *IEE Proceedings-Optoelectronics,* vol. 150, no. 3, pp. 205-209, 2003.

[98] B. M. Al-Nedawe, A. M. Buhafa, M. J. Sibley, and P. J. Mather, "Improving error performance of dicode pulse position modulation system using forward error correction codes," in *Telecommunications Forum (TELFOR), 2013 21st*, 2013, pp. 331-334: IEEE.

[99] M. J. I. P.-O. Sibley, "Performance analysis of a dicode PPM system, operating over plastic optical fibre, using maximum likelihood sequence detection," vol. 152, no. 6, pp. 337-343, 2005.

[100] M. J. J. I. P.-O. Sibley, "Suboptimal filtering in a zero-guard, dicode PPM system operating over dispersive optical channels," vol. 151, no. 4, pp. 237-243, 2004.

[101] R. Cryan and M. J. Sibley, "Minimising intersymbol interference in optical-fibre dicode PPM systems," *IEE Proceedings-Optoelectronics,* vol. 153, no. 3, pp. 93-100, 2006.

[102] M. J. Sibley, "Suboptimal filtering in a zero-guard, dicode PPM system operating over dispersive optical channels," *IEE Proceedings-Optoelectronics,* vol. 151, no. 4, pp. 237-243, 2004.

[103] M. Sibley, "Performance analysis of a dicode PPM system, operating over plastic optical fibre, using maximum likelihood sequence detection," *IEE Proceedings-Optoelectronics,* vol. 152, no. 6, pp. 337-343, 2005.

[104] R. Charitopoulos, "Implementation & Performance Investigation of Dicode PPM over Dispersive Optical Channels," Dissertation/Thesis, 2009.

[105] R. Charitopoulos, M. J. Sibley, and P. Mather, "Maximum likelihood sequence detector for dicode pulse position modulation," *IET optoelectronics,* vol. 5, no. 6, pp. 261-264, 2011.

[106] H. Wang, G. Cheng, X. Sun, and T. Zhang, "Performance analysis of dicode pulse position modulation for optical wireless communications," in *2007 International Conference on Wireless Communications, Networking and Mobile Computing*, 2007, pp. 3027-3030: IEEE.

[107] R. Charitopoulos and M. J. Sibley, "Slot and frame synchronisation in dicode pulse-position modulation," *IET optoelectronics,* vol. 4, no. 4, pp. 174-182, 2010.

[108] R. C. M. Sibley, "Experimental verification of the power spectral density of dicode pulse-position modulation with practical impairments," 2011.

[109] A. J. T. o. t. A. I. o. E. E. Lender, Part I: Communication and Electronics, "The duobinary technique for high-speed data transmission," vol. 82, no. 2, pp. 214-218, 1963.

[110] K. Mostafa, M. J. Sibley, and P. J. J. I. O. Mather, "Duobinary pulse position modulation–a novel coding scheme for the dispersive optical channel," vol. 8, no. 6, pp. 264-269, 2014.

[111] M. J. Sibley, "Analysis of offset pulse position modulation-a novel reduced bandwidth coding scheme," *IET optoelectronics,* vol. 5, no. 4, pp. 144-150, 2011.

[112] I. Ray, M. J. Sibley, and P. J. Mather, "Performance analysis of offset pulse-position modulation over an optical channel," *Journal of Lightwave Technology,* vol. 30, no. 3, pp. 325-330, 2012.

[113] I. Ray, M. J. Sibley, and P. J. Mather, "Spectral characterisation of offset pulse position modulation," *IET optoelectronics,* vol. 9, no. 6, pp. 300-306, 2015.

[114] M. J. J. I. P.-O. Sibley, "Dicode pulse-position modulation: a novel coding scheme for optical-fibre communications," vol. 150, no. 2, pp. 125-131, 2003.

[115] M. J. J. I. P.-O. Sibley, "Analysis of dicode pulse position modulation using a PINFET receiver and a slightly/highly dispersive optical channel," vol. 150, no. 3, pp. 205-209, 2003.

[116] R. Cryan and M. J. J. I. P.-O. Sibley, "Minimising intersymbol interference in optical-fibre dicode PPM systems," vol. 153, no. 3, pp. 93-100, 2006.

[117] M. J. J. I. o. Sibley, "Analysis of offset pulse position modulation–a novel reduced bandwidth coding scheme," vol. 5, no. 4, pp. 144-150, 2011.

[118] R. Cryan, R. T. Unwin, I. Garrett, M. J. Sibley, and N. J. I. P. J. Calvert, "Optical fibre digital pulse-position-modulation assuming a Gaussian received pulse shape," vol. 137, no. 2, pp. 89-96, 1990.

[119] PICOSECOND PULSE LABS, "Model 5575A, Bias Tee Product Specification," 2009.

[120] M. J. Sibley, *Optical communications: components and systems*. Macmillan International Higher Education, 1995.

[121] A. A. Leven, *Telecommunication circuits and technology* (no. Book, Whole). Oxford: Butterworth-Heinemann, 2000.

[122] C. H. Houpis and S. N. Sheldon, *LINEAR CONTROL SYSTEM ANALYSIS AND DESIGN WITH MATLAB*, Sixth Edition ed. New York, 2014.

[123] Z. Wang, Q. Wang, W. Huang, and Z. Xu, "Visible light communications: Channel and capacity," 2018.

[124] J.-W. Shi, *Photodiodes-Communications, Bio-Sensings, Measurements and High-Energy Physics*. 2011.

[125] M. J. Sibley, J. J. M. Bellon, and O. T. Letters, "Transit-time limitations in p-i-n photodiodes," vol. 26, no. 5, pp. 282-286, 2000.

[126] M. H. Ahfayd, M. J. Sibley, P. Mather, and P. Lazaridis, "Visible Light Communication Based On Offset Pulse Position Modulation (Offset-PPM) Using High Power LED," in *Proceedings of the XXXIInd International Union of Radio Science General Assembly & Scientific Symposium (URSI GASS),(Montreal, 19-26 August 2017)*, 2017: IEEE.

[127] M. H. Ahfayd, Z. A. Farhat, M. J. Sibley, P. J. Mather, and P. Lazaridis, "Selection of high power LEDs for Li-Fi applications," in *2018 25th International Conference on Telecommunications (ICT)*, 2018, pp. 170-174: IEEE.

[128] H. Li, X. Chen, B. Huang, D. Tang, and H. Chen, "High bandwidth visible light communications based on a post-equalization circuit," *IEEE photonics technology letters,* vol. 26, no. 2, pp. 119-122, 2014.

[129] H. Li *et al.*, "682 Mbit/s phosphorescent white LED visible light communications utilizing analog equalized 16QAM-OFDM modulation without blue filter," vol. 354, pp. 107-111, 2015.

[130] H. Li, X. Chen, B. Huang, D. Tang, and H. J. I. p. t. l. Chen, "High bandwidth visible light communications based on a post-equalization circuit," vol. 26, no. 2, pp. 119-122, 2014.

[131] H. Li, X. Chen, J. Guo, and H. J. O. e. Chen, "A 550 Mbit/s real-time visible light communication system based on phosphorescent white light LED for practical high-speed low-complexity application," vol. 22, no. 22, pp. 27203-27213, 2014.

[132] ALTERA, *Cyclone IV Device Handbook* 2016.

[133] Z. A. Farhat, M. H. Ahfayd, P. J. Mather, and M. J. Sibley, "Practical implementation of duobinary pulse position modulation using FPGA and visible light communication," in *2017 IEEE 15th Student Conference on Research and Development (SCOReD)*, 2017, pp. 253-256: IEEE.

[134] M. D. Audeh and J. M. Kahn, "Performance evaluation of L-pulse-position modulation on non-directed indoor infrared channels," in *Communications, 1994. ICC'94, SUPERCOMM/ICC'94, Conference Record,'Serving Humanity Through Communications.'IEEE International Conference on*, 1994, pp. 660-664: IEEE.

[135] R. Cryan and R. Unwin, "Optimal and suboptimal detection of optical fibre digital PPM," *IEE Proceedings J (Optoelectronics),* vol. 140, no. 6, pp. 367-375, 1993.

[136] L. N. Binh, *Optical fiber communication systems with Matlab and Simulink models*. CRC Press, 2014.

[137] M. J. Sibley and A. J. Massarella, "Detection of digital pulse position modulation over highly/slightly dispersive optical channels," in *Berlin-DL tentative*, 1993, pp. 99-110: International Society for Optics and Photonics.

[138] K. Mostafa, "Theoretical Analyses and Practical Implementation of Duobinary Pulse Position Modulation Using Mathcad, VHDL, FPGA and Purpose-built Transceiver," University of Huddersfield, 2015.

[139] I. Garrett, "Digital pulse-position modulation over slightly dispersive optical fibre channels," in *Int. Symp. Information Theory, St. Jovite*, 1983, pp. 78-79.

Appendices

Appendix A: Receiver circuit design

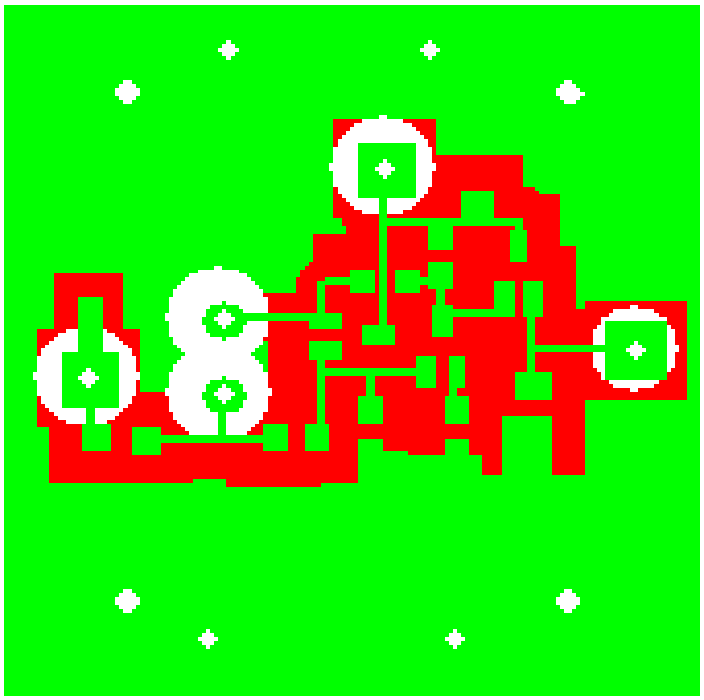

PCB Layout Components Side Transimpedance amplifier (TIA)

Printed and designed circuit of TIA

Appendix B: : Comparator Circuit Design

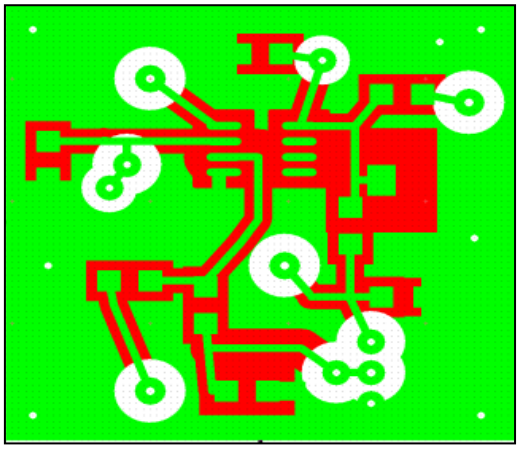

PCB Layout Components Side of comparator

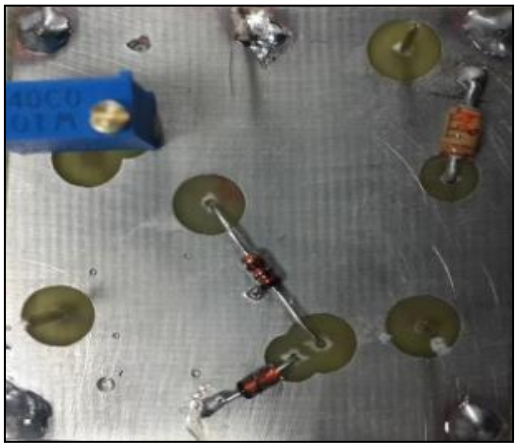

Printed and designed circuit (back)

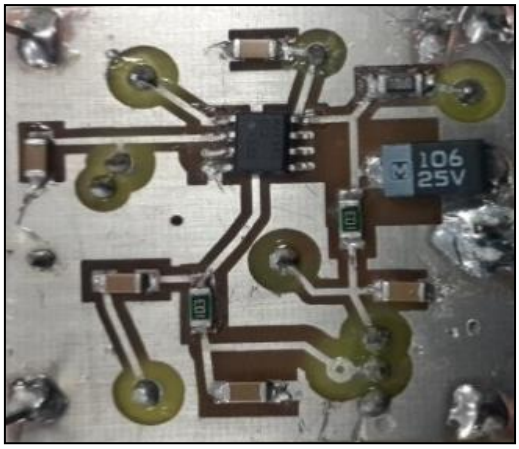

Printed and designed circuit of comparator (front)

Appendix C: Receiver sensitivity of DiPPM at 20 Mbps

Receiver sensitivity of DiPPM with zero guard at 20 Mbit/s and 3 PCM BITS for LOS Indoor VLC Link 2019

$i := 0, 1 .. 30$

$v_i := v_{off} + \frac{i}{1000}$

$n := 10$ Number of like symbols in PCM

$\eta q := 1.6 \cdot 10^{-19}$ Quantum energy

$\lambda := 820 \cdot 10^{-9}$ This is the wavelength of operation

$photon\_energy := \frac{6.63 \cdot 10^{-34} \cdot 3 \cdot 10^{8}}{\lambda}$ $gu \equiv 0$

$R_o := \frac{\eta q}{photon\_energy}$ $R_o = 659.628 \times 10^{-3}$

Preamplifier terms

$S_o := 25 \cdot 10^{-24}$ **Preamplifier input noise**

$B := 20 \cdot 10^{6}$ Bit rate

$T_b := \frac{1}{B}$ PCM bit time

Slot time $T_s := \frac{T_b}{2 + gu}$ $T_s = 25 \times 10^{-9}$

$f_c := 0.5 \cdot \frac{1}{T_s}$ $\omega_c := 2 \cdot \pi \cdot f_c$

preamplifie $H_{pre}(\omega) := \frac{1}{1 + j \cdot \frac{\omega}{\omega_c}}$

VLC impulse response

$t := 0, 0.1 .. 14$

$h(t) := \left[1 \cdot \left[\int_0^t Re\left[exp\left[i \cdot \omega \cdot (t) \cdot H_{pre}(\omega) \right] \right] d\omega \right] \right]$

Pulse shape

$$\alpha_p := \frac{0.1874 \cdot T_b}{f_n} \qquad f_n \equiv 0.65 \qquad \alpha_{pn} := \frac{\alpha_p}{T_s}$$

$$Pulse1(t) := \frac{1}{\sqrt{2 \cdot \pi} \cdot \alpha_{pn} \cdot 1} \cdot \exp\left(\frac{-t^2}{2 \cdot \alpha_{pn}^2}\right)$$

$$I_0(t) := \left(\frac{1}{T_s} \cdot \int_0^t h(\tau) \cdot Pulse1(t - \tau)\, d\tau\right)$$

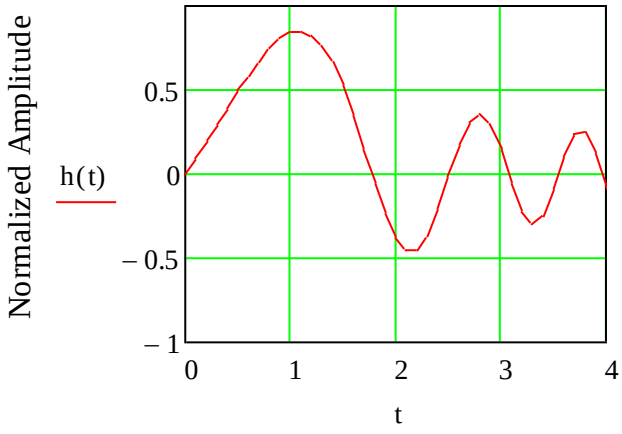

Time slot (Ts)

Pulse1(t) =

691.869·10-3
681.542·10-3
651.478·10-3
604.289·10-3
543.91·10-3
475.06·10-3
402.63·10-3
331.134·10-3
264.264·10-3
204.649·10-3
153.787·10-3
112.142·10-3
79.351·10-3
54.485·10-3
36.303·10-3
...

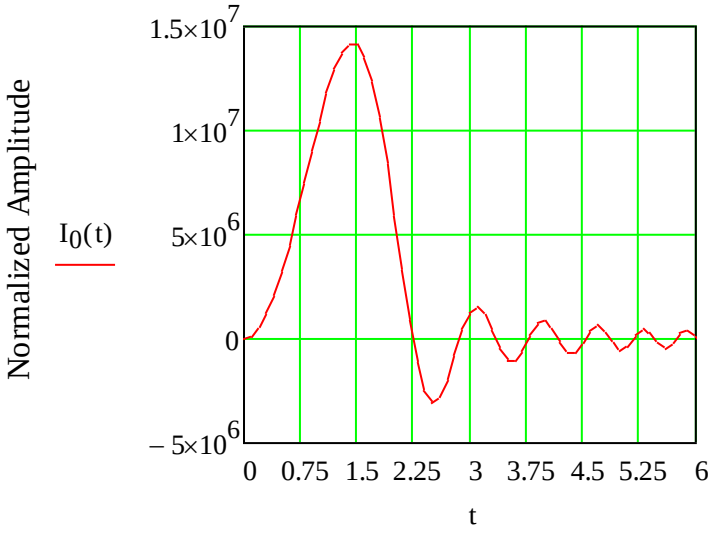

Time slot (Ts)

I0(t) =

0·10^0
138.027·10^3
547.963·10^3
1.217·10^6
2.126·10^6
3.246·10^6
4.541·10^6
5.968·10^6
7.475·10^6
9.002·10^6
10.477·10^6
11.822·10^6
12.949·10^6
13.765·10^6
14.178·10^6
...

$t := 1.5$ $I_1(t) := \frac{d}{dt} I_0(t)$ Guess at the peak time

$t_{pk} := root\left(I_1(t) \cdot T_s^{\,3}, t\right)$ $t_{pk} = 1.437 \times 10^{0}$ This is the peak time

$v_{pk} := I_0\left(t_{pk}\right)$ $v_{pk} = 14.212 \times 10^{6}$ This is the peak voltage

$noise := \frac{\pi \cdot f_c}{2}$ $noise = 31.416 \times 10^{6}$ Noise bandwidth

$S_o \cdot noise = 0 \times 10^{0}$ $\sqrt{S_o \cdot noise} = 28.025 \times 10^{-9}$

Erasure of pulse

$$Q_{e_i} := \eta q \cdot \frac{v_{pk} - v_i \cdot v_{pk}}{\sqrt{S_o \cdot noise}} \qquad P_r(b, i) := \frac{1}{2} \cdot erfc\left(\frac{Q_{e_i} \cdot b}{\sqrt{2}}\right)$$

$$P_{er}(b, i) := 2 \cdot \sum_{x=0}^{n-1} \left[\left(\frac{1}{2}\right)^{x+3} \cdot P_r(b, i) \cdot (x + 1) + \left(\frac{1}{2}\right)^{n+2} \cdot P_r(b, i) \cdot (n + 1)\right]$$

False alarm

False alarm when pulse appears in slot R can spread into S-slot of following symbol P_{efISI1}

or into previous S-slot of same symbol P_{efISI2} , $v_{oISI1} := Vo(td - Ts)$ and $v_{oISI1} := Vo(td - Ts)$

$$v_{oISI1\_Ts_i} := v_i \cdot I_0\left(t_{pk} - 1\right) \qquad v_{oISI2\_Ts_i} := v_i \cdot I_0\left(t_{pk} + 1\right)$$

$$Q_{eISI1_i} := \eta q \cdot \frac{v_i \cdot v_{pk} - v_{oISI1\_Ts_i}}{\sqrt{S_o \cdot noise}} \qquad P_{efISI1}(b, i) := \frac{1}{2} \cdot erfc\left(\frac{Q_{eISI1_i} \cdot b}{\sqrt{2}}\right)$$

$$Q_{eISI2_i} := \eta q \cdot \frac{v_i \cdot v_{pk} - v_{oISI2\_Ts_i}}{\sqrt{S_o \cdot noise}} \qquad P_{efISI2}(b, i) := \frac{1}{2} \cdot erfc\left(\frac{Q_{eISI2_i} \cdot b}{\sqrt{2}}\right)$$

$$P_{efR}(b,i) := \left[\sum_{x=0}^{n-1}\left[\left(\frac{1}{2}\right)^{x+3}\cdot P_{efISI1}(b,i)\cdot(x) + \left(\frac{1}{2}\right)^{n+2}\cdot P_{efISI1}(b,i)\cdot(n)\right]\right]\ldots$$
$$+\sum_{x=0}^{n-1}\left[\left(\frac{1}{2}\right)^{x+3}\cdot P_{efISI2}(b,i)\cdot(x+1) + \left(\frac{1}{2}\right)^{n+2}\cdot P_{efISI2}(b,i)\cdot(n+1)\right]$$

False alarm no ISI accurs between S and R and the error apears within the run of N-symbols where k is the symbol position

False alarm between R and S pulses - N to SET

$$Q_{NS}(b,i) := \eta q\cdot\frac{v_i\cdot v_{pk}}{\sqrt{S_o\cdot noise}} \qquad P_{NS}(b,i) := \frac{1}{2}\cdot erfc\left(\frac{Q_{NS}(b,i)\cdot b}{\sqrt{2}}\right)$$

$$P_{eNS}(b,i) := \left[\sum_{y=3}^{n-1}\sum_{k=2}^{y-1}\left[\left(\frac{1}{2}\right)^{y+3}\cdot P_{NS}(b,i)\cdot(y+1-k)\right]\right]\ldots$$
$$+\sum_{k=2}^{n-1}\left[\left(\frac{1}{2}\right)^{n+2}\cdot P_{NS}(b,i)\cdot(n+1-k)\right]$$

False alarm between S and R pulses - N to R

$$Q_{NR}(b,i) := \eta q\cdot\frac{v_i\cdot v_{pk}}{\sqrt{S_o\cdot noise}} \qquad P_{NR}(b,i) := \frac{1}{2}\cdot erfc\left(\frac{Q_{NR}(b,i)\cdot b}{\sqrt{2}}\right)$$

$$P_{eNR}(b,i) := \left[\sum_{x=3}^{n-1}\sum_{k=2}^{x-1}\left[\left(\frac{1}{2}\right)^{x+3}\cdot P_{NR}(b,i)\cdot(x+1-k)\right]\right]\ldots$$
$$+\sum_{k=2}^{n-1}\left[\left(\frac{1}{2}\right)^{n+2}\cdot P_{NR}(b,i)\cdot(n+1-k)\right]$$

$$P_{fN}(b,i) := P_{eNS}(b,i) + P_{eNR}(b,i)$$

$$P_{efN}(b,i) := \left[\sum_{x=1}^{n-1} \left[\left(\frac{1}{2}\right)^{x+3} \cdot \sum_{k=1}^{x} \left[P_{fN}(b,i) \cdot (x+1-k) \right] \right] \ldots \right] \ldots + \left[\left(\frac{1}{2}\right)^{n+2} \cdot \sum_{k=1}^{n} \left[P_{fN}(b,i) \cdot (n+1-k) \right] \right] + \sum_{x=2}^{n-1} \left[\left(\frac{1}{2}\right)^{x+3} \cdot \sum_{k=2}^{x} \left[P_{fN}(b,i) \cdot (x+1-k) \right] \right] \ldots + \left(\frac{1}{2}\right)^{n+2} \cdot \sum_{k=2}^{n} \left[P_{fN}(b,i) \cdot (n+1-k) \right]$$

Total Fals alarm

$$P_{ef}(b,i) := P_{efN}(b,i) + P_{efR}(b,i)$$

Total Errors

$$P_{eb}(b,i) := P_{er}(b,i) + P_{ef}(b,i)$$

$$pc(b,i) := \left(\log\left(P_{eb}(b,i)\right) + 9\right)$$ Set for 1 in 10^9 errors

$$P_{er}(b,0) = 507.784 \times 10^{-3} \quad P_{ef}(b,0) = 516.312 \times 10^{-3}$$

$$a_i := \text{root}(pc(b,i), b)$$ Find the root to give 1 in 10^9

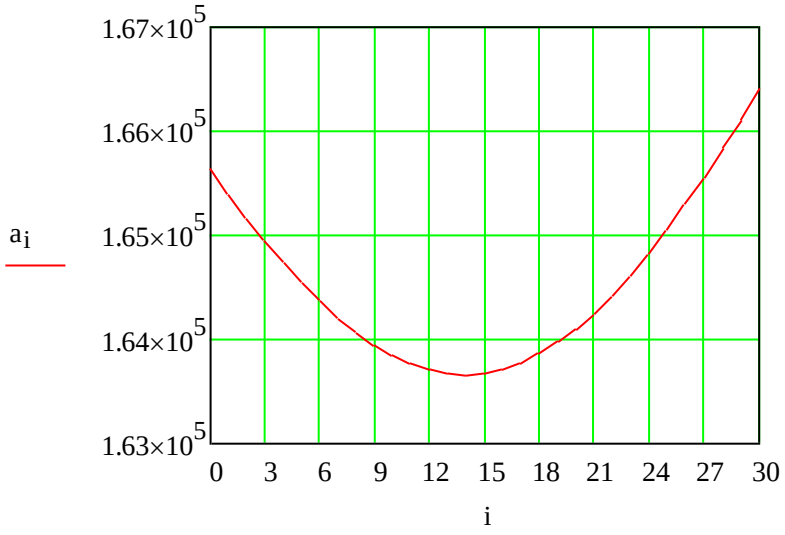

$b \equiv 1 \cdot 10^{3}$

$v_{off} \equiv 0.524$

$gu = 0 \times 10^{0}$

minimum:= min(a) $\quad$ minimum= 163.663×10^{3}

Received power

$$P_r := \left[\frac{\text{minimum}}{((gu + 2))} \cdot \text{photon\_energy}\left(\frac{1 + n}{2n} \right) \cdot B \right]$$

$P_r = 218.34 \times 10^{-9}$

Receiver sensitivity

$$P_{rdBm} := 10 \cdot \log\left(\frac{P_r}{10^{-3}} \right)$$

$P_{rdBm} = -36.609 \times 10^{0}$

$pc(minimum, 14) = -1.776 \times 10^{-15}$ closed to zero

$v_{pk} - v_i \cdot v_{pk} =$
$6.765 \cdot 10^{6}$
$6.751 \cdot 10^{6}$
$6.737 \cdot 10^{6}$
$6.722 \cdot 10^{6}$
$6.708 \cdot 10^{6}$
$6.694 \cdot 10^{6}$
$6.68 \cdot 10^{6}$
$6.665 \cdot 10^{6}$
$6.651 \cdot 10^{6}$
$6.637 \cdot 10^{6}$
$6.623 \cdot 10^{6}$
$6.609 \cdot 10^{6}$
$6.594 \cdot 10^{6}$
$6.58 \cdot 10^{6}$
$6.566 \cdot 10^{6}$
...

$v_i \cdot v_{pk} =$
$7.447 \cdot 10^{6}$
$7.461 \cdot 10^{6}$
$7.476 \cdot 10^{6}$
$7.49 \cdot 10^{6}$
$7.504 \cdot 10^{6}$
$7.518 \cdot 10^{6}$
$7.532 \cdot 10^{6}$
$7.547 \cdot 10^{6}$
$7.561 \cdot 10^{6}$
$7.575 \cdot 10^{6}$
$7.589 \cdot 10^{6}$
$7.603 \cdot 10^{6}$
$7.618 \cdot 10^{6}$
$7.632 \cdot 10^{6}$
$7.646 \cdot 10^{6}$
...

$Q_{e_i} =$
$38.623 \cdot 10^{-6}$
$38.541 \cdot 10^{-6}$
$38.46 \cdot 10^{-6}$
$38.379 \cdot 10^{-6}$
$38.298 \cdot 10^{-6}$
$38.217 \cdot 10^{-6}$
$38.136 \cdot 10^{-6}$
$38.055 \cdot 10^{-6}$
$37.973 \cdot 10^{-6}$
$37.892 \cdot 10^{-6}$
$37.811 \cdot 10^{-6}$
$37.73 \cdot 10^{-6}$
$37.649 \cdot 10^{-6}$
$37.568 \cdot 10^{-6}$
$37.487 \cdot 10^{-6}$
...

$P_{er}(b, i) =$
$507.784 \cdot 10^{-3}$
$507.818 \cdot 10^{-3}$
$507.852 \cdot 10^{-3}$
$507.886 \cdot 10^{-3}$
$507.92 \cdot 10^{-3}$
$507.954 \cdot 10^{-3}$
$507.988 \cdot 10^{-3}$
$508.022 \cdot 10^{-3}$
$508.055 \cdot 10^{-3}$
$508.089 \cdot 10^{-3}$
$508.123 \cdot 10^{-3}$
$508.157 \cdot 10^{-3}$
$508.191 \cdot 10^{-3}$
$508.225 \cdot 10^{-3}$
$508.259 \cdot 10^{-3}$
...

$v_{oISI1\_Ts_i} =$
$1.317 \cdot 10^{6}$
$1.319 \cdot 10^{6}$
$1.322 \cdot 10^{6}$
$1.325 \cdot 10^{6}$
$1.327 \cdot 10^{6}$
$1.33 \cdot 10^{6}$
$1.332 \cdot 10^{6}$
$1.335 \cdot 10^{6}$
$1.337 \cdot 10^{6}$
$1.34 \cdot 10^{6}$
$1.342 \cdot 10^{6}$
$1.345 \cdot 10^{6}$
$1.347 \cdot 10^{6}$
$1.35 \cdot 10^{6}$
$1.352 \cdot 10^{6}$
...

$v_{oISI2\_Ts_i} =$
$-1.464 \cdot 10^{6}$
$-1.467 \cdot 10^{6}$
$-1.47 \cdot 10^{6}$
$-1.472 \cdot 10^{6}$
$-1.475 \cdot 10^{6}$
$-1.478 \cdot 10^{6}$
$-1.481 \cdot 10^{6}$
$-1.484 \cdot 10^{6}$
$-1.486 \cdot 10^{6}$
$-1.489 \cdot 10^{6}$
$-1.492 \cdot 10^{6}$
$-1.495 \cdot 10^{6}$
$-1.498 \cdot 10^{6}$
$-1.5 \cdot 10^{6}$
$-1.503 \cdot 10^{6}$
...

$Q_{eISI1_i} =$
$34.998 \cdot 10^{-6}$
$35.065 \cdot 10^{-6}$
$35.132 \cdot 10^{-6}$
$35.199 \cdot 10^{-6}$
$35.266 \cdot 10^{-6}$
$35.332 \cdot 10^{-6}$
$35.399 \cdot 10^{-6}$
$35.466 \cdot 10^{-6}$
$35.533 \cdot 10^{-6}$
$35.599 \cdot 10^{-6}$
$35.666 \cdot 10^{-6}$
$35.733 \cdot 10^{-6}$
$35.8 \cdot 10^{-6}$
$35.867 \cdot 10^{-6}$
$35.933 \cdot 10^{-6}$
...

$P_{efISI1}(b, i) =$
$486.041 \cdot 10^{-3}$
$486.014 \cdot 10^{-3}$
$485.987 \cdot 10^{-3}$
$485.961 \cdot 10^{-3}$
$485.934 \cdot 10^{-3}$
$485.907 \cdot 10^{-3}$
$485.881 \cdot 10^{-3}$
$485.854 \cdot 10^{-3}$
$485.827 \cdot 10^{-3}$
$485.801 \cdot 10^{-3}$
$485.774 \cdot 10^{-3}$
$485.748 \cdot 10^{-3}$
$485.721 \cdot 10^{-3}$
$485.694 \cdot 10^{-3}$
$485.668 \cdot 10^{-3}$
...

$Q_{eISI2_i} =$
$50.875 \cdot 10^{-6}$
$50.972 \cdot 10^{-6}$
$51.07 \cdot 10^{-6}$
$51.167 \cdot 10^{-6}$
$51.264 \cdot 10^{-6}$
$51.361 \cdot 10^{-6}$
$51.458 \cdot 10^{-6}$
$51.555 \cdot 10^{-6}$
$51.652 \cdot 10^{-6}$
$51.749 \cdot 10^{-6}$
$51.846 \cdot 10^{-6}$
$51.943 \cdot 10^{-6}$
$52.04 \cdot 10^{-6}$
$52.137 \cdot 10^{-6}$
$52.235 \cdot 10^{-6}$
...

$P_{efISI2}(b,i) =$

$479.712 \cdot 10^{-3}$
$479.674 \cdot 10^{-3}$
$479.635 \cdot 10^{-3}$
$479.596 \cdot 10^{-3}$
$479.558 \cdot 10^{-3}$
$479.519 \cdot 10^{-3}$
$479.48 \cdot 10^{-3}$
$479.442 \cdot 10^{-3}$
$479.403 \cdot 10^{-3}$
$479.364 \cdot 10^{-3}$
$479.326 \cdot 10^{-3}$
$479.287 \cdot 10^{-3}$
$479.248 \cdot 10^{-3}$
$479.21 \cdot 10^{-3}$
$479.171 \cdot 10^{-3}$
...

$P_{efR}(b,i) =$

$383.405 \cdot 10^{-3}$
$383.377 \cdot 10^{-3}$
$383.35 \cdot 10^{-3}$
$383.322 \cdot 10^{-3}$
$383.295 \cdot 10^{-3}$
$383.267 \cdot 10^{-3}$
$383.24 \cdot 10^{-3}$
$383.212 \cdot 10^{-3}$
$383.185 \cdot 10^{-3}$
$383.157 \cdot 10^{-3}$
$383.13 \cdot 10^{-3}$
$383.102 \cdot 10^{-3}$
$383.075 \cdot 10^{-3}$
$383.047 \cdot 10^{-3}$
$383.02 \cdot 10^{-3}$
...

$Q_{NS}(b,i) =$

$42.517 \cdot 10^{-6}$
$42.598 \cdot 10^{-6}$
$42.679 \cdot 10^{-6}$
$42.761 \cdot 10^{-6}$
$42.842 \cdot 10^{-6}$
$42.923 \cdot 10^{-6}$
$43.004 \cdot 10^{-6}$
$43.085 \cdot 10^{-6}$
$43.166 \cdot 10^{-6}$
$43.247 \cdot 10^{-6}$
$43.329 \cdot 10^{-6}$
$43.41 \cdot 10^{-6}$
$43.491 \cdot 10^{-6}$
$43.572 \cdot 10^{-6}$
$43.653 \cdot 10^{-6}$
...

$P_{NS}(b,i) =$

$483.043 \cdot 10^{-3}$
$483.011 \cdot 10^{-3}$
$482.979 \cdot 10^{-3}$
$482.946 \cdot 10^{-3}$
$482.914 \cdot 10^{-3}$
$482.881 \cdot 10^{-3}$
$482.849 \cdot 10^{-3}$
$482.817 \cdot 10^{-3}$
$482.784 \cdot 10^{-3}$
$482.752 \cdot 10^{-3}$
$482.72 \cdot 10^{-3}$
$482.687 \cdot 10^{-3}$
$482.655 \cdot 10^{-3}$
$482.623 \cdot 10^{-3}$
$482.59 \cdot 10^{-3}$
...

$P_{eNS}(b,i) =$

$89.273 \cdot 10^{-3}$
$89.267 \cdot 10^{-3}$
$89.261 \cdot 10^{-3}$
$89.255 \cdot 10^{-3}$
$89.249 \cdot 10^{-3}$
$89.243 \cdot 10^{-3}$
$89.238 \cdot 10^{-3}$
$89.232 \cdot 10^{-3}$
$89.226 \cdot 10^{-3}$
$89.22 \cdot 10^{-3}$
$89.214 \cdot 10^{-3}$
$89.208 \cdot 10^{-3}$
$89.202 \cdot 10^{-3}$
$89.196 \cdot 10^{-3}$
$89.19 \cdot 10^{-3}$
...

$Q_{NR}(b,i) =$

$42.517 \cdot 10^{-6}$
$42.598 \cdot 10^{-6}$
$42.679 \cdot 10^{-6}$
$42.761 \cdot 10^{-6}$
$42.842 \cdot 10^{-6}$
$42.923 \cdot 10^{-6}$
$43.004 \cdot 10^{-6}$
$43.085 \cdot 10^{-6}$
$43.166 \cdot 10^{-6}$
$43.247 \cdot 10^{-6}$
$43.329 \cdot 10^{-6}$
$43.41 \cdot 10^{-6}$
$43.491 \cdot 10^{-6}$
$43.572 \cdot 10^{-6}$
$43.653 \cdot 10^{-6}$
...

$P_{NR}(b,i) =$

$483.043 \cdot 10^{-3}$
$483.011 \cdot 10^{-3}$
$482.979 \cdot 10^{-3}$
$482.946 \cdot 10^{-3}$
$482.914 \cdot 10^{-3}$
$482.881 \cdot 10^{-3}$
$482.849 \cdot 10^{-3}$
$482.817 \cdot 10^{-3}$
$482.784 \cdot 10^{-3}$
$482.752 \cdot 10^{-3}$
$482.72 \cdot 10^{-3}$
$482.687 \cdot 10^{-3}$
$482.655 \cdot 10^{-3}$
$482.623 \cdot 10^{-3}$
$482.59 \cdot 10^{-3}$
...

$P_{eNR}(b,i) =$

$89.273 \cdot 10^{-3}$
$89.267 \cdot 10^{-3}$
$89.261 \cdot 10^{-3}$
$89.255 \cdot 10^{-3}$
$89.249 \cdot 10^{-3}$
$89.243 \cdot 10^{-3}$
$89.238 \cdot 10^{-3}$
$89.232 \cdot 10^{-3}$
$89.226 \cdot 10^{-3}$
$89.22 \cdot 10^{-3}$
$89.214 \cdot 10^{-3}$
$89.208 \cdot 10^{-3}$
$89.202 \cdot 10^{-3}$
$89.196 \cdot 10^{-3}$
$89.19 \cdot 10^{-3}$
...

$P_{fN}(b,i) =$

$178.547 \cdot 10^{-3}$
$178.535 \cdot 10^{-3}$
$178.523 \cdot 10^{-3}$
$178.511 \cdot 10^{-3}$
$178.499 \cdot 10^{-3}$
$178.487 \cdot 10^{-3}$
$178.475 \cdot 10^{-3}$
$178.463 \cdot 10^{-3}$
$178.451 \cdot 10^{-3}$
$178.439 \cdot 10^{-3}$
$178.427 \cdot 10^{-3}$
$178.415 \cdot 10^{-3}$
$178.403 \cdot 10^{-3}$
$178.391 \cdot 10^{-3}$
$178.379 \cdot 10^{-3}$
...

$P_{efN}(b,i) =$

$132.907 \cdot 10^{-3}$
$132.899 \cdot 10^{-3}$
$132.89 \cdot 10^{-3}$
$132.881 \cdot 10^{-3}$
$132.872 \cdot 10^{-3}$
$132.863 \cdot 10^{-3}$
$132.854 \cdot 10^{-3}$
$132.845 \cdot 10^{-3}$
$132.836 \cdot 10^{-3}$
$132.827 \cdot 10^{-3}$
$132.818 \cdot 10^{-3}$
$132.81 \cdot 10^{-3}$
$132.801 \cdot 10^{-3}$
$132.792 \cdot 10^{-3}$
$132.783 \cdot 10^{-3}$
...

$P_{ef}(b,i) =$

$516.312 \cdot 10^{-3}$
$516.276 \cdot 10^{-3}$
$516.239 \cdot 10^{-3}$
$516.203 \cdot 10^{-3}$
$516.167 \cdot 10^{-3}$
$516.13 \cdot 10^{-3}$
$516.094 \cdot 10^{-3}$
$516.057 \cdot 10^{-3}$
$516.021 \cdot 10^{-3}$
$515.985 \cdot 10^{-3}$
$515.948 \cdot 10^{-3}$
$515.912 \cdot 10^{-3}$
$515.875 \cdot 10^{-3}$
$515.839 \cdot 10^{-3}$
$515.803 \cdot 10^{-3}$
...

$pc(b,i) =$

$9.01 \cdot 10^{0}$
$9.01 \cdot 10^{0}$
$9.01 \cdot 10^{0}$
$9.01 \cdot 10^{0}$
$9.01 \cdot 10^{0}$
$9.01 \cdot 10^{0}$
$9.01 \cdot 10^{0}$
$9.01 \cdot 10^{0}$
$9.01 \cdot 10^{0}$
$9.01 \cdot 10^{0}$
$9.01 \cdot 10^{0}$
$9.01 \cdot 10^{0}$
$9.01 \cdot 10^{0}$
$9.01 \cdot 10^{0}$
$9.01 \cdot 10^{0}$
...

$a_i =$

$165.638 \cdot 10^{3}$
$165.393 \cdot 10^{3}$
$165.159 \cdot 10^{3}$
$164.937 \cdot 10^{3}$
$164.73 \cdot 10^{3}$
$164.537 \cdot 10^{3}$
$164.36 \cdot 10^{3}$
$164.201 \cdot 10^{3}$
$164.06 \cdot 10^{3}$
$163.939 \cdot 10^{3}$
$163.839 \cdot 10^{3}$
$163.761 \cdot 10^{3}$
$163.705 \cdot 10^{3}$
$163.672 \cdot 10^{3}$
$163.663 \cdot 10^{3}$
...

Appendix D: Receiver sensitivity of DiPPM at 100 Mbps

Receiver sensitivity of DiPPM with zero guard at 100 Mbit/s and 3 PCM BITS for LOS Indoor VLC Link 2019

$i := 0, 1 .. 30$

$v_i := v_{off} + \frac{i}{1000}$

$n := 10$ Number of like symbols in PCM

$\eta q := 1.6 \cdot 10^{-19}$ Quantum energy

$\lambda := 820 \cdot 10^{-9}$ This is the wavelength of operation

$photon\_energy := \frac{6.63 \cdot 10^{-34} \cdot 3 \cdot 10^{8}}{\lambda}$ $gu \equiv 0$

$R_o := \frac{\eta q}{photon\_energy}$ $R_o = 659.628 \times 10^{-3}$

Preamplifier terms

$S_o := 25 \cdot 10^{-24}$ **Preamplifier input noise**

$B := 100 \cdot 10^{6}$ Bit rate

$T_b := \frac{1}{B}$ PCM bit time

Slot time $T_s := \frac{T_b}{2 + gu}$ $T_s = 5 \times 10^{-9}$

$f_c := 0.5 \cdot \frac{1}{T_s}$ $\omega_c := 2 \cdot \pi \cdot f_c$

preamplifie $H_{pre}(\omega) := \frac{1}{1 + j \cdot \frac{\omega}{\omega_c}}$

VLC impulse response

$t := 0, 0.1 .. 14$

$h(t) := \left[1 \cdot \left[\int_0^t Re\left[\exp\left[i \cdot \omega \cdot (t) \cdot H_{pre}(\omega) \right] \right] d\omega \right] \right]$

Pulse shape

$$\alpha_p := \frac{0.1874 \cdot T_b}{f_n} \qquad f_n \equiv 0.65 \qquad \alpha_{pn} := \frac{\alpha_p}{T_s}$$

$$Pulse1(t) := \frac{1}{\sqrt{2 \cdot \pi} \cdot \alpha_{pn} \cdot 1} \cdot \exp\left(\frac{-t^2}{2 \cdot \alpha_{pn}^2}\right)$$

$$I_0(t) := \left(\frac{1}{T_s} \cdot \int_0^t h(\tau) \cdot Pulse1(t - \tau)\, d\tau\right)$$

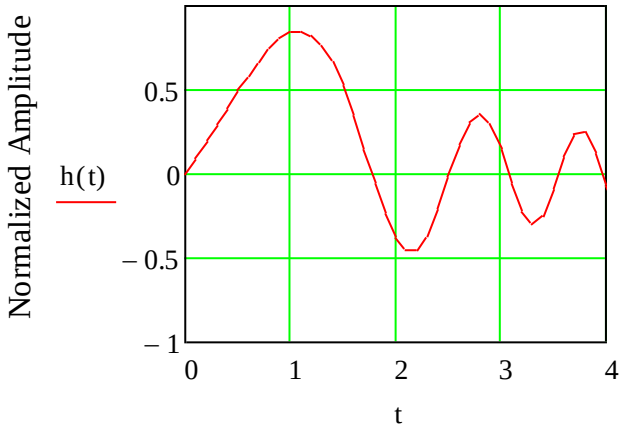

Time slot (Ts)

Pulse1(t) =

691.869·10-3
681.542·10-3
651.478·10-3
604.289·10-3
543.91·10-3
475.06·10-3
402.63·10-3
331.134·10-3
264.264·10-3
204.649·10-3
153.787·10-3
112.142·10-3
79.351·10-3
54.485·10-3
36.303·10-3
...

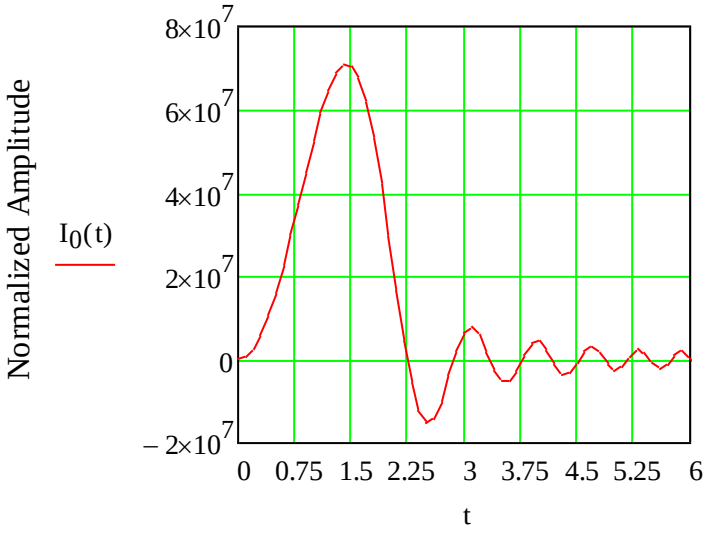

Time slot (Ts)

$I_0(t)$ =

0·10^0
690.136·10^3
2.74·10^6
6.087·10^6
10.631·10^6
16.23·10^6
22.706·10^6
29.842·10^6
37.377·10^6
45.009·10^6
52.387·10^6
59.112·10^6
64.747·10^6
68.826·10^6
70.892·10^6
...

$t := 1.5$ $I_1(t) := \frac{d}{dt} I_0(t)$ Guess at the peak time

$t_{pk} := root\left(I_1(t) \cdot T_s^{\,3}, t\right)$ $t_{pk} = 1.437 \times 10^{0}$ This is the peak time

$v_{pk} := I_0\left(t_{pk}\right)$ $v_{pk} = 71.061 \times 10^{6}$ This is the peak voltage

.

$noise := \frac{\pi \cdot f_c}{2}$ $noise = 157.08 \times 10^{6}$ Noise bandwidth

$S_o \cdot noise = 3.927 \times 10^{-15}$ $\sqrt{S_o \cdot noise} = 62.666 \times 10^{-9}$

Erasure of pulse

$Q_{e_i} := \eta q \cdot \frac{v_{pk} - v_i \cdot v_{pk}}{\sqrt{S_o \cdot noise}}$ $P_r(b, i) := \frac{1}{2} \cdot erfc\left(\frac{Q_{e_i} \cdot b}{\sqrt{2}}\right)$

$$P_{er}(b, i) := 2 \cdot \sum_{x=0}^{n-1} \left[\left(\frac{1}{2}\right)^{x+3} \cdot P_r(b, i) \cdot (x+1) + \left(\frac{1}{2}\right)^{n+2} \cdot P_r(b, i) \cdot (n+1) \right]$$

False alarm

False alarm when pulse appears in slot R can spread into S-slot of following symbol P_{efISI1}

or into previous S-slot of same symbol P_{efISI2} , $v_{oISI1} := Vo(td - Ts)$ and $v_{oISI1} := Vo(td - Ts)$

$v_{oISI1\_Ts_i} := v_i \cdot I_0\left(t_{pk} - 1\right)$ $v_{oISI2\_Ts_i} := v_i \cdot I_0\left(t_{pk} + 1\right)$

$Q_{eISI1_i} := \eta q \cdot \frac{v_i \cdot v_{pk} - v_{oISI1\_Ts_i}}{\sqrt{S_o \cdot noise}}$ $P_{efISI1}(b, i) := \frac{1}{2} \cdot erfc\left(\frac{Q_{eISI1_i} \cdot b}{\sqrt{2}}\right)$

$Q_{eISI2_i} := \eta q \cdot \frac{v_i \cdot v_{pk} - v_{oISI2\_Ts_i}}{\sqrt{S_o \cdot noise}}$ $P_{efISI2}(b, i) := \frac{1}{2} \cdot erfc\left(\frac{Q_{eISI2_i} \cdot b}{\sqrt{2}}\right)$

$$P_{efR}(b,i) := \left[\sum_{x=0}^{n-1}\left[\left(\frac{1}{2}\right)^{x+3}\cdot P_{efISI1}(b,i)\cdot(x) + \left(\frac{1}{2}\right)^{n+2}\cdot P_{efISI1}(b,i)\cdot(n)\right]\right]\ldots$$
$$+\sum_{x=0}^{n-1}\left[\left(\frac{1}{2}\right)^{x+3}\cdot P_{efISI2}(b,i)\cdot(x+1) + \left(\frac{1}{2}\right)^{n+2}\cdot P_{efISI2}(b,i)\cdot(n+1)\right]$$

False alarm no ISI accurs between S and R and the error apears within the run of N-symbols where k is the symbol position

False alarm between R and S pulses - N to SET

$$Q_{NS}(b,i) := \eta q\cdot\frac{v_i\cdot v_{pk}}{\sqrt{S_o\cdot noise}} \qquad P_{NS}(b,i) := \frac{1}{2}\cdot erfc\left(\frac{Q_{NS}(b,i)\cdot b}{\sqrt{2}}\right)$$

$$P_{eNS}(b,i) := \left[\sum_{y=3}^{n-1}\sum_{k=2}^{y-1}\left[\left(\frac{1}{2}\right)^{y+3}\cdot P_{NS}(b,i)\cdot(y+1-k)\right]\right]\ldots$$
$$+\sum_{k=2}^{n-1}\left[\left(\frac{1}{2}\right)^{n+2}\cdot P_{NS}(b,i)\cdot(n+1-k)\right]$$

False alarm between S and R pulses - N to R

$$Q_{NR}(b,i) := \eta q\cdot\frac{v_i\cdot v_{pk}}{\sqrt{S_o\cdot noise}} \qquad P_{NR}(b,i) := \frac{1}{2}\cdot erfc\left(\frac{Q_{NR}(b,i)\cdot b}{\sqrt{2}}\right)$$

$$P_{eNR}(b,i) := \left[\sum_{x=3}^{n-1}\sum_{k=2}^{x-1}\left[\left(\frac{1}{2}\right)^{x+3}\cdot P_{NR}(b,i)\cdot(x+1-k)\right]\right]\ldots$$
$$+\sum_{k=2}^{n-1}\left[\left(\frac{1}{2}\right)^{n+2}\cdot P_{NR}(b,i)\cdot(n+1-k)\right]$$

$$P_{fN}(b,i) := P_{eNS}(b,i) + P_{eNR}(b,i)$$

$$P_{efN}(b,i) := \left[\sum_{x=1}^{n-1} \left[\left(\frac{1}{2}\right)^{x+3} \cdot \sum_{k=1}^{x} \left[P_{fN}(b,i) \cdot (x+1-k) \right] \right] \ldots \right] \ldots + \left[\left(\frac{1}{2}\right)^{n+2} \cdot \sum_{k=1}^{n} \left[P_{fN}(b,i) \cdot (n+1-k) \right] \right] + \sum_{x=2}^{n-1} \left[\left(\frac{1}{2}\right)^{x+3} \cdot \sum_{k=2}^{x} \left[P_{fN}(b,i) \cdot (x+1-k) \right] \right] \ldots + \left(\frac{1}{2}\right)^{n+2} \cdot \sum_{k=2}^{n} \left[P_{fN}(b,i) \cdot (n+1-k) \right]$$

Total Fals alarm

$$P_{ef}(b,i) := P_{efN}(b,i) + P_{efR}(b,i)$$

Total Errors

$$P_{eb}(b,i) := P_{er}(b,i) + P_{ef}(b,i)$$

$$pc(b,i) := \left(\log\left(P_{eb}(b,i)\right) + 9\right)$$ Set for 1 in 10^9 errors

$$P_{er}(b,0) = 487.868 \times 10^{-3} \quad P_{ef}(b,0) = 492.779 \times 10^{-3}$$

$$a_i := \text{root}(pc(b,i), b)$$ Find the root to give 1 in 10^9

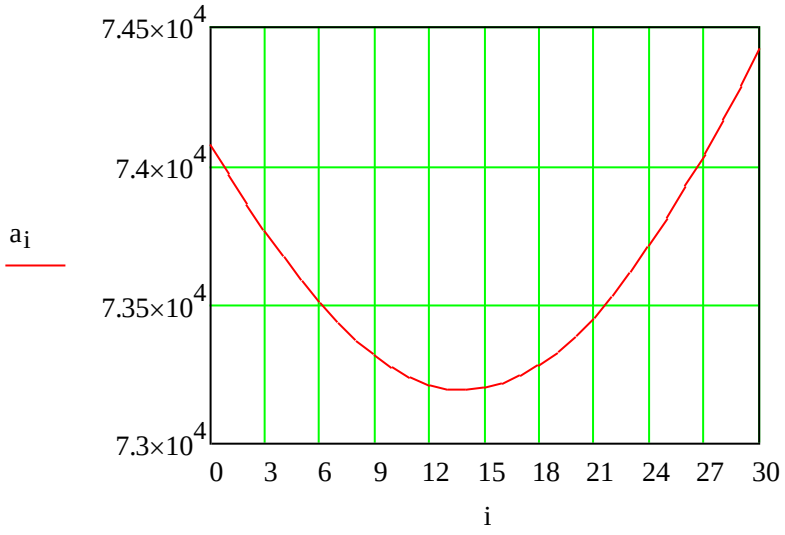

$b \equiv 1 \cdot 10^{3}$

$v_{off} \equiv 0.524$

$gu = 0 \times 10^{0}$

minimum:= min(a) $\quad$ minimum= 73.192×10^{3}

Received power

$$P_r := \left[\frac{\text{minimum}}{((gu + 2))} \cdot \text{photon\_energy}\left(\frac{1 + n}{2n} \right) \cdot B \right]$$

$P_r = 488.224 \times 10^{-9}$

Receiver sensitivity

$$P_{rdBm} := 10 \cdot \log\left(\frac{P_r}{10^{-3}} \right)$$

$P_{rdBm} = -33.114 \times 10^{0}$

$pc(minimum, 14) = 1.776 \times 10^{-15}$ closed to zero

$v_{pk} - v_i \cdot v_{pk}$ =
$33.825 \cdot 10^{6}$
$33.754 \cdot 10^{6}$
$33.683 \cdot 10^{6}$
$33.612 \cdot 10^{6}$
$33.541 \cdot 10^{6}$
$33.47 \cdot 10^{6}$
$33.398 \cdot 10^{6}$
$33.327 \cdot 10^{6}$
$33.256 \cdot 10^{6}$
$33.185 \cdot 10^{6}$
$33.114 \cdot 10^{6}$
$33.043 \cdot 10^{6}$
$32.972 \cdot 10^{6}$
$32.901 \cdot 10^{6}$
$32.83 \cdot 10^{6}$
...

$v_i \cdot v_{pk}$ =
$37.236 \cdot 10^{6}$
$37.307 \cdot 10^{6}$
$37.378 \cdot 10^{6}$
$37.449 \cdot 10^{6}$
$37.52 \cdot 10^{6}$
$37.591 \cdot 10^{6}$
$37.662 \cdot 10^{6}$
$37.733 \cdot 10^{6}$
$37.804 \cdot 10^{6}$
$37.875 \cdot 10^{6}$
$37.946 \cdot 10^{6}$
$38.017 \cdot 10^{6}$
$38.088 \cdot 10^{6}$
$38.16 \cdot 10^{6}$
$38.231 \cdot 10^{6}$
...

Q_{e_i} =
$86.363 \cdot 10^{-6}$
$86.181 \cdot 10^{-6}$
$86 \cdot 10^{-6}$
$85.818 \cdot 10^{-6}$
$85.637 \cdot 10^{-6}$
$85.455 \cdot 10^{-6}$
$85.274 \cdot 10^{-6}$
$85.093 \cdot 10^{-6}$
$84.911 \cdot 10^{-6}$
$84.73 \cdot 10^{-6}$
$84.548 \cdot 10^{-6}$
$84.367 \cdot 10^{-6}$
$84.185 \cdot 10^{-6}$
$84.004 \cdot 10^{-6}$
$83.822 \cdot 10^{-6}$
...

$P_{er}(b, i)$ =
$487.868 \cdot 10^{-3}$
$487.944 \cdot 10^{-3}$
$488.019 \cdot 10^{-3}$
$488.095 \cdot 10^{-3}$
$488.171 \cdot 10^{-3}$
$488.246 \cdot 10^{-3}$
$488.322 \cdot 10^{-3}$
$488.397 \cdot 10^{-3}$
$488.473 \cdot 10^{-3}$
$488.548 \cdot 10^{-3}$
$488.624 \cdot 10^{-3}$
$488.7 \cdot 10^{-3}$
$488.775 \cdot 10^{-3}$
$488.851 \cdot 10^{-3}$
$488.926 \cdot 10^{-3}$
...

$v_{oISI1\_Ts_i}$ =
$6.585 \cdot 10^{6}$
$6.597 \cdot 10^{6}$
$6.61 \cdot 10^{6}$
$6.623 \cdot 10^{6}$
$6.635 \cdot 10^{6}$
$6.648 \cdot 10^{6}$
$6.66 \cdot 10^{6}$
$6.673 \cdot 10^{6}$
$6.685 \cdot 10^{6}$
$6.698 \cdot 10^{6}$
$6.711 \cdot 10^{6}$
$6.723 \cdot 10^{6}$
$6.736 \cdot 10^{6}$
$6.748 \cdot 10^{6}$
$6.761 \cdot 10^{6}$
...

$v_{oISI2\_Ts_i}$ =
$-7.32 \cdot 10^{6}$
$-7.334 \cdot 10^{6}$
$-7.348 \cdot 10^{6}$
$-7.362 \cdot 10^{6}$
$-7.376 \cdot 10^{6}$
$-7.39 \cdot 10^{6}$
$-7.404 \cdot 10^{6}$
$-7.418 \cdot 10^{6}$
$-7.432 \cdot 10^{6}$
$-7.446 \cdot 10^{6}$
$-7.46 \cdot 10^{6}$
$-7.474 \cdot 10^{6}$
$-7.488 \cdot 10^{6}$
$-7.501 \cdot 10^{6}$
$-7.515 \cdot 10^{6}$
...

Q_{eISI1_i} =
$78.259 \cdot 10^{-6}$
$78.408 \cdot 10^{-6}$
$78.557 \cdot 10^{-6}$
$78.707 \cdot 10^{-6}$
$78.856 \cdot 10^{-6}$
$79.005 \cdot 10^{-6}$
$79.155 \cdot 10^{-6}$
$79.304 \cdot 10^{-6}$
$79.453 \cdot 10^{-6}$
$79.603 \cdot 10^{-6}$
$79.752 \cdot 10^{-6}$
$79.902 \cdot 10^{-6}$
$80.051 \cdot 10^{-6}$
$80.2 \cdot 10^{-6}$
$80.35 \cdot 10^{-6}$
...

$P_{efISI1}(b, i)$ =
$468.811 \cdot 10^{-3}$
$468.752 \cdot 10^{-3}$
$468.692 \cdot 10^{-3}$
$468.633 \cdot 10^{-3}$
$468.574 \cdot 10^{-3}$
$468.514 \cdot 10^{-3}$
$468.455 \cdot 10^{-3}$
$468.395 \cdot 10^{-3}$
$468.336 \cdot 10^{-3}$
$468.277 \cdot 10^{-3}$
$468.217 \cdot 10^{-3}$
$468.158 \cdot 10^{-3}$
$468.098 \cdot 10^{-3}$
$468.039 \cdot 10^{-3}$
$467.98 \cdot 10^{-3}$
...

Q_{eISI2_i} =
$113.761 \cdot 10^{-6}$
$113.978 \cdot 10^{-6}$
$114.195 \cdot 10^{-6}$
$114.412 \cdot 10^{-6}$
$114.629 \cdot 10^{-6}$
$114.846 \cdot 10^{-6}$
$115.063 \cdot 10^{-6}$
$115.28 \cdot 10^{-6}$
$115.497 \cdot 10^{-6}$
$115.715 \cdot 10^{-6}$
$115.932 \cdot 10^{-6}$
$116.149 \cdot 10^{-6}$
$116.366 \cdot 10^{-6}$
$116.583 \cdot 10^{-6}$
$116.8 \cdot 10^{-6}$
...

$P_{efISI2}(b,i) =$

$454.714 \cdot 10^{-3}$
$454.628 \cdot 10^{-3}$
$454.542 \cdot 10^{-3}$
$454.456 \cdot 10^{-3}$
$454.37 \cdot 10^{-3}$
$454.284 \cdot 10^{-3}$
$454.197 \cdot 10^{-3}$
$454.111 \cdot 10^{-3}$
$454.025 \cdot 10^{-3}$
$453.939 \cdot 10^{-3}$
$453.853 \cdot 10^{-3}$
$453.767 \cdot 10^{-3}$
$453.681 \cdot 10^{-3}$
$453.595 \cdot 10^{-3}$
$453.509 \cdot 10^{-3}$
...

$P_{efR}(b,i) =$

$365.626 \cdot 10^{-3}$
$365.564 \cdot 10^{-3}$
$365.503 \cdot 10^{-3}$
$365.442 \cdot 10^{-3}$
$365.381 \cdot 10^{-3}$
$365.32 \cdot 10^{-3}$
$365.258 \cdot 10^{-3}$
$365.197 \cdot 10^{-3}$
$365.136 \cdot 10^{-3}$
$365.075 \cdot 10^{-3}$
$365.013 \cdot 10^{-3}$
$364.952 \cdot 10^{-3}$
$364.891 \cdot 10^{-3}$
$364.83 \cdot 10^{-3}$
$364.769 \cdot 10^{-3}$
...

$Q_{NS}(b,i) =$

$95.071 \cdot 10^{-6}$
$95.253 \cdot 10^{-6}$
$95.434 \cdot 10^{-6}$
$95.616 \cdot 10^{-6}$
$95.797 \cdot 10^{-6}$
$95.979 \cdot 10^{-6}$
$96.16 \cdot 10^{-6}$
$96.341 \cdot 10^{-6}$
$96.523 \cdot 10^{-6}$
$96.704 \cdot 10^{-6}$
$96.886 \cdot 10^{-6}$
$97.067 \cdot 10^{-6}$
$97.249 \cdot 10^{-6}$
$97.43 \cdot 10^{-6}$
$97.611 \cdot 10^{-6}$
...

$P_{NS}(b,i) =$

$462.129 \cdot 10^{-3}$
$462.057 \cdot 10^{-3}$
$461.985 \cdot 10^{-3}$
$461.913 \cdot 10^{-3}$
$461.841 \cdot 10^{-3}$
$461.769 \cdot 10^{-3}$
$461.697 \cdot 10^{-3}$
$461.625 \cdot 10^{-3}$
$461.553 \cdot 10^{-3}$
$461.481 \cdot 10^{-3}$
$461.409 \cdot 10^{-3}$
$461.337 \cdot 10^{-3}$
$461.264 \cdot 10^{-3}$
$461.192 \cdot 10^{-3}$
$461.12 \cdot 10^{-3}$
...

$P_{eNS}(b,i) =$

$85.408 \cdot 10^{-3}$
$85.395 \cdot 10^{-3}$
$85.381 \cdot 10^{-3}$
$85.368 \cdot 10^{-3}$
$85.355 \cdot 10^{-3}$
$85.342 \cdot 10^{-3}$
$85.328 \cdot 10^{-3}$
$85.315 \cdot 10^{-3}$
$85.302 \cdot 10^{-3}$
$85.288 \cdot 10^{-3}$
$85.275 \cdot 10^{-3}$
$85.262 \cdot 10^{-3}$
$85.248 \cdot 10^{-3}$
$85.235 \cdot 10^{-3}$
$85.222 \cdot 10^{-3}$
...

$Q_{NR}(b,i) =$

$95.071 \cdot 10^{-6}$
$95.253 \cdot 10^{-6}$
$95.434 \cdot 10^{-6}$
$95.616 \cdot 10^{-6}$
$95.797 \cdot 10^{-6}$
$95.979 \cdot 10^{-6}$
$96.16 \cdot 10^{-6}$
$96.341 \cdot 10^{-6}$
$96.523 \cdot 10^{-6}$
$96.704 \cdot 10^{-6}$
$96.886 \cdot 10^{-6}$
$97.067 \cdot 10^{-6}$
$97.249 \cdot 10^{-6}$
$97.43 \cdot 10^{-6}$
$97.611 \cdot 10^{-6}$
...

$P_{NR}(b,i) =$

$462.129 \cdot 10^{-3}$
$462.057 \cdot 10^{-3}$
$461.985 \cdot 10^{-3}$
$461.913 \cdot 10^{-3}$
$461.841 \cdot 10^{-3}$
$461.769 \cdot 10^{-3}$
$461.697 \cdot 10^{-3}$
$461.625 \cdot 10^{-3}$
$461.553 \cdot 10^{-3}$
$461.481 \cdot 10^{-3}$
$461.409 \cdot 10^{-3}$
$461.337 \cdot 10^{-3}$
$461.264 \cdot 10^{-3}$
$461.192 \cdot 10^{-3}$
$461.12 \cdot 10^{-3}$
...

$P_{eNR}(b,i) =$

$85.408 \cdot 10^{-3}$
$85.395 \cdot 10^{-3}$
$85.381 \cdot 10^{-3}$
$85.368 \cdot 10^{-3}$
$85.355 \cdot 10^{-3}$
$85.342 \cdot 10^{-3}$
$85.328 \cdot 10^{-3}$
$85.315 \cdot 10^{-3}$
$85.302 \cdot 10^{-3}$
$85.288 \cdot 10^{-3}$
$85.275 \cdot 10^{-3}$
$85.262 \cdot 10^{-3}$
$85.248 \cdot 10^{-3}$
$85.235 \cdot 10^{-3}$
$85.222 \cdot 10^{-3}$
...

$P_{fN}(b,i) =$

$170.816 \cdot 10^{-3}$
$170.79 \cdot 10^{-3}$
$170.763 \cdot 10^{-3}$
$170.736 \cdot 10^{-3}$
$170.71 \cdot 10^{-3}$
$170.683 \cdot 10^{-3}$
$170.656 \cdot 10^{-3}$
$170.63 \cdot 10^{-3}$
$170.603 \cdot 10^{-3}$
$170.577 \cdot 10^{-3}$
$170.55 \cdot 10^{-3}$
$170.523 \cdot 10^{-3}$
$170.497 \cdot 10^{-3}$
$170.47 \cdot 10^{-3}$
$170.443 \cdot 10^{-3}$
...

$P_{efN}(b,i) =$

$127.153 \cdot 10^{-3}$
$127.133 \cdot 10^{-3}$
$127.113 \cdot 10^{-3}$
$127.094 \cdot 10^{-3}$
$127.074 \cdot 10^{-3}$
$127.054 \cdot 10^{-3}$
$127.034 \cdot 10^{-3}$
$127.014 \cdot 10^{-3}$
$126.994 \cdot 10^{-3}$
$126.975 \cdot 10^{-3}$
$126.955 \cdot 10^{-3}$
$126.935 \cdot 10^{-3}$
$126.915 \cdot 10^{-3}$
$126.895 \cdot 10^{-3}$
$126.875 \cdot 10^{-3}$
...

$P_{ef}(b, i) =$

$492.779 \cdot 10^{-3}$
$492.698 \cdot 10^{-3}$
$492.617 \cdot 10^{-3}$
$492.535 \cdot 10^{-3}$
$492.454 \cdot 10^{-3}$
$492.373 \cdot 10^{-3}$
$492.292 \cdot 10^{-3}$
$492.211 \cdot 10^{-3}$
$492.13 \cdot 10^{-3}$
$492.049 \cdot 10^{-3}$
$491.968 \cdot 10^{-3}$
$491.887 \cdot 10^{-3}$
$491.806 \cdot 10^{-3}$
$491.725 \cdot 10^{-3}$
$491.644 \cdot 10^{-3}$
...

$pc(b, i) =$

$8.992 \cdot 10^{0}$
$8.992 \cdot 10^{0}$
$8.992 \cdot 10^{0}$
$8.992 \cdot 10^{0}$
$8.992 \cdot 10^{0}$
$8.992 \cdot 10^{0}$
$8.991 \cdot 10^{0}$
$8.991 \cdot 10^{0}$
$8.991 \cdot 10^{0}$
$8.991 \cdot 10^{0}$
$8.991 \cdot 10^{0}$
$8.991 \cdot 10^{0}$
$8.991 \cdot 10^{0}$
$8.991 \cdot 10^{0}$
$8.991 \cdot 10^{0}$
...

$a_i =$

$74.076 \cdot 10^{3}$
$73.966 \cdot 10^{3}$
$73.861 \cdot 10^{3}$
$73.762 \cdot 10^{3}$
$73.669 \cdot 10^{3}$
$73.583 \cdot 10^{3}$
$73.504 \cdot 10^{3}$
$73.433 \cdot 10^{3}$
$73.37 \cdot 10^{3}$
$73.316 \cdot 10^{3}$
$73.271 \cdot 10^{3}$
$73.236 \cdot 10^{3}$
$73.211 \cdot 10^{3}$
$73.196 \cdot 10^{3}$
$73.192 \cdot 10^{3}$
...

Appendix E: Receiver sensitivity of Duo PPM at 20 Mbps

Receiver sensitivity of Duo PPM with zero guard at 20 Mbit/s and 3 PCM BITS for LOS Indoor VLC Link 2019

$i := 0, 1 .. 30$

$v_i := v_{off} + \frac{i}{1000}$

$n := 10$ Number of like symbols in PCM

$\eta q := 1.6 \cdot 10^{-19}$ Quantum energy

$\lambda := 820 \cdot 10^{-9}$ This is the wavelength of operation

$$photon\_energy := \frac{6.63 \cdot 10^{-34} \cdot 3 \cdot 10^{8}}{\lambda} \qquad gu \equiv 0$$

$$R_o := \frac{\eta q}{photon\_energy} \qquad R_o = 659.628 \times 10^{-3}$$

Preamplifier terms

$S_o := 25 \cdot 10^{-24}$ **Preamplifier input noise**

$B := 20 \cdot 10^{6}$ **Bit rate**

$T_b := \frac{1}{B}$ PCM bit time

Slot time $T_s := \frac{T_b}{2 + gu} \qquad T_s = 25 \times 10^{-9}$

$f_c := 0.5 \cdot \frac{1}{T_s} \qquad \omega_c := 2 \cdot \pi \cdot f_c \qquad f_c = 20 \times 10^{6}$

preamplifier $H_{pre}(\omega) := \frac{1}{1 + j \cdot \frac{\omega}{\omega_c}}$

Pulse shape

$t := 0, 0.1 .. 14$

VLC impulse response

$$h(t) := \left[\frac{1}{1} \cdot \left[\int_0^t \mathrm{Re}\left[\exp\left[i \cdot \omega \cdot (t) \cdot H_{pre}(\omega) \right] \right] d\omega \right] \right]$$

$$\alpha_p := \frac{0.1874 \cdot T_b}{f_n} \qquad f_n \equiv 0.6 \qquad \alpha_{pn} := \frac{\alpha_p}{T_s}$$

$$Pulse1(t) := \frac{1}{\sqrt{2 \cdot \pi} \cdot \alpha_{pn} \cdot 1} \cdot \exp\left(\frac{-t^2}{2 \cdot \alpha_{pn}^2} \right)$$

$$I_0(t) := \left(\frac{1}{T_s} \cdot \int_0^t h(\tau) \cdot Pulse1(t - \tau)\, d\tau \right)$$

$h(t) =$

$804.764 \cdot 10^{-3}$
$841.471 \cdot 10^{-3}$
$850.56 \cdot 10^{-3}$
$826.215 \cdot 10^{-3}$
$763.772 \cdot 10^{-3}$
$660.865 \cdot 10^{-3}$
$518.715 \cdot 10^{-3}$
$343.347 \cdot 10^{-3}$
$146.439 \cdot 10^{-3}$
$-54.583 \cdot 10^{-3}$
$-237.614 \cdot 10^{-3}$
$-378.401 \cdot 10^{-3}$
$-454.585 \cdot 10^{-3}$
$-450.849 \cdot 10^{-3}$
$-364.248 \cdot 10^{-3}$
...

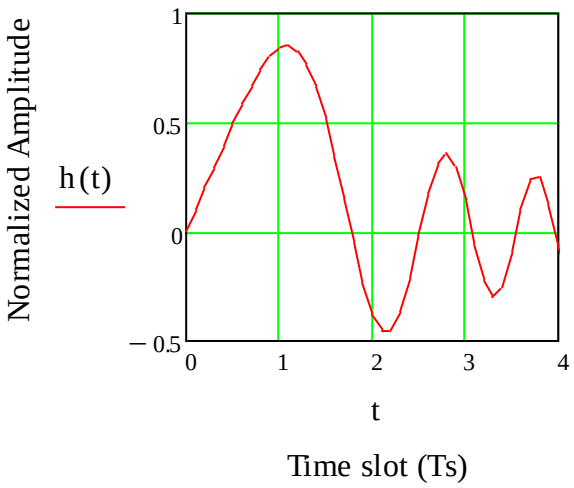

$Pulse1(t) =$

$691.869 \cdot 10^{-3}$
$681.542 \cdot 10^{-3}$
$651.478 \cdot 10^{-3}$
$604.289 \cdot 10^{-3}$
$543.91 \cdot 10^{-3}$
$475.06 \cdot 10^{-3}$
$402.63 \cdot 10^{-3}$
$331.134 \cdot 10^{-3}$
$264.264 \cdot 10^{-3}$
$204.649 \cdot 10^{-3}$
$153.787 \cdot 10^{-3}$
$112.142 \cdot 10^{-3}$
$79.351 \cdot 10^{-3}$
$54.485 \cdot 10^{-3}$
$36.303 \cdot 10^{-3}$
...

$I_0(t) =$

$0 \cdot 10^{0}$
$138.027 \cdot 10^{3}$
$547.963 \cdot 10^{3}$
$1.217 \cdot 10^{6}$
$2.126 \cdot 10^{6}$
$3.246 \cdot 10^{6}$
$4.541 \cdot 10^{6}$
$5.968 \cdot 10^{6}$
$7.475 \cdot 10^{6}$
$9.002 \cdot 10^{6}$
$10.477 \cdot 10^{6}$
$11.822 \cdot 10^{6}$
$12.949 \cdot 10^{6}$
$13.765 \cdot 10^{6}$
$14.178 \cdot 10^{6}$
...

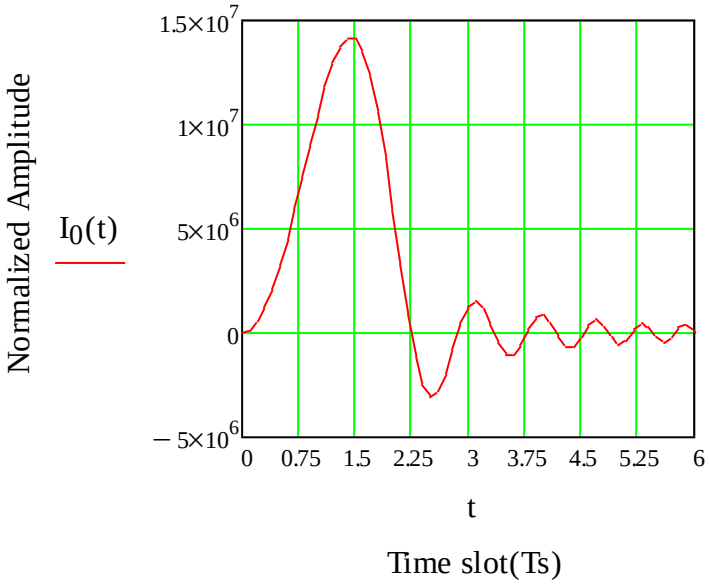

$t := 1.5$ $\quad I_1(t) := \frac{d}{dt} I_0(t)$ Guess at the peak time

$t_{pk} := root\left(I_1(t) \cdot T_s^{\,3}, t\right)$ $\quad t_{pk} = 1.437\times 10^0$ This is the peak time

$v_{pk} := I_0\left(t_{pk}\right)$ $\quad v_{pk} = 14.212\times 10^6$ This is the peak voltage

$noise := \frac{\pi \cdot f_c}{2}$ $\quad noise = 31.416\times 10^6$ Noise bandwidth

$S_o \cdot noise = 0 \times 10^0$ $\quad \sqrt{S_o \cdot noise} = 28.025\times 10^{-9}$

$x := 0..\, n$ $\quad y := 0..\, n$

Erasure of pulse

$$Q0_{e_i} := \eta q \cdot \frac{v_{pk} + v_i \cdot v_{pk}}{\sqrt{S_o \cdot noise}} \qquad Err(x, y) := \left\lceil \left\lceil \left(\frac{x - y}{2} \right) \right\rceil \right\rceil$$

$$error0(x, y) := \left[\sum_{y=0}^{n-1} \left[\left(\frac{1}{4}\right) \cdot \left(\frac{1}{2}\right)^y \cdot \left(\frac{1}{4}\right) \cdot Err(0, y) \ \ldots \right. \right. \\ \left. \left. + \left(\frac{1}{4}\right) \cdot \left(\frac{1}{2}\right)^n \cdot \left(\frac{1}{4}\right) \cdot 1.\, Err(0, n) \right] \right]$$

$$P_{r0}(b,i) := \frac{1}{2}\cdot \operatorname{erfc}\left(\frac{Q0_{e_i}\cdot b}{\sqrt{2}}\right) error0(x,y)$$

$$Q1_{e_i} := \eta q \cdot \frac{v_{pk} - v_i \cdot v_{pk}}{\sqrt{S_o \cdot noise}}$$

$$error1(x,y) := \left[\sum_{x=1}^{n-1} \left[\left[\sum_{y=0}^{n-1} \left[\left(\frac{1}{8}\right)\cdot\left(\frac{1}{2}\right)^{y}\cdot\left(\frac{1}{2}\right)^{x}\cdot\frac{1}{2}\,Err(x,y) \right] \ldots \right] \ldots \right. \right.$$
$$\left. \left. + \left(\frac{1}{4}\right)\cdot\left(\frac{1}{2}\right)^{n}\cdot\left(\frac{1}{2}\right)\cdot Err(x,n) \right] \right.$$
$$\left. + \sum_{y=0}^{n-1} \left[\left(\frac{1}{4}\right)\cdot\left(\frac{1}{2}\right)^{y}\left(\frac{1}{2}\right)^{n}\cdot\left(\frac{1}{2}\right)\cdot Err(n,y) \ldots \right] \right.$$
$$\left. \left. + \left(\frac{1}{4}\right)\cdot\left(\frac{1}{2}\right)^{n}\cdot\left(\frac{1}{2}\right)^{n}\cdot Err(n,n) \right] \right] \right]$$

$$P_{r1}(b,i) := \frac{1}{2}\cdot \operatorname{erfc}\left(\frac{Q1_{e_i}\cdot b}{\sqrt{2}}\right) error1(x,y)$$

$$P_{er}(b,i) := P_{r0}(b,i) + P_{r1}(b,i)$$

$\tau_R := \alpha_p$

$x := 0..n$

False alarm

$k := 1$

False alarm no ISI accurs between S and R and the error apears within the run of N-symbols where k is the symbol position

$ODD\cdot combinations k$ $EVEN\cdot combinations$

$$odd(k) := \frac{k}{2} - trunc\left(\frac{k}{2}\right) \qquad Erodd(x,y,k) := \frac{k}{2}$$

$$even(k) := \frac{k}{2} - trunc\left(\frac{k}{2}\right) \qquad Ereven(x,y,k) := \frac{x-k}{2}$$

$$Er(x,y,k) := Ereven(x,y,k)\cdot even(k) + Erodd(x,y,k)\cdot odd(k)$$

$$Q_{f0_i} := \frac{v_i \cdot v_{pk}}{\sqrt{S_o \cdot noise}} \qquad v_o(t) := I_0(t)$$

FALSE ALARMS

$$\text{errorf0}(x,y,k) := \left[\sum_{y=1}^{n-1} \left[\left(\frac{1}{2}\right)^{1+1} \cdot \left(\frac{1}{2}\right)^{y+1} \cdot \left(\frac{1}{4}\right) \cdot \text{Er}(1,y,1) \ \ldots \right. \right. \left. \left. + \left(\frac{1}{4}\right) \cdot \left(\frac{1}{2}\right)^{n} \cdot \left(\frac{1}{2}\right)^{2} \text{Er}(1,n,1) \right] \right]$$

$$P_{f0}(b,i) := \frac{T_s}{\tau_R} \cdot 0.5 \cdot \text{erfc}\left(\frac{b \cdot \eta q \cdot Q_{f0_i}}{\sqrt{2}} \right) \cdot \text{errorf0}(x,y,k)$$

$$\text{errorf1}(x,y,k) := \left[\sum_{x=1}^{n-1} \left[\left[\sum_{y=0}^{n-1} \left[\left(\frac{1}{8}\right) \cdot \left(\frac{1}{2}\right)^{y} \cdot \left(\frac{1}{2}\right)^{x} \cdot \frac{1}{2} \text{Err}(x,y) \right] \ldots \right] \ldots \right. \right. \left. \left. + \left(\frac{1}{4}\right) \cdot \left(\frac{1}{2}\right)^{n} \cdot \left(\frac{1}{2}\right) \cdot \text{Err}(x,n) \right] \left. \left. + \sum_{y=0}^{n-1} \left[\left(\frac{1}{4}\right) \cdot \left(\frac{1}{2}\right)^{y} \left(\frac{1}{2}\right)^{n} \cdot \left(\frac{1}{2}\right) \cdot \text{Err}(n,y) \ \ldots \right. \right. \right. \left. \left. \left. + \left(\frac{1}{4}\right) \cdot \left(\frac{1}{2}\right)^{n} \cdot \left(\frac{1}{2}\right)^{n} \cdot \text{Err}(n,n) \right] \right] \right]$$

$$P_{f1}(b,i) := 0.5 \cdot \text{erfc}\left(\frac{b \cdot \eta q \cdot Q_{f0_i}}{\sqrt{2}} \right) \cdot \text{errorf1}(x,y,k)$$

Total Fals alarm

$$P_{ef}(b,i) := P_{f0}(b,i) + P_{f1}(b,i)$$

$$P_{eb}(b,i) := P_{er}(b,i) + P_{ef}(b,i)$$

$$pc(b,i) := \left(\log\left(P_{eb}(b,i)\right) + 9\right)$$ Set for 1 in 10^9 errors

$$P_{er}(b,0) = 84.928 \times 10^{-3} \qquad P_{ef}(b,0) = 62.375 \times 10^{-3}$$

$$a_i := \text{root}(pc(b,i),b)$$ Find the root to give 1 in 10^9

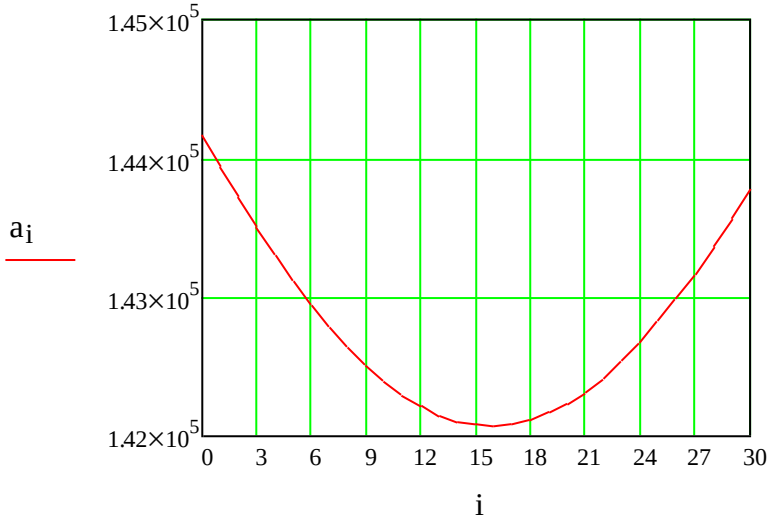

$v_{off} \equiv 0.48$

$b \equiv 1\cdot10^3$

$minimum := \min(a)$

$minimum = 142.075\times 10^3$

Received power

$$P_r := \left[\frac{minimum}{((gu + 2))}\cdot photon\_energy\cdot\left(\frac{1+n}{2n}\right)\cdot B\right]$$

$P_r = 189.541\times 10^{-9}$

Receiver sensitivity

$$P_{rdBm} := 10\cdot\log\left(\frac{P_r}{10^{-3}}\right)$$

$P_{rdBm} = -37.223\times 10^0$

$Q0_{e_i}$ =

$120.492 \cdot 10^{-6}$
$120.574 \cdot 10^{-6}$
$120.655 \cdot 10^{-6}$
$120.736 \cdot 10^{-6}$
$120.817 \cdot 10^{-6}$
$120.898 \cdot 10^{-6}$
$120.979 \cdot 10^{-6}$
$121.06 \cdot 10^{-6}$
$121.142 \cdot 10^{-6}$
$121.223 \cdot 10^{-6}$
$121.304 \cdot 10^{-6}$
$121.385 \cdot 10^{-6}$
$121.466 \cdot 10^{-6}$
$121.547 \cdot 10^{-6}$
$121.628 \cdot 10^{-6}$
...

$Err(x, y)$ =

$0 \cdot 10^{0}$
$500 \cdot 10^{-3}$
$1 \cdot 10^{0}$
$1.5 \cdot 10^{0}$
$2 \cdot 10^{0}$
$2.5 \cdot 10^{0}$
$3 \cdot 10^{0}$
$3.5 \cdot 10^{0}$
$4 \cdot 10^{0}$
$4.5 \cdot 10^{0}$
$5 \cdot 10^{0}$
$500 \cdot 10^{-3}$
$0 \cdot 10^{0}$
$500 \cdot 10^{-3}$
$1 \cdot 10^{0}$
...

$error0(x, y)$ =

$64.88 \cdot 10^{-3}$
$64.88 \cdot 10^{-3}$
$64.88 \cdot 10^{-3}$
$64.88 \cdot 10^{-3}$
$64.88 \cdot 10^{-3}$
$64.88 \cdot 10^{-3}$
$64.88 \cdot 10^{-3}$
$64.88 \cdot 10^{-3}$
$64.88 \cdot 10^{-3}$
$64.88 \cdot 10^{-3}$
$64.88 \cdot 10^{-3}$
$64.88 \cdot 10^{-3}$
$64.88 \cdot 10^{-3}$
$64.88 \cdot 10^{-3}$
$64.88 \cdot 10^{-3}$
...

$P_{r0}(b, i)$ =

$29.329 \cdot 10^{-3}$
$29.327 \cdot 10^{-3}$
$29.325 \cdot 10^{-3}$
$29.323 \cdot 10^{-3}$
$29.321 \cdot 10^{-3}$
$29.319 \cdot 10^{-3}$
$29.316 \cdot 10^{-3}$
$29.314 \cdot 10^{-3}$
$29.312 \cdot 10^{-3}$
$29.31 \cdot 10^{-3}$
$29.308 \cdot 10^{-3}$
$29.306 \cdot 10^{-3}$
$29.304 \cdot 10^{-3}$
$29.302 \cdot 10^{-3}$
$29.3 \cdot 10^{-3}$
...

$error1(x, y)$ =

$115.032 \cdot 10^{-3}$
$115.032 \cdot 10^{-3}$
$115.032 \cdot 10^{-3}$
$115.032 \cdot 10^{-3}$
$115.032 \cdot 10^{-3}$
$115.032 \cdot 10^{-3}$
$115.032 \cdot 10^{-3}$
$115.032 \cdot 10^{-3}$
$115.032 \cdot 10^{-3}$
$115.032 \cdot 10^{-3}$
$115.032 \cdot 10^{-3}$
$115.032 \cdot 10^{-3}$
$115.032 \cdot 10^{-3}$
$115.032 \cdot 10^{-3}$
$115.032 \cdot 10^{-3}$
...

$Q1_{e_i}$ =

$41.787 \cdot 10^{-6}$
$41.706 \cdot 10^{-6}$
$41.625 \cdot 10^{-6}$
$41.544 \cdot 10^{-6}$
$41.462 \cdot 10^{-6}$
$41.381 \cdot 10^{-6}$
$41.3 \cdot 10^{-6}$
$41.219 \cdot 10^{-6}$
$41.138 \cdot 10^{-6}$
$41.057 \cdot 10^{-6}$
$40.976 \cdot 10^{-6}$
$40.894 \cdot 10^{-6}$
$40.813 \cdot 10^{-6}$
$40.732 \cdot 10^{-6}$
$40.651 \cdot 10^{-6}$
...

$P_{r1}(b, i)$ =

$55.599 \cdot 10^{-3}$
$55.603 \cdot 10^{-3}$
$55.606 \cdot 10^{-3}$
$55.61 \cdot 10^{-3}$
$55.614 \cdot 10^{-3}$
$55.617 \cdot 10^{-3}$
$55.621 \cdot 10^{-3}$
$55.625 \cdot 10^{-3}$
$55.629 \cdot 10^{-3}$
$55.632 \cdot 10^{-3}$
$55.636 \cdot 10^{-3}$
$55.64 \cdot 10^{-3}$
$55.643 \cdot 10^{-3}$
$55.647 \cdot 10^{-3}$
$55.651 \cdot 10^{-3}$
...

$P_{er}(b, i)$ =

$84.928 \cdot 10^{-3}$
$84.929 \cdot 10^{-3}$
$84.931 \cdot 10^{-3}$
$84.933 \cdot 10^{-3}$
$84.934 \cdot 10^{-3}$
$84.936 \cdot 10^{-3}$
$84.938 \cdot 10^{-3}$
$84.939 \cdot 10^{-3}$
$84.941 \cdot 10^{-3}$
$84.942 \cdot 10^{-3}$
$84.944 \cdot 10^{-3}$
$84.946 \cdot 10^{-3}$
$84.947 \cdot 10^{-3}$
$84.949 \cdot 10^{-3}$
$84.951 \cdot 10^{-3}$
...

Q_{f0_i} =

$245.955 \cdot 10^{12}$
$246.462 \cdot 10^{12}$
$246.969 \cdot 10^{12}$
$247.476 \cdot 10^{12}$
$247.983 \cdot 10^{12}$
$248.49 \cdot 10^{12}$
$248.997 \cdot 10^{12}$
$249.505 \cdot 10^{12}$
$250.012 \cdot 10^{12}$
$250.519 \cdot 10^{12}$
$251.026 \cdot 10^{12}$
$251.533 \cdot 10^{12}$
$252.04 \cdot 10^{12}$
$252.547 \cdot 10^{12}$
$253.054 \cdot 10^{12}$
...

errorf0(x , y , k)

$7.935 \cdot 10^{-3}$
$7.935 \cdot 10^{-3}$
$7.935 \cdot 10^{-3}$
$7.935 \cdot 10^{-3}$
$7.935 \cdot 10^{-3}$
$7.935 \cdot 10^{-3}$
$7.935 \cdot 10^{-3}$
$7.935 \cdot 10^{-3}$
$7.935 \cdot 10^{-3}$
$7.935 \cdot 10^{-3}$
$7.935 \cdot 10^{-3}$
$7.935 \cdot 10^{-3}$
$7.935 \cdot 10^{-3}$
$7.935 \cdot 10^{-3}$
...

$P_{f0}(b , i)$ =

$6.664 \cdot 10^{-3}$
$6.664 \cdot 10^{-3}$
$6.663 \cdot 10^{-3}$
$6.663 \cdot 10^{-3}$
$6.663 \cdot 10^{-3}$
$6.662 \cdot 10^{-3}$
$6.662 \cdot 10^{-3}$
$6.661 \cdot 10^{-3}$
$6.661 \cdot 10^{-3}$
$6.66 \cdot 10^{-3}$
$6.66 \cdot 10^{-3}$
$6.659 \cdot 10^{-3}$
$6.659 \cdot 10^{-3}$
$6.659 \cdot 10^{-3}$
$6.658 \cdot 10^{-3}$
...

errorf1 (x , y , k)

$115.032 \cdot 10^{-3}$
$115.032 \cdot 10^{-3}$
$115.032 \cdot 10^{-3}$
$115.032 \cdot 10^{-3}$
$115.032 \cdot 10^{-3}$
$115.032 \cdot 10^{-3}$
$115.032 \cdot 10^{-3}$
$115.032 \cdot 10^{-3}$
$115.032 \cdot 10^{-3}$
$115.032 \cdot 10^{-3}$
$115.032 \cdot 10^{-3}$
$115.032 \cdot 10^{-3}$
$115.032 \cdot 10^{-3}$
$115.032 \cdot 10^{-3}$
...

$P_{f1}(b , i)$ =

$55.71 \cdot 10^{-3}$
$55.707 \cdot 10^{-3}$
$55.703 \cdot 10^{-3}$
$55.699 \cdot 10^{-3}$
$55.696 \cdot 10^{-3}$
$55.692 \cdot 10^{-3}$
$55.688 \cdot 10^{-3}$
$55.684 \cdot 10^{-3}$
$55.681 \cdot 10^{-3}$
$55.677 \cdot 10^{-3}$
$55.673 \cdot 10^{-3}$
$55.67 \cdot 10^{-3}$
$55.666 \cdot 10^{-3}$
$55.662 \cdot 10^{-3}$
$55.658 \cdot 10^{-3}$
...

$P_{ef}(b , i)$ =

$62.375 \cdot 10^{-3}$
$62.371 \cdot 10^{-3}$
$62.366 \cdot 10^{-3}$
$62.362 \cdot 10^{-3}$
$62.358 \cdot 10^{-3}$
$62.354 \cdot 10^{-3}$
$62.35 \cdot 10^{-3}$
$62.346 \cdot 10^{-3}$
$62.341 \cdot 10^{-3}$
$62.337 \cdot 10^{-3}$
$62.333 \cdot 10^{-3}$
$62.329 \cdot 10^{-3}$
$62.325 \cdot 10^{-3}$
$62.321 \cdot 10^{-3}$
$62.316 \cdot 10^{-3}$
...

$P_{eb}(b , i)$ =

$147.303 \cdot 10^{-3}$
$147.3 \cdot 10^{-3}$
$147.297 \cdot 10^{-3}$
$147.295 \cdot 10^{-3}$
$147.292 \cdot 10^{-3}$
$147.29 \cdot 10^{-3}$
$147.287 \cdot 10^{-3}$
$147.285 \cdot 10^{-3}$
$147.282 \cdot 10^{-3}$
$147.28 \cdot 10^{-3}$
$147.277 \cdot 10^{-3}$
$147.275 \cdot 10^{-3}$
$147.272 \cdot 10^{-3}$
$147.27 \cdot 10^{-3}$
$147.267 \cdot 10^{-3}$
...

pc(b , i) =

$8.168 \cdot 10^{0}$
$8.168 \cdot 10^{0}$
$8.168 \cdot 10^{0}$
$8.168 \cdot 10^{0}$
$8.168 \cdot 10^{0}$
$8.168 \cdot 10^{0}$
$8.168 \cdot 10^{0}$
$8.168 \cdot 10^{0}$
$8.168 \cdot 10^{0}$
$8.168 \cdot 10^{0}$
$8.168 \cdot 10^{0}$
$8.168 \cdot 10^{0}$
$8.168 \cdot 10^{0}$
$8.168 \cdot 10^{0}$
$8.168 \cdot 10^{0}$
...

a_i =

$144.164 \cdot 10^{3}$
$143.934 \cdot 10^{3}$
$143.714 \cdot 10^{3}$
$143.503 \cdot 10^{3}$
$143.304 \cdot 10^{3}$
$143.117 \cdot 10^{3}$
$142.943 \cdot 10^{3}$
$142.783 \cdot 10^{3}$
$142.637 \cdot 10^{3}$
$142.506 \cdot 10^{3}$
$142.392 \cdot 10^{3}$
$142.294 \cdot 10^{3}$
$142.214 \cdot 10^{3}$
$142.151 \cdot 10^{3}$
$142.107 \cdot 10^{3}$
...

Appendix F: Receiver sensitivity of Duo PPM at 100 Mbps

Receiver sensitivity of Duo PPM with zero guard at 100 Mbit/s and 3 PCM BITS for LOS Indoor VLC Link 2019

$i := 0, 1 .. 30$

$v_i := v_{off} + \frac{i}{1000}$

$n := 10$ Number of like symbols in PCM

$\eta q := 1.6 \cdot 10^{-19}$ Quantum energy

$\lambda := 820 \cdot 10^{-9}$ This is the wavelength of operation

$$photon\_energy := \frac{6.63 \cdot 10^{-34} \cdot 3 \cdot 10^{8}}{\lambda} \qquad gu \equiv 0$$

$$R_o := \frac{\eta q}{photon\_energy} \qquad R_o = 659.628 \times 10^{-3}$$

Preamplifier terms

$S_o := 25 \cdot 10^{-24}$ **Preamplifier input noise**

$B := 100 \cdot 10^{6}$ **Bit rate**

$T_b := \frac{1}{B}$ PCM bit time

Slot time $T_s := \frac{T_b}{2 + gu} \qquad T_s = 5 \times 10^{-9}$

$f_c := 0.5 \cdot \frac{1}{T_s} \qquad \omega_c := 2 \cdot \pi \cdot f_c \qquad f_c = 100 \times 10^{6}$

preamplifier $H_{pre}(\omega) := \frac{1}{1 + j \cdot \frac{\omega}{\omega_c}}$

Pulse shape

$t := 0, 0.1 .. 14$

VLC impulse response

$$h(t) := \left[\frac{1}{1} \cdot \left[\int_0^t \mathrm{Re}\left[\exp\left[i \cdot \omega \cdot (t) \cdot H_{pre}(\omega) \right] \right] d\omega \right] \right]$$

$$\alpha_p := \frac{0.1874 \cdot T_b}{f_n} \qquad f_n \equiv 0.6 \qquad \alpha_{pn} := \frac{\alpha_p}{T_s}$$

$$Pulse1(t) := \frac{1}{\sqrt{2 \cdot \pi} \cdot \alpha_{pn} \cdot 1} \cdot \exp\left(\frac{-t^2}{2 \cdot \alpha_{pn}^2} \right)$$

$$I_0(t) := \left(\frac{1}{T_s} \cdot \int_0^t h(\tau) \cdot Pulse1(t - \tau)\, d\tau \right)$$

$h(t) =$

$804.764 \cdot 10^{-3}$
$841.471 \cdot 10^{-3}$
$850.56 \cdot 10^{-3}$
$826.215 \cdot 10^{-3}$
$763.772 \cdot 10^{-3}$
$660.865 \cdot 10^{-3}$
$518.715 \cdot 10^{-3}$
$343.347 \cdot 10^{-3}$
$146.439 \cdot 10^{-3}$
$-54.583 \cdot 10^{-3}$
$-237.614 \cdot 10^{-3}$
$-378.401 \cdot 10^{-3}$
$-454.585 \cdot 10^{-3}$
$-450.849 \cdot 10^{-3}$
$-364.248 \cdot 10^{-3}$
...

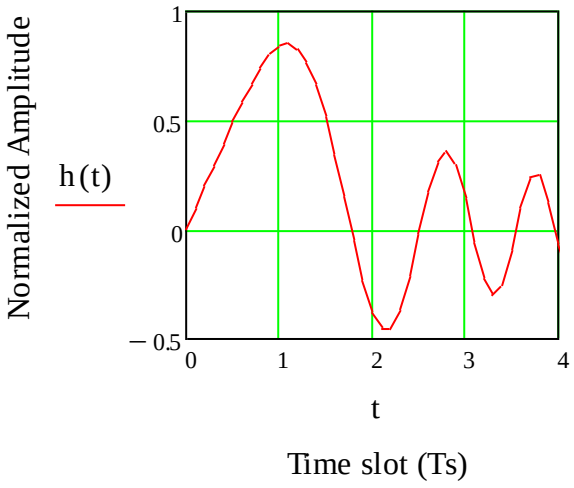

$Pulse1(t) =$

$691.869 \cdot 10^{-3}$
$681.542 \cdot 10^{-3}$
$651.478 \cdot 10^{-3}$
$604.289 \cdot 10^{-3}$
$543.91 \cdot 10^{-3}$
$475.06 \cdot 10^{-3}$
$402.63 \cdot 10^{-3}$
$331.134 \cdot 10^{-3}$
$264.264 \cdot 10^{-3}$
$204.649 \cdot 10^{-3}$
$153.787 \cdot 10^{-3}$
$112.142 \cdot 10^{-3}$
$79.351 \cdot 10^{-3}$
$54.485 \cdot 10^{-3}$
$36.303 \cdot 10^{-3}$
...

$I_0(t) =$

$0 \cdot 10^{0}$
$690.136 \cdot 10^{3}$
$2.74 \cdot 10^{6}$
$6.087 \cdot 10^{6}$
$10.631 \cdot 10^{6}$
$16.23 \cdot 10^{6}$
$22.706 \cdot 10^{6}$
$29.842 \cdot 10^{6}$
$37.377 \cdot 10^{6}$
$45.009 \cdot 10^{6}$
$52.387 \cdot 10^{6}$
$59.112 \cdot 10^{6}$
$64.747 \cdot 10^{6}$
$68.826 \cdot 10^{6}$
$70.892 \cdot 10^{6}$
...

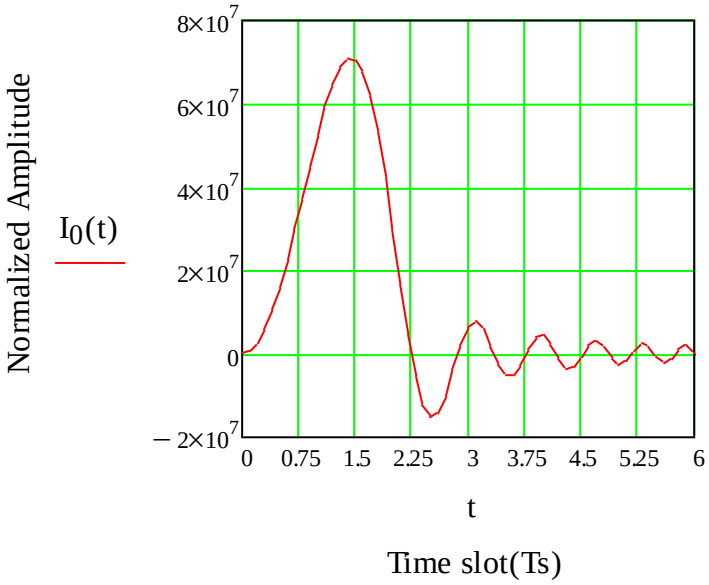

$t := 1.5$ $\quad I_1(t) := \frac{d}{dt} I_0(t)$ Guess at the peak time

$t_{pk} := root\left(I_1(t) \cdot T_s^{\,3}, t\right)$ $\quad t_{pk} = 1.437\times 10^{0}$ This is the peak time

$v_{pk} := I_0\left(t_{pk}\right)$ $\quad v_{pk} = 71.061\times 10^{6}$ This is the peak voltage

$noise := \frac{\pi \cdot f_c}{2}$ $\quad noise = 157.08\times 10^{6}$ Noise bandwidth

$S_o \cdot noise = 3.927\times 10^{-15}$ $\quad \sqrt{S_o \cdot noise} = 62.666\times 10^{-9}$

$x := 0..n$ $\quad y := 0..n$

Erasure of pulse

$$Q0_{e_i} := \eta q \cdot \frac{v_{pk} + v_i \cdot v_{pk}}{\sqrt{S_o \cdot noise}} \qquad Err(x,y) := \left|\left[\left(\left(\frac{x-y}{2}\right)\right)\right]\right|$$

$$error0(x,y) := \left[\sum_{y=0}^{n-1} \left[\begin{array}{l}\left(\frac{1}{4}\right)\cdot\left(\frac{1}{2}\right)^{y}\cdot\left(\frac{1}{4}\right)\cdot Err(0,y) \ \ldots \\ +\left(\frac{1}{4}\right)\cdot\left(\frac{1}{2}\right)^{n}\cdot\left(\frac{1}{4}\right)\cdot 1.\, Err(0,n)\end{array}\right]\right]$$

$$P_{r0}(b,i) := \frac{1}{2}\cdot \operatorname{erfc}\left(\frac{Q0_{e_i}\cdot b}{\sqrt{2}}\right) error0(x,y)$$

$$Q1_{e_i} := \eta q \cdot \frac{v_{pk} - v_i \cdot v_{pk}}{\sqrt{S_o \cdot noise}}$$

$$error1(x,y) := \left[\sum_{x=1}^{n-1} \left[\left[\sum_{y=0}^{n-1} \left[\left(\frac{1}{8}\right)\cdot\left(\frac{1}{2}\right)^{y}\cdot\left(\frac{1}{2}\right)^{x}\cdot\frac{1}{2}\,Err(x,y) \right] \ldots \right] \ldots \right. \right.$$
$$\left. \left. + \left(\frac{1}{4}\right)\cdot\left(\frac{1}{2}\right)^{n}\cdot\left(\frac{1}{2}\right)\cdot Err(x,n) \right] \right.$$
$$\left. + \sum_{y=0}^{n-1} \left[\left(\frac{1}{4}\right)\cdot\left(\frac{1}{2}\right)^{y}\left(\frac{1}{2}\right)^{n}\cdot\left(\frac{1}{2}\right)\cdot Err(n,y) \ldots \right] \right.$$
$$\left. \left. + \left(\frac{1}{4}\right)\cdot\left(\frac{1}{2}\right)^{n}\cdot\left(\frac{1}{2}\right)^{n}\cdot Err(n,n) \right] \right] \right]$$

$$P_{r1}(b,i) := \frac{1}{2}\cdot \operatorname{erfc}\left(\frac{Q1_{e_i}\cdot b}{\sqrt{2}}\right) error1(x,y)$$

$$P_{er}(b,i) := P_{r0}(b,i) + P_{r1}(b,i)$$

$\tau_R := \alpha_p$

$x := 0..n$

False alarm

$k := 1$

False alarm no ISI accurs between S and R and the error apears within the run of N-symbols where k is the symbol position

$ODD\cdot combinations k$ $EVEN\cdot combinations$

$$odd(k) := \frac{k}{2} - trunc\left(\frac{k}{2}\right) \qquad Erodd(x,y,k) := \frac{k}{2}$$

$$even(k) := \frac{k}{2} - trunc\left(\frac{k}{2}\right) \qquad Ereven(x,y,k) := \frac{x-k}{2}$$

$$Er(x,y,k) := Ereven(x,y,k)\cdot even(k) + Erodd(x,y,k)\cdot odd(k)$$

$$Q_{f0_i} := \frac{v_i \cdot v_{pk}}{\sqrt{S_o \cdot noise}} \qquad v_o(t) := I_0(t)$$

FALSE ALARMS

$$\text{errorf0}(x,y,k) := \left[\sum_{y=1}^{n-1} \left[\left(\frac{1}{2}\right)^{1+1} \cdot \left(\frac{1}{2}\right)^{y+1} \cdot \left(\frac{1}{4}\right) \cdot \text{Er}(1,y,1) \ \ldots \right. \right. \left. \left. + \left(\frac{1}{4}\right) \cdot \left(\frac{1}{2}\right)^{n} \cdot \left(\frac{1}{2}\right)^{2} \text{Er}(1,n,1) \right] \right]$$

$$P_{f0}(b,i) := \frac{T_s}{\tau_R} \cdot 0.5 \cdot \text{erfc}\left(\frac{b \cdot \eta q \cdot Q_{f0_i}}{\sqrt{2}} \right) \cdot \text{errorf0}(x,y,k)$$

$$\text{errorf1}(x,y,k) := \left[\sum_{x=1}^{n-1} \left[\left[\sum_{y=0}^{n-1} \left[\left(\frac{1}{8}\right) \cdot \left(\frac{1}{2}\right)^{y} \cdot \left(\frac{1}{2}\right)^{x} \cdot \frac{1}{2} \text{Err}(x,y) \right] \ldots \right] \ldots \right. \right. \left. \left. + \left(\frac{1}{4}\right) \cdot \left(\frac{1}{2}\right)^{n} \cdot \left(\frac{1}{2}\right) \cdot \text{Err}(x,n) \right] \left. + \sum_{y=0}^{n-1} \left[\left(\frac{1}{4}\right) \cdot \left(\frac{1}{2}\right)^{y} \left(\frac{1}{2}\right)^{n} \cdot \left(\frac{1}{2}\right) \cdot \text{Err}(n,y) \ \ldots \right. \right. \left. \left. + \left(\frac{1}{4}\right) \cdot \left(\frac{1}{2}\right)^{n} \cdot \left(\frac{1}{2}\right)^{n} \cdot \text{Err}(n,n) \right] \right]$$

$$P_{f1}(b,i) := 0.5 \cdot \text{erfc}\left(\frac{b \cdot \eta q \cdot Q_{f0_i}}{\sqrt{2}} \right) \cdot \text{errorf1}(x,y,k)$$

Total Fals alarm

$$P_{ef}(b,i) := P_{f0}(b,i) + P_{f1}(b,i)$$

$$P_{eb}(b,i) := P_{er}(b,i) + P_{ef}(b,i)$$

$$pc(b,i) := \left(\log\left(P_{eb}(b,i)\right) + 9\right)$$ Set for 1 in 10^9 errors

$$P_{er}(b,0) = 78.784 \times 10^{-3} \qquad P_{ef}(b,0) = 59.881 \times 10^{-3}$$

$$a_i := \text{root}(pc(b,i),b)$$ Find the root to give 1 in 10^9

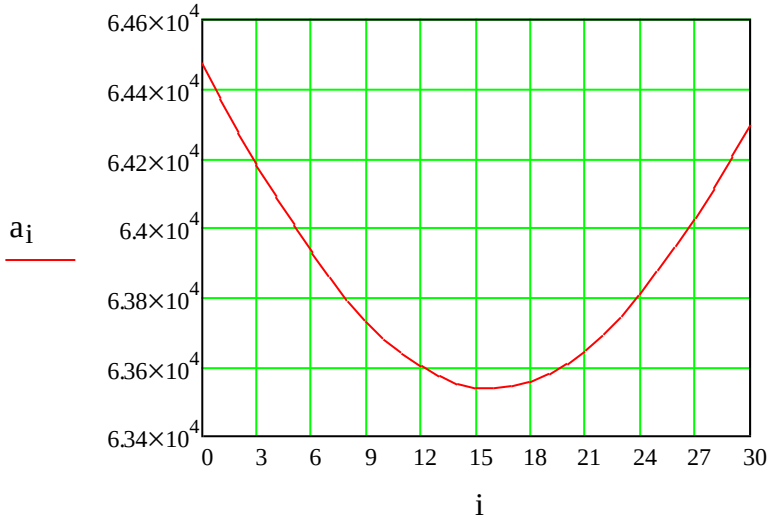

$v_{off} \equiv 0.48$

$b \equiv 1\cdot10^3$

$minimum := \min(a)$ $\quad minimum = 63.538\times 10^3$

Received power

$$P_r := \left[\frac{minimum}{((gu + 2))}\cdot photon\_energy\cdot\left(\frac{1+n}{2n}\right)\cdot B\right]$$

$P_r = 423.825\times 10^{-9}$

Receiver sensitivity

$$P_{rdBm} := 10\cdot\log\left(\frac{P_r}{10^{-3}}\right)$$

$P_{rdBm} = -33.728\times 10^0$

$Q0_{e_i}$ =

$269.429 \cdot 10^{-6}$
$269.611 \cdot 10^{-6}$
$269.792 \cdot 10^{-6}$
$269.974 \cdot 10^{-6}$
$270.155 \cdot 10^{-6}$
$270.337 \cdot 10^{-6}$
$270.518 \cdot 10^{-6}$
$270.699 \cdot 10^{-6}$
$270.881 \cdot 10^{-6}$
$271.062 \cdot 10^{-6}$
$271.244 \cdot 10^{-6}$
$271.425 \cdot 10^{-6}$
$271.607 \cdot 10^{-6}$
$271.788 \cdot 10^{-6}$
$271.969 \cdot 10^{-6}$
...

Err(x , y) =

$0 \cdot 10^{0}$
$500 \cdot 10^{-3}$
$1 \cdot 10^{0}$
$1.5 \cdot 10^{0}$
$2 \cdot 10^{0}$
$2.5 \cdot 10^{0}$
$3 \cdot 10^{0}$
$3.5 \cdot 10^{0}$
$4 \cdot 10^{0}$
$4.5 \cdot 10^{0}$
$5 \cdot 10^{0}$
$500 \cdot 10^{-3}$
$0 \cdot 10^{0}$
$500 \cdot 10^{-3}$
$1 \cdot 10^{0}$
...

error0(x , y) =

$64.88 \cdot 10^{-3}$
$64.88 \cdot 10^{-3}$
$64.88 \cdot 10^{-3}$
$64.88 \cdot 10^{-3}$
$64.88 \cdot 10^{-3}$
$64.88 \cdot 10^{-3}$
$64.88 \cdot 10^{-3}$
$64.88 \cdot 10^{-3}$
$64.88 \cdot 10^{-3}$
$64.88 \cdot 10^{-3}$
$64.88 \cdot 10^{-3}$
$64.88 \cdot 10^{-3}$
$64.88 \cdot 10^{-3}$
$64.88 \cdot 10^{-3}$
$64.88 \cdot 10^{-3}$
...

P_{r0}(b , i) =

$25.55 \cdot 10^{-3}$
$25.545 \cdot 10^{-3}$
$25.541 \cdot 10^{-3}$
$25.536 \cdot 10^{-3}$
$25.532 \cdot 10^{-3}$
$25.527 \cdot 10^{-3}$
$25.523 \cdot 10^{-3}$
$25.518 \cdot 10^{-3}$
$25.514 \cdot 10^{-3}$
$25.509 \cdot 10^{-3}$
$25.505 \cdot 10^{-3}$
$25.5 \cdot 10^{-3}$
$25.496 \cdot 10^{-3}$
$25.491 \cdot 10^{-3}$
$25.486 \cdot 10^{-3}$
...

error1(x , y) =

$115.032 \cdot 10^{-3}$
$115.032 \cdot 10^{-3}$
$115.032 \cdot 10^{-3}$
$115.032 \cdot 10^{-3}$
$115.032 \cdot 10^{-3}$
$115.032 \cdot 10^{-3}$
$115.032 \cdot 10^{-3}$
$115.032 \cdot 10^{-3}$
$115.032 \cdot 10^{-3}$
$115.032 \cdot 10^{-3}$
$115.032 \cdot 10^{-3}$
$115.032 \cdot 10^{-3}$
$115.032 \cdot 10^{-3}$
$115.032 \cdot 10^{-3}$
$115.032 \cdot 10^{-3}$
...

$Q1_{e_i}$ =

$93.438 \cdot 10^{-6}$
$93.257 \cdot 10^{-6}$
$93.076 \cdot 10^{-6}$
$92.894 \cdot 10^{-6}$
$92.713 \cdot 10^{-6}$
$92.531 \cdot 10^{-6}$
$92.35 \cdot 10^{-6}$
$92.168 \cdot 10^{-6}$
$91.987 \cdot 10^{-6}$
$91.806 \cdot 10^{-6}$
$91.624 \cdot 10^{-6}$
$91.443 \cdot 10^{-6}$
$91.261 \cdot 10^{-6}$
$91.08 \cdot 10^{-6}$
$90.898 \cdot 10^{-6}$
...

P_{r1}(b , i) =

$53.234 \cdot 10^{-3}$
$53.242 \cdot 10^{-3}$
$53.251 \cdot 10^{-3}$
$53.259 \cdot 10^{-3}$
$53.267 \cdot 10^{-3}$
$53.276 \cdot 10^{-3}$
$53.284 \cdot 10^{-3}$
$53.292 \cdot 10^{-3}$
$53.3 \cdot 10^{-3}$
$53.309 \cdot 10^{-3}$
$53.317 \cdot 10^{-3}$
$53.325 \cdot 10^{-3}$
$53.334 \cdot 10^{-3}$
$53.342 \cdot 10^{-3}$
$53.35 \cdot 10^{-3}$
...

P_{er}(b , i) =

$78.784 \cdot 10^{-3}$
$78.788 \cdot 10^{-3}$
$78.792 \cdot 10^{-3}$
$78.795 \cdot 10^{-3}$
$78.799 \cdot 10^{-3}$
$78.803 \cdot 10^{-3}$
$78.807 \cdot 10^{-3}$
$78.81 \cdot 10^{-3}$
$78.814 \cdot 10^{-3}$
$78.818 \cdot 10^{-3}$
$78.822 \cdot 10^{-3}$
$78.825 \cdot 10^{-3}$
$78.829 \cdot 10^{-3}$
$78.833 \cdot 10^{-3}$
$78.837 \cdot 10^{-3}$
...

Q_{f0_i} =

$549.972 \cdot 10^{12}$
$551.106 \cdot 10^{12}$
$552.239 \cdot 10^{12}$
$553.373 \cdot 10^{12}$
$554.507 \cdot 10^{12}$
$555.641 \cdot 10^{12}$
$556.775 \cdot 10^{12}$
$557.909 \cdot 10^{12}$
$559.043 \cdot 10^{12}$
$560.177 \cdot 10^{12}$
$561.311 \cdot 10^{12}$
$562.445 \cdot 10^{12}$
$563.579 \cdot 10^{12}$
$564.713 \cdot 10^{12}$
$565.847 \cdot 10^{12}$
...

errorf0(x , y , k)

$7.935 \cdot 10^{-3}$
$7.935 \cdot 10^{-3}$
$7.935 \cdot 10^{-3}$
$7.935 \cdot 10^{-3}$
$7.935 \cdot 10^{-3}$
$7.935 \cdot 10^{-3}$
$7.935 \cdot 10^{-3}$
$7.935 \cdot 10^{-3}$
$7.935 \cdot 10^{-3}$
$7.935 \cdot 10^{-3}$
$7.935 \cdot 10^{-3}$
$7.935 \cdot 10^{-3}$
$7.935 \cdot 10^{-3}$
$7.935 \cdot 10^{-3}$
...

$P_{f0}(b , i)$ =

$6.398 \cdot 10^{-3}$
$6.397 \cdot 10^{-3}$
$6.396 \cdot 10^{-3}$
$6.395 \cdot 10^{-3}$
$6.394 \cdot 10^{-3}$
$6.393 \cdot 10^{-3}$
$6.392 \cdot 10^{-3}$
$6.391 \cdot 10^{-3}$
$6.39 \cdot 10^{-3}$
$6.389 \cdot 10^{-3}$
$6.388 \cdot 10^{-3}$
$6.387 \cdot 10^{-3}$
$6.386 \cdot 10^{-3}$
$6.385 \cdot 10^{-3}$
$6.384 \cdot 10^{-3}$
...

errorf1(x , y , k)

$115.032 \cdot 10^{-3}$
$115.032 \cdot 10^{-3}$
$115.032 \cdot 10^{-3}$
$115.032 \cdot 10^{-3}$
$115.032 \cdot 10^{-3}$
$115.032 \cdot 10^{-3}$
$115.032 \cdot 10^{-3}$
$115.032 \cdot 10^{-3}$
$115.032 \cdot 10^{-3}$
$115.032 \cdot 10^{-3}$
$115.032 \cdot 10^{-3}$
$115.032 \cdot 10^{-3}$
$115.032 \cdot 10^{-3}$
$115.032 \cdot 10^{-3}$
$115.032 \cdot 10^{-3}$
...

$P_{f1}(b , i)$ =

$53.483 \cdot 10^{-3}$
$53.475 \cdot 10^{-3}$
$53.466 \cdot 10^{-3}$
$53.458 \cdot 10^{-3}$
$53.45 \cdot 10^{-3}$
$53.441 \cdot 10^{-3}$
$53.433 \cdot 10^{-3}$
$53.425 \cdot 10^{-3}$
$53.417 \cdot 10^{-3}$
$53.408 \cdot 10^{-3}$
$53.4 \cdot 10^{-3}$
$53.392 \cdot 10^{-3}$
$53.383 \cdot 10^{-3}$
$53.375 \cdot 10^{-3}$
$53.367 \cdot 10^{-3}$
...

$P_{ef}(b , i)$ =

$59.881 \cdot 10^{-3}$
$59.871 \cdot 10^{-3}$
$59.862 \cdot 10^{-3}$
$59.853 \cdot 10^{-3}$
$59.844 \cdot 10^{-3}$
$59.834 \cdot 10^{-3}$
$59.825 \cdot 10^{-3}$
$59.816 \cdot 10^{-3}$
$59.806 \cdot 10^{-3}$
$59.797 \cdot 10^{-3}$
$59.788 \cdot 10^{-3}$
$59.779 \cdot 10^{-3}$
$59.769 \cdot 10^{-3}$
$59.76 \cdot 10^{-3}$
$59.751 \cdot 10^{-3}$
...

$P_{eb}(b , i)$ =

$138.665 \cdot 10^{-3}$
$138.659 \cdot 10^{-3}$
$138.654 \cdot 10^{-3}$
$138.648 \cdot 10^{-3}$
$138.643 \cdot 10^{-3}$
$138.637 \cdot 10^{-3}$
$138.632 \cdot 10^{-3}$
$138.626 \cdot 10^{-3}$
$138.621 \cdot 10^{-3}$
$138.615 \cdot 10^{-3}$
$138.61 \cdot 10^{-3}$
$138.604 \cdot 10^{-3}$
$138.599 \cdot 10^{-3}$
$138.593 \cdot 10^{-3}$
$138.588 \cdot 10^{-3}$
...

pc(b , i) =

$8.142 \cdot 10^{0}$
$8.142 \cdot 10^{0}$
$8.142 \cdot 10^{0}$
$8.142 \cdot 10^{0}$
$8.142 \cdot 10^{0}$
$8.142 \cdot 10^{0}$
$8.142 \cdot 10^{0}$
$8.142 \cdot 10^{0}$
$8.142 \cdot 10^{0}$
$8.142 \cdot 10^{0}$
$8.142 \cdot 10^{0}$
$8.142 \cdot 10^{0}$
$8.142 \cdot 10^{0}$
$8.142 \cdot 10^{0}$
$8.142 \cdot 10^{0}$
...

a_i =

$64.472 \cdot 10^{3}$
$64.369 \cdot 10^{3}$
$64.271 \cdot 10^{3}$
$64.177 \cdot 10^{3}$
$64.088 \cdot 10^{3}$
$64.004 \cdot 10^{3}$
$63.926 \cdot 10^{3}$
$63.854 \cdot 10^{3}$
$63.789 \cdot 10^{3}$
$63.731 \cdot 10^{3}$
$63.68 \cdot 10^{3}$
$63.636 \cdot 10^{3}$
$63.6 \cdot 10^{3}$
$63.572 \cdot 10^{3}$
$63.552 \cdot 10^{3}$
...

Appendix G: Receiver sensitivity of Offset PPM at 20 Mbps

Receiver sensitivity of Offset PPM at 20 Mbit/s and 3 PCM BITS for LOS Indoor VLC Link 2019

$i := 0, 1 .. 30$ $\quad v_i := v_{off} + \frac{i}{1000}$

$\eta q := 1.6 \cdot 10^{-19}$ Quantum energy $\quad \lambda := 820 \cdot 10^{-9}$ This is the wavelength of operation

$$photon\_energy := \frac{6.63 \cdot 10^{-34} \cdot 3 \cdot 10^{8}}{\lambda}$$

$$R_o := \frac{\eta q}{photon\_energy} \qquad R_o = 659.628 \times 10^{-3}$$

Preamplifier terms

$S_o := 25 \cdot 10^{-24}$ **Preamplifier input noise** $\quad N \equiv 3$

$B := 20 \cdot 10^{6}$ Bit rate $\quad n := 2^{N-1}$

$T_b := \frac{1}{B}$ PCM bit time $\quad T_n := \frac{N}{B}$ frame time for N bits of pcm

$T_b = 50 \times 10^{-9}$ $\quad T_s := \frac{T_n}{n}$ $\quad T_s = 37.5 \times 10^{-9}$ average slot width

$f_c := 0.5 \cdot \frac{1}{T_s}$ $\quad \omega_c := 2 \cdot \pi \cdot f_c$ $\quad f_c = 13.333 \times 10^{6}$

preamplifier $\quad H_{pre}(\omega) := \frac{1}{1 + j \cdot \frac{\omega}{\omega_c}}$

Pulse shape

VLC impulse response

$$h(t) := \left[\frac{1}{1} \cdot \left[\int_0^t \mathrm{Re}\left[\exp\left[i \cdot \omega \cdot (t) \cdot H_{pre}(\omega) \right] \right] d\omega \right] \right]$$

$t := 0, 0.1 .. 14$

$h(t) =$

$0 \cdot 10^{0}$
$99.998 \cdot 10^{-3}$
$199.947 \cdot 10^{-3}$
$299.595 \cdot 10^{-3}$
$398.296 \cdot 10^{-3}$
$494.808 \cdot 10^{-3}$
$587.124 \cdot 10^{-3}$
$672.323 \cdot 10^{-3}$
$746.494 \cdot 10^{-3}$
$804.764 \cdot 10^{-3}$
$841.471 \cdot 10^{-3}$
$850.56 \cdot 10^{-3}$
$826.215 \cdot 10^{-3}$
$763.772 \cdot 10^{-3}$
$660.865 \cdot 10^{-3}$
...

$$\alpha_p := \frac{0.1874 \cdot T_b}{f_n} \qquad f_n \equiv 0.6$$

$$\alpha_{pn} := \frac{\alpha_p}{T_s}$$

$$Pulse1(t) := \frac{1}{\sqrt{2 \cdot \pi} \cdot \alpha_{pn} \cdot 1} \cdot \exp\left(\frac{-t^2}{2 \cdot \alpha_{pn}^2} \right)$$

$Pulse1(t) =$

$1.038 \cdot 10^{0}$
$1.003 \cdot 10^{0}$
$906.433 \cdot 10^{-3}$
$765.353 \cdot 10^{-3}$
$603.946 \cdot 10^{-3}$
$445.394 \cdot 10^{-3}$
$306.974 \cdot 10^{-3}$
$197.728 \cdot 10^{-3}$
$119.027 \cdot 10^{-3}$
$66.963 \cdot 10^{-3}$
$35.207 \cdot 10^{-3}$
$17.3 \cdot 10^{-3}$
$7.944 \cdot 10^{-3}$
$3.409 \cdot 10^{-3}$
$1.368 \cdot 10^{-3}$
...

$$I_0(t) := \left(\frac{1}{T_s} \cdot \int_0^t h(\tau) \cdot Pulse1(t - \tau)\, d\tau \right)$$

$I_0(t) =$

$0 \cdot 10^{0}$
$137.598 \cdot 10^{3}$
$541.291 \cdot 10^{3}$
$1.185 \cdot 10^{6}$
$2.031 \cdot 10^{6}$
$3.032 \cdot 10^{6}$
$4.137 \cdot 10^{6}$
$5.298 \cdot 10^{6}$
$6.461 \cdot 10^{6}$
$7.577 \cdot 10^{6}$
$8.588 \cdot 10^{6}$
$9.434 \cdot 10^{6}$
$10.051 \cdot 10^{6}$
$10.37 \cdot 10^{6}$
$10.327 \cdot 10^{6}$
...

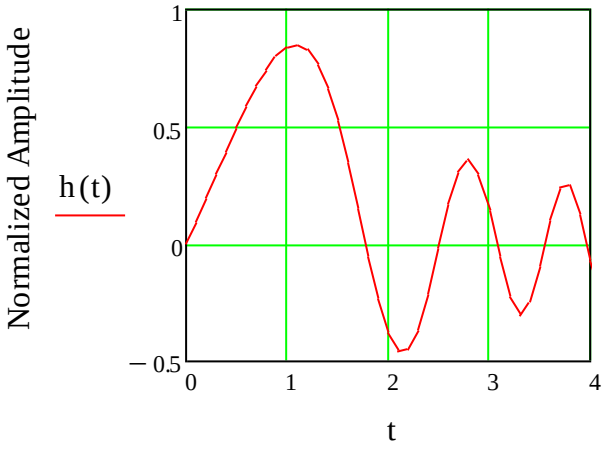

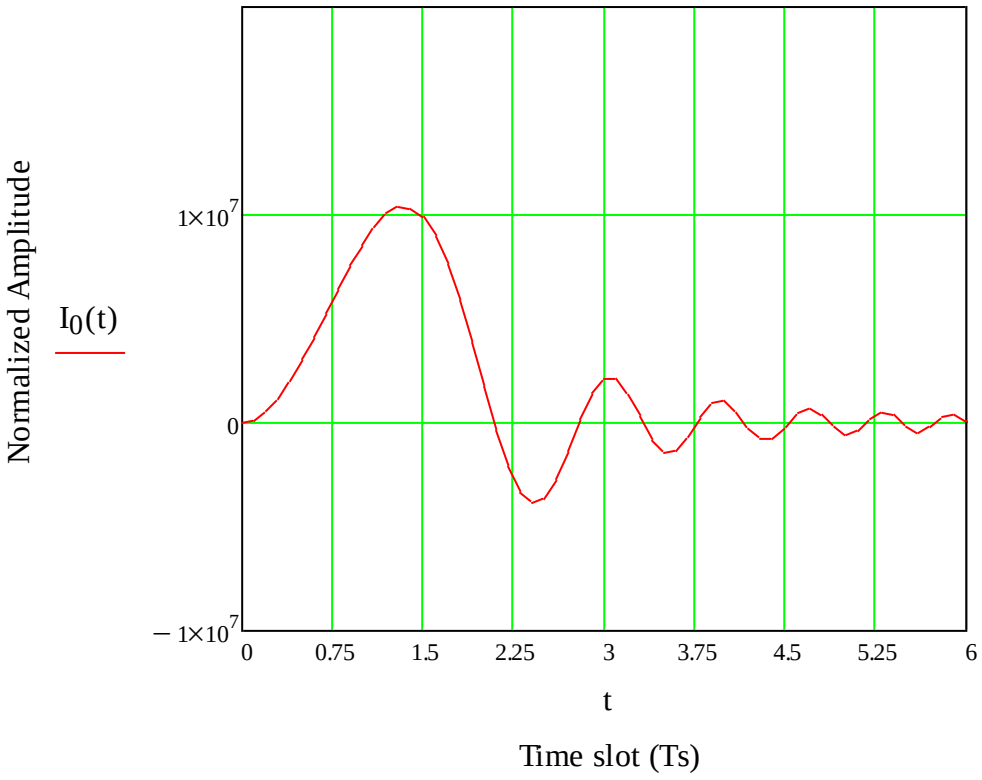

$t := 1.3$

$I_1(t) := \frac{d}{dt} I_0(t)$ Guess at the peak time

$t_{pk} := root\left(I_1(t) \cdot T_s^{\,3}, t\right)$ $t_{pk} = 1.34 \times 10^0$ This is the peak time

$v_{pk} := I_0\left(t_{pk}\right)$ $v_{pk} = 10.4 \times 10^6$ This is the peak voltage

$noise := \frac{\pi \cdot f_c}{2}$ $noise = 20.944 \times 10^6$ Noise bandwidth

$S_o \cdot noise = 0 \times 10^0$ $\sqrt{S_o \cdot noise} = 22.882 \times 10^{-9}$

Erasure of pulse

$$Q_{e_i} := \eta q \cdot \frac{v_{pk} - v_i \cdot v_{pk}}{\sqrt{S_o \cdot noise}} \qquad P_r(b,i) := \frac{1}{2} \cdot erfc\left(\frac{Q_{e_i} \cdot b}{\sqrt{2}}\right)_{0.5}$$

$$P_{er}(b,i) := P_r(b,i)$$

False alarm

False alarm no ISI accurs between S and R and the error apears within the run of N-symbols where k is the symbol position

$$\tau_R := \alpha_p \qquad v_o(t) := I_0(t) \qquad temp(i,t) := \frac{I_0(t)}{v_i \cdot I_0\left(t_{pk}\right)} - 1$$

FALSE ALARMS STANDARD

$$Q_{f_i} := \frac{v_i \cdot v_{pk}}{\sqrt{S_o \cdot noise}}$$

$$P_f(b,i) := \frac{T_s}{\tau_R} \cdot 0.5 \cdot erfc\left(\frac{b \cdot \eta q \cdot Q_{f_i}}{\sqrt{2}}\right) \cdot 0.5$$

Total Fals alarm

$$P_{ef}(b,i) := P_f(b,i)$$

$$P_{eb}(b,i) := P_r(b,i) + P_{ef}(b,i)$$

$$pc(b,i) := \left(\log\left(P_{eb}(b,i)\right) + 9\right)$$ Set for 1 in 10^9 errors

$$P_{er}(b,0) = 169.853 \times 10^{-3} \qquad P_{ef}(b,0) = 644.383 \times 10^{-3}$$

$$a_i := root(pc(b,i),b)$$ Find the root to give 1 in 10^9

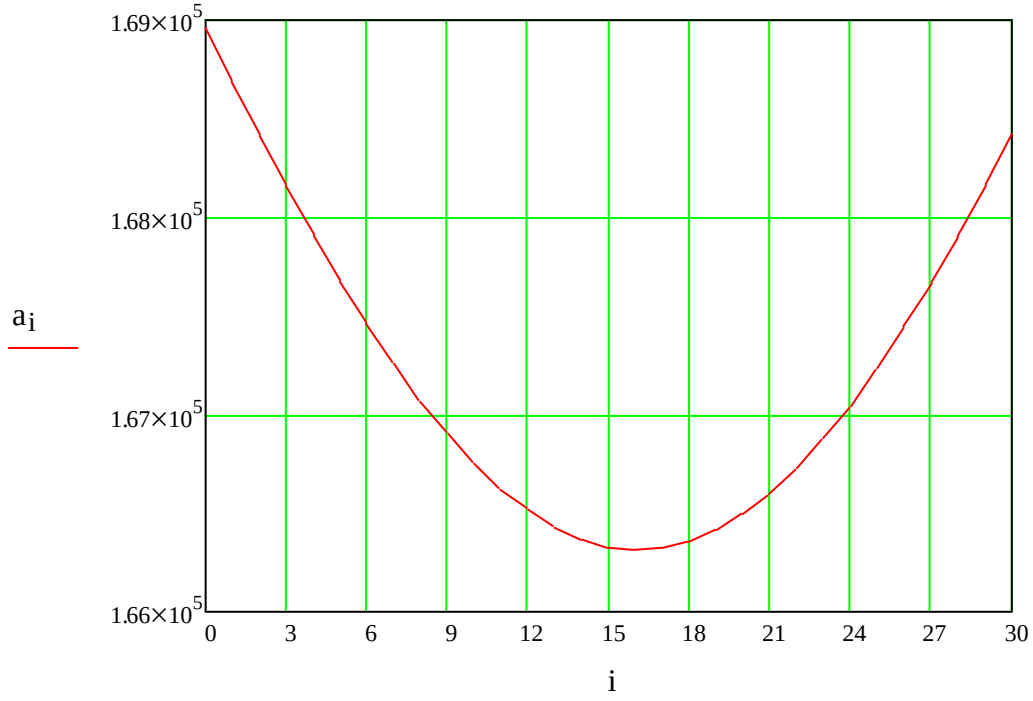

$v_{off} \equiv 0.49$

$b \equiv 1 \cdot 10^{3}$

$minimum := \min(a)$ $\quad minimum = 166.313 \times 10^{3}$

$$dBm := 10 \cdot \log\left(\frac{minimum}{3} \cdot \frac{photon\_energy}{10^{-3}} \cdot B\right)$$

$dBm = -35.703 \times 10^{0}$

Q_{e_i} =

$36.868 \cdot 10^{-6}$
$36.795 \cdot 10^{-6}$
$36.723 \cdot 10^{-6}$
$36.65 \cdot 10^{-6}$
$36.577 \cdot 10^{-6}$
$36.504 \cdot 10^{-6}$
$36.432 \cdot 10^{-6}$
$36.359 \cdot 10^{-6}$
$36.286 \cdot 10^{-6}$
$36.214 \cdot 10^{-6}$
$36.141 \cdot 10^{-6}$
$36.068 \cdot 10^{-6}$
$35.995 \cdot 10^{-6}$
$35.923 \cdot 10^{-6}$
$35.85 \cdot 10^{-6}$
...

$P_r(b, i)$ =

$169.853 \cdot 10^{-3}$
$169.863 \cdot 10^{-3}$
$169.874 \cdot 10^{-3}$
$169.884 \cdot 10^{-3}$
$169.894 \cdot 10^{-3}$
$169.904 \cdot 10^{-3}$
$169.914 \cdot 10^{-3}$
$169.924 \cdot 10^{-3}$
$169.934 \cdot 10^{-3}$
$169.945 \cdot 10^{-3}$
$169.955 \cdot 10^{-3}$
$169.965 \cdot 10^{-3}$
$169.975 \cdot 10^{-3}$
$169.985 \cdot 10^{-3}$
$169.995 \cdot 10^{-3}$
...

Q_{f_i} =

$224.063 \cdot 10^{12}$
$224.517 \cdot 10^{12}$
$224.972 \cdot 10^{12}$
$225.426 \cdot 10^{12}$
$225.881 \cdot 10^{12}$
$226.335 \cdot 10^{12}$
$226.79 \cdot 10^{12}$
$227.244 \cdot 10^{12}$
$227.699 \cdot 10^{12}$
$228.153 \cdot 10^{12}$
$228.608 \cdot 10^{12}$
$229.062 \cdot 10^{12}$
$229.517 \cdot 10^{12}$
$229.971 \cdot 10^{12}$
$230.426 \cdot 10^{12}$
...

$P_f(b, i)$ =

$644.383 \cdot 10^{-3}$
$644.345 \cdot 10^{-3}$
$644.306 \cdot 10^{-3}$
$644.268 \cdot 10^{-3}$
$644.229 \cdot 10^{-3}$
$644.191 \cdot 10^{-3}$
$644.152 \cdot 10^{-3}$
$644.114 \cdot 10^{-3}$
$644.075 \cdot 10^{-3}$
$644.037 \cdot 10^{-3}$
$643.999 \cdot 10^{-3}$
$643.96 \cdot 10^{-3}$
$643.922 \cdot 10^{-3}$
$643.883 \cdot 10^{-3}$
$643.845 \cdot 10^{-3}$
...

$P_{eb}(b, i)$ =

$814.236 \cdot 10^{-3}$
$814.208 \cdot 10^{-3}$
$814.18 \cdot 10^{-3}$
$814.151 \cdot 10^{-3}$
$814.123 \cdot 10^{-3}$
$814.095 \cdot 10^{-3}$
$814.067 \cdot 10^{-3}$
$814.038 \cdot 10^{-3}$
$814.01 \cdot 10^{-3}$
$813.982 \cdot 10^{-3}$
$813.953 \cdot 10^{-3}$
$813.925 \cdot 10^{-3}$
$813.897 \cdot 10^{-3}$
$813.868 \cdot 10^{-3}$
$813.84 \cdot 10^{-3}$
...

$pc(b, i)$ =

$8.911 \cdot 10^{0}$
$8.911 \cdot 10^{0}$
$8.911 \cdot 10^{0}$
$8.911 \cdot 10^{0}$
$8.911 \cdot 10^{0}$
$8.911 \cdot 10^{0}$
$8.911 \cdot 10^{0}$
$8.911 \cdot 10^{0}$
$8.911 \cdot 10^{0}$
$8.911 \cdot 10^{0}$
$8.911 \cdot 10^{0}$
$8.911 \cdot 10^{0}$
$8.911 \cdot 10^{0}$
$8.911 \cdot 10^{0}$
$8.911 \cdot 10^{0}$
...

a_i =

$168.963 \cdot 10^{3}$
$168.684 \cdot 10^{3}$
$168.414 \cdot 10^{3}$
$168.155 \cdot 10^{3}$
$167.909 \cdot 10^{3}$
$167.676 \cdot 10^{3}$
$167.457 \cdot 10^{3}$
$167.254 \cdot 10^{3}$
$167.068 \cdot 10^{3}$
$166.9 \cdot 10^{3}$
$166.751 \cdot 10^{3}$
$166.622 \cdot 10^{3}$
$166.514 \cdot 10^{3}$
$166.429 \cdot 10^{3}$
$166.366 \cdot 10^{3}$
...

Appendix H: Receiver sensitivity of OffsetPPM at 100 Mbps

Receiver sensitivity of Offset PPM at 100 Mbit/s and 3 PCM BITS for LOS Indoor VLC Link 2019

$i := 0, 1 .. 30$ $\quad v_i := v_{off} + \frac{i}{1000}$

$\eta q := 1.6 \cdot 10^{-19}$ Quantum energy $\quad \lambda := 820 \cdot 10^{-9}$ This is the wavelength of operation

$$photon\_energy := \frac{6.63 \cdot 10^{-34} \cdot 3 \cdot 10^{8}}{\lambda}$$

$$R_o := \frac{\eta q}{photon\_energy} \qquad R_o = 659.628 \times 10^{-3}$$

Preamplifier terms

$S_o := 25 \cdot 10^{-24}$ **Preamplifier input noise** $\quad N \equiv 3$

$B := 100 \cdot 10^{6}$ Bit rate $\quad n := 2^{N-1}$

$T_b := \frac{1}{B}$ PCM bit time $\quad T_n := \frac{N}{B}$ frame time for N bits of pcm

$T_b = 10 \times 10^{-9}$ $\quad T_s := \frac{T_n}{n}$ $\quad T_s = 7.5 \times 10^{-9}$ average slot width

$f_c := 0.5 \cdot \frac{1}{T_s}$ $\quad \omega_c := 2 \cdot \pi \cdot f_c$ $\quad f_c = 66.667 \times 10^{6}$

preamplifier $\quad H_{pre}(\omega) := \frac{1}{1 + j \cdot \frac{\omega}{\omega_c}}$

Pulse shape

VLC impulse response

$$h(t) := \left[\frac{1}{1} \cdot \left[\int_0^t \mathrm{Re}\left[\exp\left[i \cdot \omega \cdot (t) \cdot H_{pre}(\omega) \right] \right] d\omega \right] \right]$$

$t := 0, 0.1 .. 14$

$h(t) =$

$0 \cdot 10^{0}$
$99.998 \cdot 10^{-3}$
$199.947 \cdot 10^{-3}$
$299.595 \cdot 10^{-3}$
$398.296 \cdot 10^{-3}$
$494.808 \cdot 10^{-3}$
$587.124 \cdot 10^{-3}$
$672.323 \cdot 10^{-3}$
$746.494 \cdot 10^{-3}$
$804.764 \cdot 10^{-3}$
$841.471 \cdot 10^{-3}$
$850.56 \cdot 10^{-3}$
$826.215 \cdot 10^{-3}$
$763.772 \cdot 10^{-3}$
$660.865 \cdot 10^{-3}$
...

$$\alpha_p := \frac{0.1874 T_b}{f_n} \qquad f_n \equiv 0.6$$

$$\alpha_{pn} := \frac{\alpha_p}{T_s}$$

$$Pulse1(t) := \frac{1}{\sqrt{2 \cdot \pi} \cdot \alpha_{pn} \cdot 1} \cdot \exp\left(\frac{-t^2}{2 \cdot \alpha_{pn}^2} \right)$$

$Pulse1(t) =$

$1.038 \cdot 10^{0}$
$1.003 \cdot 10^{0}$
$906.433 \cdot 10^{-3}$
$765.353 \cdot 10^{-3}$
$603.946 \cdot 10^{-3}$
$445.394 \cdot 10^{-3}$
$306.974 \cdot 10^{-3}$
$197.728 \cdot 10^{-3}$
$119.027 \cdot 10^{-3}$
$66.963 \cdot 10^{-3}$
$35.207 \cdot 10^{-3}$
$17.3 \cdot 10^{-3}$
$7.944 \cdot 10^{-3}$
$3.409 \cdot 10^{-3}$
$1.368 \cdot 10^{-3}$
...

$$I_0(t) := \left(\frac{1}{T_s} \cdot \int_0^t h(\tau) \cdot Pulse1(t - \tau)\, d\tau \right)$$

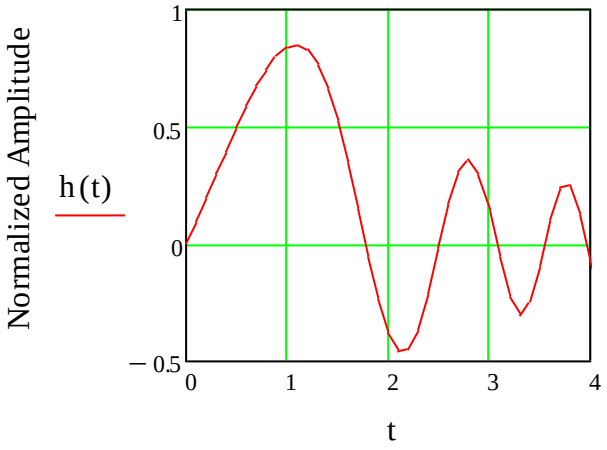

Time slot (Ts)

$I_0(t) =$

$0 \cdot 10^{0}$
$687.99 \cdot 10^{3}$
$2.706 \cdot 10^{6}$
$5.926 \cdot 10^{6}$
$10.154 \cdot 10^{6}$
$15.158 \cdot 10^{6}$
$20.687 \cdot 10^{6}$
$26.488 \cdot 10^{6}$
$32.307 \cdot 10^{6}$
$37.884 \cdot 10^{6}$
$42.939 \cdot 10^{6}$
$47.171 \cdot 10^{6}$
$50.255 \cdot 10^{6}$
$51.851 \cdot 10^{6}$
$51.636 \cdot 10^{6}$
...

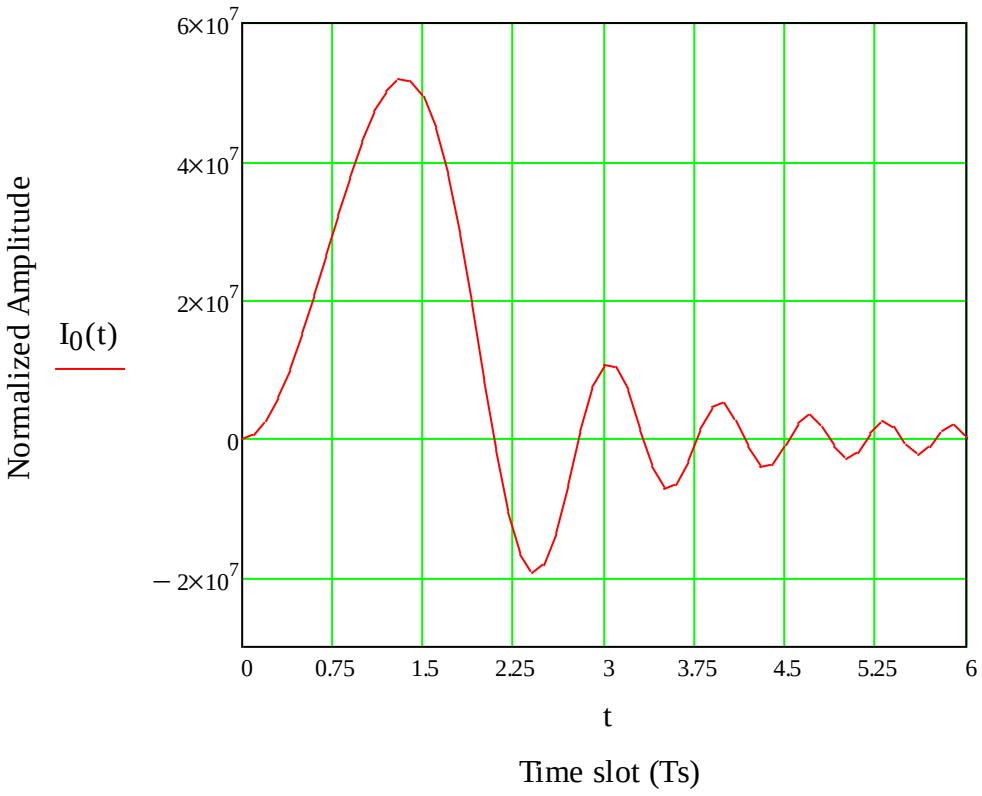

$t := 1.3$

$I_1(t) := \frac{d}{dt} I_0(t)$ Guess at the peak time

$t_{pk} := \text{root}\left(I_1(t) \cdot T_s^{\,3}, t\right)$ $t_{pk} = 1.34\times 10^0$ This is the peak time

$v_{pk} := I_0\left(t_{pk}\right)$ $v_{pk} = 51.999\times 10^6$ This is the peak voltage

$noise := \frac{\pi \cdot f_c}{2}$ $noise = 104.72\times 10^6$ Noise bandwidth

$S_o \cdot noise = 2.618\times 10^{-15}$ $\sqrt{S_o \cdot noise} = 51.166\times 10^{-9}$

Erasure of pulse

$$Q_{e_i} := \eta q \cdot \frac{v_{pk} - v_i \cdot v_{pk}}{\sqrt{S_o \cdot noise}} \qquad P_r(b,i) := \frac{1}{2} \cdot erfc\left(\frac{Q_{e_i} \cdot b}{\sqrt{2}}\right)_{0.5}$$

$$P_{er}(b,i) := P_r(b,i)$$

False alarm

False alarm no ISI accurs between S and R and the error apears within the run of N-symbols where k is the symbol position

$$\tau_R := \alpha_p \qquad v_o(t) := I_0(t) \qquad temp(i,t) := \frac{I_0(t)}{v_i \cdot I_0(t_{pk})} - 1$$

FALSE ALARMS STANDARD

$$Q_{f_i} := \frac{v_i \cdot v_{pk}}{\sqrt{S_o \cdot noise}}$$

$$P_f(b,i) := \frac{T_s}{\tau_R} \cdot 0.5 \cdot erfc\left(\frac{b \cdot \eta q \cdot Q_{f_i}}{\sqrt{2}}\right) \cdot 0.5$$

Total Fals alarm

$$P_{ef}(b,i) := P_f(b,i)$$

$$P_{eb}(b,i) := P_r(b,i) + P_{ef}(b,i)$$

$$pc(b,i) := \left(\log\left(P_{eb}(b,i)\right) + 9\right)$$ Set for 1 in 10^9 errors

$$P_{er}(b,0) = 163.502 \times 10^{-3} \qquad P_{ef}(b,0) = 620.97 \times 10^{-3}$$

$$a_i := root(pc(b,i),b)$$ Find the root to give 1 in 10^9

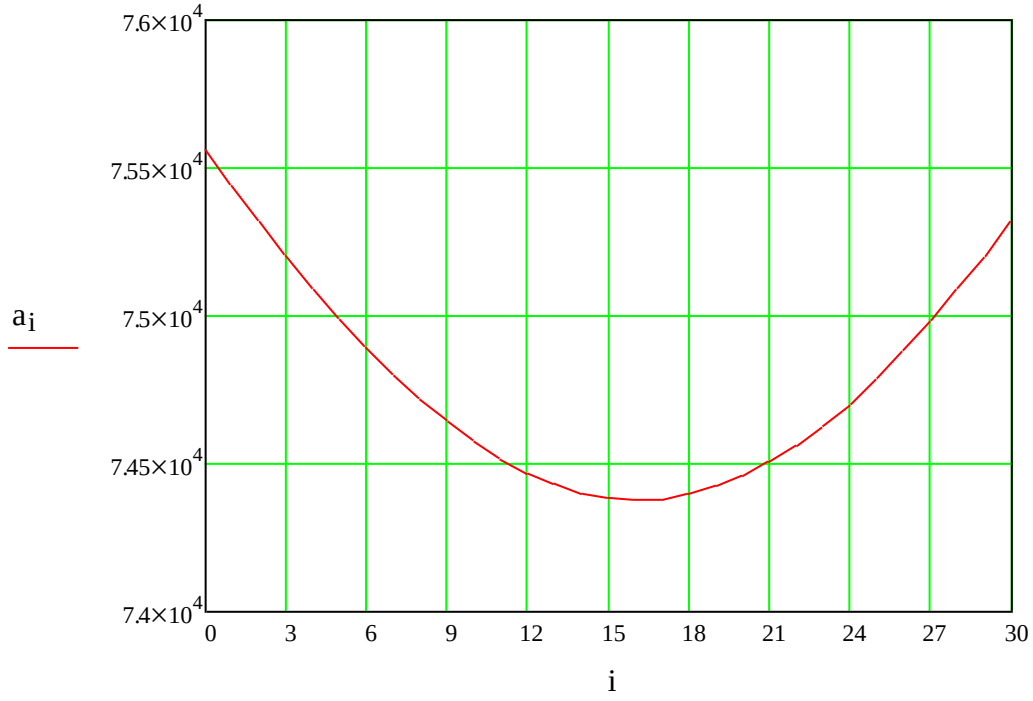

$v_{off} \equiv 0.49$

$b \equiv 1 \cdot 10^{3}$

$minimum := \min(a)$ $\quad minimum = 74.377 \times 10^{3}$

$$dBm := 10 \cdot \log\left(\frac{minimum}{3} \cdot \frac{photon\_energy}{10^{-3}} \cdot B\right)$$

$dBm = -32.209 \times 10^{0}$

Q_{e_i} =

$82.44 \cdot 10^{-6}$
$82.277 \cdot 10^{-6}$
$82.114 \cdot 10^{-6}$
$81.952 \cdot 10^{-6}$
$81.789 \cdot 10^{-6}$
$81.627 \cdot 10^{-6}$
$81.464 \cdot 10^{-6}$
$81.301 \cdot 10^{-6}$
$81.139 \cdot 10^{-6}$
$80.976 \cdot 10^{-6}$
$80.814 \cdot 10^{-6}$
$80.651 \cdot 10^{-6}$
$80.488 \cdot 10^{-6}$
$80.326 \cdot 10^{-6}$
$80.163 \cdot 10^{-6}$
...

$P_r(b, i)$ =

$163.502 \cdot 10^{-3}$
$163.525 \cdot 10^{-3}$
$163.547 \cdot 10^{-3}$
$163.57 \cdot 10^{-3}$
$163.593 \cdot 10^{-3}$
$163.615 \cdot 10^{-3}$
$163.638 \cdot 10^{-3}$
$163.66 \cdot 10^{-3}$
$163.683 \cdot 10^{-3}$
$163.706 \cdot 10^{-3}$
$163.728 \cdot 10^{-3}$
$163.751 \cdot 10^{-3}$
$163.774 \cdot 10^{-3}$
$163.796 \cdot 10^{-3}$
$163.819 \cdot 10^{-3}$
...

Q_{f_i} =

$501.019 \cdot 10^{12}$
$502.036 \cdot 10^{12}$
$503.052 \cdot 10^{12}$
$504.068 \cdot 10^{12}$
$505.084 \cdot 10^{12}$
$506.101 \cdot 10^{12}$
$507.117 \cdot 10^{12}$
$508.133 \cdot 10^{12}$
$509.15 \cdot 10^{12}$
$510.166 \cdot 10^{12}$
$511.182 \cdot 10^{12}$
$512.198 \cdot 10^{12}$
$513.215 \cdot 10^{12}$
$514.231 \cdot 10^{12}$
$515.247 \cdot 10^{12}$
...

$P_f(b, i)$ =

$620.97 \cdot 10^{-3}$
$620.885 \cdot 10^{-3}$
$620.799 \cdot 10^{-3}$
$620.713 \cdot 10^{-3}$
$620.627 \cdot 10^{-3}$
$620.542 \cdot 10^{-3}$
$620.456 \cdot 10^{-3}$
$620.37 \cdot 10^{-3}$
$620.284 \cdot 10^{-3}$
$620.198 \cdot 10^{-3}$
$620.113 \cdot 10^{-3}$
$620.027 \cdot 10^{-3}$
$619.941 \cdot 10^{-3}$
$619.855 \cdot 10^{-3}$
$619.77 \cdot 10^{-3}$
...

$P_{eb}(b, i)$ =

$784.472 \cdot 10^{-3}$
$784.409 \cdot 10^{-3}$
$784.346 \cdot 10^{-3}$
$784.283 \cdot 10^{-3}$
$784.22 \cdot 10^{-3}$
$784.157 \cdot 10^{-3}$
$784.094 \cdot 10^{-3}$
$784.03 \cdot 10^{-3}$
$783.967 \cdot 10^{-3}$
$783.904 \cdot 10^{-3}$
$783.841 \cdot 10^{-3}$
$783.778 \cdot 10^{-3}$
$783.715 \cdot 10^{-3}$
$783.652 \cdot 10^{-3}$
$783.588 \cdot 10^{-3}$
...

$pc(b, i)$ =

$8.895 \cdot 10^{0}$
$8.895 \cdot 10^{0}$
$8.895 \cdot 10^{0}$
$8.894 \cdot 10^{0}$
$8.894 \cdot 10^{0}$
$8.894 \cdot 10^{0}$
$8.894 \cdot 10^{0}$
$8.894 \cdot 10^{0}$
$8.894 \cdot 10^{0}$
$8.894 \cdot 10^{0}$
$8.894 \cdot 10^{0}$
$8.894 \cdot 10^{0}$
$8.894 \cdot 10^{0}$
$8.894 \cdot 10^{0}$
$8.894 \cdot 10^{0}$
...

a_i =

$75.563 \cdot 10^{3}$
$75.438 \cdot 10^{3}$
$75.317 \cdot 10^{3}$
$75.201 \cdot 10^{3}$
$75.091 \cdot 10^{3}$
$74.987 \cdot 10^{3}$
$74.889 \cdot 10^{3}$
$74.798 \cdot 10^{3}$
$74.715 \cdot 10^{3}$
$74.64 \cdot 10^{3}$
$74.573 \cdot 10^{3}$
$74.516 \cdot 10^{3}$
$74.467 \cdot 10^{3}$
$74.429 \cdot 10^{3}$
$74.401 \cdot 10^{3}$
...